Spring 2013

Heat transfer and bubble dynamics in bubble and slurry bubble columns with internals for Fischer-Tropsch synthesis of clean alternative fuels and chemicals

Moses Odongo O. Kagumba

Department: Chemical and Biochemical Engineering

HEAT TRANSFER AND BUBBLE DYNAMICS IN BUBBLE AND SLURRY BUBBLE COLUMNS WITH INTERNALS FOR FISCHER-TROPSCH SYNTHESIS OF CLEAN ALTERNATIVE FUELS AND CHEMICALS

by

MOSES ODONGO O. KAGUMBA

A DISSERTATION

Presented to the Faculty of the Graduate School of the

MISSOURI UNIVERSITY OF SCIENCE AND TECHNOLOGY

In Partial Fulfillment of the Requirements for the Degree

DOCTOR OF PHILOSOPHY

in

CHEMICAL ENGINEERING

2013

Approved by

Muthanna H. Al-Dahhan, Advisor
Pathasakha Neogi
Joseph Smith
Douglas Ludlow
Shoaib Usman

ABSTRACT

Synthesis gas, a mixture of CO and H_2 obtained from coal, natural gas and biomass are increasingly becoming reliable sources of clean synthetic fuels and chemicals and via Fischer-Tropsch (F-T) synthesis process. Slurry bubble column reactor is the reactor of choice for the commercialization of the F-T synthesis. Even though the slurry bubble column reactors and contactors are simple in structures, their design, scale-up, operation, and performance prediction are still challenging and not well understood due to complex interaction of phases. All the studies of heat transfer have been performed without simultaneously investigating the bubble dynamics adjacent to the heat transfer surfaces, particularly in slurry with dense internals.

This dissertation focuses on enhancing the understanding of the role of local and overall gas holdup, bubble passage frequency, bubble sizes and bubble velocity on the heat transfer characteristics by means of a hybrid measurement technique comprising an advanced four-point optical probe and a fast response heat transfer probe used simultaneously, in the presence and absence of dense internals. It also seeks to advance a mechanistic approach for estimating the needed parameters for predicting the heat transfer rate in two phase and three phase systems.

The results obtained suggest that the smaller diameter internals gives higher heat transfer coefficient, higher local and overall gas holdup, bubble passage frequency and specific interfacial area but smaller bubble sizes and lower axial bubble velocities. The presence of dense internals enhances the heat transfer coefficient in both the large and smaller columns, while increased column diameter increases the heat transfer coefficient, axial bubble velocity, local and overall gas holdup, bubble chord lengths and specific interfacial area. Addition of solids (glass beads) leads to increased bubble chord lengths and increase in axial bubble velocity, but a decrease in local and overall gas holdup, a decrease in bubble passage frequency and decrease in the heat transfer coefficient.

Further, a mechanistic assessment of the dependence of the heat transfer coefficient on the bubble dynamics shows that the contact time needed in the heat transfer coefficient estimation is indeed a function of the bubble passage frequency and local gas holdup. Hence the variation of the heat transfer coefficient with contact time is via bubble passage frequency and local gas phase holdup, which are related with sizes and velocity.

ACKNOWLEDGMENTS

A little over four and a half years of my graduate studies seem to have come to an end. Many have crossed my path during this endeavor and contributed directly or indirectly in my work. When I first met with Prof, Muthanna. H. Al-Dahhan in early 2009 as my academic and research advisor, I knew making friends with chemical reactors was inevitable. It has been an excellent opportunity working under him who sees an opportunity in every challenge. I sincerely thank him for his insightful thoughts, encouragement, advice and valuable suggestions throughout the journey.

I wish to express my sincere gratitude to all my Ph.D. committee members, Prof. J. Smith, Prof. P. Neogi, Prof. D. Ludlow and Prof. S. Usman for finding the time to be on my Ph.D. dissertation committee. I also wish to thank the funding agency which made this work possible. To the Chemical Engineering staff, thank you for answering my questions and clearing my doubts. Special thanks to Adam Lenz. To my labmates, past and present thank you for your numerous help and support.

I am eternally indebted to my parents, family, and friends for their support and encouragement throughout this endeavor. To my elder brother Jackson, for the sacrifices, unwavering support, belief in me and constant encouragement even when nothing seemed possible, I am forever grateful. To my dad who instilled the sense of hard work in me, to my mom for her unbounded love and support you remained the pillar of this work. To my wife, Celline, I owe you probably more than I can ever pay back, without you none of this could have been achieved. To our lovely girls Gloria and Ashley, days turned into years but you never doubted I would be home with you soon. You were all the motivation I had to get this work done. I dedicate this dissertation to you.

TABLE OF CONTENTS

Page

LIST OF ILLUSTRATIONS

Figure Page

LIST OF TABLES

NOMENCLATURE

Symbol	Description
a	Specific interfacial area, cm^2/cm^3
A_f	Free cross-sectional area of the column, m^2
C_p	Heat capacity, kJ/(kg.K)
D	Column diameter, m
d_b	Bubble diameter, cm
D_c	Column diameter, m
D_i	Inner diameter, m
ID	Inner diameter, m
d_l	Bubble chord length, cm
D_o	Outer diameter, m
D_R	Ratio of gas and liquid/slury phase densities, dimensionless
D_r	Ratio of gas phase density to liquid/slurry phase, dimensionless
d_s	Sauter mean bubble diameter, cm
d_{tube}	tube diameter, cm
Eo	Etovos number, dimensionless
f	Frequency, Hz
Fr	Froude number, dimensionless
g	Gravity constant, $m.s^{-2}$
h	Heat transfer coefficient, $W/(m^2.K)$

H	Height of liquid, m
h_{ave}	Time averaged heat transfer coefficient, W/(m^2.K)
h_w	Time averaged heat transfer coefficient, W/(m^2.K)
H_d	Dynamic height, m
h_i	Instantaneous heat transfer coefficient, W/(m^2.K)
H_S	Static height, m
$h_{w,max}$	Maximum heat transfer coefficient, W/(m^2.K)
k	Thermal conductivity, W/(m.K)
$k_L a$	Volumetric mass transfer coefficient, s^{-1}
L	Column length, m
L	Length of probe, m
l_c	bubble chord length, cm
m	mean of lognormal distribution
Mo	Morton number, dimensionless
N	Length of time series, dimensionless
n	Sampling number
N	Sampling number
Nu	Nusselt number, dimensionless
Pe	Peclet number, dimensionless
Pr	Prandtl's number, dimensionless
q	Heat flux across the sensor, (kW/(m^2. K))

r	Radial location in the column, m
R	Radius of column, m
Re	Reynolds number, dimensionless
St	Stanton Number, dimensionless
T	Length of time series, s
T	Total sampling time, s
t	time, s
t_l	Contact time, s
T_b	Bulk temperature, K
t_c	Contact time, s
t_R	Inter-tube gap, cm
T_i	Contact time between by bubble and probe measured by tip i
T_s	Surface temperature of the probe, K
t_{tube}	tube pitch, m
U_b	Bubble velocity, m/s
$U_{B\infty}$	Terminal bubble rise velocity, $m.s^{-1}$
U_G	Superficial gas velocity, $m.s^{-1}$
U_g	Superficial gas velocity, $m.s^{-1}$
$U_{g,L}$	Large bubble rise velocity, m/s
$U_{g,sm}$	Small bubble rise velocity, m/s
U_L	Superficial liquid velocity, $m.s^{-1}$

U_{lb}	Large bubble rise velocity, $m.s^{-1}$
U_{sb}	Small bubble rise velocity, $m.s^{-1}$
U_{slip}	Slip velocity, $m.s^{-1}$
V_c	Circulation velocity, m/s
V_g	Superficial gas velocity, m/s
We	Weber number, dimensionless group
x	thickness of the tube, m
y	Distance from wall, m
Z	Axial distance above the gas distributor, m
z	Axial position, m
Z/D	Dimensionless height above distributor

Greek Letters

$\bar{\varepsilon}_G$	Cross-sectionally averaged gas holdup, dimensionless
ε_G	Overall gas hold up, dimensionless
μ	Mean of a time-series, dimension of time-series
θ	Contact time, s
σ	Standard deviation of a time series, dimension of time-series
	Surface tension, $dyne.cm^{-1}$
τ	Sampling period, s
ρ_g	Gas phase density, $kg\ m^{-3}$

ρ_L	Liquid phase density, kg m^{-3}
ρ_S	Solids phase density, kg m^{-3}
ρ_{SL}	Slurry phase density, kg m^{-3}
σ_L	Liquid surface tension, N m^{-1}
μ_L	Liquid viscosity, kg m^{-1} s^{-1}
α	Thermal diffusivity, m^2/s
δ	Film thickness, m
δ_0	Viscous sublayer thickness, m
ε_g	local gas holdup, dimensionless
$\varepsilon_{g,l}$	Large bubble gas holdup, dimensionless
$\varepsilon_{g,sm}$	Small bubble gas holdup, dimensionless
$\varepsilon_{g,T}$	Time based gas holdup, dimensionless
φ	Angle between bubble velocity vector and the normal vector of the bubble's symmetry plane
φ_s	Volume based solids loading, vol.%
ϕ	Angle between the projection of the normal vector on the xy plane and the x axis
μ	Mean of log-normal distribution Viscosity, Pa.s
ν	Kinetic viscosity, m^2/s

	variance of log-normal distribution
θ	Angle between the normal vector of the bubble's symmetry plane to the probe's axial direction
ρ	phase density, kg m^{-3}
τ	Sampling time, (s)

Subscripts

avg	Average
d	Downward
Exp.	Experimental data
g	Gas phase
G	Gas phase
l	Liquid phase
L	Liquid phase
	Large bubble
max	Maximum
Pred.	Predicted value
s	Solid phase
sl	Slurry phase
sm	Small bubble
u	Upward

Abbreviations

AARD	Average Absolute Relative Difference
AARE	Average Absolute Relative Error

ANN	Artificial Neural Network
ARD	Absolute Relative Difference
BTL	Biomass to liquids
CARPT	Computer Automated Radioactive Particle Tracking
CFD	Computational Fluid Dynamics
CREL	The chemical reaction engineering laboratory (Washington University)
CSA	Cross-Sectional Area,
CT	Computed Tomography
CTL	Coal to Liquids
DAQ	Data acquisition
DGD	Dynamic Gas Disengagement
ECT	Electrical Capacitance Tomography
EIA	Energy Information Administration
FT	Fischer-Tropsch
GTL	Gas-to-Liquids
ID	Inner diameter
NDG	Nuclear Gauge Densitometry
PDF	Probability Density Function
PIV	Particle imaging velocimetry
SBC	Slurry bubble column
SBCR	Slurry bubble column reactor
SCHF	Standard Cubic Feet per Hour
TKE	Turbulent kinetic energy

1. INTRODUCTION

1.1. ENERGY CONCERNS, FISCHER-TROPSCH AND SLURRY BUBBLE COLUMNS

Energy is a fundamental driver of economic development and a major contributor to people's quality of life. It sustains the living standards of developed countries to a high level of comfort and convenience while at the same time leads people out of poverty in the developing world. For instance, according to the World Health Organization (WHO) report 2012, access to electricity increases life expectancy, reduces infant mortality, facilitates education and improves productivity. Thus energy provides a window to the wider world. Therefore, there is no doubt that energy is fundamental to our development and a stable and sustainable energy supply is one of the major issues of this Century. In fact, the combination of increased energy demand and declining petroleum supply can be a threat to political and economic stability, and even likely to lead to further shifts towards coal and non-conventional oil fuels from energy sources such as natural gas and biomass

Economic growth in the developing countries over the past decade, the expanding world population, and an increase in the purchasing power of individuals has lead to the increase in energy demand globally. Over the same decade, new technologies for recovering crude oil, changes in the yields of existing crude oil fields, and a global increase in exploration have expanded the number and variety of crude oil types (U.S. Energy Information Administration | International Energy Outlook, June/2012). Global production of natural gas, coal, biomass and biofuel is growing rapidly due to the

increasing price of fossil fuels, growing environmental concerns, and considerations with regards to the security and diversification of energy supply.

During the past 25 years, the production of liquid fuels has changed from being based on petroleum primarily to using a wide range of feedstock as well as completed products from numerous sources around the globe. Changes in environmental regulatory policies have resulted in the use of feedstocks other than crude oil, such as natural gas and renewable biomass, and a renewed interest in the use of other feedstocks such as coal.

According to the U.S. Energy Information Administration | International Energy Outlook, 2007, the global energy demand is projected to grow in the region of 50 % by 2030 which is approximately 2.3 % annually for the next 18 years. Oil remains the single dominant energy source for the transport sector; however it cannot meet the ever increasing demand indefinitely and sufficiently. Thus the oil demand, supply security and price concerns also occasioned by the latest turmoil that has been witnessed in the Middle-East (which has nearly 67 % of the worlds proven crude oil) has led to renewed interest in coal, natural gas, and biomass as alternative feedstock for the production of clean transportation fuels and chemicals. The variety and changing dynamics of petroleum and nonpetroleum feedstocks and the resulting end-use products are illustrated in Figure 1.1.

Natural gas, coal, and biomass are set to play an ever-increasing role if the energy challenge is to be met effectively. In the recent history, Natural gas, Coal, and Biomass have taken significant market share from petroleum feedstocks, correlated with shifts in product yields, a trend that is expected to continue in the future, along with further diversification into non-petroleum fossil feedstocks. In 2000, nearly all liquid fuels were

derived from petroleum. Since then, however, the share of petroleum has dropped while the shares of biomass and other non-fossil fuels have increased. According to the U.S. Energy Information Administration | International Energy Outlook, June/2012, (Figure 1.1) the demand for natural gas, biomass, and coal combined is projected to account for nearly 60 % of the total energy demand by 2035.

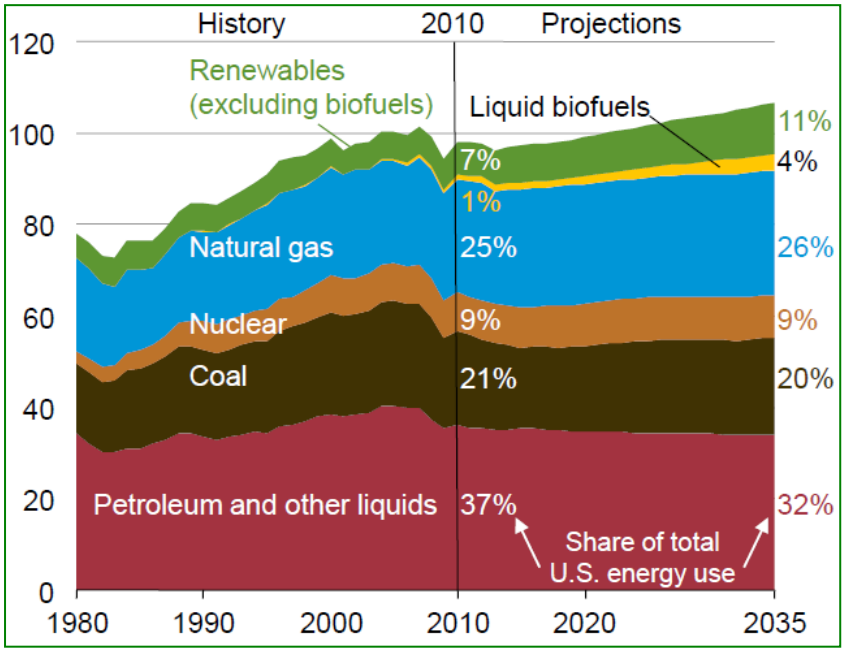

Figure 1.1 Variety and changing dynamics of nonpetroleum feedstocks
(Source : U.S. Energy Information Administration | International Energy Outlook, June/2012)

Synthesis gas (Syngas) (a mixture of CO and H_2) produced via gasification of coal, natural gas and biomass are increasingly becoming reliable sources of energy and chemicals. The Fischer-Tropsch (F-T) synthesis process is a well proven technology for making synthetic fuels and chemicals derived from syngas obtained from coal, natural

gas, and biomass which are more environmentally friendly alternatives to the petroleum. The F-T process was first developed by Franz Fischer and Hanz Tropsch in Germany in the 1920s and 1930s at the Kaiser-Wilhelm (presently Max Plank) Institute for Coal Research in Mülheim. The F-T chemistry is based on making longer chains of hydrocarbons from a mixture of CO and H_2 at elevated pressure and temperature and in the presence of a catalyst, usually cobalt or iron depending on the raw material. The excess heat generated from the reaction has typically been removed by heat exchanging fluid such as water tubes that carry water; other reactor is trickle bed in shell and tubes configuration where water flows in the shell. In reality, any source of carbon can be used to generate the synthesis gas. The first step in the FT process is the production of the synthesis gas, which is usually carried out by the gasification of coal or biomass or the conversion of natural gas by steam or other method of reforming. The manufacture of the synthesis gas is of prime importance, since it comprises the most capital-intensive part of the Fischer-Tropsch commercial process (Geerlings, 1999).

In the F-T process, syngas is passed after cleaning through a suspension of small (< 150 micron) solid catalyst particles in molten wax. To achieve economically high space-time yields, high slurry concentration (typically (30-40 % vol.), (Krishna et al., 1997) needs to be employed, while to suspend such high quantity of solids, high energy input is needed which is provided by high superficial gas velocity consequently giving rise to higher productivity. Figure 1.2 shows a schematic of a typical slurry bubble column used in the Fischer-Tropsch synthesis process.

Slurry bubble column reactor has been demonstrated to be the reactor of choice for the clean utilization and conversion of syngas and commercialization of the F-T synthesis due to it's advantages over other multiphase flow reactors, particularly trickle

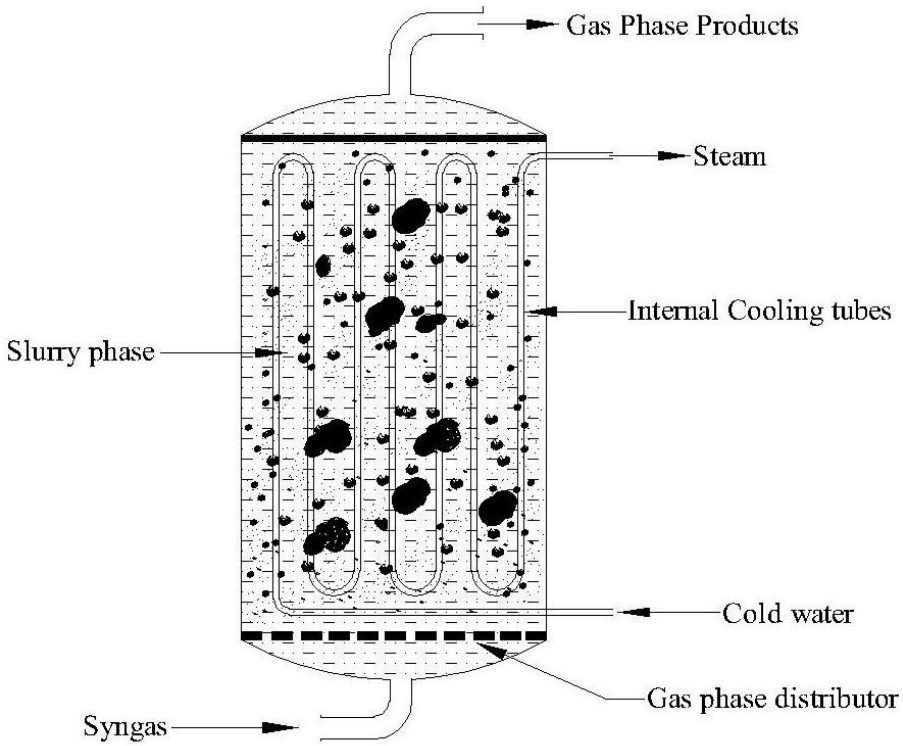

Figure 1.2 Established slurry bubble column reactor configuration with internal cooling for Fischer-Tropsch synthesis

bed reactors that have been also utilized for F-T synthesis in the form of shell and tubes configuration where the heat is removed by water passing through the shell. Multiphase reactors and contactors in general are widely used in the chemical, petroleum, and bioprocessing industries among others for gas liquid operations and for heterogeneous reactions such as gas-liquid, gas-solid, liquid-solid, gas-liquid-liquid and gas-liquid-solid

reactions. Bubble and slurry bubble columns, three-phase fluidized bed reactors, stirred tank reactors, packed bed reactors, rotating disk contactors, and monolith reactors, and ebulated bed reactors are some of the multiphase reactors currently used in the chemical industry.

Bubble columns (BC) and slurry bubble columns (SBC) have several advantages over other conventional multiphase reactors giving them an edge as gas-liquid and gas-liquid-solid contactors and reactors. Among the desired characteristics of slurry bubble column reactors (Kolbel and Ralek, 1980; Deckwer, 1980; Tang and Fan, 1990; Karamanev et al., 1992; Deckwer and Schumpe, 1993; Kluytmans et al., 2001; Degaleesan et al. 2001; Joshi, J.B 2001; Dudukovic, M.P., 2002; Li and Prakash, 2002; Li et al., 2003; Barghi et al., 2004) are;

- Uniformity in temperature and high rate of heat transfer and mass transfer characteristics due to strong mixing and phase interactions.
- Simple to construct structures which do not involve mechanically moving parts; hence competitive investment, operating and maintenance costs, and
- High durability of the catalyst.

Online catalyst addition and withdrawal ability and plug-free operation are other advantages that render slurry bubble columns as an attractive reactor choice.

Conceptually, a slurry bubble column reactor (SBCR) is a vertical cylindrical vessel in which gas containing one or more reactants (e.g syngas for F-T processes) is sparged through a liquid containing liquid reactant(s) and or products (F-T processes) and a finely dispersed solids catalyst. The solid particles are suspended and dispersed by the liquid movement induced by the bubble motion. The bubble and slurry bubble columns

are extensively used as multiphase contactors and reactors in chemical, petrochemical, biochemical, pharmaceutical, metallurgical, and mineral industrial processes (Carra and Morbidelli 1987, Deckwer, 1992, Deckwer and Alper 1980, Fan 1989, Dudukovic et al., 1999, Holladay et al., 1978). Examples of such processes besides F-T synthesis are the partial oxidation of ethylene to acetaldehyde, wet-air oxidation (Deckwer, 1992), hydrogenation of maleic acid (MAC), hydro conversion of heavy oils and petroleum feedstocks, cultivation of bacteria, cultivation of mold fungi, production of single cell protein, animal cell culture (Lehmann and Hammer 1978), and liquid phase methanol synthesis (LPMeOH) (Wender, 1996).

Even though the slurry bubble column reactors are simple in design and structures, their design, scale-up, operation, and prediction and understanding of their performance are still challenging and not well understood due to the complexity in the interaction among the phases (gas-liquid-solid). For instance, numerous design and operating variables, physicochemical and thermodynamic properties of the fluids together affect the various hydrodynamic and transport parameters such as of heat and mass. In order to accomplish high efficiency reaction systems that offer lower capital and operational costs for syngas conversion into high-value fuels and chemicals via Fischer-Tropsch processes, further investigations of the fluid dynamics and transport properties are needed. Figure 1.3 illustrates the utilization of Syngas obtained from coal, biomass and natural gas into clean fuels and chemicals.

From economics point of view, heat transfer, and high volumetric productivity, a high catalyst loading is desired. For optimal product yield, Slurry bubble column reactors must be operated at high gas velocities in the churn turbulent flow regime. Hence, the

gas-liquid interfacial dynamics control the hydrodynamics and the flow pattern of the system provided that the SBCR is operating at liquid superficial velocity in the order of magnitude smaller than the superficial gas velocity and the catalyst particles are not excessively heavy and ~50 μ in size.

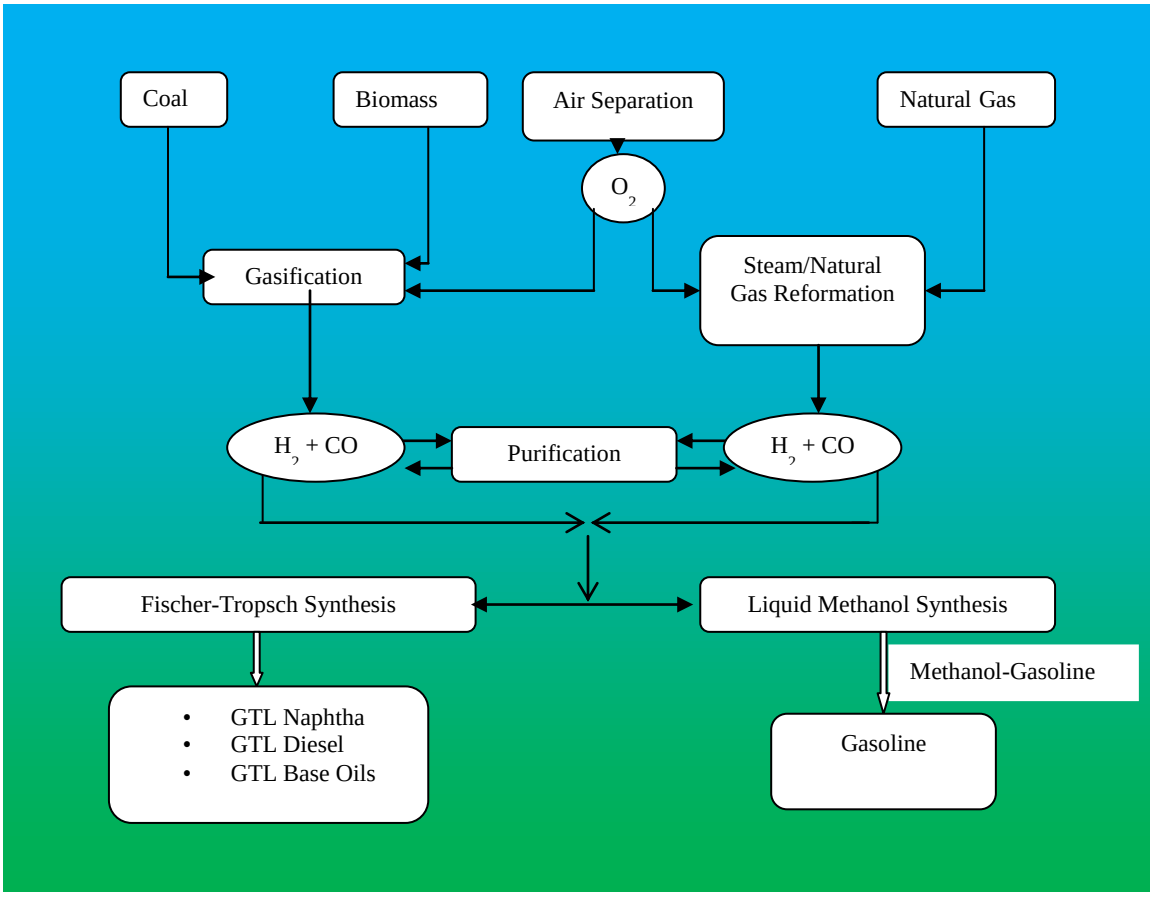

Figure 1.3 Synthesis gas utilization into fuels and chemicals

1.2. MOTIVATION AND RESEARCH OBJECTIVES

Removal of large quantities of excess generated heat by the exothermic synthesis reactions is one of the major challenges facing FT synthesis, whereas one of the most

desired characteristics in the operation of bubble and slurry bubble columns is the high heat transfer rate. Therefore, the slurry bubble column is the most suited reactor for the syngas conversion via the FT process. If the heat is not removed sufficiently, catalyst poisoning and deactivation might occur due to local heating that creates hotspots and carbon deposition on the catalyst that renders the catalyst inactive. Particularly the cobalt based F-T catalysts, like many other systems lose their activity with time on stream, (van Berge et al., 1997). The heat transfer rate is influenced by a number of parameters including design and operating conditions as well as physical properties of the liquid/slurry. More specifically bubble dynamics including local and overall phase hold ups, bubble velocity, bubble sizes, interfacial area and bubble frequency, superficial gas velocity, and liquid circulation velocity all of which are interrelated and highly interactive thus controlling the bubble column performance.

The majority of industrial multiphase flow systems and processes requires different forms of heat supply or heat removal particularly when isothermal or near isothermal operation is desired. Most of these processes involve heat transfer between different configurations of immersed heat transfer surfaces or jacket surfaces and the surrounding gas-liquid or gas-liquid-solid systems. Therefore, there is a need for proper design of heat removal in these reactor systems to allow optimal temperature control for desired product quality and yield (Duduković et al., 2002) and also to avoid a broad product spectrum. In industry, various designs and configurations of internals or means of supplying or removing heat have been developed including vertical or horizontal internals, jackets at the wall, among others. The internals are of different types and are required in a number of industrial applications of bubble columns to achieve the desired

mixing or to remove the heat of reaction so as to maintain the desired temperature and near isothermal conditions of operation.

Examples of these applications include Fischer-Tropsch synthesis process for clean alternative fuels and chemicals production from natural gas, coal and biomass, liquid-phase methanol synthesis, (LMeOH), oxidation, hydrogenations, and production of dimethyl ether (DME). However a few studies have shown that the presence of internals can alter the column hydrodynamics and mixing patterns (Youssef and Al-Dahhan, 2009; Larachi et al., 2006; and Chen et al., 1999). The altered column hydrodynamics might not only have significant influence on the reactor performance but also the heat and mass transfer characteristics.

The generated or removed heat can be transferred directly from the surfaces that generate or receive the heat to the contacting medium of gas-liquid or gas-liquid-solid. Gas-liquid and gas-liquid-solid systems are characterized by high heat-transfer rate and hence, these systems have widespread use as reactors and contactors. Bubble and slurry bubble column reactors are characterized by high heat-transfer rate and hence these systems have widespread use as reactors and contactors.

Heat transfer from solid surfaces to gas-liquid and gas-liquid-solid systems have been studied experimentally and analytically in the literature (Kim and Kang, 1997, Hulet et al., 2009, Kumar and Fan; 1994, Yang et al., 2000, Kumar et al., 1992 among others). However, all these studies have been performed without simultaneously investigating the bubble properties adjacent to the heat transfer surfaces. It has been shown fundamentally that there is strong tie and interactions between heat transfer rate from or to the surface and the bubble dynamics adjacent to the surface in bubble columns since bubble

dynamics affect the renewal rate of liquid and slurry elements on the heat transfer surface (Wu, 2007 and Kumar et al., 1992). Hence, turbulence and mixing that are induced by gas bubbles play important role in heat transfer in gas-liquid and gas-liquid-solid systems. Both experimental and theoretical results reported in the literature (Li and Fan, 2001; Yang et al., 2000; Kumar and Fan 1994; Wasan and Ahluwalia, 1969) suggest that there is a series of film and surface renewal that govern the heat exchange between a surface and flowing fluid. Therefore, there is a need to investigate heat transfer rate and bubble dynamics simultaneously and to use the obtained data to mechanistically assess the dependence of heat transfer coefficient on the multiple bubble properties; Including, local and overall gas holdup, bubble passage frequency, specific interfacial area, axial bubble velocity (both upward and downward), bubble sizes as well as the bubble directions.

Even though the slurry bubble column reactors are simple in design and structures, their design, scale-up, operation, prediction and understanding the performance of the bubble and slurry bubble column reactors are still challenging and not well understood due to the complexity in the interaction among the phases (gas-liquid-solid). For instance, numerous design and operating variables, physicochemical and thermodynamic properties of the fluids together affect the various hydrodynamic and transport parameters. To achieve high volumetric throughput the use of large diameter reactors (typically, > 5 m) are required, which by means is almost two orders of magnitude larger than most of the laboratory scale columns and reactors. Heat removal internals may be installed in the bubble columns during the design and construction, while addition of solids is inevitable if high product yield is to be achieved. The flow

structure would be greatly altered in the larger column, nor stay the same with inserted internals while the physical properties of the fluid/slurry and the general rheology of the suspension would be altered by the added solids (Van Baten and Krishna, 2004; Krishna and Morreto, 1999; Saxena, et al., 1989.

Therefore, in order to accomplish high efficiency reaction systems that offer lower capital and operational costs for syngas conversion into high-value fuels and chemicals via Fischer-Tropsch processes, further investigations of the fluid dynamics and transport properties such as of heat and mass need to be done.

Accordingly, the main objective of this work is to investigate the effect of bubble dynamics on the heat transfer coefficient in bubble columns and slurry bubble columns equipped with mimicked dense heat exchanging internals using a hybrid measurement technique consisting of a fast response heat transfer probe for heat transfer coefficient and four-points fiber optic probe for bubble dynamics. In order to achieve this objective, the following tasks have been set.

- Task 1. Study the effect of dense (25 % cross-sectional area, CSA) internals and solids loading (up to 40 % vol) on bubble dynamics and heat transfer coefficient in two pilot scales bubble and slurry bubble columns (6-inch diameter and 18-inch diameter.)
- Task 2. Assessment of the mechanistic analysis of the heat transfer coefficient and its distribution based on bubble properties and their distribution in the studied bubble and slurry bubble columns. Performing also evaluation of the reported correlations against the obtained data.

- Task 3. Investigating the effect of column diameter on the bubble dynamics and on heat transfer coefficient in bubble and slurry bubble columns using 6-inch and 18-inch diameter bubble columns with and without internals

In order to accomplish the stated objective and tasks, detailed experimental investigations have been performed on the heat transfer coefficient measurements and bubble properties including local and overall gas hold-up, bubble velocity (both axial and radial), bubble passage frequency, specific interfacial area, and bubble sizes.

1.3. THESIS STRUCTURE

This dissertation consists of the following seven sections:

Section 1 introduces the energy concerns and the F-T synthesis process as an alternative solution towards cleaner liquid fuels and chemicals from alternative feedstocks which are more abundant resources than oil. It also outlines the relevance of slurry bubble columns to the FT process. The motivation and research objective for this study as well as the tasks are also presented in this chapter.

Section 2 presents the pertinent literature review to this work. It critically evaluates and highlights the previous work on bubble dynamics, heat transfer and scale-up issues.

In Section 3, the results obtained from the investigated effects of different sizes and hence configurations of dense internals occupying the same cross-sectional area (CSA) on the bubble dynamics in 6-inch diameter column are presented. In the same chapter, the impact of solids loading and dense internals on the bubble dynamics

investigated in 6-inch diameter column and in 18-inch diameter column are reported and discussed.

Section 4 discusses the impact of dense internals in two pilot scales bubble columns on the investigated heat transfer coefficient in light of the bubble dynamics presented in Section3.

In Section 5, the heat transfer coefficient is mechanistically examined. A contact time model that depends only on the bubble dynamics is proposed and used in a mechanistic equation to predict the heat transfer coefficient.

Section 6 discusses and highlights the effect of scale and diameter of slurry bubble column on the bubble dynamics as well as heat transfer coefficient in bubble and slurry bubble columns equipped with the dense mimicked heat exchanging internals.

Finally, Section 7 summarizes the conclusions drawn from different sections of the entire study and presents recommendations for future work on bubble dynamics and heat transfer studies in slurry bubble columns with dense internals.

Appendices are then annexed to provide further details of operating procedures, and additional results.

2. BACKGROUND AND LITERATURE SURVEY

2.1. BUBBLE DYNAMICS IN BUBBLE AND SLURRY BUBBLE COLUMNS

The knowledge of bubble properties, including local and overall gas holdup, bubble velocity, bubble size, bubble frequency and specific interfacial area, is of great importance for the proper design and operation of bubble columns. Besides, the bubble properties play key roles in determining the heat and mass transfer rates in bubble columns (Yang et al., 2000; Kumar et al., 1992; Kumar and Fan, 1994; Wu, 2007; Jhawar, 2011). Many researchers in the past decades have extensively studied the bubble and slurry bubble columns (SBCs) experimentally and also modeled the behavior of SBCs. However, most of these studies on bubble dynamics in bubble columns have been focused on overall gas hold-up and bubble sizes (Luo et al., 1999; Bouaifi et al., 2001; Shimizu et al., 2000; Anabtawi et al., 2002; Wang et al., 2003; Forret et al., 2003; Tang and Heindel, 2003; and Veera et al., 2004).

The first comprehensive study of bubble properties in bubble columns was done by Xue, 2004. In his work conducted in 16.2 cm diameter bubble column at pressures up to 1.0 MPa, and superficial gas velocity, up to 60 cm/s, and with three different gas spargers, he studied both overall and local gas hold-up, bubble frequency, bubble velocity, bubble chord length (which is characteristic of bubble sizes) and the specific interfacial area. It was established that the radial profiles of local gas holdup, specific interfacial area, mean bubble velocity, and bubble frequency profiles exhibit the same trends. The radial profiles evolve from flat at low superficial gas velocity to highly parabolic at high superficial gas velocity. The effects of axial position, pressure, spargers,

and elevation in the column were also investigated. Xue et al., 2008, and Xue, 2004 showed that the effect of sparger diminishes at higher gas velocities in the fully developed flow region. Besides, Xue, 2004 also demonstrated that higher pressure leads to the evolution of smaller bubbles with low bubble velocity and enhanced frequency, hence higher residence time, consequently increasing both the overall and local gas holdup. Within the fully developed flow region at axial position $z/D \geq 2.0$, above the gas distributor, the bubble properties did not exhibit any significant change. Figure 2.1 and Figure 2.2 compare some of the obtained bubble properties with different spargers and at different axial positions respectively

Unfortunately this work was carried out in empty bubble column thus the effect of dense internals which are encountered in exothermic systems such as the F-T Synthesis process cannot be deduced from this work. Furthermore, solids influence on the bubble dynamics was not examined, neither was the effect of scale.

It is noteworthy to mention that most of the studies in the literature on the effects of operating and design variables on the hydrodynamic parameters and transport of heat and mass have been performed in empty bubble and slurry bubble columns, (Wu, 2007; Youssef, 2010; and Youssef and Al-Dahhan, 2009). Therefore, the effects of heat exchanging internals on the hydrodynamic and transport parameters have not been well understood. Only a limited number of studies have been carried out in bubble and slurry bubble columns equipped with heat exchanging internals.

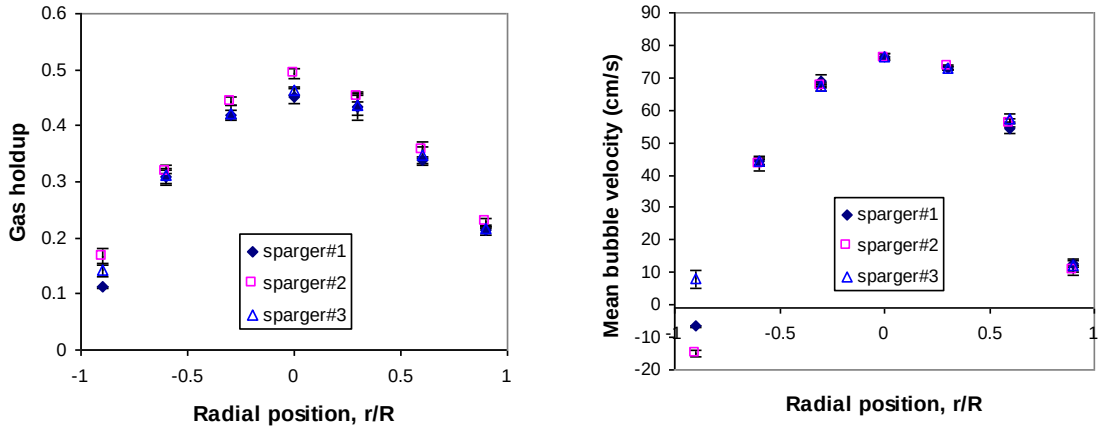

Figure 2.1 Bubble properties at z/D=5.1 for different spargers at Ug = 30 cm/s (from Xue, 2004)

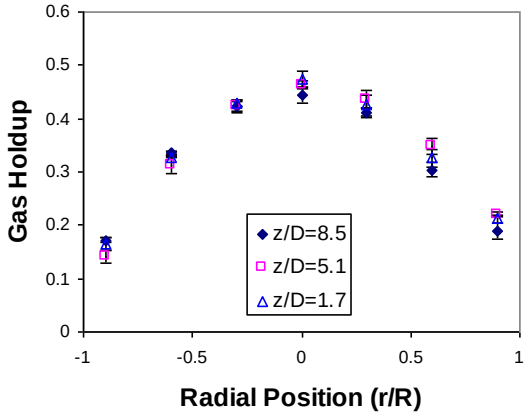

Figure 2.2 Gas holdup radial profiles at different axial positions at, Ug = 30 cm/s (from Xue, 2004)

Pradhan et al., 1993 used two types of internals (helical coils and a vertical straight tube bundle) in a 0.102 m diameter and 2.5 m height Plexiglas column and superficial gas velocities of up to 9 cm/s to investigate the effect of volume fraction of internals on overall gas holdup. The volume fractions covered by the internals

configurations varied from 0.014 to 0.193 were studied, and their results showed that gas holdup increased with an increase of volume fractions. In addition, helical coils provided higher gas holdup than vertical tubes. The difference was attributed to large intertube gaps for the vertical tube internals that provided more space for larger bubbles escape, thus decreasing the gas holdup, unlike the helical coil internals in which only smaller gaps were present. They claimed that the gas holdup enhancement of up to 55 % was achieved when the helical coil internals was used. However, the range of the superficial gas velocity used is still in the transition flow regime and cannot suspend sufficiently the large quantities of solids used in the F-T synthesis process.

Chen et al., 1999 using gamma ray computed tomography (CT) and computer automated radioactive particle tracking (CARPT) techniques, investigated the effect of internals on gas holdup, liquid velocity, turbulent stresses and eddy diffusivities both radial and axial in a 0.44 m diameter column. The column was equipped with internals similar to those used in industrial scale units covering 5 % of the column's total cross-sectional area to mimic liquid phase methanol (LPMeOH) synthesis using both air-water and air-drakeoil 10 and superficial gas velocities from 2-10 cm/s. The configuration of the internals used is shown in Figure 2.3. They reported that internals covering 5 % of the total column cross-sectional area have no significant effect on liquid recirculation velocity, while gas holdup increases slightly. The turbulent stresses and eddy diffusivities were lower in the presence of internals. In this work the range of superficial gas velocity covered was low. Thus it is not possible to evaluate with confidence the effect of internals at high superficial gas velocity that would guarantee a high volumetric productivity as desired especially in the FT process. Furthermore, the low cross-sectional

area internals cannot effectively remove the generated heat from a highly exothermic processes, hence the need to evaluate the impact of dense internals. In addition the observed changes in the gas holdup and turbulent parameters could have come from the increased mass flow rate of the gas since the gas velocity was calculated based on the total cross-sectional area thus same amount of mass for smaller cross- sectional area.

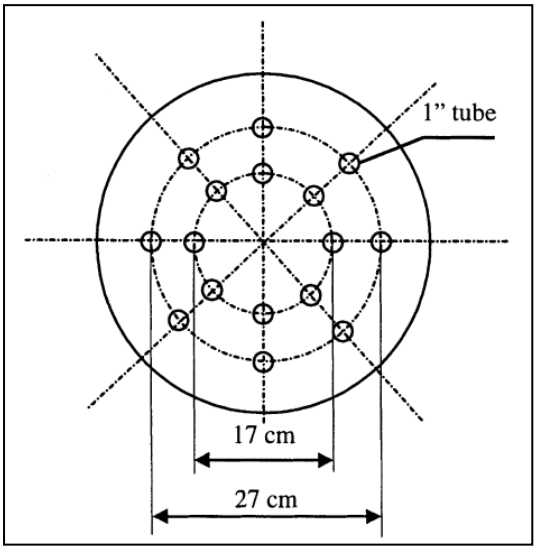

Figure 2.3 Configuration of internals covering 5 % of column's Cross-Sectional Area (from Chen et al., 1999)

Forret et al., 2003 studied the effect of internals on liquid dispersion and liquid mixing in a 1 m diameter bubble column, with internals occupying 22 % of the column cross-sectional area (CSA) and superficial gas velocity of 15 cm/s. They used a basic tracer technique and also, assessed a 1D-axial dispersion model (ADM) on the empty column and developed a 2D model to account for the effect of internals on the liquid mixing. They observed a decrease in the liquid fluctuating velocity and an enhancement

of large scale liquid recirculation with internals. Thus the presence of internals significantly affects both large scale recirculation and local dispersion as illustrated in Figure 2.4.

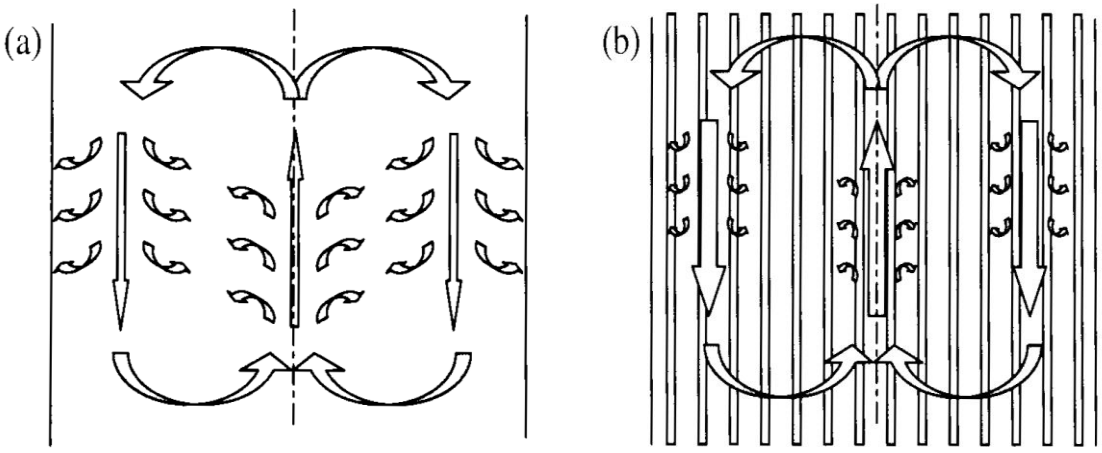

Figure 2.4 Schematic representation of enhanced large scale liquid recirculation and reduced small scale liquid recirculation in bubble columns (a) Empty column (b) with internals (from Forret et al., 2003)

Larachi et al., 2006 studied the effect of internals and their configuration on bubble column hydrodynamics using computational fluid dynamics (CFD). They used vertical heat-exchange tubes with occluded cross-sectional area ranging between 2 to 16.2 %, and tubes of 1 inch diameter arranged in a triangular pitch configuration. Transient 3-D computational fluid dynamic simulations were carried out for five bubble column internals geometries. The study revealed that circulation and mixing patterns in bubble columns with internals were affected in a very complex manner by the inserted tubes. They concluded that in the presence of internals, the large-scale and coherent meandering gas winding around, as observed in hollow bubble columns, could not be sustained and were replaced by smaller pockets whose size was dictated by the inter-tube

gaps. They also reported that gap scale was important in the longitudinal funneling of liquid flow. A sharp decrease of the liquid kinetic turbulent energy upon insertion of the heat-exchange tubes in the bubble column was also observed. They assumed a constant bubble size (neglecting coalescence/dispersion effects) and a steady drag force as the sole interfacial force (neglecting all other forces such as lift, wall, and turbulent diffusion). Whereas the occluded column cross-sectional area was reasonably high, these CFD results were not evaluated and validated against any benchmark experimental data due to the lack of such data. Further work which utilizes solids is still required.

Recently, Youssef and Al-Dahhan, 2009 and Youssef, 2010 did the first systematic and comprehensive study of bubble properties in bubble columns equipped with mimicked dense heat-exchanging internals. The studies were conducted in two bubble columns of diameter 0.19 m and 0.44 m with superficial gas velocity varied between 3 - 45 cm/s. The internals used were of different configurations with cross-sectional area covering 0 - 24.5 % of columns total cross-sectional area. The details of internals bundles and configurations used in the 0.44 m bubble column are shown in Figure 2.5. The detailed studies were carried out on overall gas holdup and local gas holdup radial profiles, bubble velocity, bubble sizes as well as specific interfacial area. They reported enhanced overall gas holdup with increased percentage coverage of column cross-sectional area by internals which was also consistent with the findings of Bernemann, 1989. With dense internals that obstructed high fraction of the column, an increase in the gas holdup radial profiles was observed as illustrated in Figure 2.6. The internals also led to higher bubble break-up rate giving rise to smaller bubble chord

lengths. Thus increased specific interfacial area between the gas and liquid phases was higher for systems equipped with internals. No significant differences were noted on the

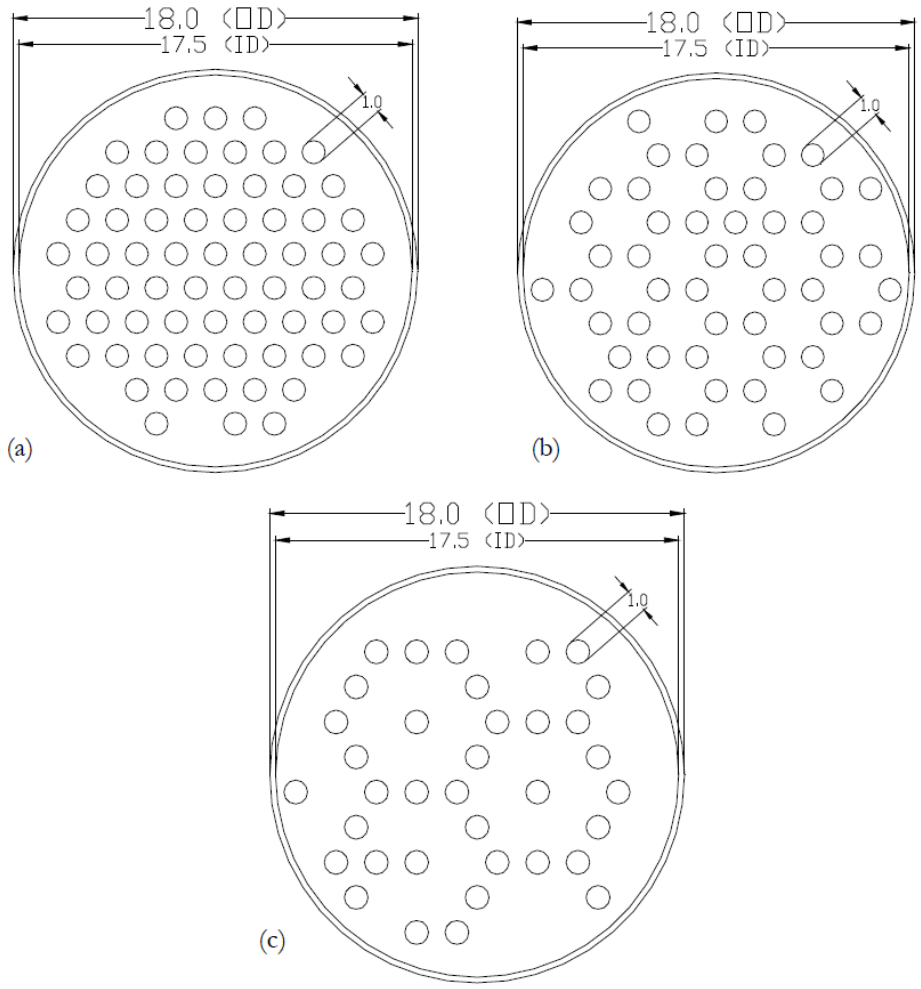

Figure 2.5 Different configurations of internals bundles covering (a) 20 %, (b) 15 %, and (c) 10 % of the total column's cross-sectional area (from Youssef, 2010).

bubble velocity probability distributions at the column's center between the case of no internals and that of 25 % CSA internals, particularly at high superficial gas velocity. However, at the 0.44 m diameter column's wall region, a higher probability of bubbles

moving downward was obtained with nearly no bubbles moving upwards at the wall region. This work (Youssef, 2009) provided a greater insight on the detailed impact of internals on bubble properties in bubble columns. However it was limited to air-water systems while the FT synthesis involves a three-phase system. Therefore, it is imperative that studies be conducted which mimic the 3-phase FT conditions to guarantee the validity of their results. Moreover, it is important to discuss in further detail the utilization of superficial gas velocity for open area only and how this affects the bubble dynamics. For the latter to be achieved, investigations using the superficial velocity need to be compared with the results from the data at superficial gas velocity for open area only and further validation be done for systems containing solids.

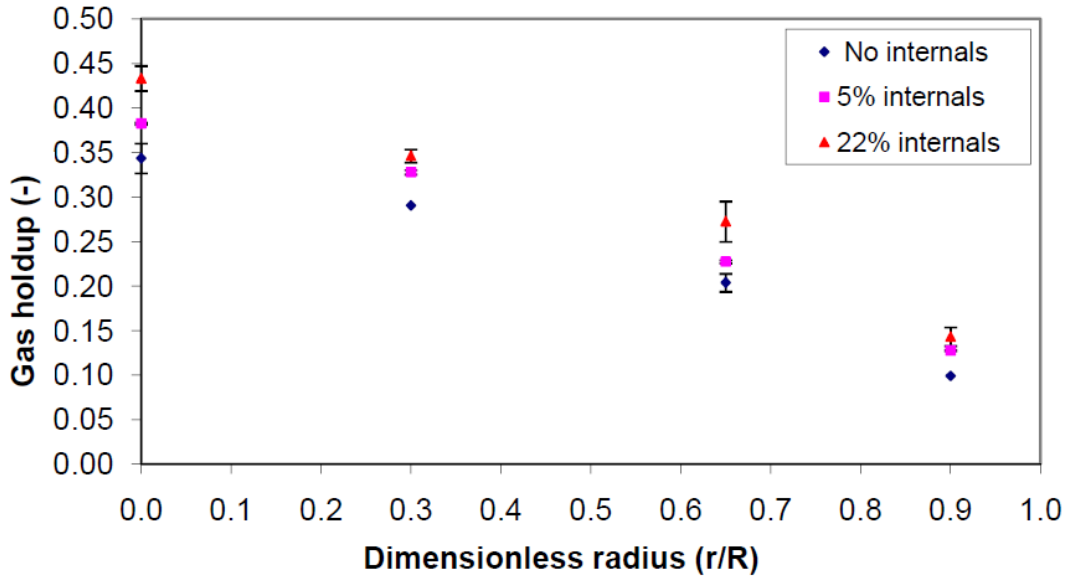

Figure 2.6 Effect of vertical internals on the local gas holdup at U_g = 20 cm/s (from Youssef and Al-Dahhan, 2009)

2.2. HEAT TRANSFER IN BUBBLE AND SLURRY BUBBLE COLUMNS

Proper design of the heat removal surfaces such as cooling tubes is crucial in order to maintain catalyst activity, reaction integrity, and product quality in bubble columns. A number of processes carried out in bubble and slurry bubble columns are highly exothermic, for instance the Fischer-Tropsch synthesis process is a highly exothermic process with a heat of reaction in the order of -172 kJ/mol of CO converted (Maretto and Krishna, 1999).

Heat transfer in two and three-phase gas suspension reactors as well as heat transfer from the solid surfaces have been investigated by several researchers both experimentally and analytically in the literature (Baker et al., 1978; Deckwer et al., 1980; Kato et al., 1981; Chiu and Ziegler, 1983; Kang et al., 1985; Kim et al., 1986; Magiliotou et al., 1988; Saxena et al., 1990a, b and 1992, Kantarci et al., 2005b). Majority of these studies have been captured in the past several reviews about the fundamental heat transfer studies in gas-liquid and gas-liquid-solid systems. Including the reviews published by Pandit and Joshi, 1986; Kim and Laurent, 1991; Saxena and Chen, 1994; Saxena, 1995; Nigam and Schumpe, 1996; Kim and Kang, 1997; Li and Prakash, 2001; Kantarci et al., 2005; Hulet et al., 2009 and most recently an overview of heat transfer in a slurry bubble column by Jhawar and Prakash, 2012, include the details of heat transfer experimental investigations in multiphase flow systems, particularly bubble and slurry bubble columns.

In this section, the key studies on heat transfer most relevant to of this work are reviewed and critically highlighted.

Korte, 1987 studied in details heat transfer from horizontal and vertical tube bundles with an embedded heat transfer probe in three different columns of 0.12 m i.d.

(4.5 m high), 0.196 m i.d. (6.8 m high) and 0.45 m i.d (6.2 m high), and concluded that the bundle's density and configuration has extensive effect on the heat transfer coefficient. Different liquids were also used in the studies and it was shown that even with high viscosity liquids, (which can be mimicked by addition of solid particles to the liquid), which promote coalescence of bubbles, and dampen the bubble instabilities, the presence of internals may inhibit any decrease on the values of the heat transfer coefficient by enhancing the bubble break-up rate. Korte, 1987 correlated his results for the tube bundles taking into account the internals by the following equation:

$$St = 0.139\left[\left(Re_g Fr_g {Pr_l}^{2.26}\right)^{-\frac{1}{3}}\right]^{0.84} {A_f}^{-0.2}\left(\frac{t_{tube}}{d_{tube}}\right)^{0.14}\left(\frac{\mu_l}{\mu_w}\right)^{0.3} \quad (2.1)$$

where A_f is the free cross-sectional area of the column, t_{tube} is the tube pitch (m), and d_{tube} (m), the tube diameter with the dimensionless numbers based on the following definitions:

$$St = \frac{h}{\rho_l C_{pl} U_g} \quad , \quad Re_g = \frac{\rho_l D_c U_g}{\mu_l} \, , \; Pr_l = \frac{\mu_l C_{pl}}{k_l} \, , \text{ and } \; Fr_g = \frac{{U_g}^2}{g D_c} \, .$$

Korte, 1987 in his studies also used a microturbine velocimeter to determine the liquid velocity through the columns. However in this work, generally heat transfer coefficients were measured on the basis of the measurement of energy input using a slow-response assembly probe (Saxena and Chen, 1994). Wu and Al-Dahhan, 2011; Wu et al., 2007; Wu, 2007 and Abdulmohsin and Al-Dahhan, 2012 claimed that in this methodology, error in the calculation of heat flux based on the energy input is inevitable because the heat losses in heating up all the surrounding materials, including the connecting fittings and/or column wall, were also counted into the heat transferred from the heat source to the bulk flow. Furthermore, detailed hydrodynamics studies were not

conducted in order to elucidate the dependence of heat transfer rate on the bubble properties.

Saxena, 1989, Saxena et al., 1989, 1990, and 1991 did numerous heat transfer studies in two phase-flows and three-phase flow systems equipped with mimicked heat exchanging internals with in-built heaters. The main parameters in their studies included column diameter, particle sizes and fines, solids concentration, the superficial gas velocity, bed temperature and the number and configuration of the internals. Saxena, 1989, using 0.108 m diameter column and glass beads as solids reported that the gas holdup decreased with solids loading at higher superficial gas velocities while the heat transfer coefficient initially increased rapidly with increasing U_g and then reached an asymptotic value. They also reported that heat transfer coefficient was consistently higher with solids loading, and with decreased liquid and pseudo-slurry viscosity. However, when they used different sizes of glass beads (50, 119, 143 μm) at concentrations of 0 and 10 wt. %, with the gas and liquid phases consisting of air and water, they reported that the gas hold-up and heat transfer coefficient were both independent of the particle diameter and solids concentration.

Westermeyer, 1992 studied heat transfer in bubble columns. Their studies were an extension of the work done by Korte, 1987 where they introduced the solids in the same systems. They also used a conductivity probe to measure the radial solids phase hold-up. They concluded that the heat transfer coefficient increased with decreasing liquid viscosity but independent of column diameter. The experimental data of their results were correlated by the following equation;

$$St = 0.115\left(\left(Re_g Fr_g {Pr_l}^2\right)^{-\frac{1}{3}}\right)\left[{Re_g}^{1/36} Fr_g {We_g}^{5/48}\right]{A_f}^{-1/6} \tag{2.2}$$

where $We_g = \frac{\rho_l D_c {U_g}^2}{\sigma_l}$ and the rest of the dimensionless numbers defined the same way as Korte, 1987.

Yang et al., 2000, conducted heat transfer studies in slurry bubble columns at elevated pressures up to 4.2 MPa and temperatures up to 81 ^{0}C using nitrogen as the gas phase, Paratherm NF heat-transfer fluid as the liquid phase, and 53 μm glass beads as the solids. The solids concentrations were varied up to 35 vol %, while the superficial gas velocities up to 20 cm/s was used. They examined the effect of gas velocity, solids concentration, pressure and temperature on the heat transfer coefficient. They noted that the variation of heat transfer coefficient with pressure and temperature was due to the counteracting effects of the liquid and pseudo-slurry viscosity, bubble sizes, and gas holdup. They reported an increase in heat-transfer coefficient in slurry bubble column with temperature and solids loading and appreciable decrease with an increase in pressure. Even-though in this work the bubble sizes were not measured, the decrease in heat-transfer coefficient with pressure was attributed to the decreased bubble sizes, increased liquid viscosity, and increased gas holdup as the pressure increases.

Yang et al., 2000 also used a consecutive film and surface renewal model that will be discussed later in chapter 5 to analyze their heat-transfer results. On the basis of the model they claimed that the main resistance to heat-transfer in high pressure slurry bubble columns lies within a fluid film surrounding the heating surface. However, they assumed that the liquid elements move at the same velocity as the bubbles around the heat transfer resistance film and thus the contact time between the liquid elements and the film is equal to the contact time between the bubbles and the film, when the bubble motion is considered as the driving force of the liquid elements. In their study, the contact

time between the liquid elements and heat transfer resistance film was estimated from; $t_c = \frac{L}{U_b}$ where t_c is the contact time, L is the vertical length of the heat flux sensor, and U_b is the bubble rise velocity. Figure 2.7 illustrates the variation of the estimated contact time with bubble rise velocity according to Yang et al., 2000. Their study also did not elucidate the effect of radial location. It should be noted that the bubble velocity in bubble or slurry bubble columns are both axial (upward and downward) and radial and bubble-turbulence induced heat transfer only depends on the bubble passage and not direction. Using the bubble rise velocity as the only determinant of the contact time is likely to overestimate the heat transfer coefficient.

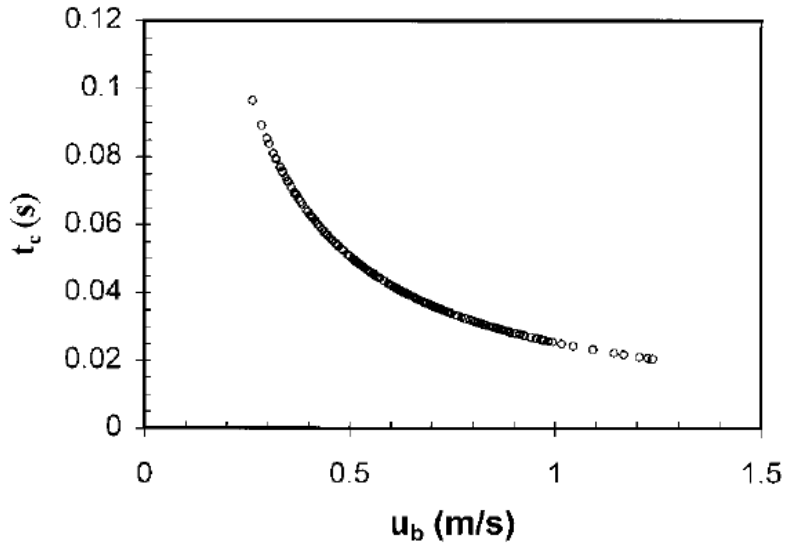

Figure 2.7 Contact time between liquid elements and the film under various operating conditions (from Yang et al., 2000)

Kumar et al., 1992 and Kumar and Fan, 1994 studied the effect of bubbles and their sizes on the instantaneous heat-transfer rate in gas-liquid and gas-liquid-solid

systems. They reported that when a single bubble is injected into liquid or liquid-solid systems the heat-transfer rate through the bubble wake is enhanced. Figure 2.8 illustrates the system set-up used and the effect of bubble sizes on the instantaneous heat transfer coefficient due to the passage of bubble in a liquid for probe located at the column center. They found that the wake is proportional to bubble size and maximum heat transfer occurs in the wake region a short distance behind the bubble in the upward flow. The observed heat transfer enhancement was thus attributed to the bubble wake created by the bubble(s) passing over the heat transfer surface. Larger bubbles would have larger wakes and stronger vortices associated with the wake, thereby enhancing the rate of heat transfer. The strong vortices and turbulence in the bubble wake region increase the heat-transfer surface renewal rate. They demonstrated that the heat transfer rate is proportional to the bubble sizes. These studies did not elucidate the effect of larger bubble population as they were limited to single bubbles or a chain of bubbles. They also did not cover the range of gas velocities suitable for most commercial applications. Moreover the measurements were limited to column center and thus no local variations in the heat transfer rates were reported. However, at any superficial gas velocity, a large population of bubbles is evolved with a range of velocities (Xue, 2004; Youssef and Al-Dahhan, 2009), which is the case in a real system of commercial interest.

Li and Prakash, 1997 studied the instantaneous and time-averaged heat transfer coefficients as well as averaged gas holdups in a 0.28 m diameter slurry bubble column for air-water and air-water-glass beads (35 μm) system. The influence of high superficial gas velocities (up to 0.35 m/s) and high solids concentrations (up to 40 vol %) were investigated. A decrease in gas holdup with increasing slurry concentrations was reported

(a)

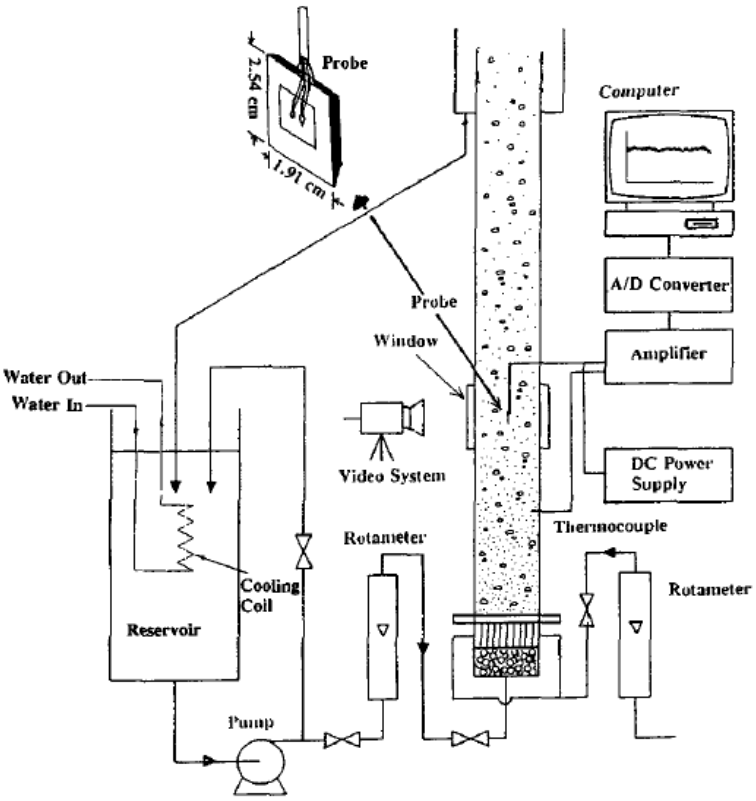

(b)

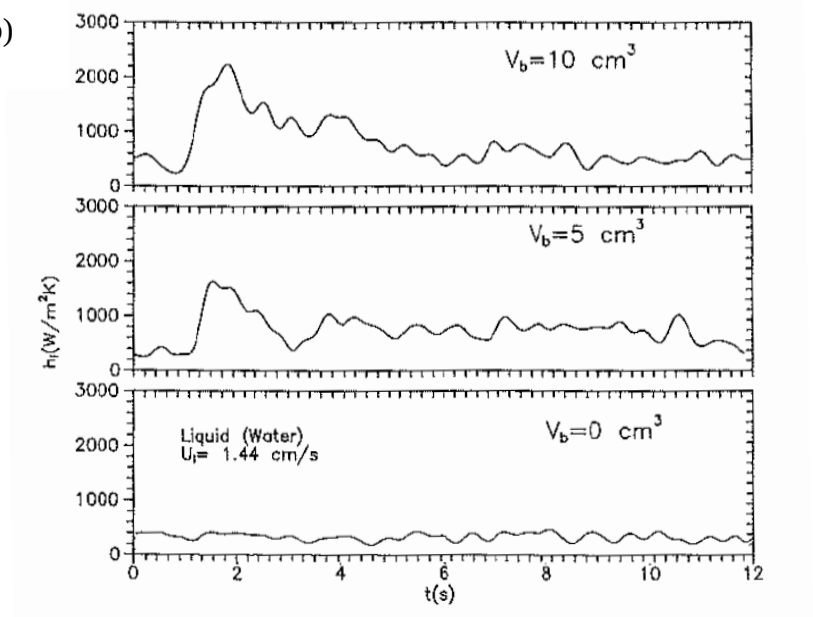

Figure 2.8 Bubble wake enhanced heat transfer coefficient (a) Experimental system and (b) Effect of bubble size on instantaneous heat transfer coefficient due to the passage of bubble in liquid for probe located at center, r/R (-) = 0.0 (from Kumar and Fan, 1994).

and a rapid rate of decline at high superficial gas velocities. The instantaneous local heat transfer measurements were analyzed to study the bubble behavior in the regions near the wall and at the center for different solids concentrations. They reported larger bubbles in the column wall region in three phase system as compared to the solid-free system. The average heat transfer coefficient decreased with increasing slurry concentrations, contrary to what Yang et al., 2000, observed with the same type of solids but different gas and liquid phases. The heat transfer coefficient was always lower at the wall than at the center.

Kolbel et al., 1958 reported the first correlation to predict the heat transfer in bubble columns. Their studies were conducted in 9.2 cm and 29.2 cm bubble columns with superficial gas velocity varied from 1 – 10 cm/s. They measured the heat transfer from a wall in bubble column based on certain thermal output generated by a heating cartridge in a metal cylinder. They supposed that the heat transfer enhancement produced by the gas bubble in bubble columns was related to the removal of stagnant liquid portions (boundary layer) from the heat transfer surface. They attributed the heat transfer resistance to wall boundary layer. They argued that the boundary layer decreases and becomes independent of gas velocity at very low gas velocities and are not broken up. This claim however seem to be contrary to others. Where, the boundary layer grows with reduction in gas velocity and or liquid velocity, but instead diminishes with increase in gas velocity to become nearly independent with further increase. Based on their experimental data they proposed the following correlations:

$$Nu_{(d_t)} = 43.7Re^{0.22} \; for \;\; Re > 150 \tag{2.3}$$

$$Nu_{(d_t)} = 22.4Re^{0.36} \;\; \text{for} \;\; Re < 150 \tag{2.4}$$

Where d_t is the tube diameter, $Re = \frac{\rho_l V_g d_t}{\mu_l}$ is the gas Reynolds number, $Nu_{(d_t)} = \frac{h d_t}{k_l}$ is the Nusselt number based on tube diameter, d_t, with the heat transfer coefficient, h, liquid thermal conductivity, k_l, the superficial gas velocity, V_g, and liquid viscosity, μ_l. Whereas the correlation accounts for the liquid system properties, the gas velocity used is not beneficial to processes which require high volumetric productivity such as the Fischer-Tropsch synthesis. The effect of solids and or heat exchanging internals was also not examined. Besides, the mode of heat transfer measurement was based on the thermal output. This method is prone to large errors since even the heat used in heating up the column walls and fittings are assumed to be transferred to the medium, as explained earlier on.

Kast, 1962 indicated that the concept of heat transfer through the boundary layer plays negligible or no role in the bubble agitated systems such as bubble columns. By analyzing the fluid motion around a bubble in the upward flow Kast, 1962 proposed the first semi-theoretical correlation to estimate the heat transfer coefficient in bubble columns.

$$St = f(Re^a Fr^b Pr^c)^m \tag{2.5}$$

They proposed the constant values as, f = 0.1, a = 1, b = 1, c = 2 and m= -0.22. Many researchers (KoIbel et al., 1964; Burkel, 1972; Shaykhutdinov et al., 1971; Hart, 1976; Steiff and Weinspach, 1978) have modified the values of the constants to fit their experimental data. In this analysis, a fluid element in the front of a rising bubble receives radial momentum and thus moves towards the heating surface. This lateral transport of mass resulting from axial motion of the bubble weakens and breaks up, the boundary layer (thin film lying parallel to and covering the heat transfer surface) at the wall

surface. Whereas from Kast's point of view this indicates that the boundary layer heat transfer enhancement is negligible, it should be construed that the phenomena of bubble-wake induced heat transfer enhancement due to surface renewal rate plays crucial role in the heat transfer in bubble columns as will be illustrated in Section 5.

Deckwer, 1980 by applying the surface renewal theory (Higbie, 1935) of interphase mass transfer and Kolmogoroff's theory of isotropic turbulence improved the theoretical interpretation of the heat transfer model proposed by Kast, 1962 and obtained the values of the constants of Kast's correlation as f = 1, a = 1, b = 1, c = 2, m = -0.25. This correlation was extended to gas-liquid-fine solid systems (slurry bubble columns) by Deckwer et al., 1980. Using the surface renewal model analysis, Deckwer, 1980 argued that the occurrence of fast radial exchange flow rates can be regarded as lateral eddy diffusivity with radial mass dispersion. Thus owing to the radial eddy diffusivity, there does not exist boundary layer at the wall at all, instead it is reasonable that in the vicinity of wall surface there is irregular back and forth but steady flow of fluid eddies from the bulk to the wall. According to this analysis, the fluid element stays in contact with the heat transfer surface then leaves to enter the bulk medium. Hence, applying the surface renewal theory of interface mass transfer Higbie, 1935 and a 1-D unsteady state heat conduction equation,

$$\frac{\partial T}{\partial t} = \alpha \frac{\partial^2 T}{\partial T^2} \tag{2.6}$$

With the boundary/initial conditions;

$$T = T_w \qquad x = 0 \qquad t \geq 0$$

$$T = T_B \qquad x > 0 \qquad t = 0$$

$$T = T_B \qquad x = \infty \qquad t > 0$$

The average heat transfer coefficient during the contact time θ between the fluid eddy and the heat transfer surface can be calculated as follows;

$$h = 2\sqrt{\left(\frac{\alpha}{\pi\theta}\right)\rho c_p} \tag{2.7}$$

with the contact time estimated as $\theta = \frac{d_B \in_G}{U_G}$

This model (Kast's, 1962) suggests that there is no stagnant film on the heat transfer surface hence no resistance due to the boundary layer thickness. The contact time estimation approach may contain large errors since the estimation of the bubble diameter is not easy. In fact at higher superficial gas velocity encountered in the churn turbulent flow regime that is of great commercial interest, the bubbles have no definite geometric shape making estimating their diameter extremely difficult.

Wu, 2007 and Wu and Al-Dahhan, 2011 demonstrated in a 0.16 m ID bubble column the variation of heat transfer coefficient with superficial gas velocity up to 30 cm/s, pressure up to 10 bar and solids loading up to 25 % by volume. They observed that the heat transfer coefficient increases with superficial gas velocity, but the rate of increase slows significantly at high range of superficial gas velocity. At the same gas flow rate they noted an increase of heat transfer coefficient with solids loading and a reversed trend with pressure. Based on a wide data bank of heat transfer coefficient spanning over 30 years, they proposed an artificial neural network (ANN) based correlation for predicting the heat transfer rate. They also proposed the following power law correlation based on their experimental data.

$$St = 0.0323 Dr^{0.3915} Pr^{-0.1276} We^{0.285} D^{-0.711} \tag{2.8}$$

With dimensionless groups as;

$$Dr = \frac{\rho_g}{\rho_{sl}}, D = \frac{{U_g}^2 \rho_g}{g\sigma}, We = \frac{d{U_g}^2 \rho_g}{\sigma}, \text{Pr} = \frac{Cp_{sl}\mu_{sl}}{K_{sl}}$$

Generally, the centerline heat transfer coefficient values were higher than at the wall with the radial profiles being flatter at increased pressure. They also mimicked the heat exchanging internals by using inbuilt cartridge heaters on the internal in order to assess the effect of internals on the heat transfer coefficient. The internals used in this work covered very low cross-sectional area (5 % CSA). The presence of internals led to slight increase in the heat transfer coefficient and this was attributed to the changes in bubble dynamics and hydrodynamics owing to altered flow field. They strongly recommended further studies of heat transfer, bubble dynamics and hydrodynamics in slurry bubble columns equipped with dense internals for better understanding of commercial operations with heat exchanging internals. Though both the heat transfer studies as well as detailed bubble dynamics studies were conducted, the heat transfer measurements were done at separate times from the bubble dynamics measurements hence the direct link between the bubble dynamics could not be elucidated. It should also be noted that the observed effect of internals could be misleading since higher gas mass rate was employed with the internals. The need to use superficial gas velocity based on open cross-sectional area for the flow is essential in order to assert the reported internals effect. Furthermore, detailed studies of effect of dense internals on the bubble dynamics (Youssef and Al-Dahhan, 2009 and Youssef, 2010) have shown that internals with low CSA coverage have no significant effect on the bubble dynamics, hence the need for more studies with dense internals.

Abdulmohsin and Al-Dahhan, 2012 recently reported the effect of heat exchanging internals on the heat-transfer coefficient from a 0.19 m diameter bubble column for an air−water system with superficial gas velocities varying from 3 to 20 cm/s using a fast response heat-transfer probe. In their study, they examined the effect of

internals occupying 0 % (empty column), 5 % (simulating methanol synthesis), and 22 % (simulating Fischer−Tropsch synthesis) of the column cross-sectional area. Their results indicate that the presence of a high percentage of internals causes an increase in the heat-transfer coefficient at the same gas velocity that is based on free cross-sectional area for flow. Figure 2.9 (Abdulmohsin and Al-Dahhan, 2012) illustrates the effect of internals and gas velocity on the heat transfer coefficient. The method of determining the

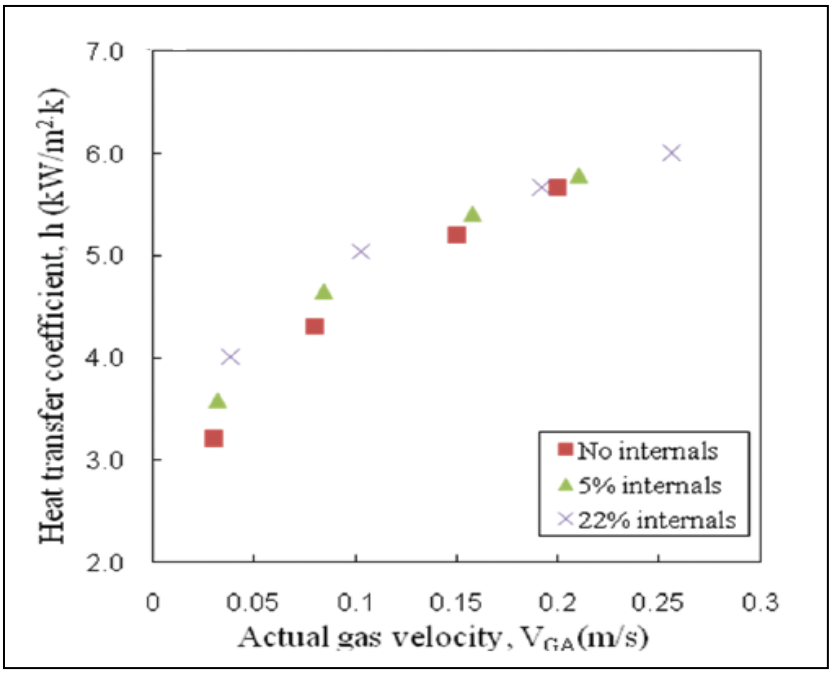

Figure 2.9 Effect of internals and actual gas velocity on the heat-transfer coefficients at the column center (from Abdulmohsin and Al-Dahhan, 2012)

superficial gas velocity when the internals was used does not allow for proper comparison since the same mass flow rate was employed as for empty column, then back-calculated for the corresponding Ug with internals. This work was also limited to two phase-systems and effect of scale was also not examined. In order to assess the

dependence of heat transfer coefficient on bubble dynamics, there is still need to carry out measurements simultaneously of both the heat transfer coefficient and bubble properties at the same time and same location while utilizing the gas flow rate that is based on the free area for flow only.

Most recently, Jhawar and Prakash, 2012 and Jhawar, 2011 studied local heat transfer and column hydrodynamics in a 0.15 m ID bubble column with and without solids in the presence of internals of different configurations and superficial gas velocity covering homogenous, transition, and churn turbulent flow regimes. Local heat transfer variations were measured with a fast response probe capable of capturing bubble dynamics as well as detecting local flow direction. Glass beads averaging 49 μm in size was used as the solids with loading varied up to 20 % by volume. Different configurations of internals were used occupying 6 % of the cross-sectional area of the column and water as the liquid phase. They observed a decrease in the heat transfer coefficient with increase in the slurry concentration. Figure 2.10 shows the variation of heat transfer coefficient at the center of bubble column without internals measured by Jhawar, 2011. They also demonstrated that the internals configuration had significant effect on the steepness of the radial profiles of both the liquid velocity and heat transfer coefficient. With the tube bundle type of configuration the heat transfer coefficient had steeper radial profiles and the rate of decrease in the heat transfer coefficient with slurry was affected by internals configuration. From this work, the hydrodynamics studies were limited to liquid velocity and overall gas holdup thus, many other bubble properties including bubble velocity, frequency, sizes, and the local gas holdup radial profiles which

control the column hydrodynamics and consequently their effect on the heat transfer coefficient were not investigated or reported.

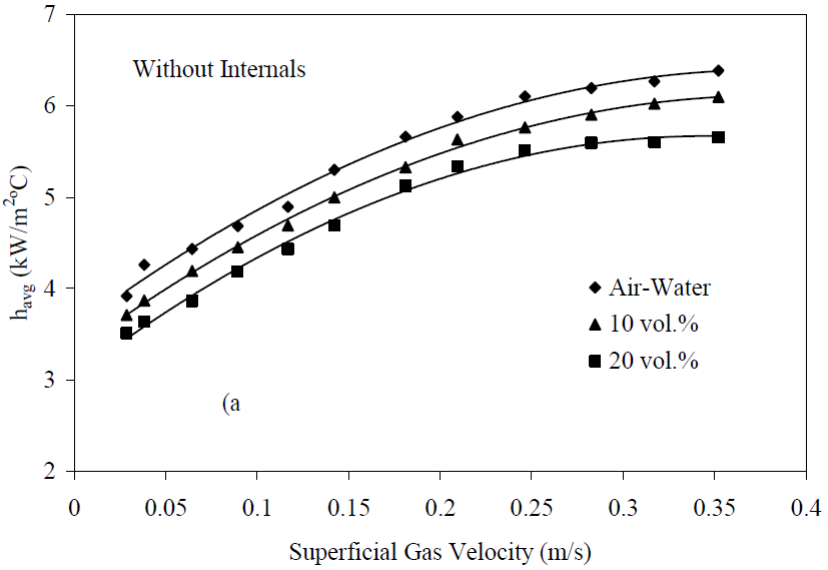

Figure 2.10 Effect of solids loading and gas velocity on the heat-transfer coefficients at the column center (from Jhawar, 2011)

2.3. EFFECT OF SCALE IN BUBBLE AND SLURRY BUBBLE COLUMNS

The prevailing market oil prices determines the profitability of FT synthesis process, while to be economically viable and independent of market oil prices, capital expenditure (CAPEX) of such process needs to be equal to or below $20 000 Barrels/day of installment cost (Shaikh and Al-Dahhan, 2010). The scale-up of slurry bubble column reactor for Fischer-Tropsch synthesis can only be achieved with successful and proper description of hydrodynamics and transports phenomena as a function of reactor scale. A comprehensive approach, which consists of improved catalyst selectivity and efficiency in FT synthesis and economies of scale in larger reactor sizes, is needed to achieve this

goal. The economies of scale demands reduced risk in scale up to build large diameter reactors, which in turn necessitates reliable similarity criteria. A vast majority of studies in bubble and slurry bubble columns have been done on small diameter columns and only a few have been done in bubble columns of diameter greater than 0.308 m and even much fewer on effect of scale. Of the studies conducted on the effect of scale and column diameter only those which are pertinent to this work are examined in this section.

Wilkinson et al., 1992 carried out experiments in two sizes of bubble columns for a number of liquids at pressures between 0.1 and 2.0 MPa. Using their experimental results as well as extensive literature data, the extent of the effect of column dimensions on gas holdup were determined, both at low and high pressures (which is of importance to scale-up). They also claimed that none of the published empirical gas holdup correlations incorporates accurately the influence of gas density. Therefore, a new improved gas hold-up equation was developed that incorporates the influence of gas and liquid properties with an average error of approximately 10 %. It also discussed the extent of the influence of pressure on other important design parameters such as the interfacial area, the liquid volumetric mass transfer coefficient, and gas and liquid mixing. According to this study, the gas holdup was found to be nearly independent of the column dimensions and the sparger layout (for low as well as high pressures) provided that: (1) the column diameter is larger than 15 cm; (2) the column height to diameter ratio is in excess of 5; and (3) the hole diameter of the sparger is larger than 1–2 mm.

Degaleesan, 1997 addressed scale-up issues from the experimental data of fluid dynamics obtained using computer automated radioactive particle tracking (CARPT) in

bubble columns of 14 cm, 19 cm and 44 cm diameter operated in the churn-turbulent flow regime. Based on her experimental data and literature information, she developed correlations for predicting the mean liquid recirculation velocity and average eddy diffusivities in air-water atmospheric systems. Degaleesan, 1997 also using a unified characterization of churn-turbulent bubble columns, proposed a scale up methodology that enables the estimation of the mean liquid recirculation velocity and average eddy diffusivities in bubble columns operated in the churn-turbulent flow regime, higher pressure and temperature all which are of industrial importance, using data generated from the air-water systems. She claimed that any gas–liquid/slurry would exhibit the similar hydrodynamic behavior as air–water system if both the systems have the same overall gas holdup. It was suggested that hydrodynamics and mixing at the equivalent superficial gas velocity, in an atmospheric air–water system that results in the same overall gas holdups would represent the hydrodynamics and mixing in scaled up hot unit

The equations and scale up methodology of churn-turbulent bubble columns which she proposed require the knowledge of and substantial experimental data for additional bubble properties including the bubble velocity, bubble frequency and bubble sizes among other parameters.

Inga and Morsi, 1997 working on a similar experimental unit as Behkish, 2004 extrapolated the results of laboratory scale stirred tank reactor to design industrial scale slurry bubble column based on similarity of the relative importance of mass transfer resistance in the overall reaction resistances, defined in terms of a dimensionless parameter, β_i which represents the balance between the mass transfer coefficient and rate of consumption, pseudo kinetic constant for first order. Accordingly, maintaining the

same β in two reactors will result in the same reactant concentration and catalyst activity and thereby the conversion and selectivity in two reactors.

Fan et al., 1999 carried out experiments in a high-pressure high-temperature system of 2- inch and 4- in diameter columns. Using a vast range of data collected from both the literature and their own experimental data over a wide range of flow conditions, they proposed an empirical correlation which predicts the overall gas holdup in slurry bubble columns of different scales in terms of the following three dimensionless numbers; slurry Morton number, (Mo_{sl});

$Mo_{sl} = g(\rho_{sl} - \rho_g)\mu_{sl}^4/\rho_{sl}^2\sigma^3$, ρ_g/ρ_{sl}, $U_g^4\rho_g/(\sigma g)$. They suggested that maintaining these dimensionless groups the same in two systems would lead to similar overall gas holdup and hence mixing and hydrodynamics. This approach is similar to Degaleesan, 1997. They also employed a similarity rule which is revealed for the overall hydrodynamics of high-pressure slurry bubble columns, which takes into account the operating conditions (such as high pressure), the maximum stable bubble size, and the physical properties of the gas, liquid, and solids. The heat transfer characteristics under high pressures were also investigated and a consecutive film and surface renewal model used to characterize the heat transfer mechanism. It should be noted from this work that the experimental work done were limited to very small columns thus extension of the findings to larger columns of industrial interest cannot be confidently achieved.

Safoniuk et al., 1999 and Macchi et al., 2001, employed dynamic similitude approach in which ratios of all forces acting on corresponding fluid particles and boundary surfaces in the two systems are constant. In this mechanism, they presented a scale-up method for three phase fluidized beds with the aid of the Buckingham pi

theorem, which yielded five dimensionless numbers that have a significant effect on overall gas holdup. These dimensionless groups are Morton number, $Mo = g(\rho_l - \rho_g)\mu_l{}^4/\rho_l{}^2\sigma^3$ Etovos number, $Eo = g(\rho_l - \rho_g){d_p}^2/\sigma$, Reynolds number, $Re = \rho_l d_p U_l/\mu_l$; Density ratio ρ_p/ρ_l; and Superficial gas and liquid velocity ratio, U_g/U_l. Later, Macchi et al., 2001 tested the scaling approach of Safoniuk et al., 1999 in three phase fluidized beds where aqueous solution of glycerol (a liquid mixture) was used as the liquid phase in one column and silicone oil (a pure liquid) in the other. It was observed that, whenever five dimensionless numbers were the same in these systems, the overall gas holdups were within 11 % of root mean standard deviations. Macchi et al., 2000 concluded that matching these five dimensionless numbers is inadequate to ensure hydrodynamic similarity

Van Baten et al., 2003 developed a scale-up procedure that relies on the use of computational fluid dynamics (CFD), with Eulerian descriptions of the gas and slurry phases. Interactions between the bubbles and the slurry were taken into account by means of a momentum exchange, or drag, coefficient; this coefficient is estimated from the experimental measurements of gas holdup in a column of 0.051m diameter. They proposed a modified strategy for the use of CFD approach to scale up bubble column reactors. The drag coefficient and bubble diameter were calculated utilizing only overall gas holdup data in small diameter column (5.1 cm). The CFD model was first validated by comparison with the measured overall gas holdup data for a range of superficial gas velocities. Figure 2.11 illustrates a comparison for different column diameters, the radial distribution of the liquid and gas (bubble) velocities. However, the validation of CFD simulation results with experiments in large diameter columns was not established.

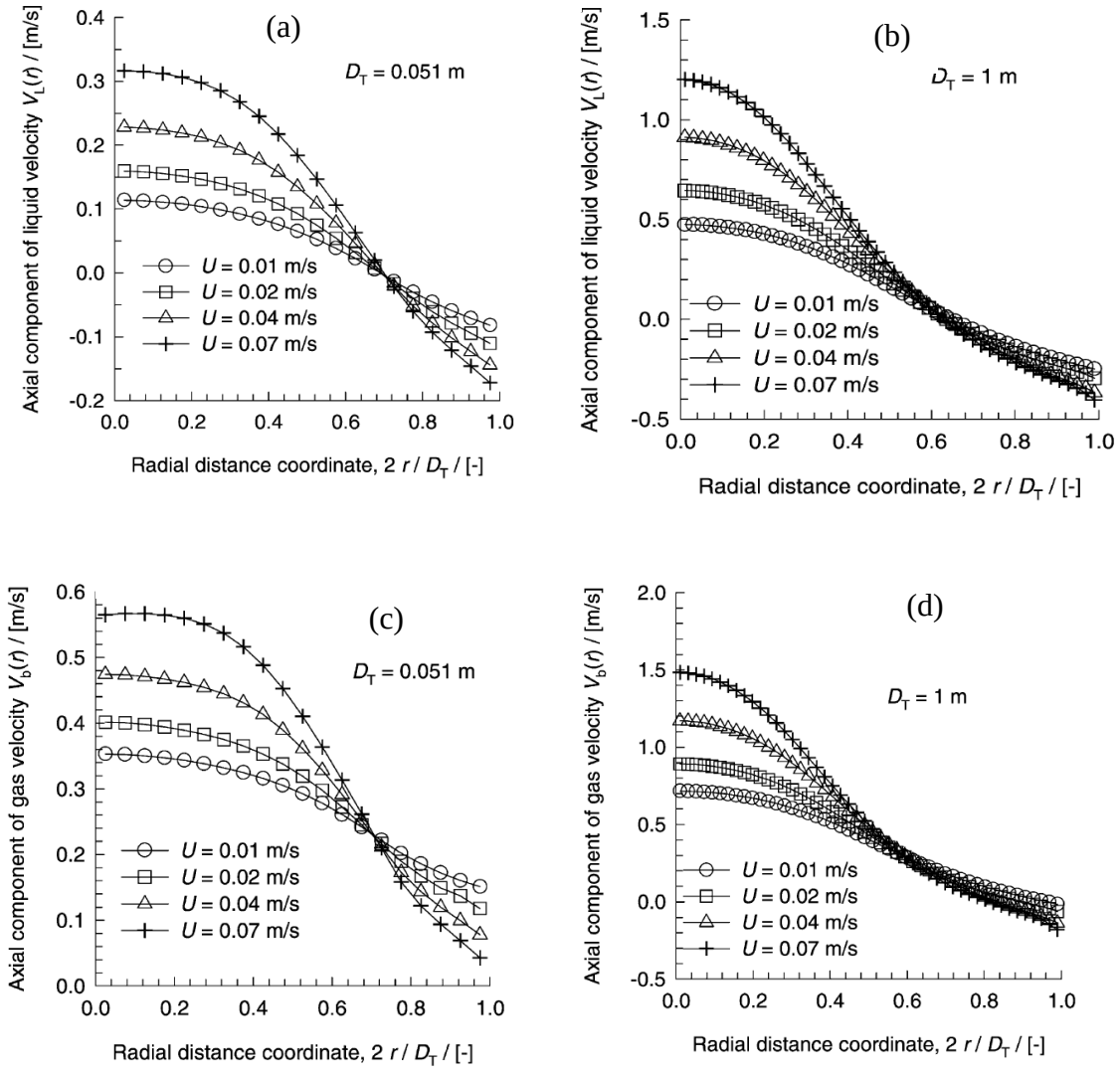

Figure 2.11 Radial profiles of (a) liquid velocity in 0.051 diameter column (b) liquid velocity in 1 m (c) gas velocity in 0.051 m diameter column and (d) gas velocity in 1 m diameter column (from Van Baten et al., 2003)

Zhang and Zhao, 2006 presented a scale up methodology that takes care of hydrodynamics in cold flow units, catalyst performance evaluation in an autoclave, and process investigation in a pilot-scaled circulating slurry bubble column reactor. Their experiments were conducted in columns ranging from 4.2 cm – 10 cm in diameters. A new suite of tools for developing low-temperature methanol synthesis in circulating

slurry bubble reactors was explored in their study. They proposed a strategy that tied flow behavior and catalysis studies with that of process engineering which involved studying hydrodynamics in cold flow units, catalyst performance evaluation in an autoclave, and process investigation in pilot-scale continuous slurry bubble column reactor. It should be noted that while their studies included cold mockups and hot units they did not provide any guidelines regarding hydrodynamic similarity in cold and hot unit nor any results with successful scale-up were shown. Besides the column sizes used were relatively smaller than desired in commercial FT systems and variation in the presence of dense internals is still missing.

Forret et al., 2006 using 0.15 m, 0.40 m and 1 m diameter bubble columns presented the effects of scale and the presence of internals on hydrodynamic characteristics, for scale-up purposes based on experiments in cold mockups. They worked out a scale-up methodology based on phenomenological models that require the knowledge of overall gas holdup, center-line liquid velocity, and axial dispersion. Two methods were proposed to predict scale effect on liquid velocity: an empirical correlation proposed in the literature and a phenomenological model. They reconfirmed that the overall gas holdup is independent of the column's diameter for columns larger than 15 cm in diameter (Figure 2.12). They obtained the liquid phase velocity profile using a) an empirical correlation for the center-line liquid velocity as a function of gas velocity and column diameter, and b) the simplified one-dimensional two-fluid model accompanied by adjustment of the turbulent viscosity as a function of column diameter and gas velocity.

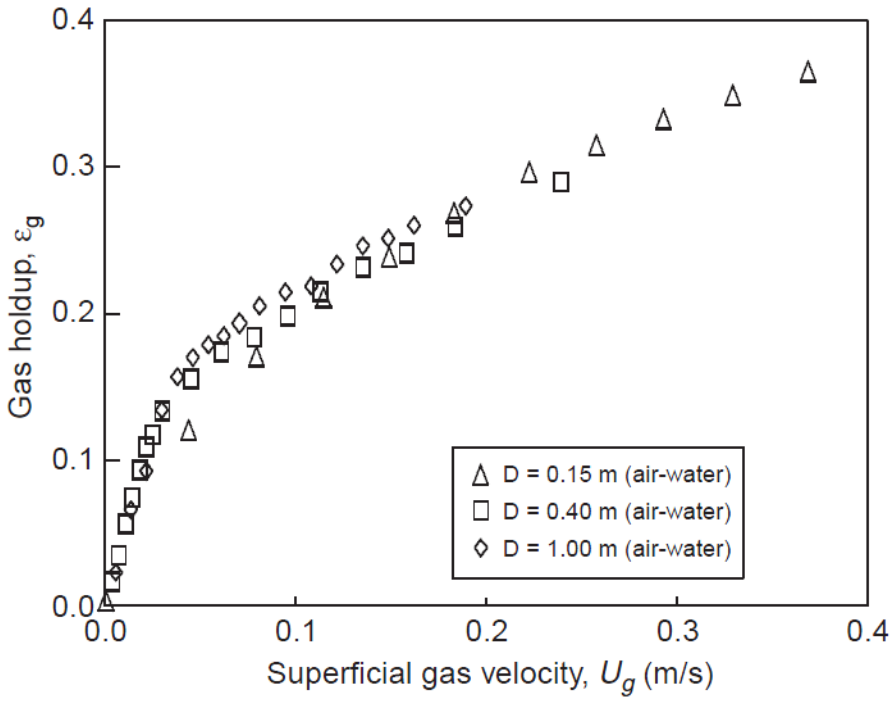

Figure 2.12 Overall gas holdup as a function of column diameter and superficial gas velocity (from Forret et al., 2006)

Further they proposed a two-dimensional (2D) model to estimate the dispersion coefficient in large columns, taking into account both the axial dispersion and the radial dispersion. Whereas their study also included some data in columns equipped with internals, the cross-sectional area occupied by the internals remained low and the effect of solids especially the high solids loading on the measured parameters were not evaluated.

Recently, Shaikh and Al-Dahhan, 2010 proposed a hypothesis for hydrodynamic similarity that can be subsequently used for scale-up of bubble column reactors. Their findings were mainly supported by experimental work carried out in a 0.162 m diameter column using water and a mixture of C_9–C_{11} to account for the effect of varying liquid physical properties by gamma-ray computed tomography (CT) and computer automated

radioactive particle tracking (CARPT) techniques. They proposed a hypothesis that takes into account both global (by matching overall gas holdup) as well as local hydrodynamics (by matching time-averaged radial profile/cross-sectional distribution of gas holdup) to maintain similarity in two systems. They also demonstrated that similarity based only on global hydrodynamics does not necessarily ensure similar mixing and turbulence in two systems. They claimed that the hydrodynamic similarity can be obtained by matching the commonly used dimensionless groups as were also evaluated at the experimental conditions. They recommended that such evaluation of the demonstrated methodology be further extended to study its utility in different column diameters. The validity of such methodology in bubble columns equipped with dense internals is yet to be checked.

The most recent work on scale effect in bubble columns was done by Youssef, 2010. They proposed a scaling methodology based on the reactor compartmentalization approach by using the heat exchanging tubes to create column wall of 6-inch diameter and compared the findings with those of solid column wall of same diameter, conducted by Xue, 2004 and found close match. The proposed reactor compartmentalization methodology, which has various issues and uncertainties (Youssef, 2010), still needs to be evaluated and validated in systems of at least two different physico-chemical properties and solids for reliability of the scaling method.

The studies captured above on scale-up have at least one of the following drawbacks: (1) Examined global parameters only and mainly the overall gas holdup; (2) Mostly applicable to the homogenous flow regime; (3) Did not account for the presence of dense internals and solids; (4) they are based on dynamic similarity but with no actual

scaling validation; (5) they are missing experimental validation in large scale units particularly the CFD simulations studies; (6) limited to hydrodynamics studies.

2.4. SUMMARY

As noted from the foregoing review, the role of bubble dynamics on the heat transfer coefficient in bubble and slurry bubble columns is undisputed. The following observations and conclusions can be made on the state of knowledge on the relevant heat transfer and bubble dynamics studies in bubble and slurry bubble columns.

Bubble dynamics and heat transfer coefficient have been studied separately under different operating conditions, thus the need for simultaneous measurements and evaluation of heat transfer and bubble dynamics at the same time.

Most of the studies in the literature on the effects of operating and design variables on the hydrodynamic and transport parameters have been performed in empty bubble and slurry bubble columns. Hence the need to study the hydrodynamics and transport parameters, such as heat and mass in columns inserted with mimicked dense heat exchanging internals.

Most of the previous studies reported time-averaged heat transfer coefficients obtained with slow response probes, which are unable to detect instantaneous variations in the heat transfer rate, besides the heat transfer coefficients were measured on the basis of the energy input (Saxena and Chen, 1994). In this approach the results were prone to large errors since the energy used in heating up the column walls, column base and fittings are counted as part of the heat transferred to the flowing liquid/fluid medium. Hence adopting heat transfer measurement that is based on the measurement of the direct

heat flux using fast-response probe (Prakash et al., 1997; Wu et al., 2007) could be more appropriate.

In bubble columns equipped with internals, effect of internals was evaluated based on same gas volumetric flow rate as empty column, hence the observed and reported effects could be attributed to more kinetic energy introduced in to the system by high mass of the gas that creates greater turbulence in the system. Hence the need to use same mass gas flow rate evaluated on free cross-sectional area open for the flow only.

No heat transfer and bubble dynamics studies have been reported in the literature for measurements conducted at the same time in bubble columns and slurry bubble columns equipped with dense (25 % CSA) internals that mimic the 3-phase FT synthesis operation system.

Whereas the diameter of internals play crucial role in bubble columns and slurry bubble columns, the diameter effect of internals occupying the same CSA remains largely uninvestigated in the reported bubble dynamics studies or heat transfer studies.

To the best of our knowledge, no study in the literature has examined through simultaneous measurements the dependence of heat transfer coefficient on bubble dynamics and at the same time in bubble and slurry bubble columns with or without mimicked dense heat exchanging internals together with their radial distributions. Thus, this forms the backbone of the current study as indicated in Section 1.2. Hence, this study is focused on the effect of solids loading and dense internals on the heat transfer rate and bubble dynamics in bubble columns of 6-inch and 18-inch diameter.

3. EFFECT OF DENSE HEAT EXCHANGING INTERNALS ON BUBBLE DYNAMICS IN BUBBLE AND SLURRY BUBBLE COLUMNS

The installation of internals is the most suitable way of removing excess heat generated by exothermic process reactions such the FT synthesis and LPMeOH synthesis since they (internals) provide both reasonable ratio of reaction volume to heat transfer area and they preclude the need for either an external heat exchanger or large and expensive slurry pumps (Carleton, 1967, Balamurugan and Subbaro, 2006). In Section 2 it was demonstrated that no single study has been reported in the literature on bubble dynamics in bubble columns or slurry bubble columns equipped with dense internals of different diameters, covering the same cross-sectional area. The effect of solids loading in the presence of dense internals is yet to be reported too. The current section of this study seeks to address this missing knowledge to provide a benchmarking database for future studies in this direction and in view of modeling and scaling of systems with dense internals. As described in Section 3.1.1, four point optical probe is utilized for the measuring of the bubble dynamics and the local gas holdup, while the overall gas holdup is visually estimated from the method of bed expansion.

3.1. MEASUREMENTS TECHNIQUE

In this work combined measurements technique has been used to measure simultaneously the heat transfer coefficient and bubble dynamics. The combined measurements have been achieved by using a hybrid probe which conceptually consists of two independently fabricated probes, namely the advanced four-point fiber optical probe and a fast response heat transfer probe. The advanced four-points fiber optical

probe was used to measure the bubble properties which include local gas hold up, bubble passage frequency, axial bubble velocity (upward and downward), specific interfacial area, as well as the bubble chord lengths which is characteristic of bubble sizes. The fast response heat transfer probe was used to measure the heat flux from which the heat transfer coefficient can be estimated. The details of the fast response heat transfer probe will be highlighted later in Section 4 and the heat transfer measurement procedures detailed in Appendix B. Therefore, in this section only the details of four-point optical probe is discussed

3.1.1. Four-Point Fiber Optical Probe. The four-point optical probe has been successfully used in gas-liquid and gas-liquid- solid systems (Xue, 2004; Xue et al., 2008; Wu, 2007; Youssef and Al-Dahhan, 2009 and, Youssef, 2010). It is an excellent tool to use in systems including those with internals, solids and fines. As mentioned above, it can provide insight into the bubble characteristics (local gas holdup, bubble chord length, specific interfacial area, bubble frequency, bubble velocity (both radial and axial) among other properties, adjacent to the axial cooling tubes frequently used in industrial applications. It can provide local information on the effect of solids loading on bubble properties as well. Though originally developed and successfully implemented in gas-liquid systems, it was observed during the data acquisition in the current study that far high signal to noise ratio was achieved with solids loading than in gas-liquid systems only.

The four points optical probe used in the current study is an advanced version of the one originally developed and employed by Frijlink, 1987 at Kramers laboratory in the Department of Multiscale Physics at the Technical University of Delft in the Netherlands.

It was refined by Xue et al., 2003, Xue, 2004; and Xue et al., 2008 in the Chemical Reaction Engineering Laboratory (CREL) at Washington University in Saint Louis, who developed and validated a new data processing algorithm in columns without internals. It has since been used and further validated by Wu et al., 2007 and Wu, 2007 in three phase systems and Youssef and Al-Dahhan, 2009, and Youssef, 2010 who extended it to bubble columns equipped with dense internals structure at the same laboratory. The four points probe consists of four tips, three of which are of the same length and form an equilateral triangle. The fourth central tip is positioned through the geometric centre of this triangle measuring about 2.0 mm longer than the three peripheral tips. Each fiber consists of three layers: a quartz glass core having a refraction index of 1.45 and a diameter of 200 μm, a silicon cladding to make the diameter of 380 μm and a further protective layer of Teflon making the overall diameter of 600 μm. The cladding and Teflon layers are removed from the last centimeters of the probe. Figure 3.1 shows the four points optical probe tips, views and configurations, while Figure 3.2 shows the fiber optic coupling scheme and probe tip with the probe response to a bubble strike.

Each optical fiber sensitive part is shaped by over-heating it, resulting in a round shaped glass core end much like Figure 3.1c. The manufacturing of the probe has been done in our laboratory at Missouri University of Science and Technology (Missouri S&T) which is equipped with all the needed tools and equipment. The light is sent into each fiber by a Laser Emitting Diode (LED) of wave-length 680 nm via standard glass fiber connectors and is detected by a photodiode. Due to the difference in refractive index between liquid and the gas phase, when the fiber tip is in a liquid medium, most of the

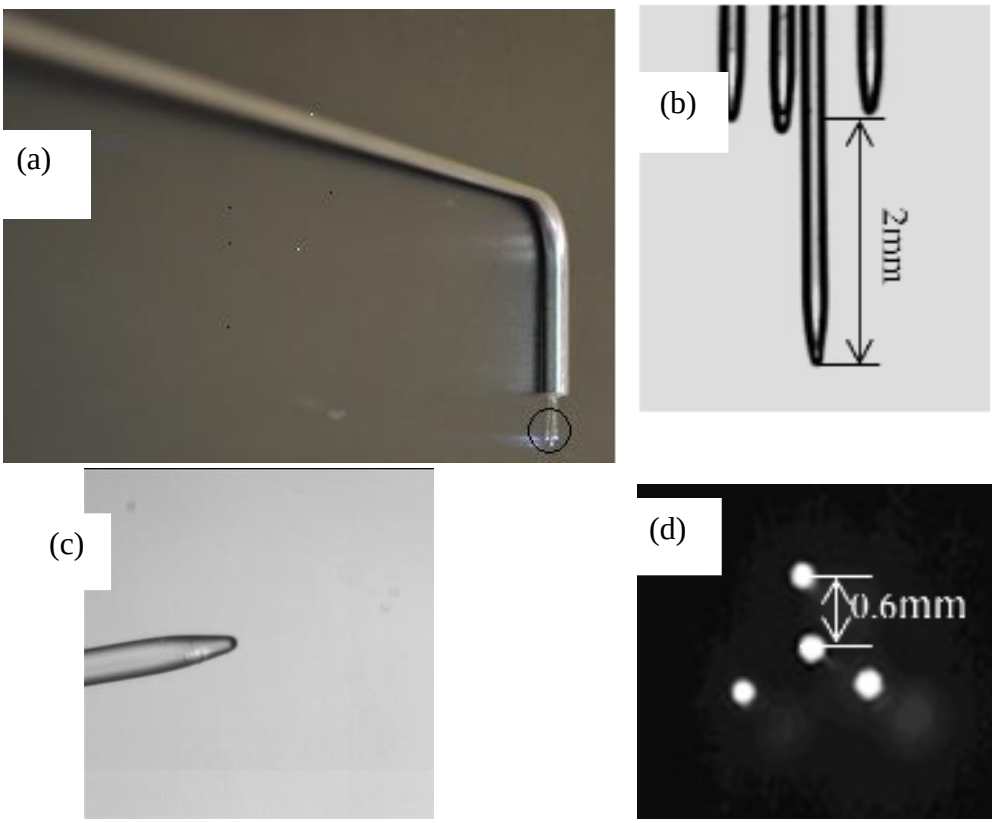

Figure 3.1 Configurations of four-point optical probe (a) Optical probe tips (b) Side view of four points probe tip (c) TEM image of finished tip, (d) Top view of four points probe tip

light is refracted into the liquid and very little light is sent back up the fiber. However, when the tip is in the gas bubble, most of the light is reflected and travels back into the coupler that channels about 50 % of the reflected light into a photodiode (see Figure 3.2 a) which finally transforms the light photons into a voltage much like in Figure 3.1 b. Finally, the voltage signals are collected by a data acquisition board (PowerDAQ PD2-MFS-8-1M/12) at a sampling frequency of 40 kHz. This data acquisition board was purchased from United Electronics Industries.

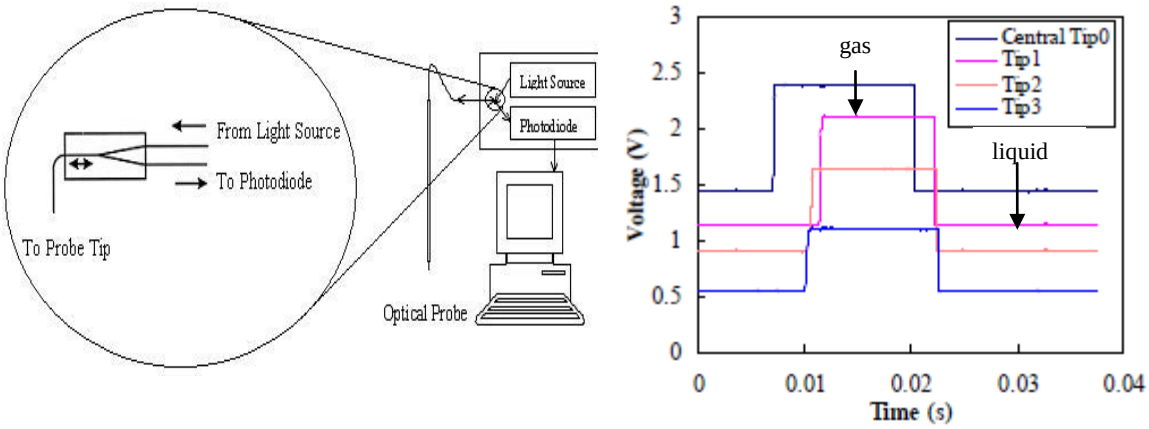

Figure 3.2 Fiber optic coupling scheme and probe tip with the probe response to a bubble strike (a) Fiber coupling and probe tip (b) Bubble striking four-point optical probe tips

3.1.2. Data Processing and Optical Probe Signal Analysis: From the captured signal with a probe response to bubble strike such as illustrated in Figure 3.2(b), the bubble parameters already stated can be determined by following the algorithm advanced by Xue, 2004. In this section the algorithm for extracting the bubble velocity, bubble chord length, specific interfacial area and the local gas holdup is presented.

For a single bubble movement, the bubble velocity vector aligns itself with the bubble orientation due to the balance of the forces on bubbles and the shape flexibility of gas bubbles (Xue, 2004; Xue et al., 2008; Wu, 2007). However, in churn-turbulent flow regime, sometimes the direction of bubble's motion changes significantly due to the strong turbulence, thus the bubble velocity vector might deviate from the normal vector of the bubble's symmetry plane by an angle ϕ. Such a deviation may cause errors in the bubble velocity vector and bubble chord length measured by the four-point optical probe. The sketches of the physical situation of the bubble velocity and chord length measurements in churn-turbulent flow are as shown in Figure 3.3 (Xue, 2004).

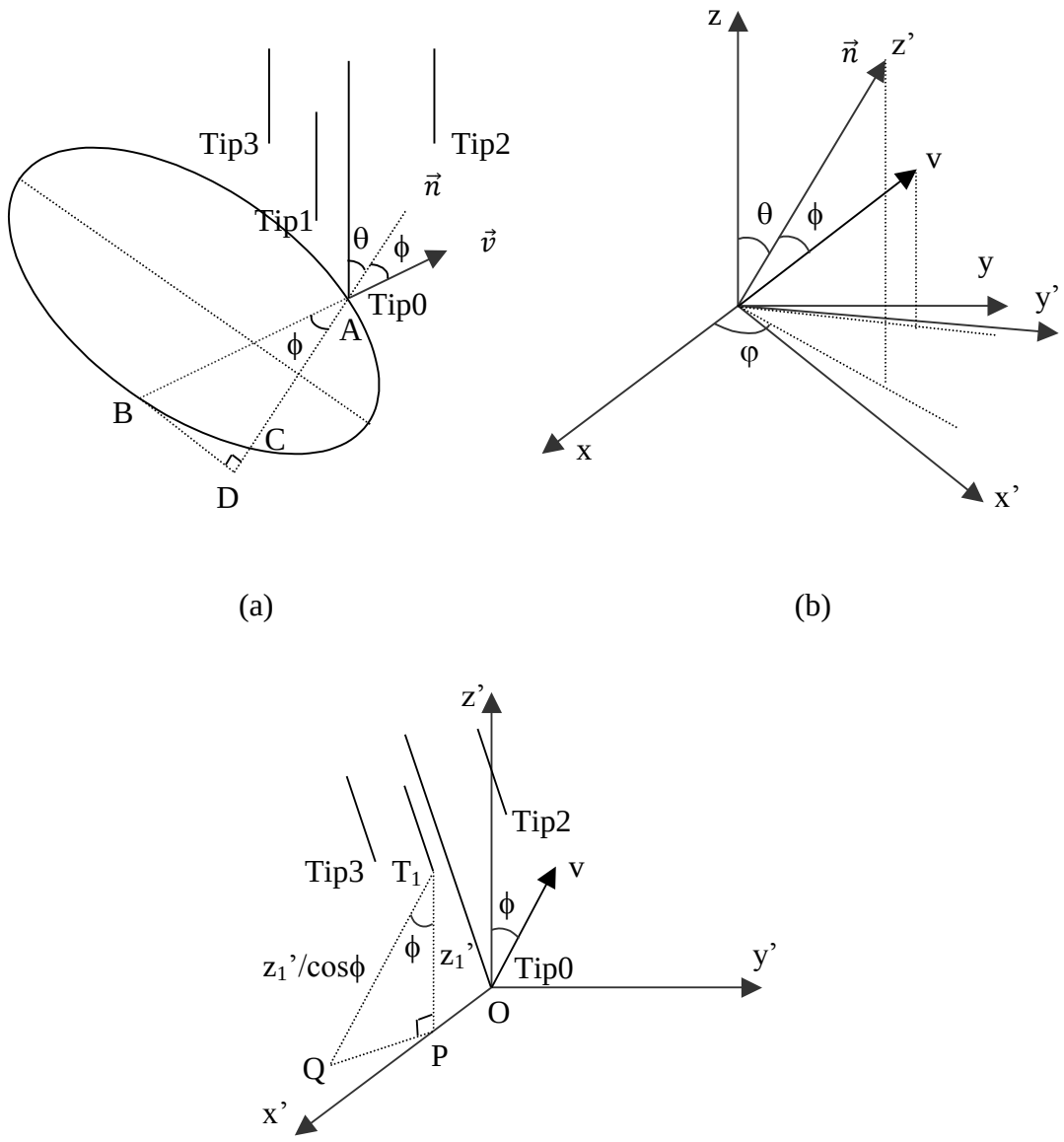

Figure 3.3 The physical situation of the bubble velocity and chord length measurements (from Xue, 2004)

In order to obtain the bubble velocity and chord length particularly in the churn-turbulent flow regime that is desired in the LPMeOH synthesis and FT process the following procedure is adopted as proposed by Xue, 2004 and Xue et al., 2008. Using the

central tip, (Tip0) as the reference for each bubble strike, it can be derived from Figure 3.3c that the time intervals between the instant when a bubble hits the central Tip0 and when it hits each of the other peripheral tips, Tip i, with i=1,2,3 are:

$$\Delta t_1 - \frac{T_0 - T_1}{2} = \frac{z_1^{'} / \cos\phi}{v} = \frac{x_1 \cdot \sin\theta\cos\varphi + y_1 \cdot \sin\theta\sin\varphi + z_1 \cdot \cos\theta}{v \cdot \cos\phi} \tag{3.1a}$$

$$\Delta t_2 - \frac{T_0 - T_2}{2} = \frac{z_2^{'} / \cos\phi}{v} = \frac{x_2 \cdot \sin\theta\cos\varphi + y_2 \cdot \sin\theta\sin\varphi + z_2 \cdot \cos\theta}{v \cdot \cos\phi} \tag{3.1b}$$

$$\Delta t_3 - \frac{T_0 - T_3}{2} = \frac{z_3^{'} / \cos\phi}{v} = \frac{x_3 \cdot \sin\theta\cos\varphi + y_3 \cdot \sin\theta\sin\varphi + z_3 \cdot \cos\theta}{v \cdot \cos\phi} \tag{3.1c}$$

where θ is the angle between the normal vector (vector $\vec{n}$ in Figure 3.3b) of the bubble's symmetry plane to the probe's axial direction, and φ is the angle between the projection of the normal vector on the xy plane and the x axis (Figure 3.3b). As shown in Figure 3.3b, the xyz coordinate system is transformed to x'y'z' system with its z'-axis in the direction of the bubble's normal vector, $\vec{n}$. With four variables (v, θ, φ and ϕ) and three equations (Equations 3.1a, 3.1b, 3.1c), it is only possible to obtain θ, φ and the product $v \cdot \cos\phi$ instead of each of the variables separately. Once the bubble velocity is known, the bubble chord length L_i pierced by tip i is simply given by the product $v \cdot T_i \cdot \cos\phi$, thus,

$$L_i = v \cdot \cos(\phi) \cdot T_i \tag{3.2}$$

While in Figure 3.3a, the chord length from the point where the probe's central tip hits the bubble's surface, A, is AC, with the product $v \cdot T_0 \cdot \cos\phi$ actually being the distance

AD. Hence, in the case where the bubble velocity vector does not align with the bubble's orientation, the determined bubble velocity vector and bubble chord length contain a systematic error. However, the error is small when the value of ϕ is small.

For the measurement of the specific interfacial area between the bubble and the liquid for each bubble strike, Kataoka et al., 1986 derived the equation for specific interfacial area as;

$$a = \frac{1}{\Delta T} \cdot \sum_{N} \frac{1}{v \cdot \cos\phi} \tag{3.3}$$

Where N is the total number of the gas-liquid interfaces passing though the probe during the measurement time ΔT, and ϕ is the angle between the velocity vector and the normal vector of the gas-liquid interface. According to Xue, 2004, the equations describing the velocity of the bubble's surface section pierced by the four-point probe are;

$$\Delta t_1 = \frac{x_1 \cdot \sin\theta\cos\varphi + y_1 \cdot \sin\theta\sin\varphi + z_1 \cdot \cos\theta}{v \cdot \cos\phi} \tag{3.4a}$$

$$\Delta t_2 = \frac{x_2 \cdot \sin\theta\cos\varphi + y_2 \cdot \sin\theta\sin\varphi + z_2 \cdot \cos\theta}{v \cdot \cos\phi} \tag{3.4b}$$

$$\Delta t_3 = \frac{x_3 \cdot \sin\theta\cos\varphi + y_3 \cdot \sin\theta\sin\varphi + z_3 \cdot \cos\theta}{v \cdot \cos\phi} \tag{3.4c}$$

The unknowns in these equations are now θ, φ, and $v \cdot \cos(\phi)$, and the three equations can be solved numerically to find $v \cdot \cos(\phi)$ which is the needed component in Kataoka's equation to directly determine interfacial area without assuming the bubble geometry.

The overall gas holdup defined as the ratio of volume of the gas-liquid mixture occupied by the gas. The local gas holdup can be defined in a similar way but at an infinitesimal volume within the reactor. By invoking the ergodic principle, which states that "the ensemble average is equivalent to the time average", the spatially (volume) averaged local gas holdup can be replaced by its equivalent time-averaged local gas holdup and thus estimated using the following equation:

$$\varepsilon_{G,local} = \frac{t_G}{t_G + t_L} \tag{3.5}$$

Where t_G and t_L is the time the probe spends in the gas bubbles and liquid respectively. The details for the local gas holdup estimation are presented in Section 5.

3.2. IMPACT OF INTERNALS SIZE AND CONFIGURATION ON LOCAL GAS HOLDUP AND BUBBLE PROPERTIES IN 6" BUBBLE COLUMN

Whereas the impact of internals on bubble dynamics have been investigated comprehensively by only one researcher, (Youssef and Al-Dahhan, 2009), no studies have been reported in the open literature on the effect of dense internals with different diameters and covering the same cross-sectional area and hence configuration on bubble properties. Therefore in this section, the effect of size of internals on bubble dynamics is discussed for a 6-inch diameter column.

3.2.1. Experimental System and Setup. The experiments were carried out in a Plexiglas column of 0.14 m in diameter and 1.83 m in height. The dynamic bed height was estimated visually and maintained at a constant level of about 1.56 m (z/D = 11.3) above the gas distributor by adjusting the amount of liquid loaded in the column. All the measurements were done at z/D = 5.6 which represents the fully developed flow region.

At this height above the distributor, the bubble properties remain nearly unchanged as it falls within the fully developed flow region. This height was chosen since the experimental results show that within this flow region, bubble properties including gas holdup, bubble velocity, specific interfacial area, and bubble frequency are independent of axial position (Ong et al., 2009, Xue, 2004).

A schematic diagram of the experimental setup is shown in Figure 3.4. In this work, the gas phase used was compressed oil-free dry air passed through filters and introduced continuously from the bottom of the column with the flow regulated by a set of calibrated rotameters. The high range rotameters were custom made and purchased from Brooks Instruments (1024NL0D1AA3F9C00001 and 1024NP0A1AA5F9C00001) with the capacity to deliver between 330-3,200 SCFH and 2,000 - 19,000 SCFH of air, respectively. While the lower range rotameter (FL-1501A-B) was purchased from Omega Engineering Inc. with air flow capacity of 0.317-3.17 SCFM. This set of rotameters gives the gas flow rate that covers both the bubble flow regime and churn turbulent flow regime. The compressed air was supplied by industrial scale high capacity air compressor purchased from Ingersoll Rand. It is a two stage rotary screw type air compressor, which can deliver compressed air at the rate of 44 100 CFH and at a pressure up to 200 psig. Soft filtered tap water was used as liquid phase.

Perforated plate with 121 holes and diameter of 1.32 mm arranged in a triangular pattern with a total free area of 1.09 % was used as the gas distributor which yields an intermediate flow condition characterized by the dimensionless capacitance number N_c defined by; $N_c = 4V_c g\rho_l/\pi {D_0}^2 P_s$ (Kumar and Kuloor, 1970; Tsuge and Hibino, 1983). When *Nc* is smaller than 1, the gas flow rate through the orifice is constant, which is

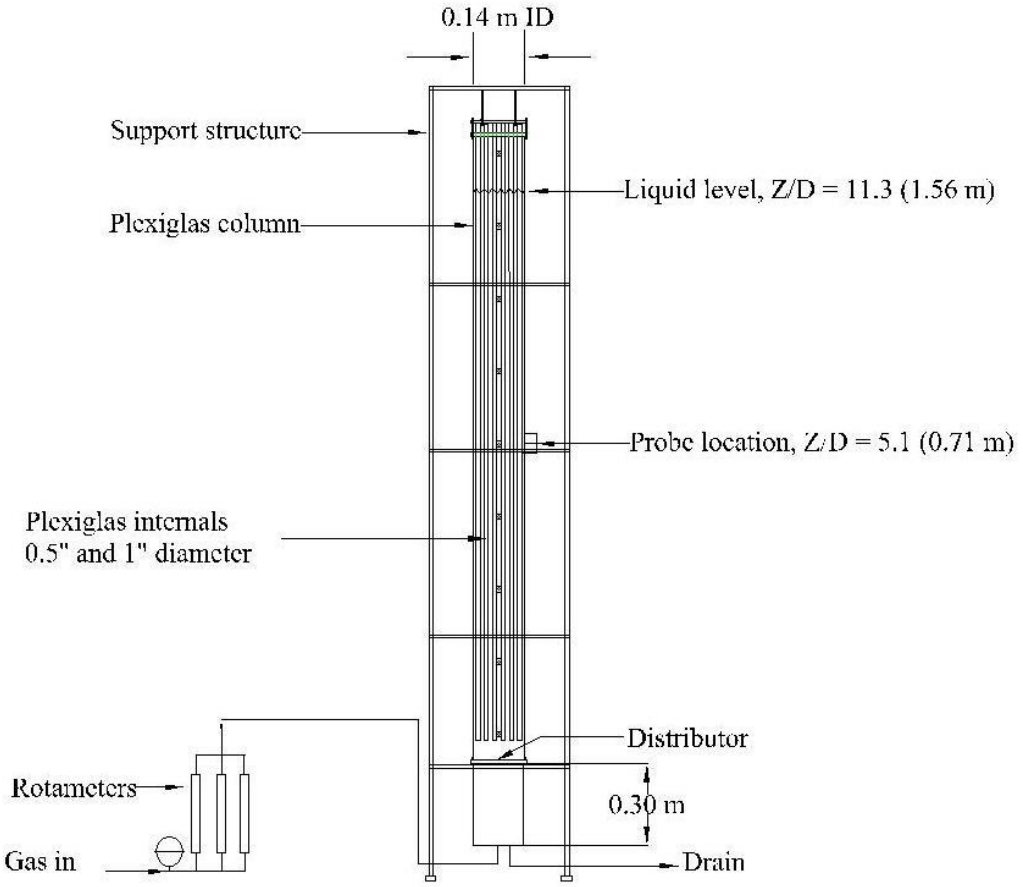

Distributor details	
No of holes	121
Hole diameter	1.32 mm
Occluded area	1.09%

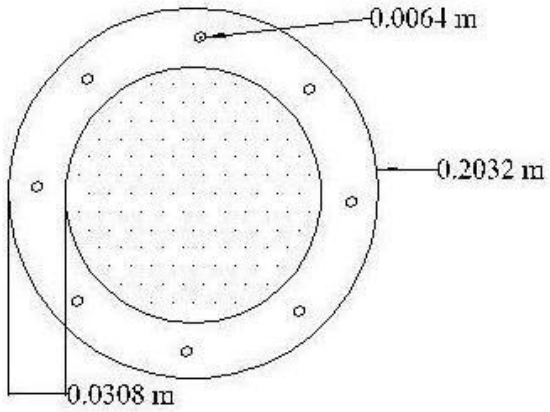

Figure 3.4 Schematic diagram of the experimental system with dense internals in 6-inch column

characterized as constant flow conditions. When *Nc* is larger than 9, the gas flow rate yields a variable pressure, and is dependent on the pressure difference between the gas chamber and bubble. The capacitance number in this case was 1.65 that lies between 1-9.

The experiments were carried out at a range of superficial gas velocities covering homogenous flow regime, transition flow regime and the churn turbulent flow regimes. The superficial gas velocities were varied from 0.03 to 0.45 m/s based on both the total cross-sectional area (CSA) of the column and also based on the free cross-sectional area. Two different sizes of internals were used in each case covering 25 % of the column cross-sectional area that simulates the Fischer-Tropsch synthesis process. For reference and to form a basis for comparison, experiments and measurements were also done on empty bubble columns. The internals used in this study were vertical Plexiglas rods of 0.5-inch and 1-inch diameter. The configurations of the internals design used are shown in Figure 3.5.

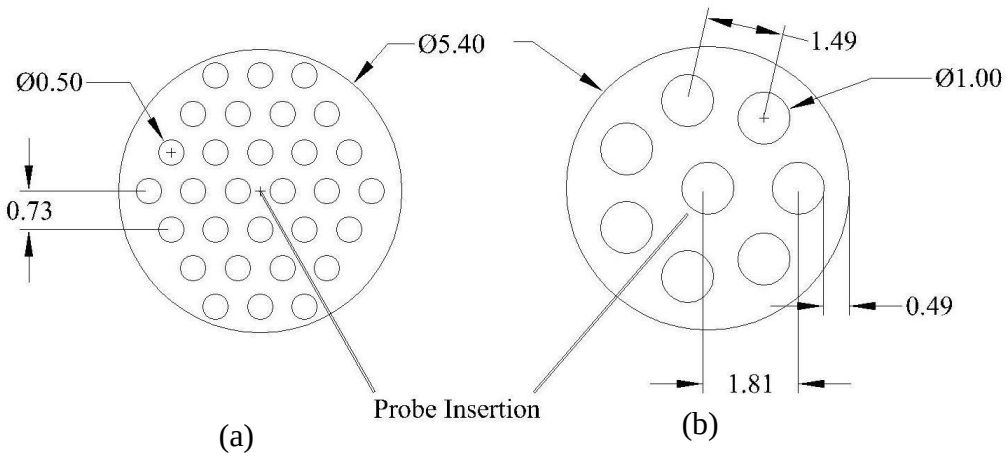

Figure 3.5 Internals configurations covering 25 % CSA (a) 0.5-inch diameter (b) 1-inch diameter

For superficial gas velocity calculations, the free cross-sectional area of the column was determined from the following relation;

$$\left\{\begin{matrix}Free\\Cross-Sectional\\Area\end{matrix}\right\}=\left\{\begin{matrix}Cross-Sectional\\Area\ of\\Empty\ Column\end{matrix}\right\}-\left\{\begin{matrix}Cross-Sectional\\Area\ Occupied\\by\ Internals\end{matrix}\right\}$$

3.2.2 Results and Discussion. Even though combined measurements approach was used to simultaneously measure both the bubble dynamics and the heat flux at the same time, only the bubble dynamics results are presented and discussed in this section. Whereas a few studies have examined the impact of internals on bubble dynamics, the mode of determining the gas flow rate and hence the gas velocity into the column has remained questionable. The use of empty cross-sectional area (open cross-sectional area available for flow only) is emphasized in calculating the superficial gas velocity in order to determine the effect of internals which should be free from the influence of the higher mass rate of the gas which may result when the cross-sectional area of empty column is used in calculating the superficial gas velocity.

3.2.2.1 Overall and local gas holdup. Overall gas holdup may be defined as the volume fraction of gas in the gas-liquid dispersion (Joshi J.B, 1998). It is one of the important design parameters in the bubble and slurry bubble column reactors. It not only governs the overall reactor performance but also determines the volume of the reactor since it is the fraction of the column volume occupied by the gas phase. The local spatial variation of the gas holdup is yet another key parameter of the gas holdup since it gives rise to pressure variation radially and axially leading to varied strengths in the large scale and small scale liquid re-circulations which are important aspects for both mass and heat transfer in bubble and slurry bubble columns. It should be noted that the overall gas

holdup was measured in the Plexiglas columns by visual observation using the bed expansion approach in the lab. Other means or technique may be adopted for opaque systems such as the stainless steel columns in which visualization may not be possible.

Local gas holdup at an interrogation point is the fraction of an infinitesimal volume around this point that is occupied by the gas phase (Drew, 1983; Kumar, 1994). While the overall phase holdup is important in determining the gas phase residence time and the system pressure drop, the local void fraction provides information about the phase interactions, the interfacial areas, and phase recirculation; which are all related to the heat transfer mechanisms. Consequently, local gas holdup and its distribution have been identified as among the most important parameters that govern liquid recirculation in bubble column operation. Figure 3.6 illustrates the influence of superficial gas velocity based on both the free cross-sectional area and total cross-sectional area of the column on the overall gas holdup (Figure 3.6a) and local gas holdup (Figure 3.6b) at the center of the column, r/R(-) = 0.0. It is evident that the effect is significant when the Ug is based on the empty column's cross-section area. This result shows that the dense internals have little effect on the overall gas holdup and local gas holdup at the center of the column, r/R(-)= 0.0 particularly at higher gas velocities. However, the observed enhancement at superficial gas velocity based on total cross-sectional area can be attributed to same mass flow rate of the gas as that of empty column passing through a smaller cross-sectional area. To quantify the reproducibility of measurements the use of error bars have been made which show very little deviations. Thus for the purposes of clarity, the error bars have not been plotted in most of the subsequent bubble dynamics figures. Figure 3.7 shows the effect of different diameters of internals on radial profiles of local gas holdup

with gas velocities based on free cross-sectional area (Figure 3.7a) and also based on total cross-sectional area (Figure 3.7b) at U_g = 3 cm/s (bubbly flow regime).

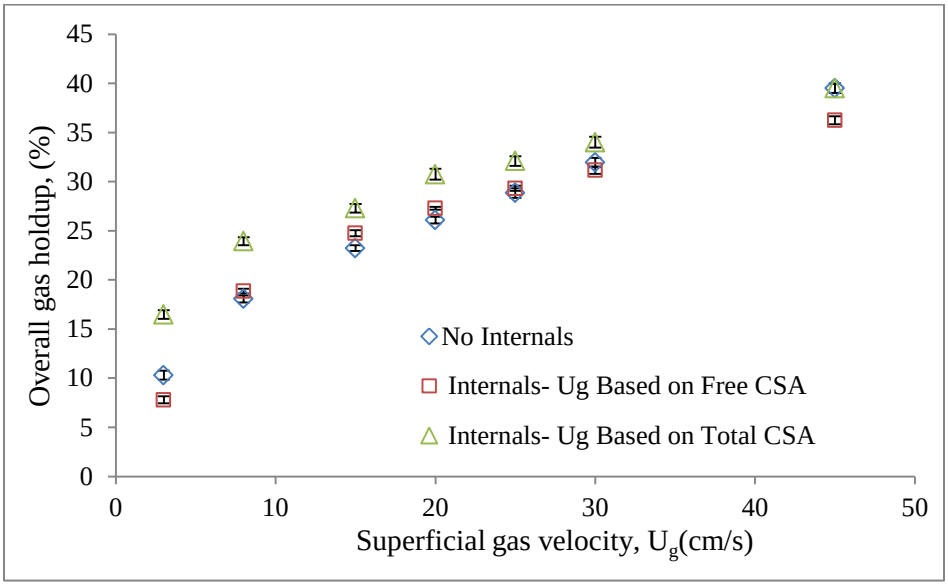

(a)

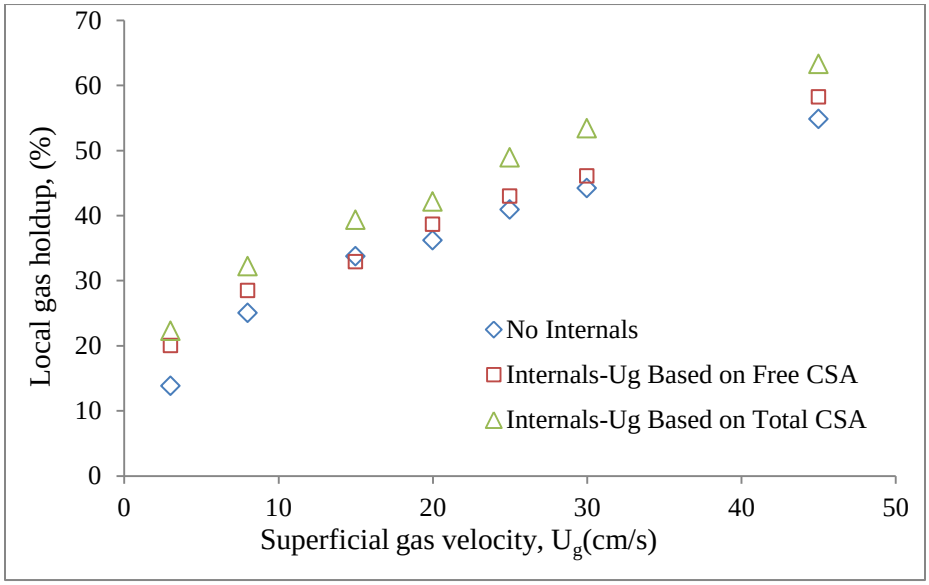

(b)

Figure 3.6 Effect of dense internals (0.5 inch diameter) on (a) Overall gas holdup and (b) Local gas holdup at r/R(-) = 0.0, with superficial gas velocity based on the total cross-sectional area and free cross-sectional area of the column

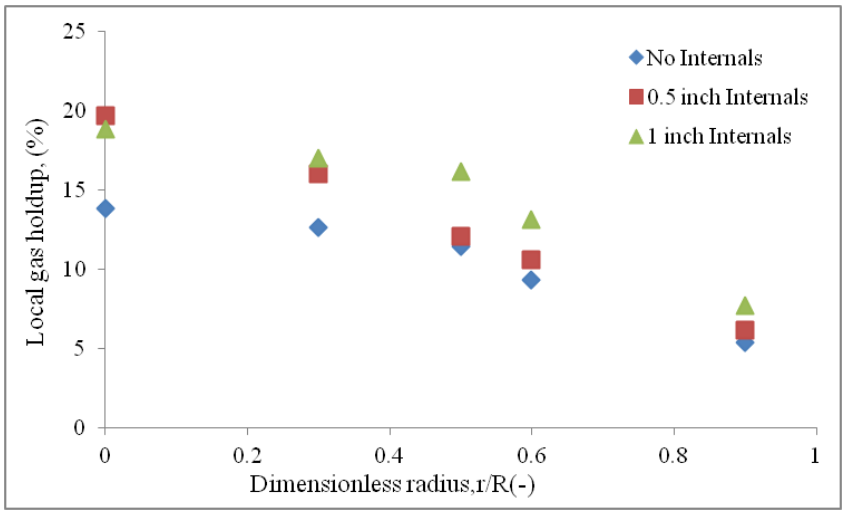

(a)

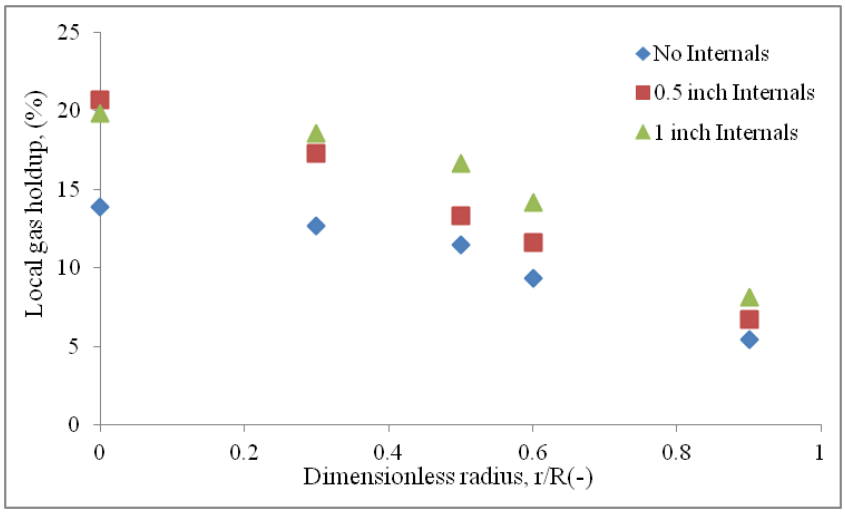

(b)

Figure 3.7 Effect of size of internals on radial profiles of local gas holdup at U_g = 3 cm/s (a) Ug based on free cross-sectional area (b) Ug based on total cross-sectional area

As noted in Section 2, most of the bubble dynamics studies including gas holdup were conducted in empty bubble columns. When the columns are inserted with internals, the flow rate of the gas into the system should be employed based on the free area of the column cross-section available for the flow in order to assess the effect of internals only. It is observed that when 25 % of the cross-sectional area is occupied by internals the local

gas hold-up is enhanced by up to 40 % at U_g = 3 cm/s at the column center (r/R = 0.0), with 0.5-internals giving higher values which are also within 5 % of the values obtained with 1-inch internals. Close to the column wall region regardless of the cross-sectional area used in calculating the superficial gas velocity, the internals have little effect. A key observation that has been made is that in the bubbly flow regime (Ug = 3cm/s), the 1-inch internals enhances the local gas holdup in the middle region between the column center and the column wall by between 25 % and 20 % more than the 0.5-inch internals when the gas velocity is based on free CSA and total CSA, respectively. Therefore in the homogenous (bubbly) flow regime, the difference caused by the dense internals on the local gas hold up is significant. Consequently the local gas holdup results obtained in the empty columns operated in the bubbly (homogenous) flow regime cannot be extrapolated to columns equipped with dense internals

Figure 3.8 shows the effect of different diameters of internals on radial profiles of local gas holdup with gas velocities based on free cross-sectional area (Figure 3.8a) and also based on total cross-sectional area (Figure 3.8b) at U_g = 45 cm/s, which is in the churn turbulent flow regime. At Ug = 45 cm/s based on free cross-sectional area the gas holdup is enhanced by up to 6 % close to the column wall region with 1-inch diameter internals. Elsewhere along the radial locations, the enhancement of local gas holdup by different internals sizes lie within 3 % of each other, with average increase of less than 2 % for both the 0.5-inch diameter and 1-inch diameter internals. However, when the Ug is based on total cross-sectional area then the effect is noticeably higher. The local gas holdup is increased by up to 17 % at the column center by 0.5-inch diameter internals with a mean increase in radial gas holdup of 12 % when 0.5-inch diameter internals are

used. Up to 21 % increase is attained closer to the column wall by 1-inch internals and radial average increase of 13 % in the local gas holdup with the same (1-inch) internals. Again this is due to same mass of gas flow rate introduced through smaller cross-sectional area in the case of dense internals

It is obvious therefore that whereas the presence of internals affects the flow field behavior in bubble columns, the gas holdup enhancement attributable to higher break up rates due to dense internals is negligible at higher superficial gas velocity. Youssef and Al-Dahhan, 2009, reported enhanced bubbles breakup rate when the gas velocity is based on total cross-sectional area, where same volumetric flow of gas flowing through a smaller cross-section of the column with dense internals compared to that without internals. The same volumetric flow rate of gas through smaller cross-section would yield higher gas velocity inside the column with internals. This higher gas velocity inside the column with internals would give rise to large population of bubbles with higher bubble passage frequency and hence higher gas holdup is obtained.

Also worth mentioning is the fact that at the column core region within r/R(-) $\leq$ 0.3, the 0.5-inch diameter internals gave consistently higher gas holdup while 1-inch diameter internals gave higher values at r/R(-) = 0.9. Thus local gas holdup radial profiles obtained with 0.5-inch diameter internals are steeper than those obtained with 1-inch diameter internals. Hence, higher large-scale liquid recirculation velocity is expected with 0.5-inch internals which needs to be experimentally evaluated. In this case the heat transfer rates obtained with 0.5-internals is likely to be higher than those obtained with 1-inch diameter internals or no internals, which is experimentally evaluated in Section 4.4.

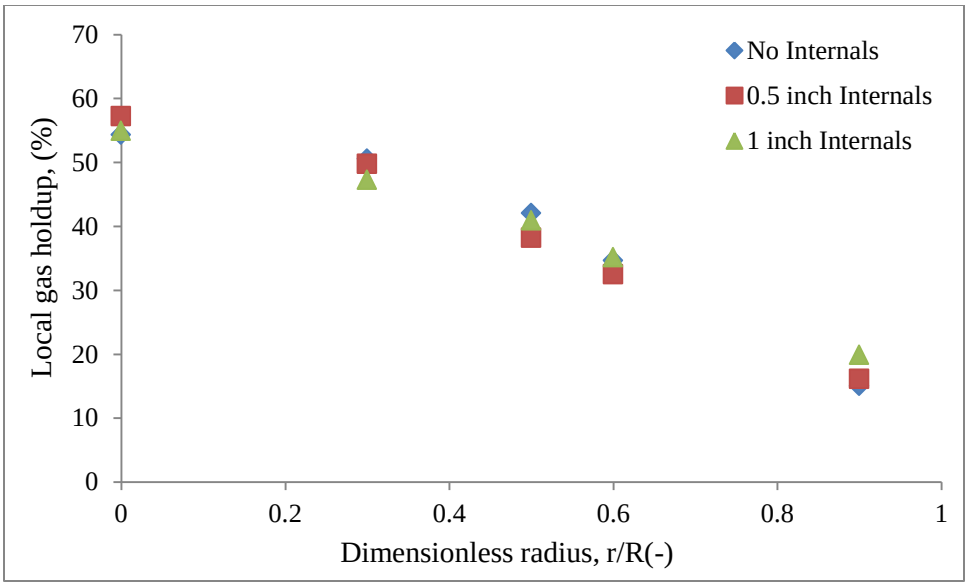

(a)

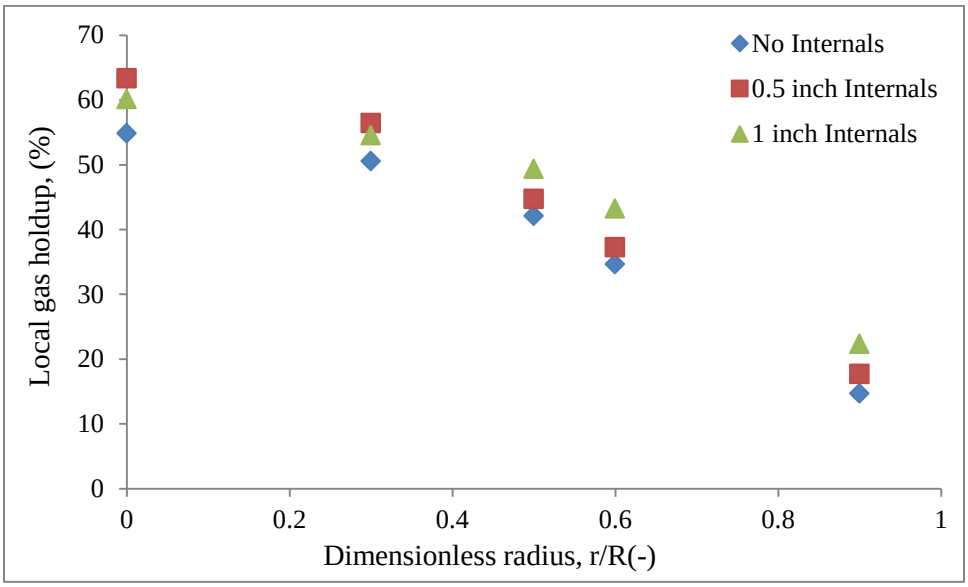

(b)

Figure 3.8 Effect of size of internals on radial profiles of local gas holdup at U_g = 45 cm/s (a) Ug based on free cross-sectional area. b) Ug based on total cross-sectional area

From this section, it can be concluded that in the churn turbulent flow regime at very high gas velocity, Ug = 45 cm/s, the overall gas holdup or local gas holdup results

obtained from investigations in empty bubble columns can be extrapolated to columns with dense internals. This can be achieved by matching the superficial gas velocity in columns with dense internals to those of empty columns by using the gas velocity based on the free cross-sectional area available for flow.

In order to assess the performance of the four-point optical fiber probe in this work, the radial profiles of gas holdup obtained by the probe was compared with those predicted by correlation of Schweitzer et al., 2001 (Equation 3.6) which was obtained based on experiments performed in smaller columns ($D \leq 0.4$ m) without internals.

$$\varepsilon_g(r) = \bar{\varepsilon_g}\left\{1.7889\left(1-\left(\frac{r}{R}\right)^6\right) - 1.228\left(1-\left(\frac{r}{R}\right)^4\right) + 0.930\left(1-\left(\frac{r}{R}\right)^2\right)\right\} \tag{3.6}$$

Where $\bar{\varepsilon_g}$ is the cross-sectional average gas holdup and the only required input. Futher comparison was made with the correlation of Wu and Al-Dahhan, 2001 (Equation 3.7a) that was developed based on extensive gas holdup and radial gas holdup profiles acquired in the Chemical Reaction Engineering Laboratory (CREL) by using gamma ray Computed Tomography (CT) in columns ranging in diameter from 0.19-0.44 m.

$$\varepsilon_g(r) = \bar{\varepsilon_g}\left(\frac{n+2}{n+2-2c}\right)\left[1-c\left(\frac{r}{R}\right)^n\right] \tag{3.7a}$$

$$n = 2.188 * 10^3 {Re_G}^{-0.598} {Fr_G}^{0.146} {Mo_L}^{-0.004} \tag{3.7b}$$

$$c = 4.32 * 10^{-2} {Re_G}^{0.2492} \tag{3.7c}$$

$$Re_G = \frac{D_c U_g(\rho_L - \rho_g)}{\mu_L}, \quad Fr_G = \frac{{U_g}^2}{gD_c}, \quad Mo_L = \frac{g{\mu_L}^4}{(\rho_L - \rho_g){\sigma_L}^3}$$

Where, n is indicative of the steepness of the gas holdup profiles, c is indicative of the gas holdup value near the column wall and $\bar{\varepsilon_g}$ is the cross-sectional average gas holdup.

Kumar, 1994 has shown that the cross-sectional average gas holdup measured at heights above the distributor larger than 4 to 5 column diameters is in close agreement with the overall gas holdup in the column. Thus the overall gas holdup estimated by visual observation using the bed expansion approach in the current work is utilized in Equation 3.5 and Equation 3.6 to predict the radial profiles of the gas holdup. The comparison is made between the four-point optical probe measurements in this study and predicted radial profiles. Figure 3.9 shows the comparison at 8 cm/s and at 45 cm/s of superficial gas velocity based on free CSA (Figure 3.9a) and also based on total CSA (Figure 3.9b). A close match between the radial profiles obtained by measurements and using predictions from the correlations was realized. The main conclusion that can be drawn is that the influence of internals on the gas holdup in bubble column can as well be determined by estimating the gas holdup in empty bubble columns at same superficial gas velocity equivalent to that in the column with internals estimated based on free CSA. While the effect of the configuration and diameter of internals is only significant at lower range of gas velocity.

3.2.2.2 Bubble passage frequency. The bubble passage frequency may be defined as the number of bubbles that pass through a unit volume in space within the reactor in a unit time. In order to quantify the bubble passage frequency in the current work, the total number of bubbles that hit the probe's central tip was divided by the total sampling time. For the bubble passage frequency and specific interfacial area, the effect of internals diameter and configuration on bubble properties is presented only for the churn

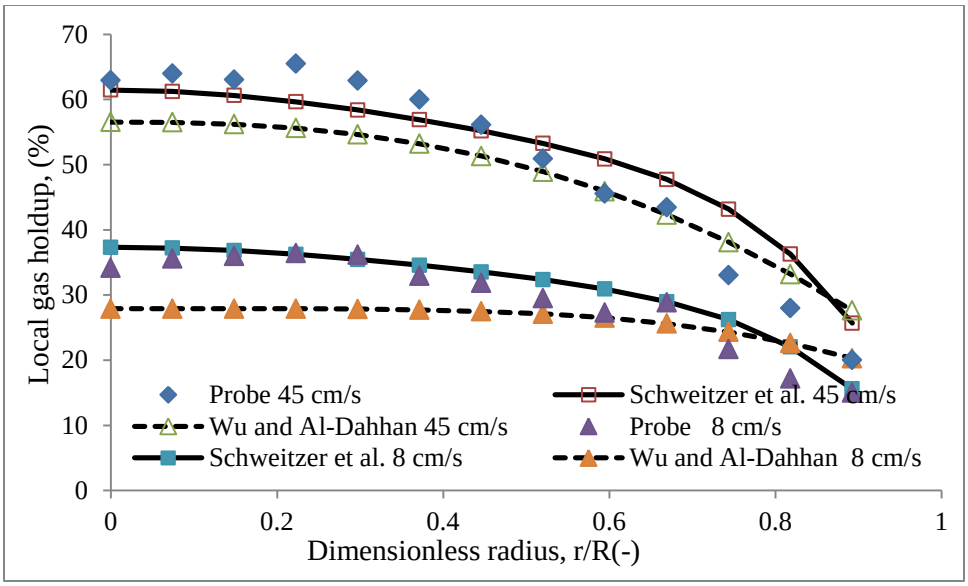

(a)

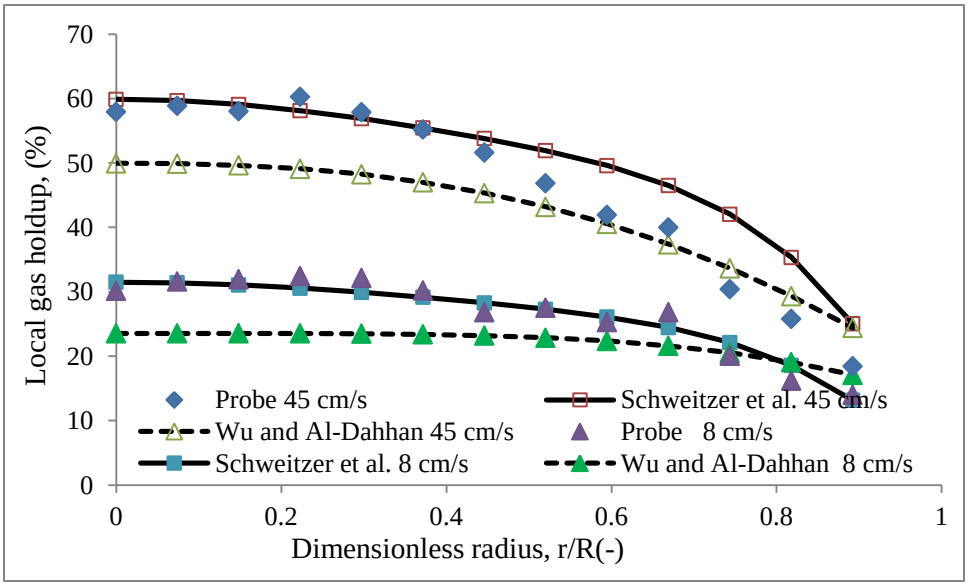

(b)

Figure 3.9 Optical probe measurements comparison with literature correlations in bubble column with 0.5- inch diameter internals with superficial gas velocity based on (a) Free cross-sectional area (b) Total cross-sectional area

turbulent bubble column operation since trends similar to those of local gas holdup were observed for the low range of gas velocity as discussed for local gas holdup at Ug = 3

cm/s. Additional results at 3 cm/s are available in Appendix C-1. Only a few studies have examined the bubble passage frequency in bubble columns, (Choi and Lee, 1992; Xue, 2004; Wu, 2007; Shin et al., 2009, and Youssef and Al-Dahhan, 2010). However, none has examined the effect of size of internals and the internals configuration on bubble passage frequency.

Figure 3.10 shows the radial profiles of bubble passage frequency for different diameters of internals with superficial gas velocity (45 cm/s) based on both free CSA (Figure 3.10a) and total CSA (Figure 3.10b). Similar profiles were obtained at 20 cm/s and 30 cm/s and have not been re-plotted here. Like gas holdup, the radial bubble frequency, is governed by bubble slip velocity generated by the net radial force and turbulent dispersion. Choi and Lee, 1992 reported that the bubble frequency is influenced by the gas holdup, bubble size, bubble rise velocity as well as the intensity of the liquid turbulence. It is evident from Figure 3.10, that the bubble passage frequency is significantly increased when column is inserted with internals particularly the 0.5-inch internals. The intertube gap, t_R for the 0.5-inch internals is much smaller than that of 1-inch internals (less than half of that of 1-inch). This restricts the coalescence of bubbles and enhances the bubble break-up rate thus many bubbles appear in the column per unit time. It is also noted that when 1-inch diameter internals are used and the superficial gas velocity is based on free CSA, up to 49 % increase in bubble passage frequency is obtained close to the column wall region with a cross-sectional radial average increase of 9.2 %. While for 0.5-inch diameter internals an average increase of 40 % is attained with twice as many bubbles in wall region than without the internals. A similar trend is

observed when the superficial gas velocity is based on total CSA where the average increase when 0.5-inch internals are used is 30 % higher than with 1-inch internals.

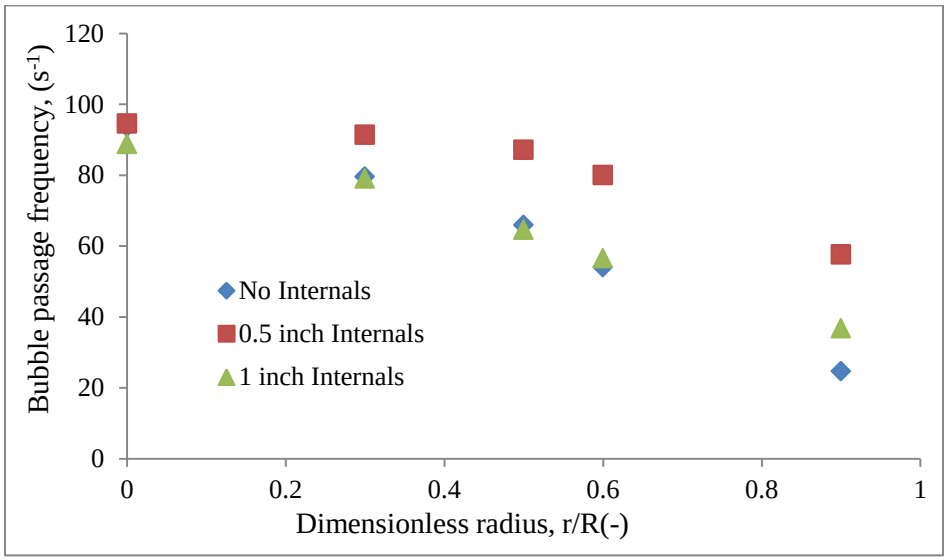

(a)

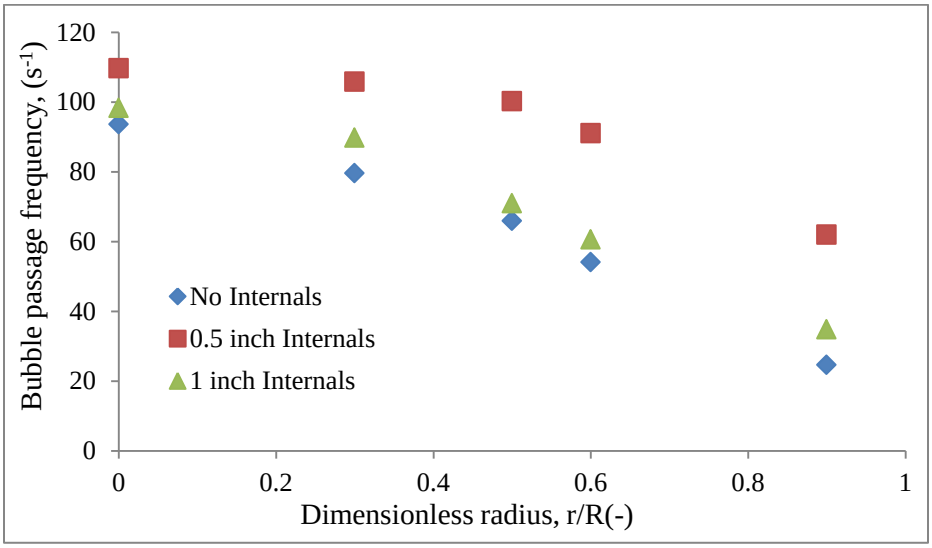

(b)

Figure 3.10 Effect of size of internals on radial profiles of bubble passage frequency at U_g = 45 cm/s (a) Ug based on free cross-sectional area (b) Ug based on total cross-sectional area.

3.2.2.3 Specific interfacial area. According to Sehabiague, 2012, specific interfacial area is usually defined as the ratio of the surface of the gas bubbles per unit liquid-phase volume. In bubble and slurry bubble columns, the overall mass transfer rate per unit volume of the dispersion is governed by the liquid-side mass transfer coefficient, k_La since $k_La << k_Ga$ (Lye et al., 2001) hence the volumetric mass transfer coefficient k_La is the key parameter needed in order to determine the bubble column reactor performance. Behkish, 2004 studied the volumetric liquid-side mass transfer coefficient, k_La, using the transient physical gas absorption technique in the cold and hot slurry bubble column reactors (SBCRs). He reported that the k_La values in the slurry bubble column reactors were found to vary only due to the alteration of the gas-liquid interfacial area, a. Similar conclusions were arrived at by Fan et al., 1985, and Kantarci et al., 2004. Thus, a proper knowledge of the specific gas-liquid interfacial area and the radial distribution is required for proper design and optimal operation of bubble and slurry bubble column reactors.

Figure 3.11 shows the effect of internals size and configuration on the specific interfacial. The specific interfacial area has been found to increase with superficial gas velocity. The change in specific interfacial area with respect to superficial gas velocity is higher at low range of Ug (0 – 10 cm/s) and gets lower or less at higher range of Ug (10 – 45 cm/s), see Figure 3.11. Similar trend was also reported from the experimental findings of Xue, 2004 and Xue et al., 2008 and various empirical correlations and CFD models of several researchers including, Krishna and Van Baten, 2003; Behkish et al.,

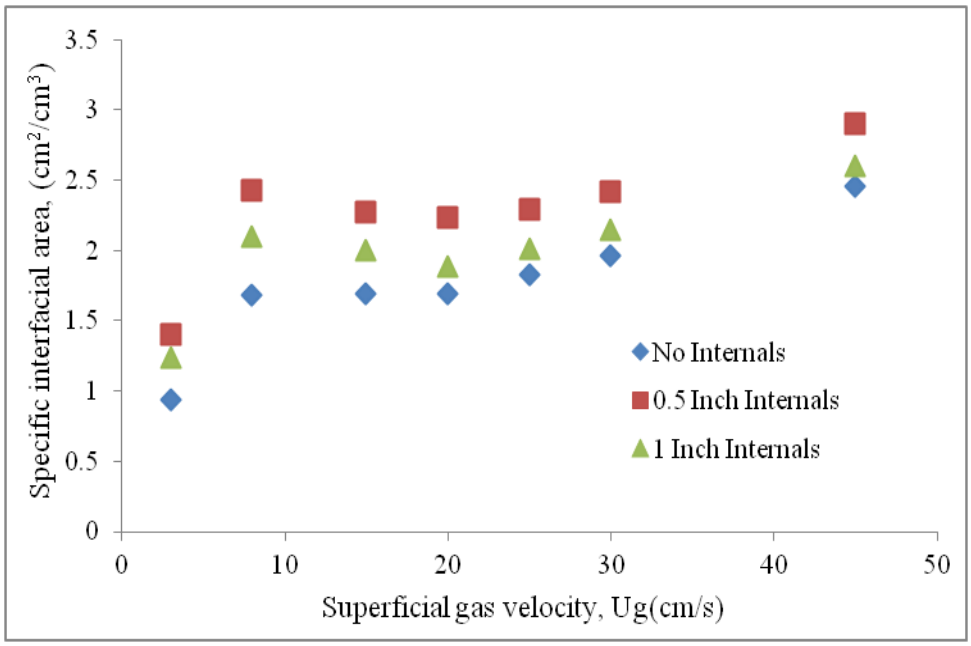

Figure 3.11 Effect of size of internals size on specific interfacial area at r/R(-) = 0.0, with U_g based on free cross-sectional area.

2002; and Akita and Yoshida, 1974. With increasing superficial gas velocity, more bubbles appear in the column. Xue, 2004 and Youssef and Al-Dahhan, 2009 reasoned that the population of bubbles increases with superficial gas velocity, at the same time the bubbles breakup rate and coalescence is enhanced. The coalescence of bubbles leads to formation of larger bubbles, at the same time the population of small bubbles also increase significantly that gives rise to many bubbles in the column hence increased interfacial area with the superficial gas velocity.

It is noteworthy that the profiles of specific interfacial area exhibit local maximum then continues to rise with the superficial gas velocity. Local maxima are characteristic of the region or range of superficial gas velocity where the flow regime transitions into churn turbulent from the transition flow regime range. A similar trend has

been reported before for the overall gas holdup measurements, from which the three flow regimes can also be identified (Jhawar and Prakash, 2007; Krishna et al., 1997). Figure 3.12 obtained from Jhawar and Prakash, 2007 compares the gas holdups obtained with two types of spargers, a fine and a coarse sparger, with a fine sparger showing clearly this

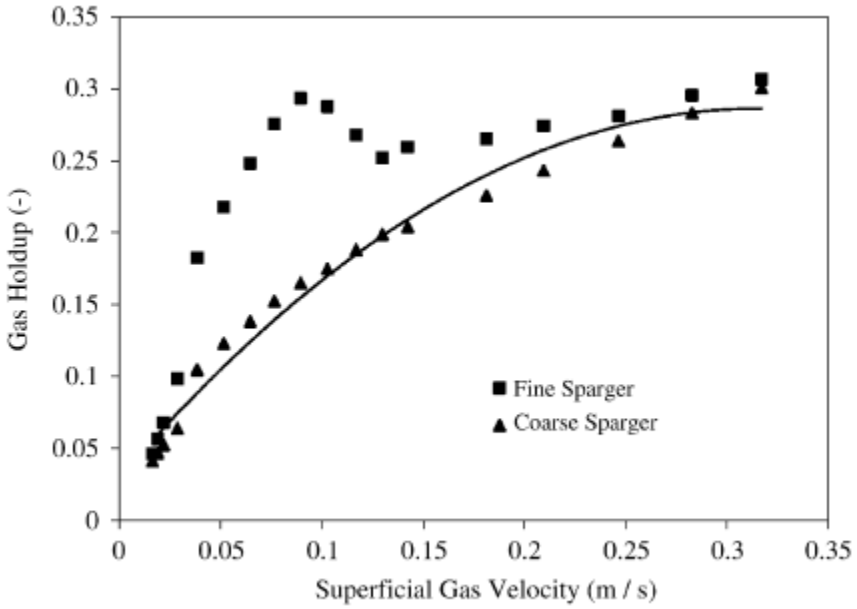

Figure 3.12 Variation of overall gas holdup with superficial gas velocity with fine and coarse sparger. (Obtained from: Jhawar and Prakash, 2007)

range where a local maximum occurs for the overall gas holdup. Therefore with a local maxima occurring at the same superficial gas velocity, it is possible that specific interfacial area can be used to pin-point where the flow regime changes from transition flow into the churn turbulent flow, Figure 3.11. Use of dense internals leads to enhancement of the specific interfacial area, with 0.5-inch diameter internals exhibiting greater enhancement. As noted earlier the tube pitch for 0.5-inch internals restrict the

maximum bubble sizes which can pass between the tubes hence higher break-up rate leading to smaller bubbles with higher specific interfacial area per unit volume. The radial profiles of the specific interfacial area at Ug = 45 cm/s is shown in Figure 3.13. Like the gas hold-up, the 0.5-inch diameter internals have steeper radial profiles of specific interfacial area compared with empty column or with 1-inch diameter internals.

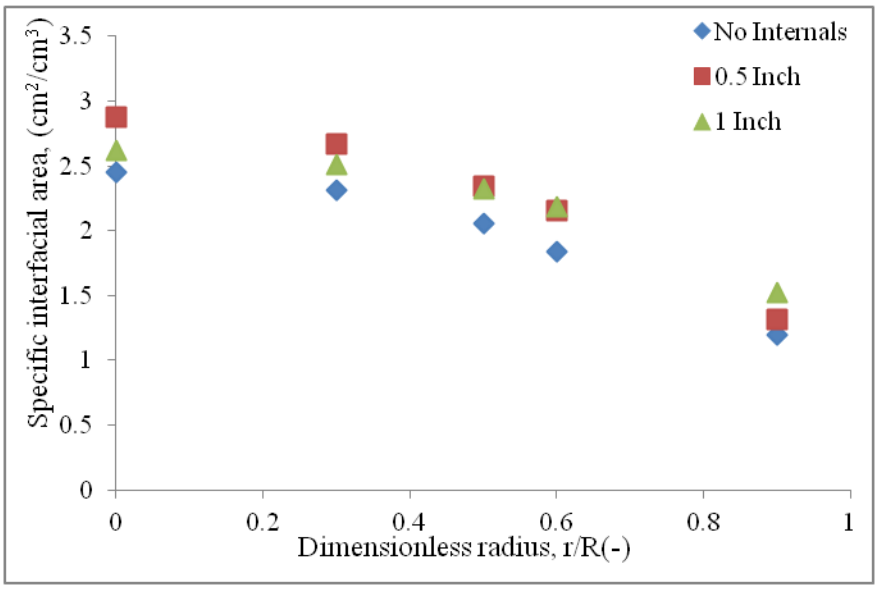

Figure 3.13 Effect of size of internals and configuration on radial profiles of specific interfacial area at U_g = 45 cm/s based free cross-sectional area

With 0.5-inch diameter internals an increase of 15 % is attained at the column core region, $\left(\frac{r}{R} \leq 0.3\right)$ while 7 % increase is attained with 1-inch diameter internals at the same region. Closer to the column wall, the interfacial area is increased by 10 % and 20 % with 0.5-inch and 1-inch diameter internals respectively. Previous studies by Youseff and Al-Dahhan, 2009, Xue, 2004 Xue et al., 2008 and Wu, 2007 on bubble

passage frequency have demonstrated that an increase in bubble frequency leads to an increase in gas holdup and specific interfacial area.

It was found that a larger interfacial area existed at the column's center than in the region near the wall which is similar to the findings of Xue et al., 2008. This difference is due to enhanced rates of breakup and coalescence among bubbles in the central region of the column in the churn turbulent flow regime, which was confirmed by the bubble frequency measured by the probe. An increase in bubble frequency leads to an increase in specific interfacial area. Speaking generally, an increase in bubble frequency leads to an increase in gas holdup and specific interfacial area.

3.2.2.4 Bubble chord length. By taking into account the column hydrodynamics, mass transfer, kinetics, and bubble-bubble interaction, Bauer and Eigenberger, 2001 demonstrated that in multiscale modeling the change in local bubble size, due to mass transfer with reaction, and change in local mass fluxes between the gas and liquid phases can significantly change the hydrodynamics of the bubble column. Thus it is necessary to examine the bubble sizes which are characterized by the bubble chord lengths in this work. Bubble chord lengths have been used as the characteristic length for bubble sizes by a number of researchers, (Choi and Lee, 1992; Schweitzer et al., 2001; Xue, 2004; Xue et al., 2008; Wu, 2007; Shin et al., 2009; Youssef and Al-Dahhan, 2009 and Youssef, 2010). Whereas the mean of the chord length has been used as the characteristic bubble size, it does not give the correct picture of the size of bubbles in the system. Therefore, the use of bubbles chord lengths distribution has been adopted in this work and reporting the mean bubble chord lengths where necessary. A large population of smaller bubbles and smaller population of large bubbles was noted by histogram plot as

shown in the following sections (Figure 5.12a and b). However, the bubbles size structure is best represented by using a lognormal distribution. Akita et al., 1974 were the first to report that bubble size distribution follows a lognormal distribution and similar findings have thereafter been reported by; Glasgow et al.,1984; Yasunishi et al., 1986; Luewisutthchat, et al., 1997, and Pohorecki et al., 2001. The lognormal distribution for the bubble sizes, $f(l_c)$ is expressed as:

$$f(l_c) = \frac{1}{\sigma l_c \sqrt{2\pi}} exp\left[-\frac{(lnl_c - \mu)^2}{2\sigma^2}\right] \tag{3.8}$$

Where, l_c , is the measured chord length obtained directly from the four points optical probe and the parameters μ and σ are related to the mean, m, and variance, υ , of the measured chord lengths as follows;

$$\mu = \log\frac{m^2}{\sqrt{\upsilon+m^2}} \text{ and } \sigma = \sqrt{\log\frac{\upsilon}{m^2+1}}$$

Accordingly, in this work the measured chord lengths, l_c that are directly obtained from the four-points optical probe are represented by Equation 3.8 by using the chord length, l_c for each measured data point obtained during a bubble passage. This equation hence, is used here to plot all the probability density functions, (pdf) as demonstrated in Figures 3.14 through 3.16. Figures 3.14 through 3.16 show the effect of internals sizes and configuration at U_g = 3 cm/s and at U_g = 45 cm/s of gas flow rate based on free cross-sectional area measured within the column center, (r/R (-) = 0.0) and at two other different radial locations, r/R (-) = 0.5, and r/R (-) = 0.9). The bubble chord lengths have been further analyzed statistically by providing the mean and the variance, as shown in Table 3.1. The variance of the distribution, υ is defined as $\upsilon = \frac{1}{n-1}\sum_{i=1}^{n}(x_i - m)^2$, where n is the number of data points and m is the mean. Here in this section, to avoid

confusion with the parameters in equation 3.8, mean and variance are represented by m and υ and summarized in Table 3.1. At U_g = 3 cm/s the size of bubbles exhibits a narrow distribution which indicates near uniform size in the column while in churn turbulent flow regime, at U_g = 45 cm/s, a wide bubble size distribution is observed.

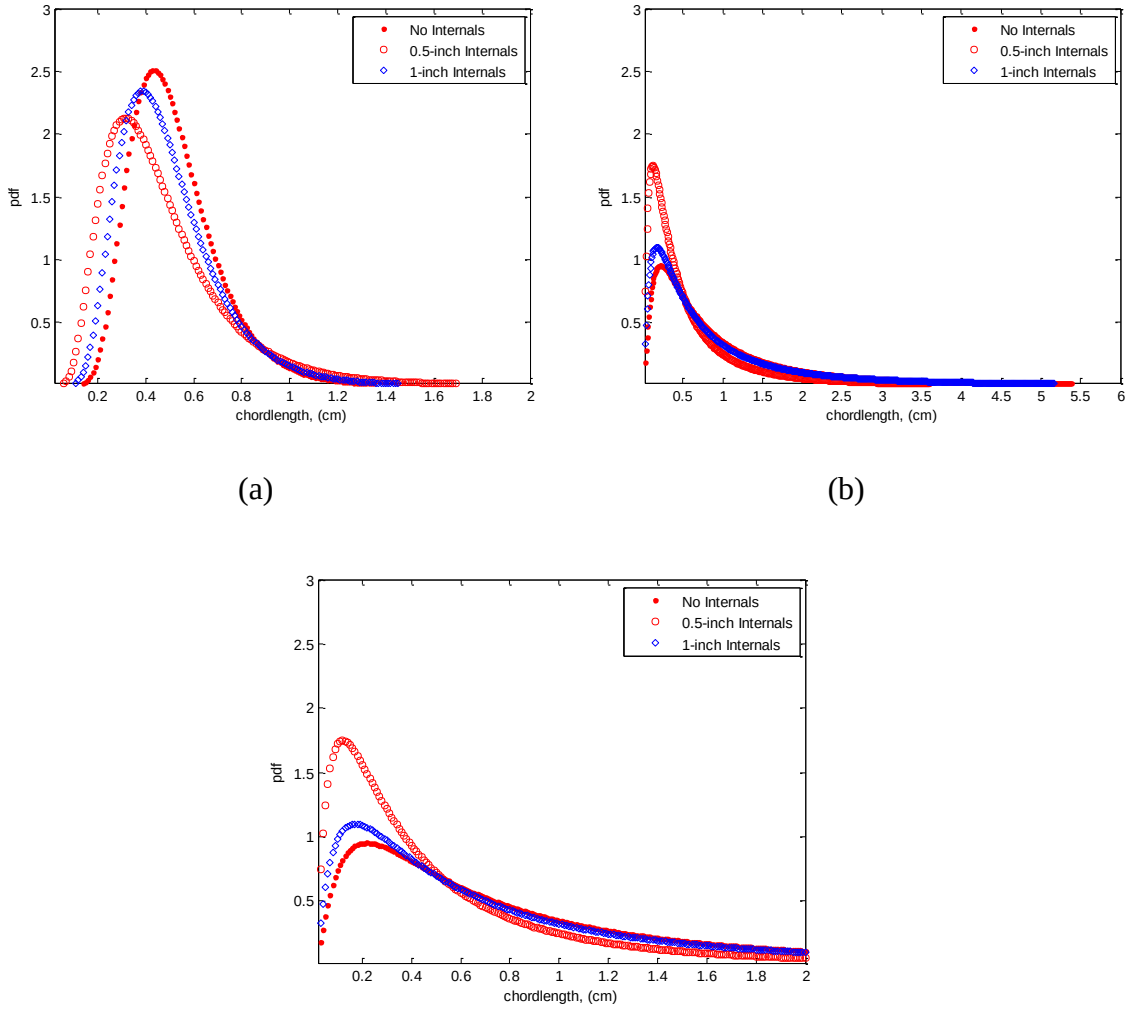

Figure 3.14 Effect of size of internals and configuration on the bubble chord length distributions at r/R(-) = 0.0, (a) at Ug = 3 cm/s based on free cross sectional area (b) at Ug = 45 cm/s based on free cross-sectional area (c) large-scale view of Figure(b), (Equation 3.8)

At low gas velocity, smaller bubbles with near uniform size form in the column and in this regime there is little or no coalescence hence a narrow size range while at high superficial gas velocity, there is enhanced bubble coalescence as well as bubble break-up which gives rise to larger bubbles as well as smaller ones. However the population of smaller bubbles has also been observed to increase significantly hence a wider range in distribution of the bubble sizes as evidenced from the mean and variance shown in Table 3.1. With 0.5-inch dense internals at low gas velocity (3 cm/s) at the column center, the chord length distribution exhibit lower mean value of 0.4730 cm as compared to 0.4946 cm of 1-inch diameter internals and 0.5182 cm for empty column. This finding suggests that the bubble size gets smaller when high density internals are used. Moreover, the mean chord lengths for the 1-inch internals and empty column cases are close to each other, implying that the effect of 1-inch internals is nearly negligible. Similar trends are also observed at the other radial locations. At high superficial gas velocity (45 cm/s), there is higher probability of getting smaller bubbles with dense internals than without internals. The probability increases further or at least shifts towards smaller values of chord lengths with 0.5-inch diameter internals relative to the 1-inch diameter internals.

This difference is attributed to much higher break-up rate enhancement with 0.5-inch internals than with 1-inch for similar reasons discussed in preceding sections. Similar observation was made by Youssef and Al-Dahhan, 2009. In the churn turbulent flow regime, the influence of dense internals on bubble sizes becomes less. From the mean of the chord lengths presented, it was found that an average decrease of 6 % is obtained with 0.5-inch internals at 45 cm/s while up to 12 % average increment is

obtained at 3 cm/s. This can be attributed to higher turbulence of the system brought about by the incoming gas where the breakage and coalescence of the bubbles is due to the churning of the system and the internals contribution becomes negligible.

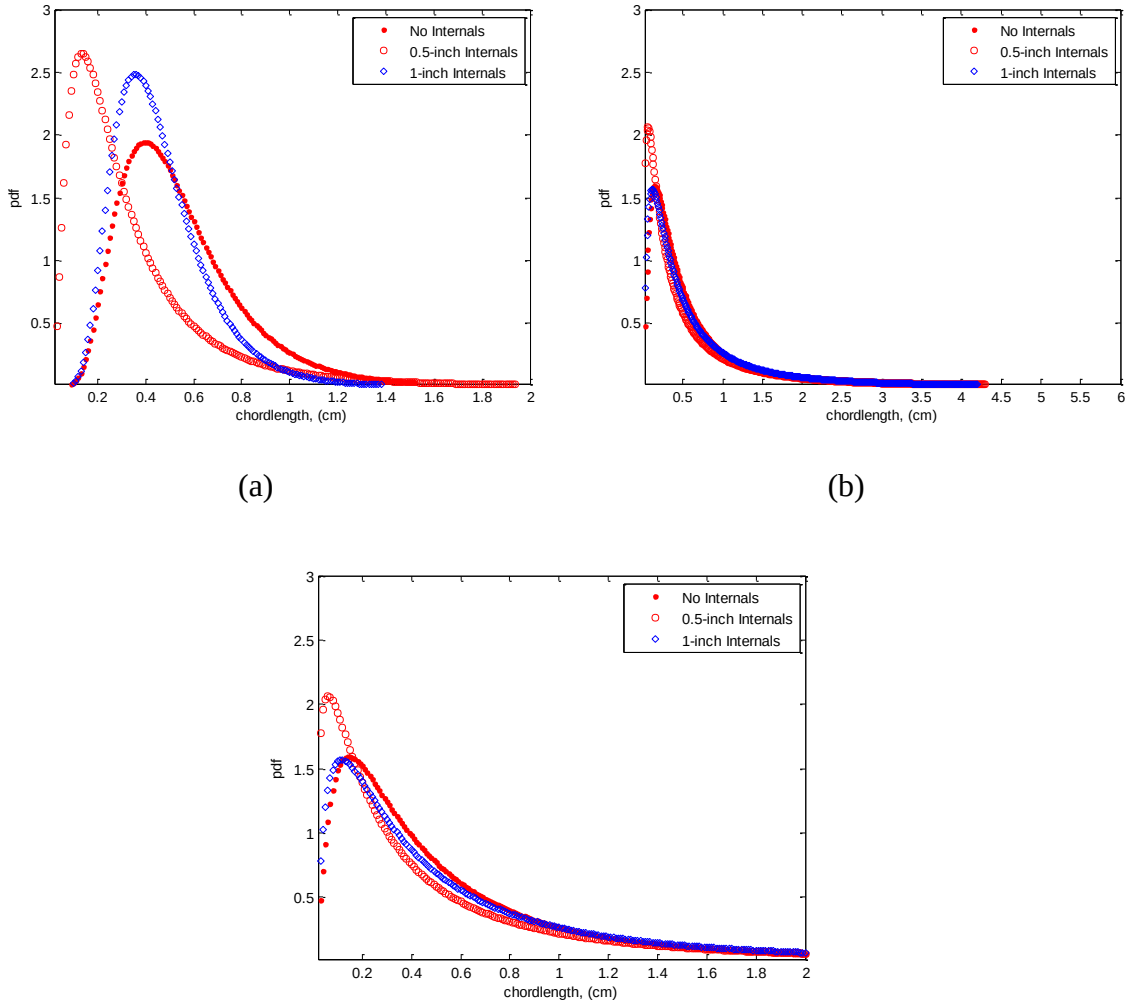

(a) (b)

(c)

Figure 3.15 Effect of size of internals and configuration on the bubble chord length distributions at r/R(-) = 0.5, (a) at Ug = 3 cm/s based on free cross-sectional area (b) at Ug = 45 cm/s based on free cross-sectional area (c) large-scale view of Figure(b), (Equation 3.8)

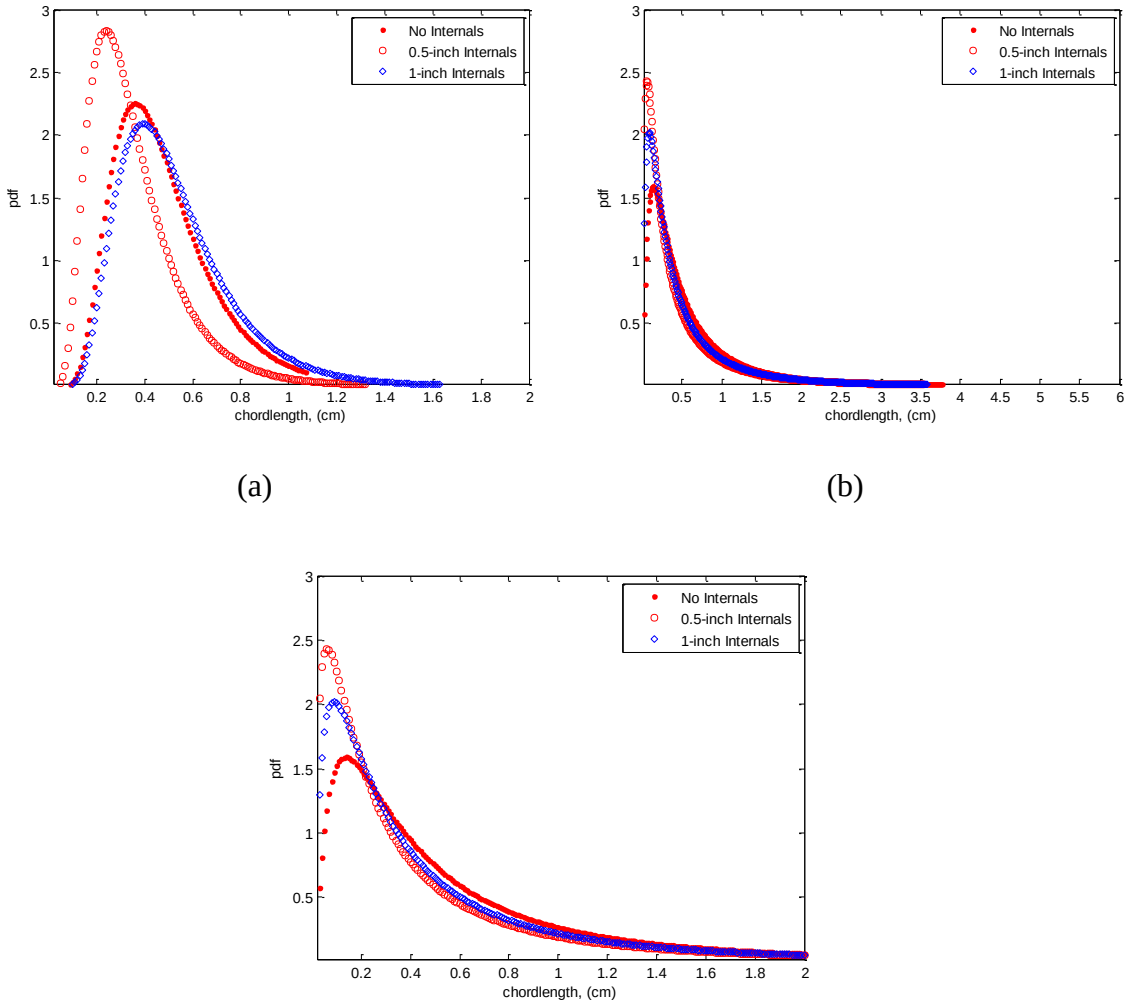

Figure 3.16 Effect of size of internals and configuration on the bubble chord length distributions at r/R(-) = 0.9, (a) at Ug = 3 cm/s based on free cross-sectional area (b) at Ug = 45 cm/s based on free cross-sectional area (c) large-scale view of Figure(b) (Equation 3.8)

Table 3.1 Statistical measures for the chord length distributions in 6-inch diameter column at different radial locations, with m and υ used in Equation 3.8

r/R(-) = 0.0				
	Ug = 3 cm/s		Ug = 45 cm/s	
	Mean (m)	Variance (υ)	Mean (m)	Variance (υ)
No Internals	0.5082	0.03941	0.8534	3.4010
0.5-inch Internals	0.4470	0.0369	0.8123	2.822
1-inch Internals	0.4746	0.0444	0.8466	3.3611
r/R(-) = 0.5				
	Ug = 3 cm/s		Ug = 45 cm/s	
	Mean (m)	Variance (υ)	Mean (m)	Variance (υ)
No Internals	0.4841	0.0841	0.7939	1.2717
0.5-inch Internals	0.3749	0.1301	0.8029	2.0185
1-inch Internals	0.4507	0.0565	0.8226	2.1087
r/R(-) = 0.9				
	Ug = 3 cm/s		Ug = 45 cm/s	
	Mean (m)	Variance (υ)	Mean (m)	Variance (υ)
No Internals	0.4250	0.0357	0.7252	1.0789
0.5-inch Internals	0.3971	0.0270	0.6099	1.3369
1-inch Internals	0.4398	0.0412	0.6421	1.1281

3.2.2.5. Axial bubble velocity. The quality of mixing in bubble and slurry bubble columns is governed by among other factors the gas phase residence time in bubble and slurry bubble columns. The residence-time and its distribution in the reactor must be

controlled so that the desired reactions go as far as possible without the occurrence of undesirable reaction(s) to significant levels, while at the same time ensuring large mass and heat transfer rates, high degree of mixing, complete suspension of the catalyst particles and high reactor productivity (Raje et al., 1997). Furthermore controlling the gas phase reactant residence time is essential in order to avoid a broad product spectrum. Since the velocity of the gas phase in the bubble column usually differs from the other phases (liquid/solids), the volumetric flow rate fraction of the gas phase is not equal to its corresponding holdup, and hence the slip velocity, U_s, between the gas and the liquid is introduced to account for this difference. According to Behkish, 2004, for a semi-batch process the slip velocity is given by

$$U_s = \frac{U_G}{\varepsilon_G} \tag{3.9}$$

The bubble velocity U_b, at any given location depends on mainly two factors: the local liquid velocity, U_l and the local slip velocity, U_s at that location, (Gupta, 1998 and Hamed, 2012).

$$U_b = U_l + U_s \tag{3.10}$$

Thus, not only operating variables such as superficial gas velocities, solid catalysts loading and physical properties of the liquid mixture but also design parameters such as internals presence, size and configurations affect the bubble velocity since the internals will alter the intensity of large-scale liquid recirculating velocity.

For consistency, the bubble velocity results are shown in terms of their distribution. In this work the axial bubble velocity was estimated from both the upward and downward bubble velocities at the same point. The downward bubble velocity was measured by flipping the optical fiber probe to face up while the upward bubble velocity

was measured by the probe facing downward. The probability density function (pdf) of the axial bubble velocity is then obtained by dividing the number of bubbles which have a particular velocity by the total number of bubbles that hit all the four tips of the optical fiber probe during the sampling period. Details of how the axial bubble velocities were obtained are given in Section 3.3.3.5. Figures 3.17 through 3.19 show the effect of internals size and configuration on the distribution of the axial bubble velocity in 6-inch bubble column at r/R(-) = 0.0 and at two other radial locations, with gas velocity based on the free cross-sectional area of the column at 3 cm/s and 45 cm/s. The axial bubble velocity distribution is analyzed further statistically by using the mean and variance of the distribution.

At Ug = 3 cm/s the 0.5-inch internals reduces the axial bubble velocity by ~ 20 % while the 1-inch internals gives a reduction of 10 % as reflected from the mean of the axial bubble velocity distribution in Table 3.2. This difference is attributed to larger space between the 1-inch internals relative to those of 0.5-inch internals. However in the churn turbulent flow regime (Ug = 45 cm/s) a relatively smaller decrease of about 6 % was observed with 0.5-inch internals and 1-inch internals. From the overall gas hold up and the local gas holdup radial profiles discussed earlier, there is a near match in column without internals and that with dense internals by applying gas velocity based on free CSA. Al-Mesfer, 2013 experimentally demonstrated that even though such similarity in both the overall and local gas holdup, (i.e radial profiles of local gas holdup) was attained; it is not possible to show similarity in the liquid recirculation velocity at such high gas velocities. This has been attributed to the non-similarity in the design and configuration between these columns (one without internals while the other with dense

internals) where smaller CSA available for flow in the column with internals than that without. Therefore, to maintain a mass balance of the batch operated liquid phase between the upward flow in the column central region and down flow at the column wall region while maintaining the same inversion point, the axial liquid velocity should increase with dense internals.

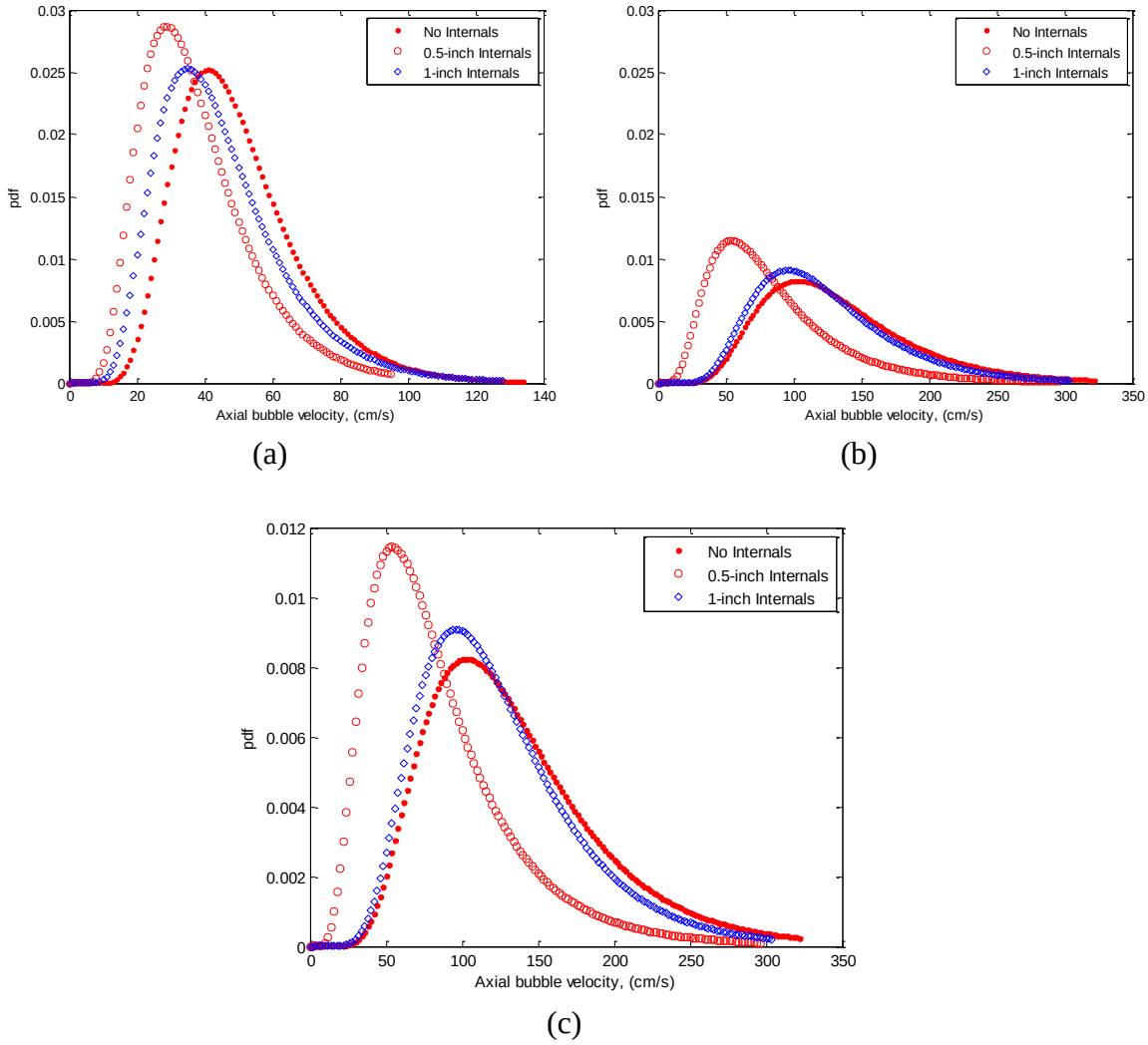

Figure 3.17 Effect of size of internals and configuration on the axial bubble velocity distributions at r/R(-) = 0.0 (a) Ug = 3 cm/s based on free cross-sectional area (b) Ug = 45 cm/s based on free cross-sectional area (c) Large-scale view of Figure(b)

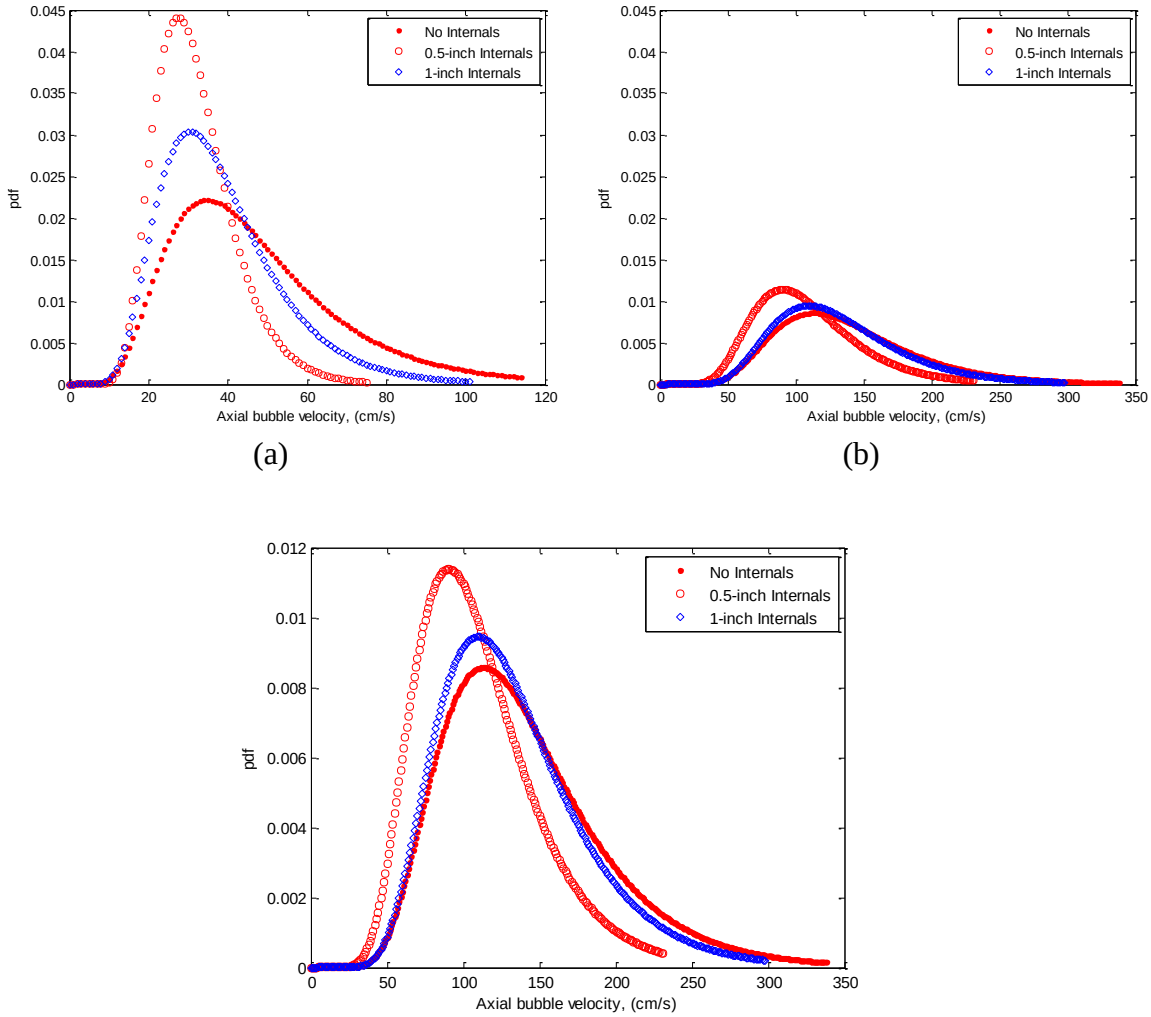

Figure 3.18 Effect of size of internals and configuration on the axial bubble velocity distributions at r/R(-) = 0.5 (a) Ug = 3 cm/s based on free cross-sectional area (b) Ug = 45 cm/s based on free cross-sectional area (c) Large-scale view of Figure(b)

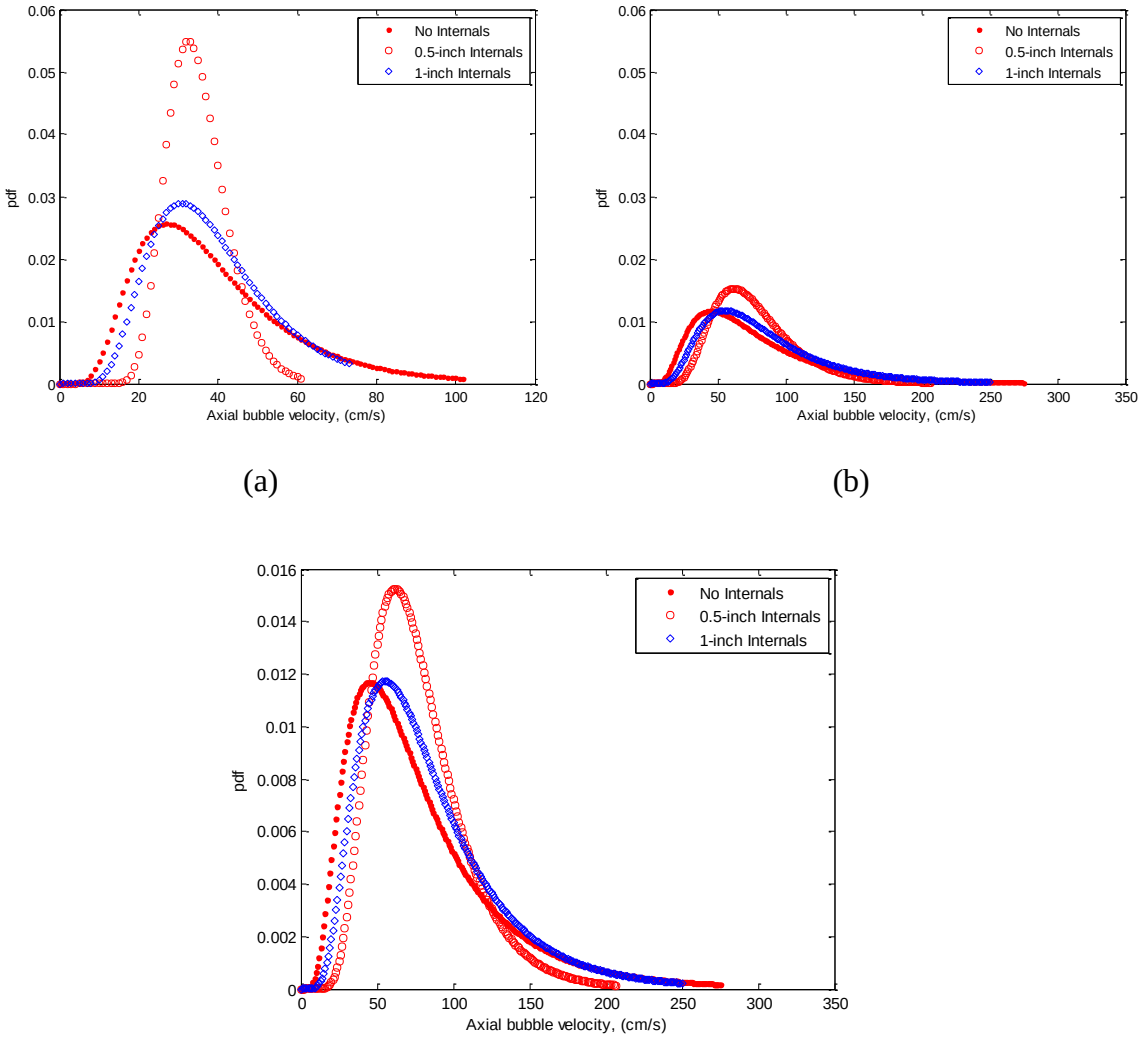

Figure 3.19 Effect of size of internals and configuration on the axial bubble velocity distributions at r/R(-) = 0.9 a) Ug = 3 cm/s based on free cross-sectional area (b) Ug = 45 cm/s based on free cross-sectional area (c) Large-scale view of Figure(b)

3.3. IMPACT OF SOLIDS LOADING AND DENSE INTERNALS ON BUBBLE PROPERTIES IN 6" AND 18" BUBBLE COLUMNS

3.3.1. Scope. In bubble and slurry bubble column reactors and contactors, the size of the solid particles ranges from 5 to 150 μm, with solids loading up to 50 % volume

(Krishna et al., 1997). The gas phase contains one or more reactants, while the liquid phase usually contains product and/or reactants and in some cases inerts. The solid particles are typically catalyst or the catalyst carrier. In the bubble and slurry bubble column reactors (B/SBCRs), momentum is transferred from the faster, upward moving

Table 3.2 Statistical parameters for the axial bubble velocity distributions 6-inch diameter column at different radial locations

r/R(-) = 0.0				
	Ug = 3 cm/s		Ug = 45 cm/s	
	Mean (m)	Variance (υ)	Mean (m)	Variance (υ)
No Internals	50.89	348.33	135.23	3724
0.5-inch Internals	38.36	314.94	125.47	2288
1-inch Internals	45.15	382.37	125.01	3002
r/R(-) = 0.5				
	Ug = 3 cm/s		Ug = 45 cm/s	
	Mean (m)	Variance (υ)	Mean (m)	Variance (υ)
No Internals	47.06	424.41	118.29	5291
0.5-inch Internals	40.34	105.99	110.34	1709
1-inch Internals	39.88	256.25	105.22	2471
r/R(-) = 0.9				
	Ug = 3 cm/s		Ug = 45 cm/s	
	Mean (m)	Variance (υ)	Mean (m)	Variance(υ)
No Internals	39.81	457.48	80.76	3079
0.5-inch Internals	34.91	59.38	77.95	1006
1-inch Internals	39.80	290.30	84.85	2363

gas phase to the slower liquid or slurry phase. The operating superficial gas velocity is in the range of 1-50 cm/s while the liquid superficial velocity in the range of 0 to 2 cm/s which is an order of magnitude lower than the superficial gas velocity. Hence, the hydrodynamics and transport in such reactors are mainly controlled by the gas flow.

One of the main disadvantages of bubble column reactors is significant back-mixing, which can reduce product conversion and selectivity, and also induce a broad product spectrum. The significant back-mixing requires to be reduced if not completely eliminated. Among the means of eliminating such problem is the reactor modification in the design of bubble column reactors; including the addition of internals and or baffles (Deckwer, 1991), or use of sieve plates (Maretto and Krishna, 2001).

The investigation of the impact of solids loading and dense internals is extremely useful. For one, the optimum amount of catalyst to be employed for maximum reactor performance is of particular interest. Pohorecki et al., 2001 observed that the bubble dynamics at conditions of industrial interest may show different behavior than at laboratory conditions. Thus, one needs to know in detail the fluid dynamics and mixing characteristics at the conditions similar to those of industrial interest, not only in laboratory scale systems of 6-inch diameter but also in pilot scale unit such as of 18-inch diameter. This can be achieved either by performing experiments at the industrial conditions using the real system or by mimicking the industrial system at laboratory operating conditions. With the latter option being more attractive due to limitations encountered in laboratory studies.

Glass beads with an average size of 150 μm and particle density of 2500 kg/m^3 were selected as the solids phase. The main reason was the fact that a few research have

been successfully done using 150 μm glass beads as the solids phase in slurry bubble column using an (air-water-glass beads system), (Rados, 2003, Wu, 2007), forming a basis for comparison. Besides the glass-beads are more safe to use and environmentally benign. The density of the glass beads is also close to the apparent density (density of solids filled with liquid in its pores) of FT catalyst, i.e., 2200 kg/m^3, which has a mean size of 70-90 μm, with 45 % of the solids 90 μm and above. Thus these glass beads present an opportunity to study the effect of non-porous solids close in density to that of FT catalyst that can provide a benchmark for future studies on porous FT catalyst.

3.3.2. Experimental System. The experimental set up and system used in this section is highlighted. The experimental set up is made up of 6-inch (0.14 m) diameter and 18-inch (0.44 m) diameter columns mounted with threaded ports to implement probe and sensor measurements. The heat flux and surface temperature sensor measurements will be discussed in Section 4. For the 6-inch diameter column, measurement conditions are the same as those described in Section 3.2.1. with 0.5-inch diameter Plexiglas rods as internals. A schematic diagram of the experimental system is shown in Figure. 3.20. The experiments in the 18-inch (Dc = 0.44 m) column were conducted in a pilot scale bubble column made of Plexiglas. The pilot scale had a 0.44 m inside diameter and 3.66 m height with dynamic bed height in all the experiments, maintained constant at a level of about 2.67 m (z/D = 6.0) above the gas distributor by adjusting the amount of liquid, and liquid-solids loaded in the column. In this study, compressed filtered oil-free dry air introduced continuously from the bottom of the column was used as the gas phase. Soft filtered tap water was used as liquid phase. Glass beads with an average size of 150 μm and density of 2500 kg/m^3 was used as the solids phase. The solids loading was based on

the wet volume and the concentrations varied between 0 % vol – 40 % vol in the 6-inch diameter column while 0 % vol – 25 % vol solids loading was used in the 18-inch diameter column because of large amounts of solids required for same % vol. and hence 40 % vol would be too much for 18-inch column.

A steel perforated plate with 241 holes of 3 mm diameter each, distributed in a square pitch and with a total free area of 1.09 % was used as the gas distributor. The superficial gas velocities were from 0.03 to 0.45 m/s based on the total cross-sectional area (CSA), (see additional results in appendix A) as well as free cross-sectional area. The free cross-sectional area was employed in this work for two main reasons. The first was to get the effect of dense internals only and not the effect of higher gas velocity inside the column where same mass flow rate of the column without internals is used in that with internals by using total cross-sectional area of the column. The second reason was to examine whether the column without internals, results can be extrapolated to the one with dense internals by matching the same gas velocity based on free cross-sectional area available for flow. The internals used in this study were vertical Plexiglas rods which occupy 25 % of the column cross-sectional area that simulates the Fischer-Tropsch synthesis process. The internals used in the 18-inch column were 1-inch in diameter. 0.5-inch diameter internals was chosen over the 1-inch diameter internals in the 6-inch column since the 0.5-inch internals have comparable intertube gaps to column diameter as the intertube gaps in the 1-inch diameter internals used in the 18-inch column as illustrated in Table 3.3. The details of the configurations of the internals used in 6-inch and 18-inch diameter columns are shown in Figure 3.21 while the photos of the bubble and slurry bubble columns used in this work are shown in Figure 3.22.

Combined measurements technique comprising an advanced heat transfer probe and four-points optical probe was used to simultaneously measure the local heat flux and the local bubble properties, including local gas hold up, bubble passage frequency, axial bubble velocity, specific interfacial area, as well as the bubble chord lengths which is characteristic of bubble sizes. However in this section only the bubble properties are reported, while the heat transfer coefficient results will be discussed in Section 4. The local measurements by the probe were taken at seven dimensionless radial positions; r/R (-) = 0.0, ± 0.3, ± 0.6, ± 0.9. Since there was near axis-symmetry, only results on one half (+ r/R) have been reported. Similarly local measurements by the probe were taken in 6-inch column at five dimensionless radial positions; r/R (-) = 0.0, ± 0.5, ± 0.9, and in some cases including r/R = ± 0.3 but only results on one half (+ r/R) have been reported. Due to the smaller nature of the column, fewer radial positions of measurements were taken in the 6-inch column, though it is still possible to get measurements at more radial points. Table 3.4 shows the selected experimental conditions for both the 6-inch and 18-inch diameter columns whose results are reported here in Section 3.3.3

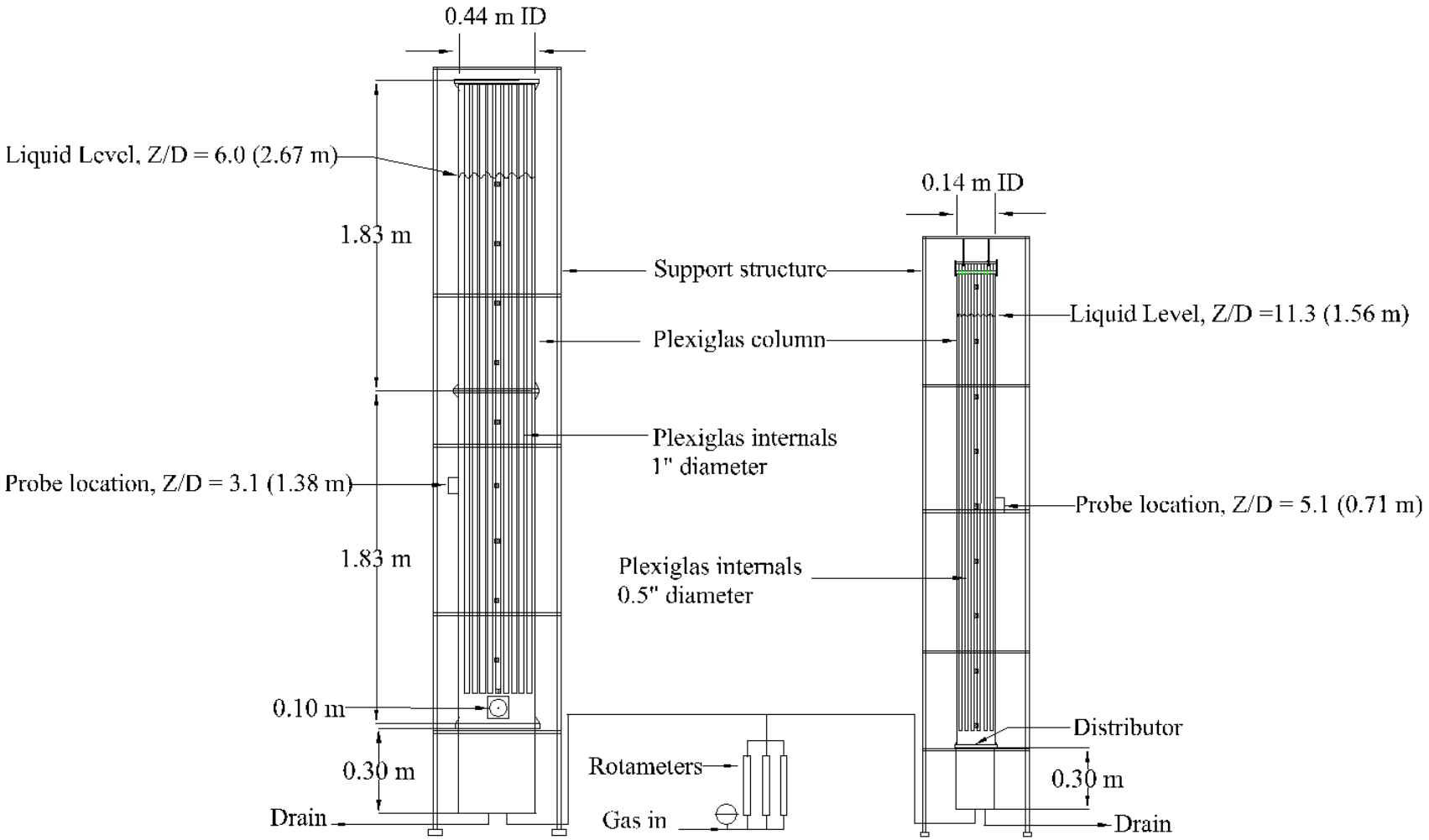

Figure 3.20 Schematic diagram of the pilot plant experimental setups (Not drawn to scale)

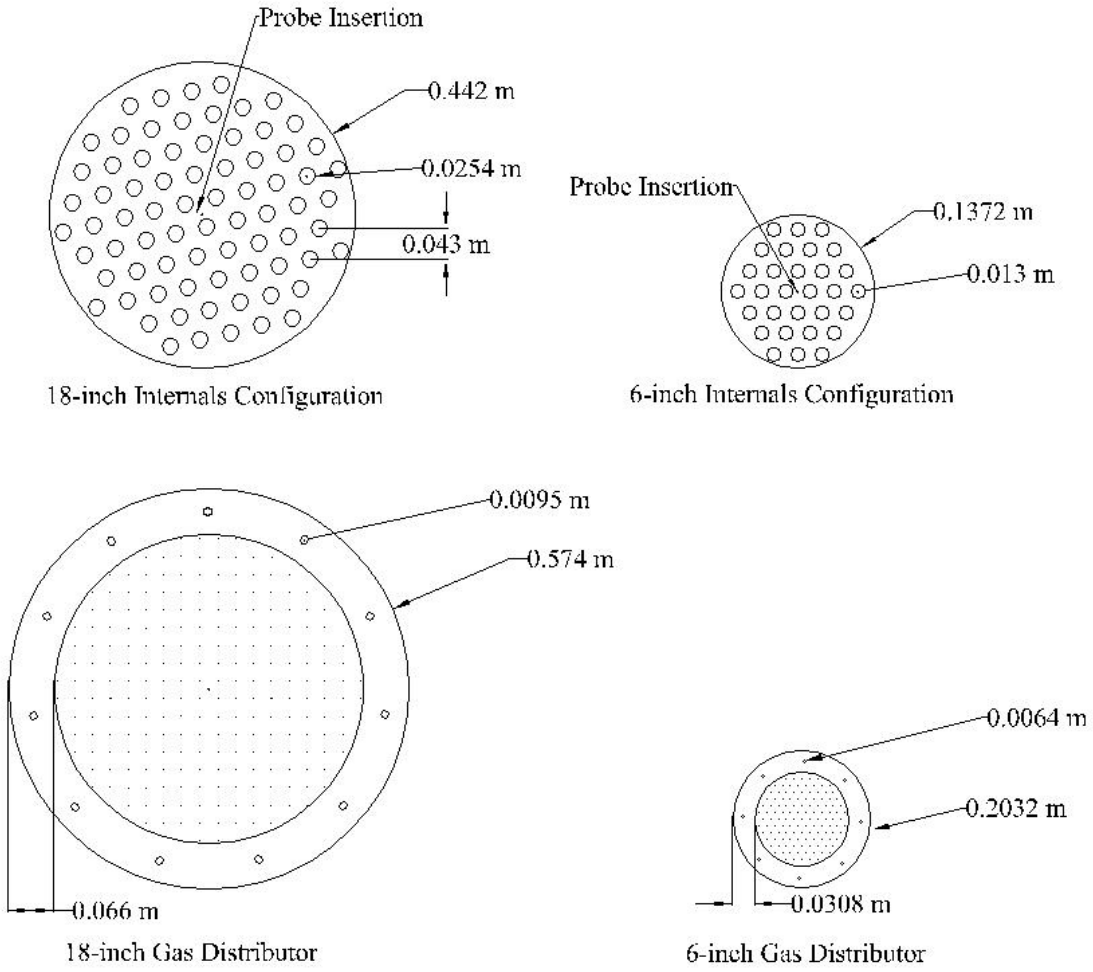

Figure 3.21 Dense internals configuration and details of gas distributor for both 6-inch and 18-inch diameter columns.

Table 3.3. Internals size selection in 6-inch column for comparison in 18-inch column

Column diameter (D_c)	Tube diameter (t_D)	Inter-tube gap (t_R)	t_R/ D_c
14 cm	1.27 cm	0.60 cm	0.0430
	2.54 cm	1.22 cm	0.0873
44 cm	2.54 cm	1.60 cm	0.0360

(a) (b)

Figure 3.22 Experimental setup photos (a) 18-inch diameter column no internals (b) 18-inch with dense internals (left) and 6-inch column with dense internals

3.3.3. Results and Discussion. In this section, the effects of solids loading and dense internals, occupying 25 % of the cross-sectional area on bubble dynamics is highlighted for two pilot scale bubble columns 6-inch and 18-inch in diameters. The measurement technique and algorithm is the same as detailed in Section 3.1.1.

Table 3.4 Experimental conditions for impact of solids and dense internals on bubble dynamics for 6-inch column and 18-inch column

Column diameter (m)	Radial location r/R (-)	Internals (% CSA)	Solids loading (% vol.)
Dc = 0.14	r/R (-) = 0.0, ± 0.5, ± 0.9	0.0	0.0
	r/R (-) = 0.0, ± 0.5, ± 0.9	25 %	0.0
	r/R (-) = 0.0, ± 0.5, ± 0.9	0.0	9.1 %
	r/R (-) = 0.0, ± 0.5, ± 0.9	25 %	9.1 %
	r/R (-) = 0.0, ± 0.5, ± 0.9	0.0	25 %
	r/R (-) = 0.0, ± 0.5, ± 0.9	25 %	25 %
	r/R (-) = 0.0, ± 0.5, ± 0.9	0.0	40 %
	r/R (-) = 0.0, ± 0.5, ± 0.9	25 %	40 %
Dc = 0.44	r/R (-) = 0.0, ± 0.3, ± 0.6, ± 0.9	0.0	0.0
	r/R (-) = 0.0, ± 0.3, ± 0.6, ± 0.9	25 %	0.0
	r/R (-) = 0.0, ± 0.3, ± 0.6, ± 0.9	0.0	25 %
	r/R (-) = 0.0, ± 0.3, ± 0.6, ± 0.9	25 %	25 %

3.3.3.1 Local gas holdup and overall gas holdup. As mentioned earlier, gas holdup is one of the most important operating parameters because it not only governs phase fraction and gas-phase residence time but is also crucial for mass transfer between liquid and gas. Gas holdup depends chiefly on gas flow rate, but also to a great extent on the gas-liquid or gas-liquid-solids system involved. Figure 3.23 shows the effect of solids

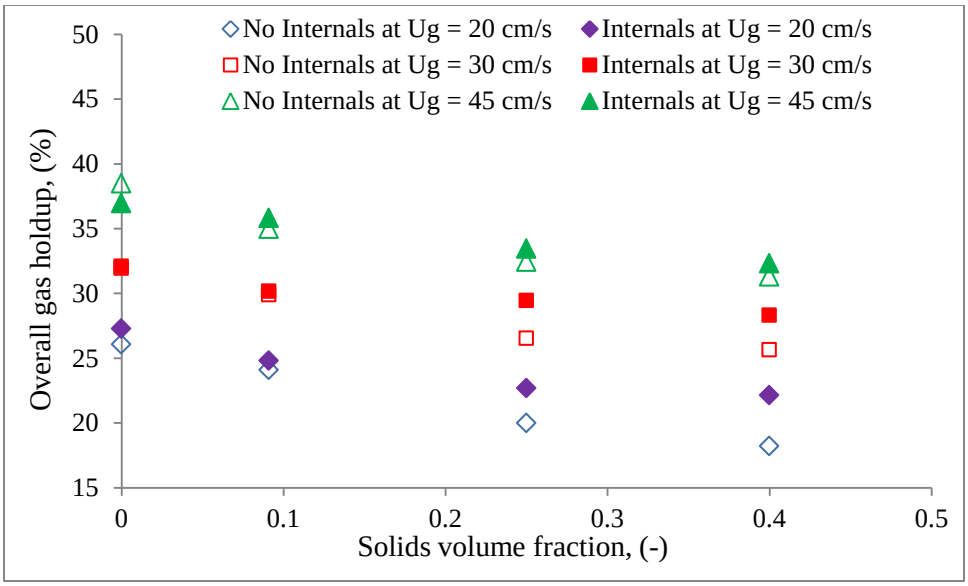

(a)

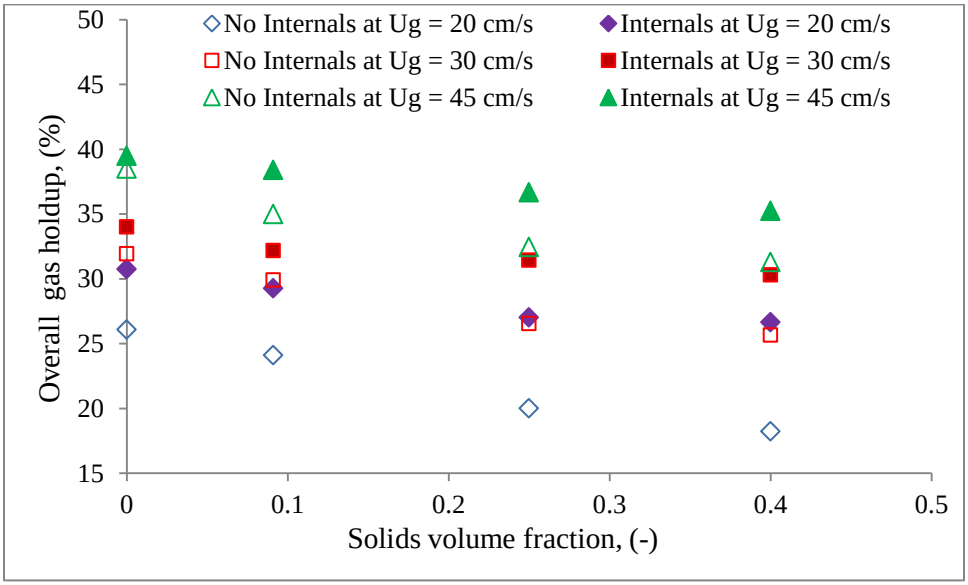

(b)

Figure 3.23 Effect of solids loading, dense internals and superficial gas velocity on overall gas holdup (a) Based on free cross-sectional area (b) Based on total cross-sectional area

loading and presence and absence of dense internals on overall gas holdup for different gas velocities in 6-inch diameter column, while Figure 3.24 illustrates the effect of solids

loading and presence of dense internals on local gas holdup at different gas velocities at the center (r/R = 0.0) of 6-inch diameter column. A comparison is also made when the Ug is based on free cross-sectional area and when the Ug based on total cross-sectional area of the column.

It is clearly noticed that the gas holdup is increased with increasing superficial gas velocity for all solids concentration. With increasing Ug from 20-45 cm/s, an increase of 40 % in overall gas holdup in empty column with no solids but up to 60 % increase is realized when 40 % vol solids are used. With dense internals, an increase in gas velocity from 20 – 45 cm/s based on free cross-sectional area leads to an increase in overall gas holdup by 35 % at no solids and up to 40 % when 40 % vol solids are used. This increase is due to increment in number of bubbles with increasing gas flow rate as determined by Youssef and Al-Dahhan, 2009 and Chen et al., 1999. They argued that with increasing superficial gas velocity the bubbles coalescence is enhanced, leading to a growth in number of large bubbles while at the same time the break-up rate also goes up giving rise to many smaller bubbles.

When dense internals are used and Ug = 20 cm/s based on free cross-sectional area, a 3 % increase in overall gas holdup is realized at 9.1 % volume solids or no solids and up to 20 % increase is obtained for 25 % volume solids or more. While the dense internals and at Ug = 45 cm/s based on free cross-sectional area, leads to less than 3 % increase in overall gas holdup at all the solids loading. When Ug = 20 cm/s based on total cross-sectional area, the dense internals increases the overall gas holdup by 15 % at no solids or low solids loading (9.1 % vol solids) and up to 40 % at higher solids loading, (40 % vol solids). However, 3 % and 10 % increase in overall gas holdup is attained at

low (9.1 % vol solids) or no solids and at higher solids loading, (40 % vol solids) respectively at 45 cm/s based on total cross-sectional area.

On the other hand, it was found that the local gas holdup decreases with increase in the solids loading. This can be attributed to increased pseudo-slurry viscosity, which promotes coalescence of large bubbles (Crabtree and Bridgewater, 1971, Li and Prakash, 1997), whereas the bubble break-up rate decreases due to dampening of instabilities at bubble-liquid interface. In addition, the possibility of formation of smaller bubbles which lead to the increase in the rise velocity and reduce the residence time of the bubbles as a result the gas holdup would be reduced (Kara et al., 1982; Koide et al., 1984; Li and Prakash, 1987, and Saxena et al., 1989). The presence of dense internals, that occupy 25 % of the column CSA, leads to general increase in the local gas hold-up regardless of the solids loading. This trend is due to the enhancement of bubble brake up which yields relatively smaller bubbles, with higher bubble passage frequency and lower velocity hence higher residence time in the column and enhanced gas holdup. Similar reasoning was also advanced by Youssef and Al-Dahhan, 2009. However the effect of internals on gas holdup starts to diminish at gas velocities ≥30 cm/s. With solids, effect of internals is more pronounced compared to without solids as earlier discussed.

Figure 3.25 shows the radial profiles of gas holdup in 18-inch bubble column for the systems of air-water and air-water-glass beads without internals and with dense internals at Ug = 30 cm/s (Figure 3.25a) and at Ug = 45 cm/s (Figure 3.25b). The gas holdup is high in the center and low near the wall of the column as seen from in Figure 3.25, with the slope increasing continuously towards the column wall. With no solids and

without internals, the slope of the gas holdup radial profile at the column wall region, (r/R≥0.6) is up to 5.4 times that at the column center region (r/R≤ 0.3) at Ug = 45 cm/s.

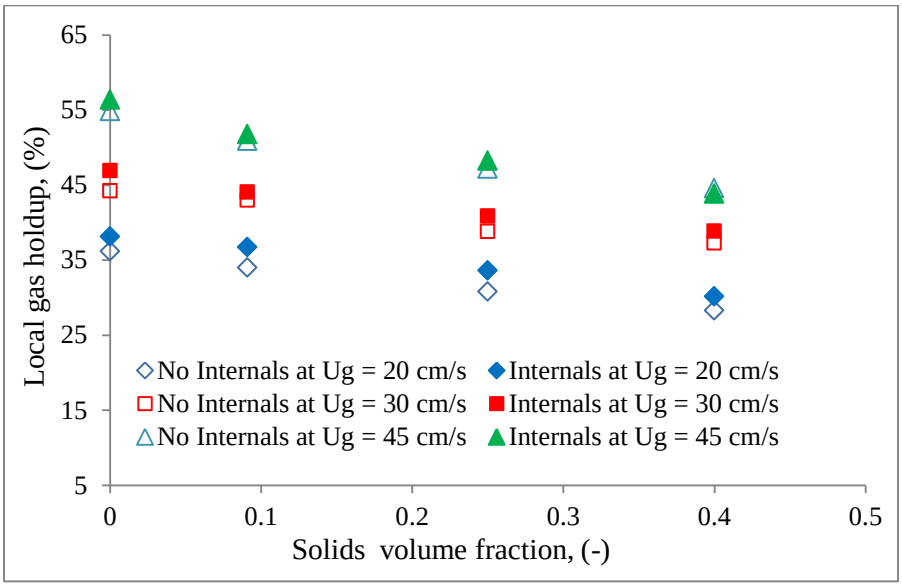

(a)

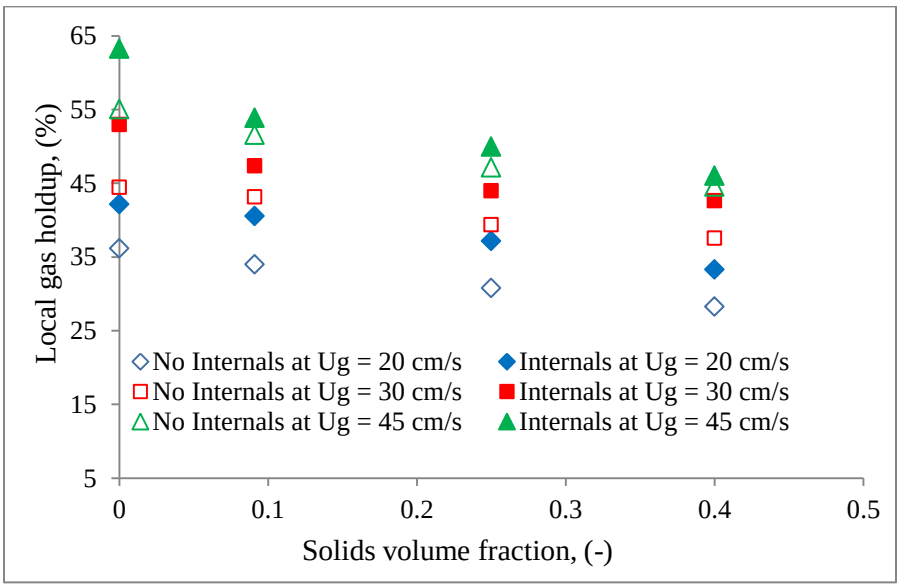

(b)

Figure 3.24 Effect of solids loading, dense internals and superficial gas velocity on local gas holdup in 6-inch diameter column at r/R(-) = 0.0. (a) Based free cross-sectional area (b) Based on total cross-sectional area

With dense internals and no solids, the slope at r/R≥0.6 is 8 times that at the column center region at r/R≤ 0.3 at the same Ug 45 cm/s. When 25 % vol solids are used, without internals, the slope of the gas holdup radial profile at the column wall region, (r/R≥0.6) is about 5 times that at the column center region (r/R≤ 0.3) at Ug = 45 cm/s. While with the dense internals the slope at r/R≥0.6 is 7.2 times that at the column center region at r/R≤ 0.3 at the same Ug. This kind of holdup distribution in the bubble column does not contradict the results obtained by CT scans in smaller diameter bubble columns (Kumar, 1994, Kumar et al., 1995, 1997, Rados, 2003) and also confirmed by other measurements obtained by Menzel et al., 1990; Franz et al., 1984; Goren et al., 1996, and Hebrard et al., 1996. Large bubbles are formed when solids are used due to increased pseudo-slurry viscosity than that of pure water, thus the gas holdup in the air- water-glass beads system without and with dense internals is lower than that in the air-water system. It is also noted that the high solids used does not have significant change on the steepness of the radial gas holdup. Rados, 2003 using the same type of glass beads as used in the current work observed from the CT scans that even-though there was a decrease in radial profiles of gas holdup with increased solids loading up to 35 % by weight, the steepness of the radial profiles only had slight decrease. Han, 2007 observed that the FT catalyst was found to exhibit significant differences from the 150 μm glass beads in profiles of gas holdup, solids velocity, and turbulence parameters which were reported by Rados, 2003.

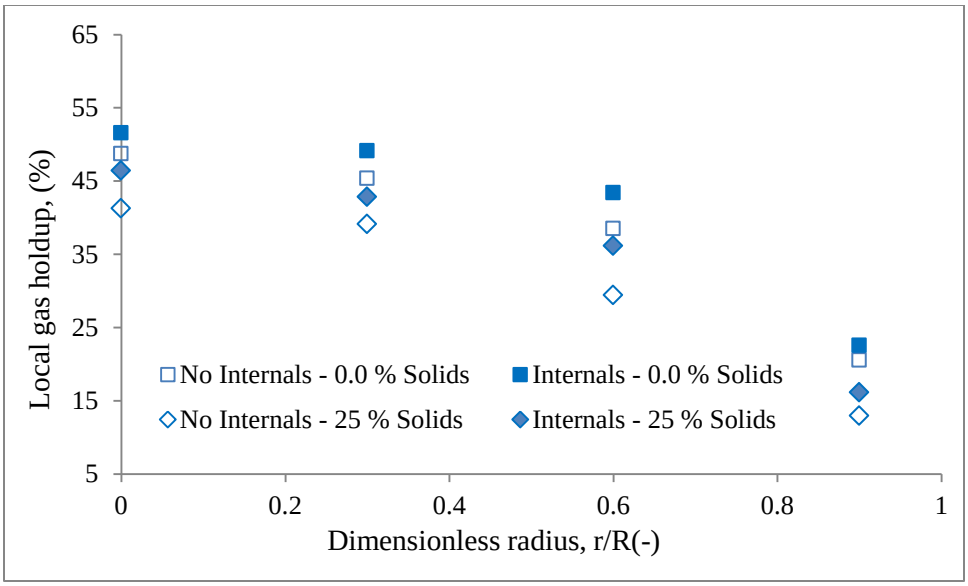

(a)

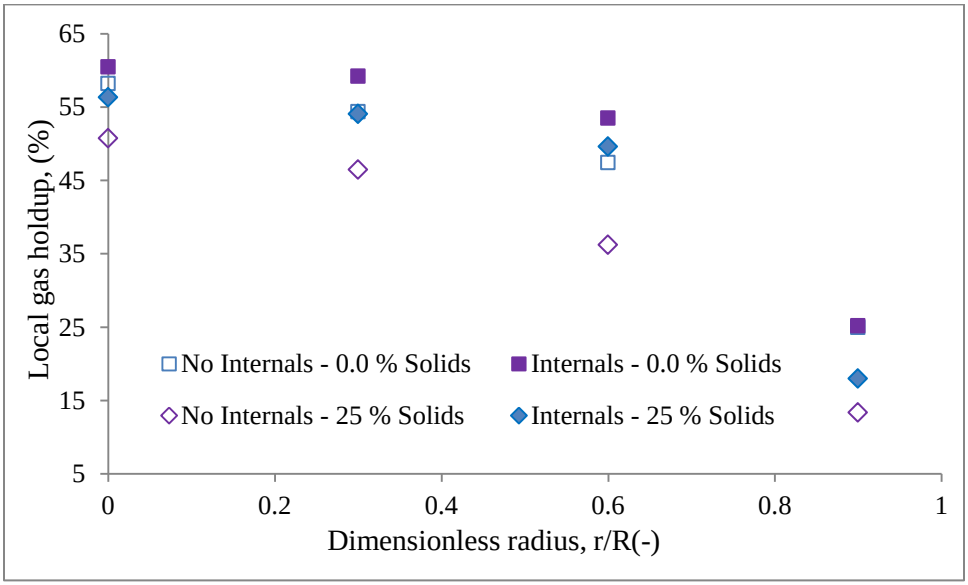

(b)

Figure 3.25 Effect of solids loading and dense internals on radial profiles of local gas holdup in 18-inch diameter column with Ug based on the free cross-sectional area at (a) Ug = 30 cm/s and (b) Ug = 45 cm/s

However the use of dense internals leads to increased steepness of the radial gas holdup profiles regardless of the solids loading. As discussed above, gas holdup in a

bubble column is high in the center and low at the wall and this leads to a gross liquid circulation throughout the column with liquid flowing up in the center and down near the wall. This kind of flow behavior was also demonstrated by Chen et al., 1999.

It has been observed that the difference in the radial local gas holdup is the driving force behind the large-scale liquid recirculation, (Chen et al., 1999, Forret et al., 2003). Thus the presence dense internals would lead to higher large-scale liquid recirculation velocity while the glass bead solids may not have profound effect on the large-scale liquid recirculation velocity, as there is little change on the driving force. As will be discussed in Section 4, the solids loading effect on the heat transfer could be due to a number of factors, including its role on determining the bubble sizes, frequency, bubble velocity and holdup. Finally the local and overall gas holdup studied in empty columns can be extrapolated to columns with dense internals in 6-inch at no and low (9.1 % vol) solids loading or at Ug $\geq$ 30 cm/s. However this extrapolation is not possible for 18-inch diameter column.

3.3.3.2 Specific interfacial area. As mentioned earlier the knowledge of mass transfer rates in bubble columns is essential for determining the maximum overall rates that can be supported in the heterogeneous flow regimes of operating bubble columns, which is of commercial interest. The overall volumetric gas-liquid mass transfer coefficient, k_La is the limiting thus an important design parameter for bubble columns, particularly in processes that involve the absorption of gases in organic liquids such as methanol synthesis and the F-T process which are at the core of this study. Thus it is necessary that the specific interfacial area a, be determined in order to obtain the liquid side volumetric mass transfer coefficient. Even though the gas-liquid interfacial area has

been a subject of studies in the past decades giving rise to dozens of publications, the influence of solids loading and the effect of dense vertical cooling internals on specific interfacial area is still missing in the open literature, particularly in the flow regime of commercial interest.

Figure 3.26 illustrate the effect of solids loading on the profiles of specific interfacial area at different gas velocities with and without dense internals in a 6-inch bubble column. It is obviously noticed that specific interfacial area decreases with increasing solids loading, a trend that is similar to that of local gas holdup as expected. For the three cases of superficial gas velocity presented, (Figure 3.26), similar trends have been noted. When 9.1 % vol solids are used without internals, a decrease of 8 % in interfacial area is attained while 11 % decrease is noted when dense internals area used at Ug = 45 cm/s based on free CSA. At higher solids loading, 40 % vol. a decrease of 18 % is obtained in empty column but up to 21 % decrease in interfacial area is attained in the presence of dense internals. The observed decrease is due to an increase in bubble coalescence, where larger bubbles are formed which give rise to a decreased specific interfacial area per unit volume hence the decrease in total interfacial area (Zahradnick et al., 1992). Thus the large coalesced bubbles have a lower interfacial area per unit volume.

It is noteworthy that increasing the superficial gas velocity leads to dramatic increase in the bubble coalescence rate. But the breakup rate of these larger bubbles also significantly increase, thus, the population of smaller bubbles increase faster than those of large bubbles, leading to increased interfacial area with superficial gas velocity.

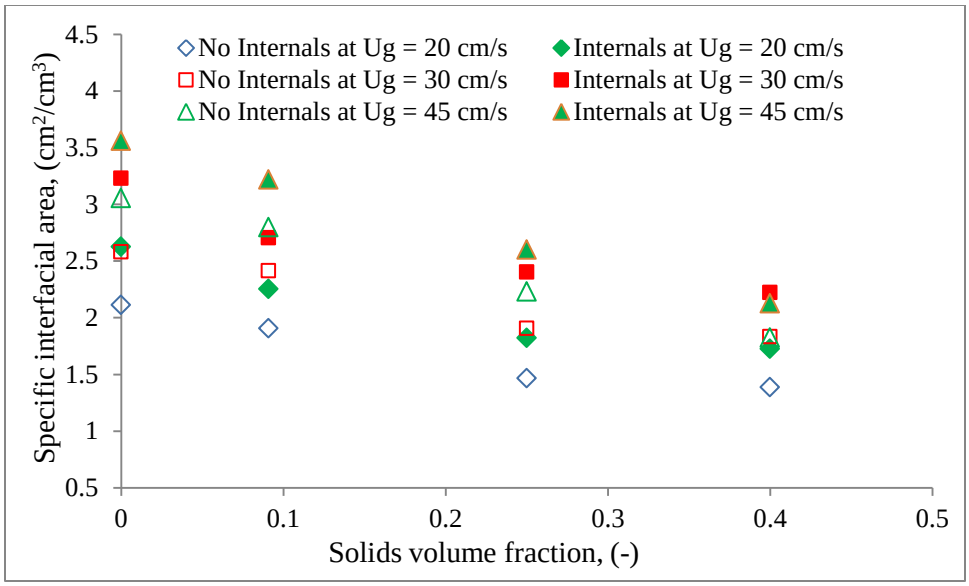

(a)

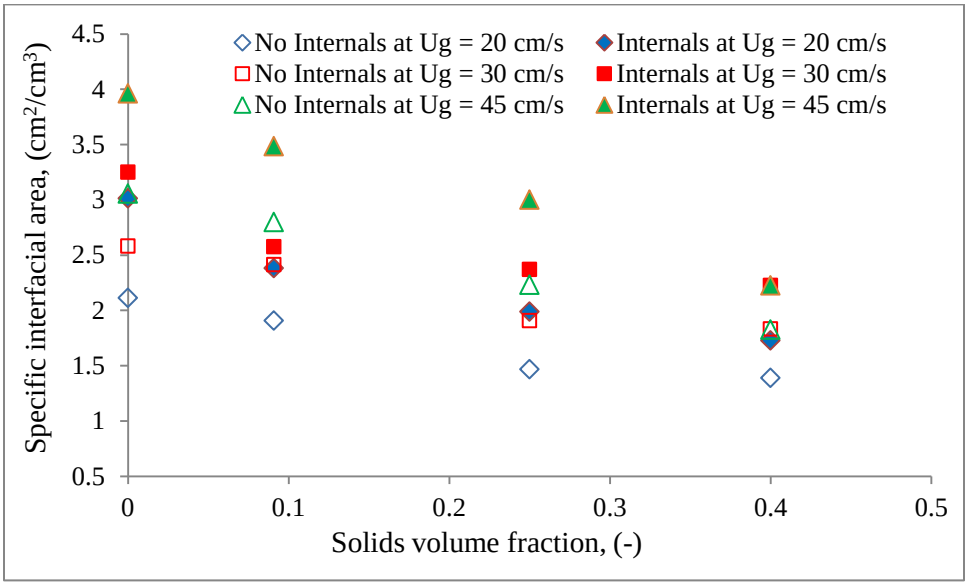

(b)

Figure 3.26 Effect of solids loading, dense internals and superficial gas velocity on specific interfacial area in 6-inch column at r/R = 0.0. (a) Based on free cross-sectional area (b) Based on total cross-sectional area.

For instance, increasing gas velocity from 20 cm/s to 45 cm/s in empty column leads to an increase in specific interfacial area by 40 % at no solids to 30 % with high solids

loading (40 % vol solids). In the presence of dense internals, same increase in Ug leads to an increase in the interfacial area by 35 % at no solids and 22 % at high solids loading. Therefore the effect of superficial gas velocity is more pronounced in the empty column regardless of the solids use. The presence of dense internals was found to increase the specific interfacial area for all the gas velocities regardless of solids loading. An average increase of 23 % is attained with internals at Ug = 20 cm/s and average increase of 16 % is attained at Ug = 45 cm/s based on free CSA. This could be attributed to the reduction in bubble sizes, and restricted formation of larger bubbles. Hence, many smaller bubbles appear in the column which have higher interfacial area in a unit volume hence a higher specific interfacial area per unit volume.

The effect of dense internals and high solids loading, (25 vol %) on the radial profiles of the specific interfacial area in the 18-inch column is shown in Figure 3.27. It is noted that at high solids loading the interfacial area remains higher in the center of the column and lower at the wall region. With dense internals up to 30 % and 20 % decrease in interfacial area is achieved in the column center and column wall region, respectively. While between 35 % and 17 % decrease is obtained in empty column at the same radial locations. On the other hand, little or no effect of internals in the wall region without solids but up to 16 % increase in interfacial area is achieved at the column center with no solids. With 25 % vol solids loading, again the effect of internals is up to 15 % higher in the wall region and 10 % in the column center.

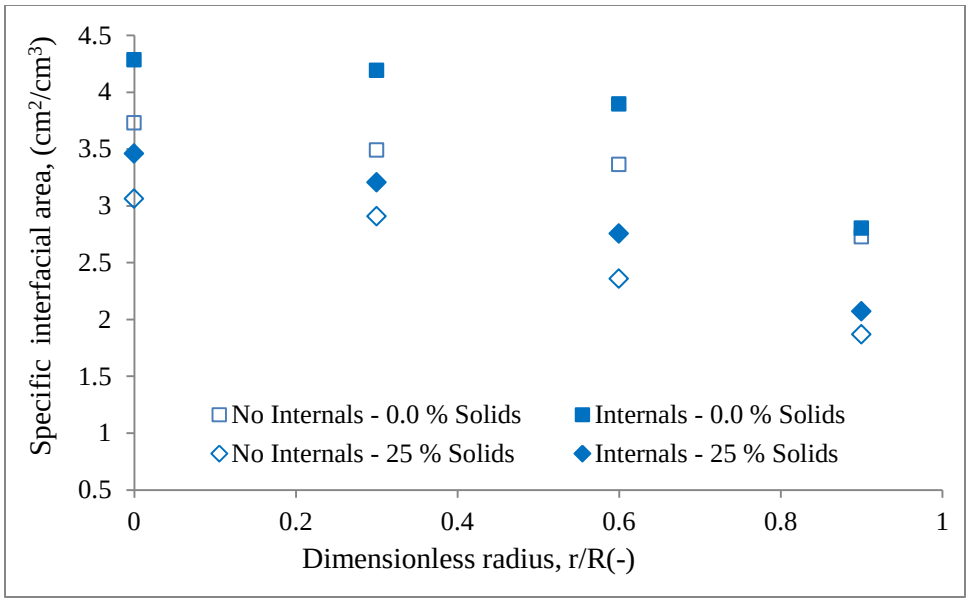

Figure.3.27 Effect of solids loading and dense internals on radial profiles of specific interfacial area in 18-inch column at Ug = 30 cm/s based on the free cross-sectional area

3.3.3.3 Bubble passage frequency. Bubble passage frequency is a count of the number of bubbles that pass through a given space in the duration of sampling. It is obtained by dividing the number of bubbles that hit the fiber probe's central tip by sampling time. Figure 3.28 shows the influence of solids loading and dense internals on the bubble passage frequency in the 6-inch pilot scale bubble column. While bubble coalescence and breakup play a significant role in determining gas holdup, bubble size and the size distribution, gas-liquid interfacial area, bubble velocity and the distribution which govern the performance of gas-liquid contractors. Thus the bubble breakup and coalescence is responsible for the bubble passage frequency across the column cross-section and thus have effect not only on the mass transfer but on the heat transfer as well.

Thus the use of solids and internals as has been demonstrated in the previous sections will have profound effect on the bubble passage frequency.

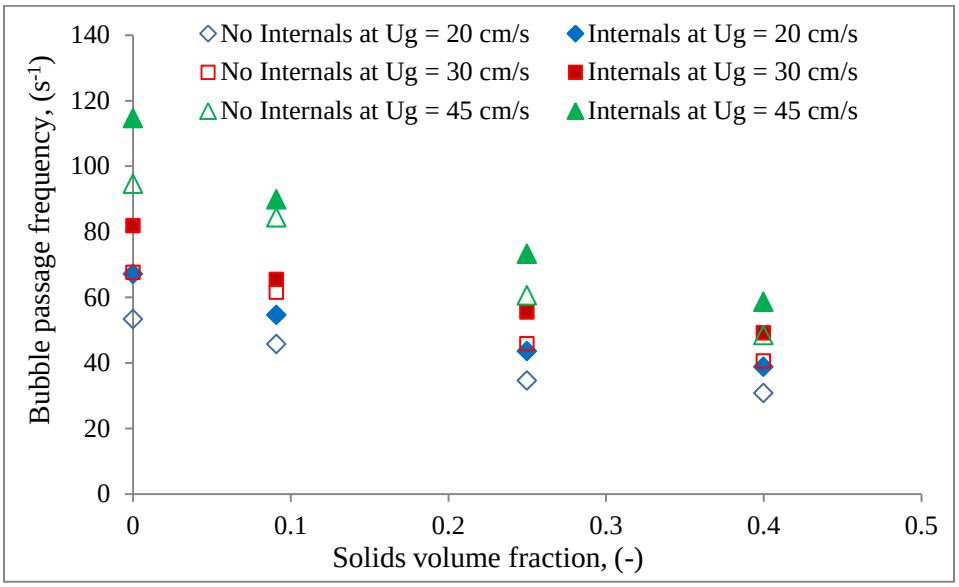

(a)

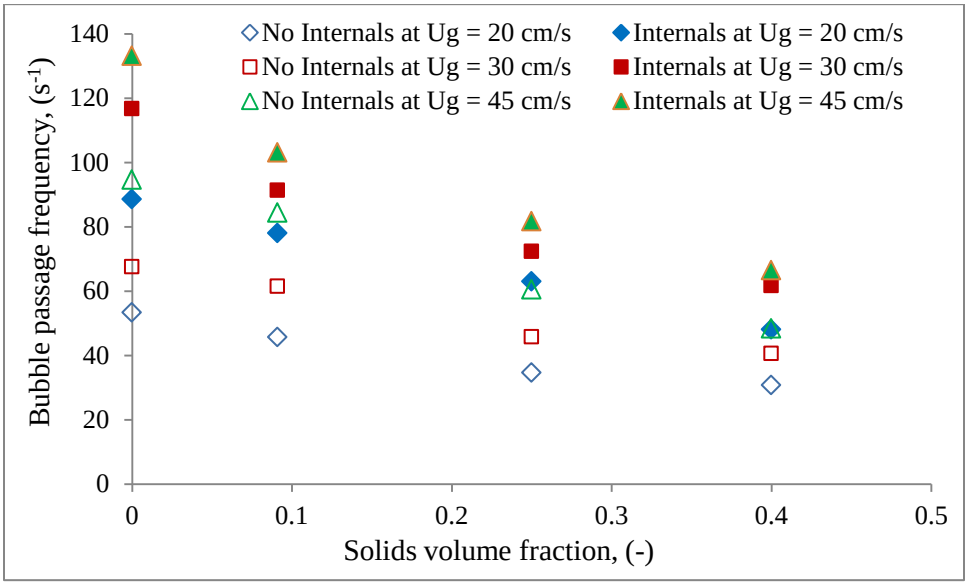

(b)

Figure 3.28 Effect of solids loading, dense internals and superficial gas velocity on bubble passage frequency at column center, r/R = 0.0 with superficial gas velocity (a) Based on free cross-sectional area and (b) Based on total cross-sectional area

When 9.1 % vol solids are used without internals, a decrease of 10 % in bubble passage frequency is attained while 21 % decrease is noted when dense internals are used at Ug = 45 cm/s based on free CSA. At higher solids loading, (40 % vol.) a decrease of 18 % is obtained in empty column but up to 21 % decrease in interfacial area is attained in the presence of dense internals. The observed decrease can be attributed to fewer bubbles resulting from the enhanced coalescence of the bubbles. The high solids loading enhances the bubble coalescence and reduces the bubble breakup rate which leads to a lower number of bubbles in a space, hence the observed decrease bubble passage frequency with solids loading. This is consistent with the interfacial area and the gas holdups presented and explained before.

With increased superficial gas velocity, the bubble population is dramatically increased. This leads to higher bubble passage frequency. Increasing superficial gas velocity from 20 cm/s to 45 cm/s in empty column leads to an increase in bubble passage frequency by 75 % at no solids and 55 % with high solids loading (40 % vol solids). In the presence of dense internals, similar increase in Ug leads to an increase in bubble passage frequency by 70 % at no solids and 43 % at high solids loading. Again it is noted that the effect superficial gas velocity is more pronounced in the empty column regardless of the solids use. When the column is inserted with dense internals the bubble passage frequency is enhanced for all the gas velocities regardless of solids loading. With an average increase of 24 % is at Ug = 20 cm/s and an average increase of 17 % is attained at Ug = 45 cm/s based on free CSA. When the column is inserted with the dense internals, the maximum bubble sizes which can be formed is restricted by the tubes, thus more smaller bubbles appear in a unit space, regardless of the solids loading.

The radial profiles of bubble passage frequency in 18-inch column and the effect solids loading and dense internals is shown in Figure 3.29. The local gas holdup, specific interfacial area and bubble passage frequency have similar distribution with and without internals, irrespective of solids use. While the large bubbles move towards the column center, they entrain with them smaller bubbles that also move at averagely the same bubble velocity as large ones. However, mainly small bubbles tend to enter the wall zone and move with the downward liquid flow.

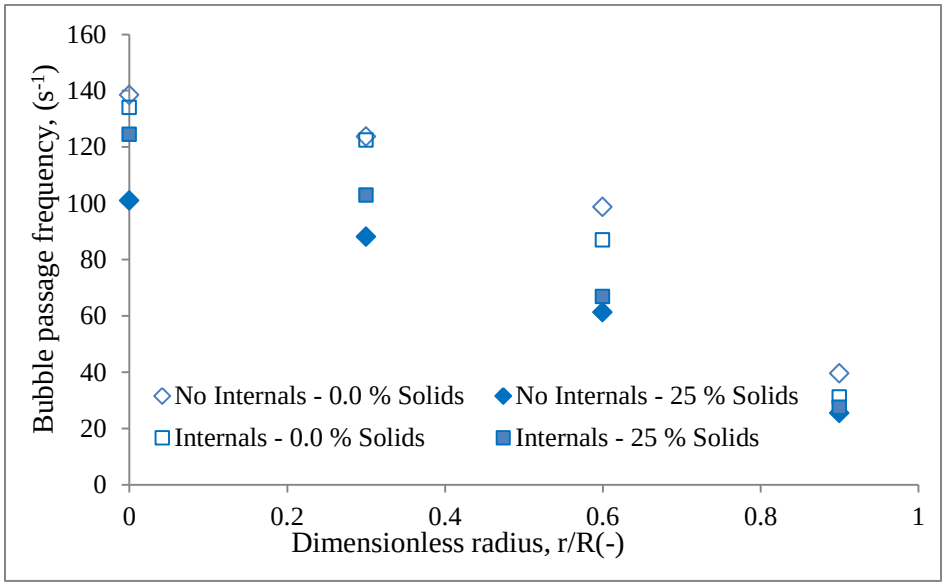

Figure 3.29 Effect of solids loading and dense internals on radial profiles of bubble passage frequency in 18-inch column at Ug = 30 cm/s based on the free cross-sectional area

3.3.3.4 Bubble chord length. Bubble sizes is apparently one of the most important parameters in the gas-liquid reactors and contactors since it controls almost all the other bubble parameters; local and over gas holdup, bubble velocity, the gas phase

residence time in terms of the bubble velocity, among others. To characterize the bubble size distribution, the Sauter mean diameter is widely used as the most representative average diameter. This however is far from the real phenomenon as the bubbles only have definite and semi-definite shape in the homogenous flow regime. This operating regime is of little benefit to industrial processes such as the methanol synthesis and F-T processes. Thus a representation of a characteristic bubble size is adopted of bubble chord-lengths. To represent the raw measured chord length data, equation 3.8 is used as was described in section 3.2.2.4. The effect of solids loading on the distribution of the measured bubble chord lengths by the 4-point optical probe in the absence of internals is shown in Figure 3.30 while the effect of solids loading in the presence of dense internals is shown in Figure 3.31. In this work, the bubbles produced at the studied gas velocities were such that a large number of disintegrated bubbles with smaller chord lengths and a small number of coalesced large bubbles, that leads to a very asymmetric bubble size distribution. Many authors (e.g., Luewisutthichat et al., 1997 and Pohorecki et al., 2001) have reported the bubble chord length distributions to be best represented by a log-normal distribution, with its upper value at the maximum bubble size. Such a distribution were also reported by Akita and Yoshida, 1974; and,Youssef and Al-Dahhan, 2009; among others.

The bubble chord length distributions have been analyzed statistically by providing the mean and the variance, as shown in Table 3.5. It can be seen that there is a higher probability of lower chord lengths at lower gas velocity. The addition of solids increases not only the mean but also the spread of the bubble chord length distribution. Without internals the mean of the distribution at Ug = 3 cm/s is 0.4729 with no solids and

it is increased to 0.5800 when 25 % vol solids are used. This implies that the formation of smaller bubbles dominates giving rise to a higher probability of small chord lengths. When 25 % vol solids are used, larger bubbles are formed which coexist with smaller ones leading to a wider spread in the size distribution. Increase in solids loading increases

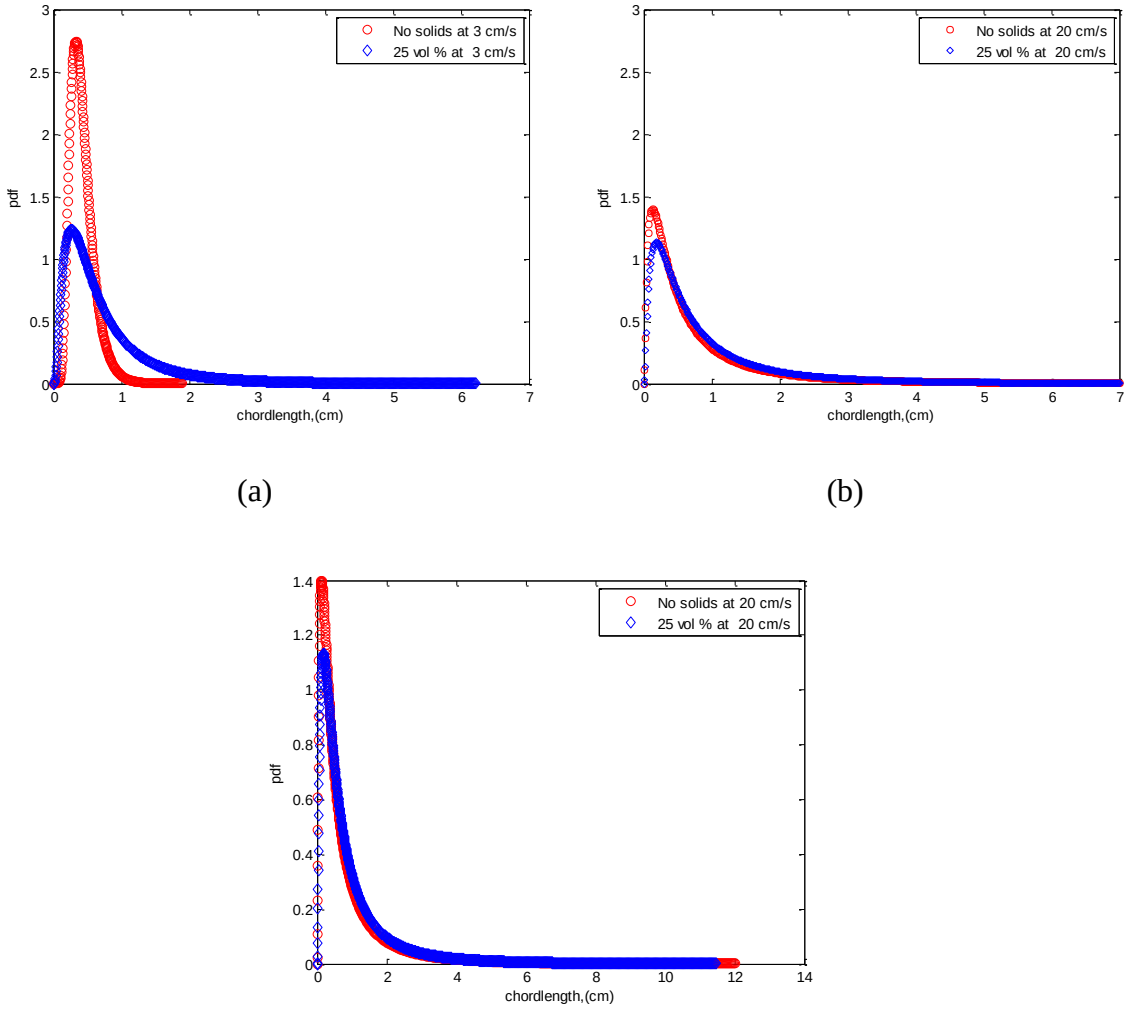

(a) (b)

(c)

Figure 3.30 Effect of solids loading in the absence of internals on bubble chord length distribution at dimensionless radius r/R(-) = 0.0 in 6-inch column (a) At Ug = 3 cm/s (b) At Ug = 20 cm/s (c) Enlarged scale of (b), (Equation 3.8)

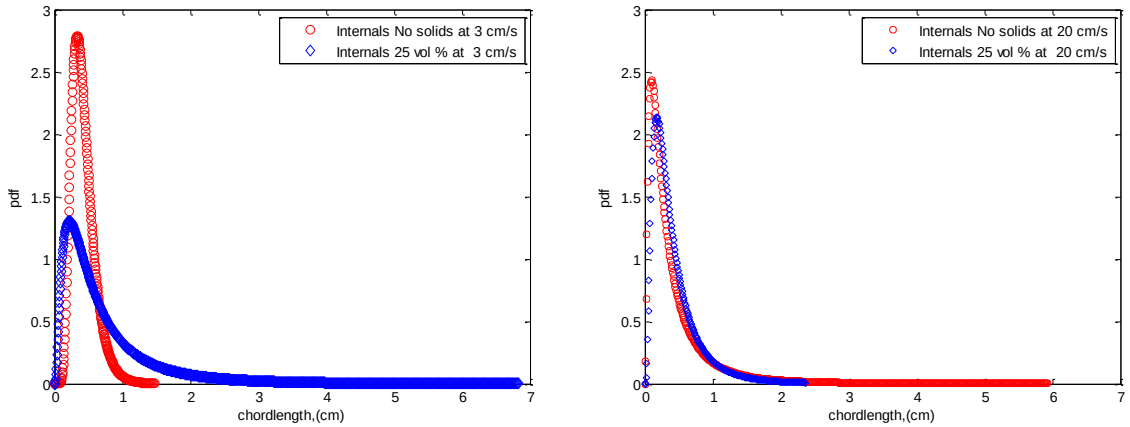

(a) (b)

Figure 3.31 Effect of solids loading in the presence of dense internals on bubble chord length distribution at dimensionless radius r/R(-) = 0.0. in 6-inch column with superficial gas velocity based on free cross-sectional area (a) at Ug = 3 cm/s (b) at Ug = 20 cm/s, (Equation 3.8)

Table 3.5 Statistical measures of the bubble chord length distribution in 6-in column at r/R = 0.0 at different conditions with m and υ used in Equation 3.8

Ug (cm/s)	Solids loading	Internals	Mean (m)	Variance (υ)
3 cm/s	0.0 % vol	0.0 % CSA	0.4729	0.0319
	25 % vol	0.0 % CSA	0.5451	0.6340
	0.0 % vol	25 % CSA	0.4437	0.0303
	25 % vol	25 % CSA	0.4763	0.3465
20 cm/s	0.0 % vol	0.0 % CSA	0.9171	1.1611
	25 % vol	0.0 % CSA	0.9941	1.3875
	0.0 % vol	25 % CSA	0.8434	0.7856
	25 % vol	25 % CSA	0.8748	0.1642

pseudo-slurry viscosity, which promotes coalescence of large bubbles (Crabtree and Bridgewater, 1971), whereas the bubble break-up rate decreases due to dampening of instabilities at bubble-liquid interface. As can be seen in Figure 3.30, the addition of solids has greater effect on the chord lengths at lower gas velocity.

The average bubble chord length radial profiles are show in Figure 3.32 for an air-water and air-water glass beads system in 18-inch diameter column. As was illustrated in the interfacial area, the effect of dense internals and high solids loading on the average chord length are nearly the same as those of interfacial area. In the absence of internals,

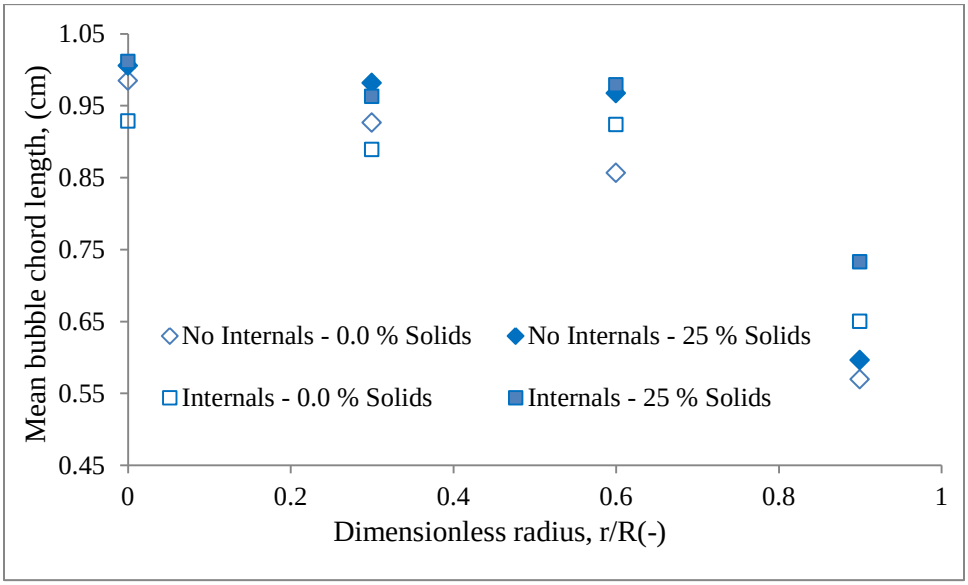

Figure.3.32 Effect of solids loading and dense internals on radial profiles of mean bubble chord length in 18-inch column at Ug = 30 cm/s based on the free cross-sectional area

larger bubble chord lengths at the column center and lower at the column wall region are obtained. With no solids, the bubble chord lengths are up 67 % higher at the column

center than wall region and 63 % higher at the column center than the wall region when 25 % vol solids are used. In the presence of dense internals the chord length at the column center is 42 % higher than at the wall region without solids and up to 38 % higher with 25 % vol solids. This variation in bubble chord lengths reinforces the earlier observations noted with the interfacial area, bubble frequency and gas holdup profiles.

3.3.3.5 Axial bubble velocity. The bubble velocity in bubble columns has been erroneously taken to mean the bubble rise velocity, but bubbles in bubble columns move downward as well. Besides, radial motion is also exhibited by the bubbles. In light of the bubble wake heat transfer enhancement, the turbulence generated plays the crucial role. The heat-transfer enhancement due to the passage of gas bubbles is caused by the bubble wake which is primarily responsible for the rapid heat transfer surface renewal of fluid on the heat-transfer surface irrespective of the bubble direction. Hence, in this work the magnitude of the axial bubble velocity for both upward bubble velocity and downward bubble velocity are considered. To measure the downward bubble velocity, the optical probe was flipped to face upward at the same point of measurement of the upward bubbles. The probability density function (pdf) of the axial bubble velocity is then obtained by dividing the number of bubbles which have a particular velocity upward or downward by the total number of bubbles that hit all the four tips of the optical fiber probe during the sampling period. The axial bubble velocity is obtained as follows;

$$U_{axial} = \frac{f_d}{f_d + f_u}\overline{U}_d + \frac{f_u}{f_d + f_u}\overline{U}_b \tag{3.11}$$

And

$$\overline{U}_d = \frac{1}{N_d}\sum_{i=1}^{N_d} U_{d,i}\ , \qquad \overline{U}_b = \frac{1}{N_u}\sum_{i=1}^{N_u} U_{u,i}$$

$$f_d = \frac{N_d}{t_d}, \qquad f_u = \frac{N_u}{t_u}$$

Where U_{axial} is the axial bubble velocity, $\overline{U}_d$ is the average value of the downward bubble velocity, obtained with probe pointing upward, $\overline{U}_b$ is the average value of the bubble rise velocity, obtained with probe pointing downward, $U_{d,i}$ is the instantaneous downward bubble velocity, $U_{u,i}$ is the instantaneous upward bubble velocity, f_d is the downward bubble passage frequency, f_u is the upward bubble passage frequency with N_d the bubble number of bubbles moving downward and N_u the bubble number of bubbles moving upward, t_d is the sampling time with probe facing upward while t_u is the sampling time with the probe pointing downward.

Figure 3.33 shows the effect of dense internals, high solids loading and the superficial gas velocity on the profiles of axial bubble velocity in the laboratory scale 6-inch diameter column based on both the free cross-sectional area (Figure 3.33a) and based on total cross-sectional area (Figure 3.33.b). The increase in solids loading increases the bubble velocity in both bubbly (Ug = 3 cm/s) and churn turbulent (Ug = 20 cm/s, 45 cm/s) flow regimes. Similar trend was observed by Li and Prakash, 1997. This increment is attributed to change in the slurry properties, where increased pseudo-slurry viscosity promotes the bubble coalescence (Crabtree and Bridgewater, 1971) and hence increase in the bubble sizes as discussed under other bubble properties in the preceding section.

With the Ug based on free cross-sectional area, dense internals lower the axial bubble velocity by 25 % on the average at Ug = 3 cm/s and 3.4 % at 20 cm/s but leads to an average increase of 6 % at 45 cm/s. Based on total cross-sectional area the dense

internals reduces the velocity by 16 % at 3 cm/s while an increase of 5 % and 8.1 % average in axial bubble velocity is attained at 20 cm/s and 45 cm/s respectively. The

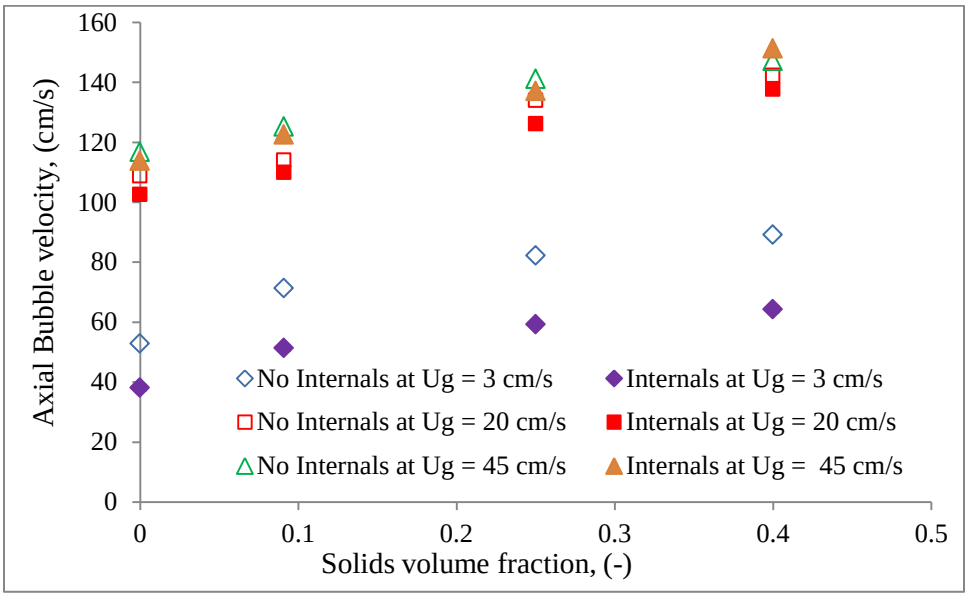

(a)

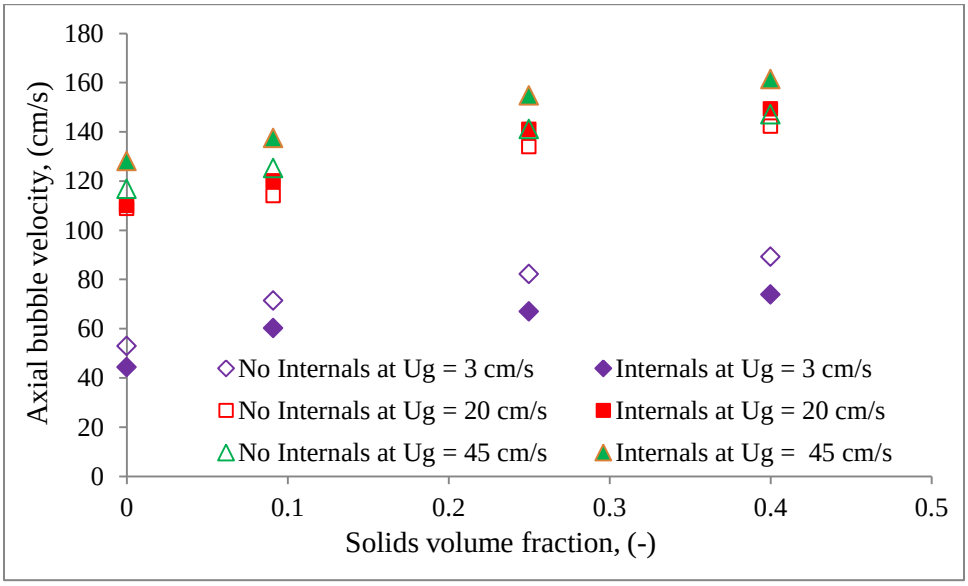

(b)

Figure 3.33 Effect of solids loading, internals and superficial gas velocity on axial bubble velocity (a) Based on free cross-sectional area (b) Based on total cross-sectional area

difference with internals is higher when Ug is based on total CSA due to same gas mass flow rate used in the column with internals as that in column without internals in which the gas/bubbles flow through a smaller CSA in column with internals. However the difference becomes less when the Ug is based on free CSA. It is apparent from these observations that it is not possible to extrapolate the bubble velocity obtained from empty columns to those with dense internals when solids are utilized.

The effect of dense internals and high solids loading on the radial profiles of axial bubble velocity with the superficial gas velocity based on the free cross-sectional area, in the pilot-scale 18-inch diameter column is presented by first analyzing the effect of the various components of the axial bubble velocity. Figure 3.34 shows the said effects on the radial profiles of the upward bubble velocity, commonly referred to as bubble rise velocity (Figure 3.34a) and the downward bubble velocity, (Figure 3.34b). Both the bubble rise and downward bubble velocities exhibit parabolic radial profiles with the bubble rise velocity highest at the column center and decreases towards the column wall. On the contrary the downward bubble velocities are lowest at the column center and highest at the column wall. The bubble rise velocity is increased by an average of 9 % when 25 % vol solids are used in the absence of dense internals. However, when the column is inserted with dense internals, 25 % vol of solids lead to an average of 6 % increase in bubble rise velocity. The effect of solids loading on the downward bubble velocity averages 11 % with or without internals.

The effect of dense internals and high solids loading on the radial profiles of axial bubble velocity with the superficial gas velocity based on the free cross-sectional area, in the pilot-scale 18-inch diameter column is shown in Figure 3.35. It is observed

that the bubble rise velocity, (Figure 3.34a) is 5 % higher than the axial bubble velocity on the average within r/R≤ 0.6 but up 50 % lower than the axial bubble velocity at the

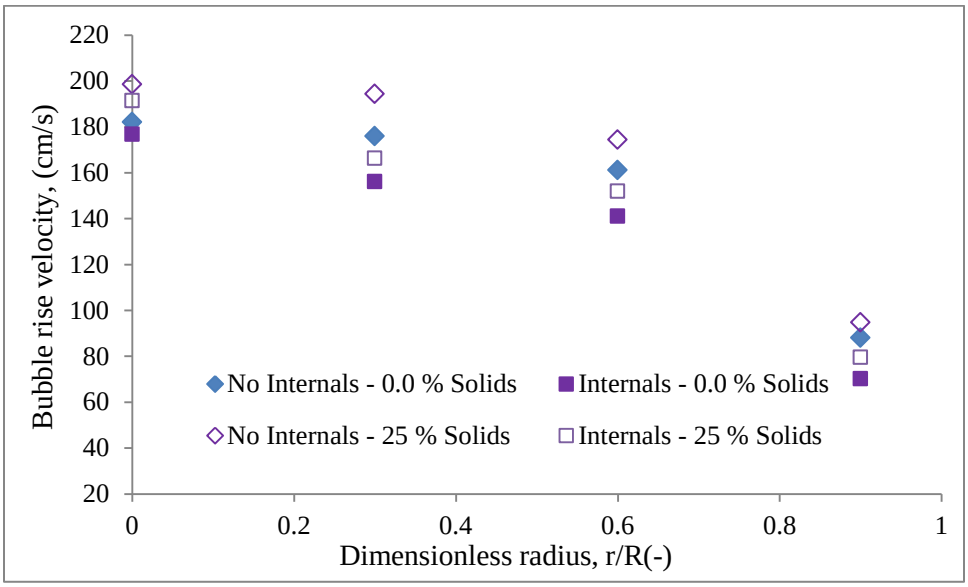

(a)

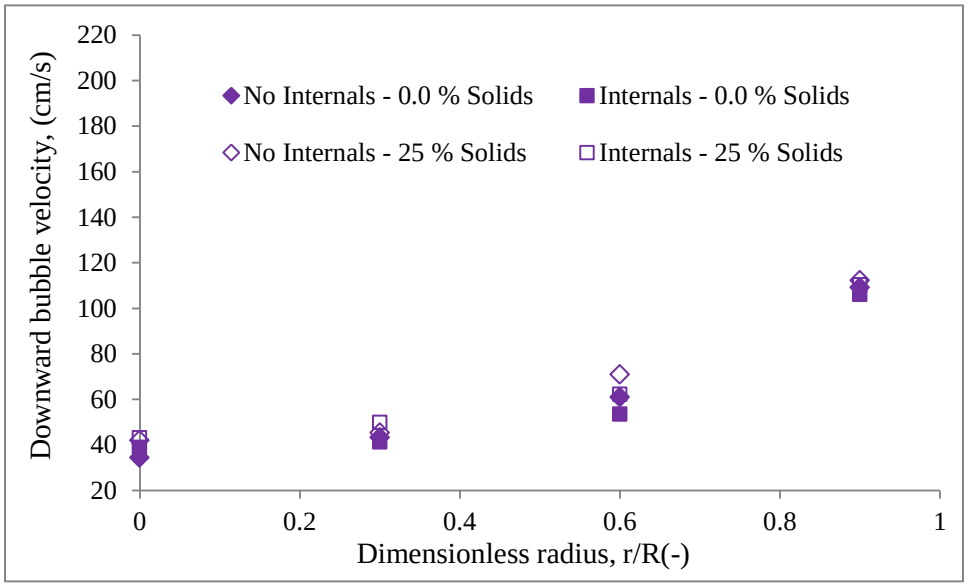

(b)

Figure 3.34 Effect of solids loading and dense internals on the radial profiles of (a) bubble rise velocity (b) downward bubble velocity at Ug = 45 cm/s based on free cross-sectional area in 18-inch diameter column

column wall. This trend can be attributed to higher passage frequency of bubbles moving at higher velocities upwards in the core region and downward closer to the wall region. In the empty column, 25 % vol solids lead to increased axial bubble velocity, with an increase of 7 % at the center and 10 % at the column wall. A similar trend is observed with dense internals where the increase of 6 % at the column center and up to 13 % increase closer to column wall.

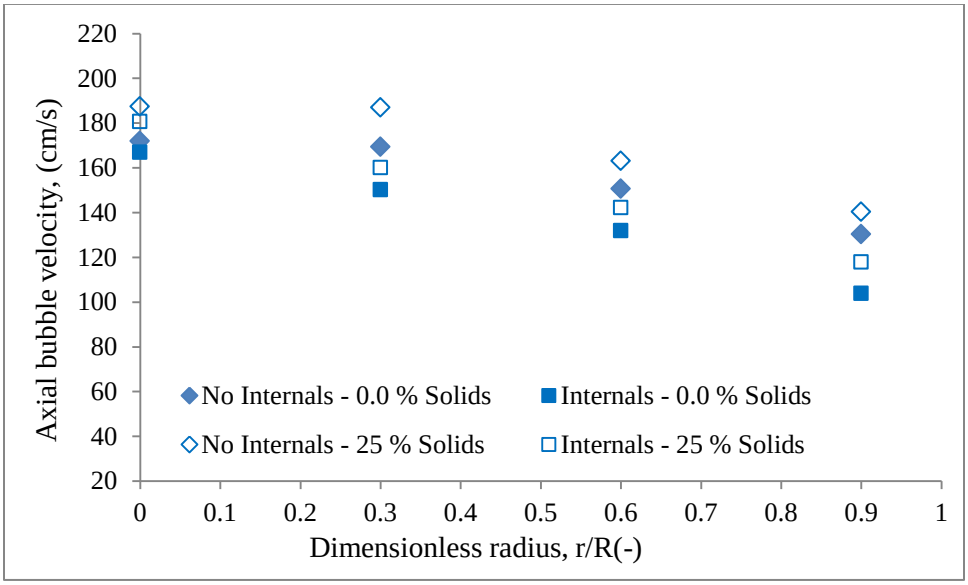

Figure 3.35 Effect of solids loading and dense internals on radial profiles of axial bubble velocity in 18-inch diameter column at Ug = 45 cm/s based on the free cross-sectional area

3.4. REMARKS

The impact of dense internals occupying 25 % of column cross-sectional area was assessed in an air-water and air-water-glass beads (150 μm) system by using the four-point optical probe in slurry bubble columns. Local gas holdup, bubble chord length, bubble

passage frequency, specific interfacial area, and axial bubble velocity were investigated under different operating conditions under ambient pressure. With the increase in superficial gas velocity, the local gas holdup, bubble chord length, bubble passage frequency, specific interfacial area, and axial bubble velocity increased. Local gas holdup, specific interfacial area, and apparent bubble frequency decreased with the increase in solids loading, but increased with dense internals, though insignificantly for gas holdup in the 6-inch column.

The impact of diameter of internals and different configurations of internals covering the same cross-sectional area (25 % CSA) was investigated and quantified over a wide range of superficial gas velocities and solids loading in 6-inch laboratory bubble column. The use of both free area cross-sectional area available for the flow and total cross-sectional area was used, to discriminate between the effect of higher gas velocity inside the column and the actual effect of the dense internals. High density of internals shows negligible effect on both overall and local gas holdup, an enhancement of bubble passage frequency, increased interfacial area and a decrease in bubble velocity and bubble chord length which was smaller with internals as result of an enhancement in bubble break-up rate. A closer comparison revealed that the use of total cross-sectional area for determining the gas flow rate gives a misleading effect. It shows that there is effect on virtually all the bubble dynamic parameters. It is also important to mention that the local and overall gas holdup studied in empty columns can be extrapolated to columns with dense internals in 6-inch at no and low (9.1 % vol) solids loading or at $Ug \geq 30$ cm/s.

Consistently higher specific interfacial area, bubble frequency was noted with 0.5-inch diameter internals, at the column center but lower elsewhere than with 1-inch diameter column. However the insignificant difference in the local gas hold ups, indicate that it is possible to extrapolate the local gas hold up results obtained from empty bubble columns of similar size to extract the influence of dense internals on the same but the effect of dense internals on the other bubble properties would still need to be done in columns equipped with dense internals.

With the increase in solids loading, both the average bubble chord length and bubble velocity bubble velocity increased though slightly. Based on bubble chord length distribution in the column center, higher probability of larger bubbles was observed with high solids loading with and without the dense internals with the effect being significantly higher at lower gas velocity. It was also established that the bubble chord length had a wider spread with increasing solids loading at lower gas velocity and a reverse trend at higher gas velocity. In fact, a closer look at the mean of the bubble chord length distributions (Table 3.1, 3.2 and 3.2) revealed that the effect of internals and solids loading is much higher in the low gas velocity and negligible at very high gas velocity.

The effect of dense internals and high solids loading on the bubble dynamics in the 18-inch diameter pilot-scale bubble column was assessed using the four-point optical probe technique. In the 18-inch column when 25 % of the total CSA of the column is obstructed by internals in the churn turbulent flow regime ($Ug \geq 30$ based on free CSA), an increase in the gas holdup radial profiles was observed, together with increased steepness of the gas holdup radial profiles compared to the column without internals. This would lead to higher large-scale liquid recirculation hence a likely increase in the

transport parameters like both of heat and mass. The use of high solids loading leads to lower gas holdup due to the enhanced bubble coalescence resulting in formation of larger bubbles with lower specific interfacial area per unit volume, lower bubble passage frequency as fewer bubbles appear in the column a unit time and slightly higher bubble velocity. However one key observation also was that the high solids loading does not lead to significant change in the steepness of the radial profiles of the local gas holdup, thus little or no change in liquid/slurry recirculation might be induced by using high solids loading with or without internals. The bubble chord length was smaller with internals as result of an enhancement in bubble break-up rate. Finally a conclusion that can be drawn from this study is that it is not possible to extrapolate any of the studied bubble parameters form an empty 18-inch column to those with dense internals by matching gas velocities regardless of solids use.

4. IMPACT OF SOLIDS LOADING AND DENSE INTERNALS ON THE HEAT TRANSFER COEFFICIENT IN BUBBLE AND SLURRY BUBBLE COLUMNS

4.1. SCOPE

As detailed in Section 2, efforts have been made to study the heat transfer coefficient in bubble and slurry bubble columns, but most of these studies were conducted in two-phase systems. Also, most of the studies in the literature on the effects of operating and design variables on the bubble dynamics and transport parameters including the heat transfer rates and coefficients have been performed in empty bubble and slurry bubble columns. Therefore, the effects of heat exchanging internals on the bubble dynamics and transport parameters have not been well understood. The most recent investigation of heat transfer coefficients in a bubble column with mimicked dense heat exchanging internals occupying 22 % of CSA at conditions of high superficial gas velocity was performed in a 0.19 m diameter column by Abdulmohsin and Al-Dahhan, 2012. But still the investigation was limited only to a two-phase system. Thus heat transfer studies are yet to be reported for three-phase (gas- liquid-solid) system bubble columns with dense internals.

The properties of liquid phase changes significantly when the solids/fines are added particularly the liquid density, liquid viscosity, liquid thermal conductivity and heat capacity. Addition of solid particles would increase or decrease the average properties of suspension depending on solids properties (Deckwer et al., 1980). The role of liquid viscosity on the heat transfer rate in multiphase systems is also well highlighted in the literature (Kim and Kang, 1997). The use of solid catalysts to improve the yield in

the FT process is inevitable. Therefore, in this chapter, the effects of operating parameters on the heat transfer coefficient in an air-water-glass beads system bubble columns with internals covering 25 % of the column CSA to mimic FT synthesis is examined.

4.2. EXPERIMENTAL SYSTEM

The combined measurement used in this work consists of two independently fabricated probes: (1) Four points fiber optical probe, whose description and features are described in Chapter 3 and further information and detailed algorithm and capabilities are available elsewhere in Xue, 2004. The other is an advanced fast response (L-shaped) rod type heat transfer probe, a modified version of the originally proposed heat transfer probe by Li and Prakash, 1997.

The instantaneous heat flux was measured using a micro-foil heat flux sensor (11 mm × 11 mm × 0.08 mm) from RdF Corporation (No. 20453-1). The micro-foil heat flux sensor was flush-mounted on the outer surface of a hollow brass cylinder. The micro-foil sensor has both the heat flux sensor and thermocouple. Thus the micro-foil sensor can measure both the local instantaneous heat flux from the probe to the bulk fluid and the instantaneous surface temperature of the probe simultaneously. A small cylindrical cartridge heater (Chromalox, model number CIR-1012) was installed inside the hollow brass cylinder. The AC power was supplied to the cartridge heater through a variac to regulate the supplied power in the range of 0 to 50 V. To complete the heat transfer probe assembly, the tube and fittings are separated by Teflon, which reduces the heat loss transferred from the heater to the connections. Two additional T-type thermocouples are installed in the column to measure the bulk fluid temperature. The measured signals of

the heat flux, in the range of microvolts, need to be amplified before being sent to the data acquisition (DAQ) system. After amplification, the heat flux signals, together with the signals from the thermocouples, were sampled at 50 Hz for between 60-90 seconds. Since this work studied the local time-averaged heat transfer coefficient in the fully developed region, the thermocouple probes were installed close to the heat transfer probe, about 0.1 m in axial distance, (above and below it). Figure 4.1 shows the schematic of the heat transfer probe and photo image of the L-shaped rod heat transfer probe.

The axial positions of the two thermocouples in the thermocouple probe were 6-inches above and below the L-shaped heat flux probe. The averaged values of the temperatures obtained by these thermocouples were representative of and used as the bulk temperature. In addition to the L-shaped rod type probe, an advanced heat transfer probe which mimics heat exchanging internals heat transfer surface has been employed in this work as will be discussed in Section 4.3.

The combined probes (consisting of the heat transfer probe and four-point optical probe) was mounted in the fully developed flow region of the columns for all the measurements, with the optical probe mounted just off the surface of the heat flux sensor. Only one axial location, in the fully developed flow region was used for all the measurements since there is negligible variation on the bubble properties within this flow region, (Xue, 2004). The combined probes were both fabricated in Professor Al-Dahhan's Lab in Missouri University of Science and Technology. This combination enables the capture of the bubble dynamics simultaneously with the heat flux in the same vicinity. The local measurements by the probe were taken at seven dimensionless radial positions r/R (-) = ± 0.0, ± 0.3, ± 0.6, ± 0.9 and in some cases nine, including ± 0.5. Since there

was axis-symmetry, only results on one half (+r/R) have been reported. Three to five test runs were performed at each condition and average values reported.

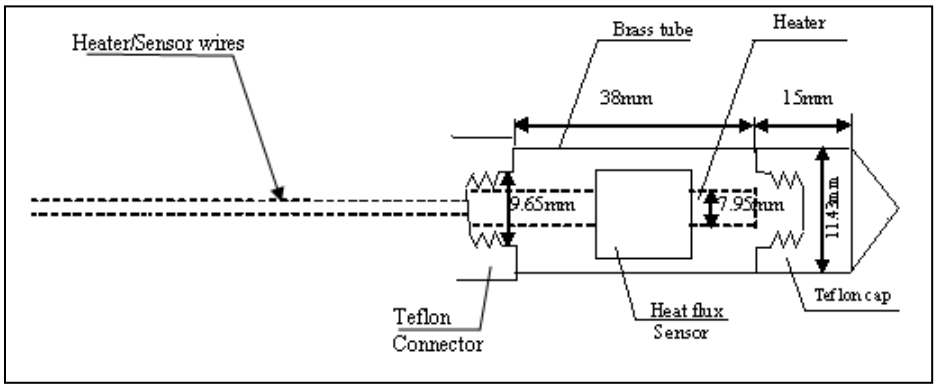

(a)

(b)

Figure 4.1 Heat transfer probe assembly: (a) Schematic of the heat flux sensor and heater, (b) Photo of the L-shaped rod heat transfer probe

According to Li and Prakash, 2001, to estimate the instantaneous heat flux and instantaneous heat transfer coefficient measured by the sensor, equation 4.1 derived for

liquid film heat transfer coefficient has been employed. From this equation, the instantaneous heat transfer coefficient could be determined by measurement of heat flux per unit area and the difference between surface temperature and the average temperatures of the bulk fluid medium at a given time.

$$\frac{1}{h_i} = \frac{T_{s_i} - T_{b_i}}{q_i} \tag{4.1}$$

Where h_i is the instantaneous local heat transfer coefficient, q_i is the instantaneous heat flux per unit area across the sensor, T_{b_i} is the instantaneous bulk temperature of the fluid media, T_{s_i} is the instantaneous temperature of the probe surface. Likewise, the time-averaged heat transfer coefficient at a given location was estimated by averaging the instantaneous heat transfer data collected after every 90s by equation 4.2.

$$h_{avg} = \frac{1}{N} \sum_{i=1}^{N} \frac{q_i}{\left(T_{s_i} - T_{b_i}\right)} \tag{4.2}$$

Where, h_{avg} is the time-averaged heat transfer coefficient, and *N* is the total number of the collected data. The value of *N* was selected to be 2 050 to ensure a stable value of heat transfer coefficients.

4.3. RESULTS AND DISCUSSION

The effect of solids loading on the heat transfer coefficient is examined in 6-inch laboratory scale and 18-inch pilot scale bubble columns without internals and with dense internals in relation to the bubble properties discussed in Section 3. It should be noted that the heat transfer coefficient results presented and discussed in this chapter was obtained at the same time as the bubble properties discussed in Section 3. For purposes of

clarity, selected relevant bubble dynamics results illustrated in chapter will be used alongside the heat transfer results in this chapter.

4.3.1. Instantaneous Heat Transfer Coefficient. First, a time series of the signals obtained from the instantaneous heat transfer coefficient is presented. Figure 4.2 shows the time series of the instantaneous heat transfer coefficient and fluctuations measured at the column center, r/R(-) = 0.0 in 6-inch diameter column without internals for an air-water system in the bubbly flow regime (Ug = 3 cm/s, Figure 4.2(a)) and in the churn turbulent flow regime, (Ug = 20 cm/s, Figure 4.2(b)) and the signal fluctuations in terms of $h_i - h_{avg}$ (Figure 4.2c). where h_i is the instantaneous heat transfer coefficient and h_{avg} is the time averaged heat transfer coefficient. It is observed that the instantaneous heat transfer coefficients obtained in bubbly region (3 cm/s) are significantly lower and relatively uniform (less fluctuation) around the mean than in the churn turbulent flow regime (20 cm/s). This is confirmed by higher fluctuation of the signal in the churn turbulent flow regime than in the bubbly flow regime as shown in Figure 4.2c and further evidenced by the mean and variances of the time averaged-instantaneous heat transfer coefficient shown in Figure 4.2a and 4.2b. This increase in instantaneous heat transfer coefficient with superficial gas velocity can be attributed to increase in bubble passage frequency, increase in number of larger bubbles which generate stronger liquid recirculation velocity thus increased bubble-wake-induced turbulence as also pointed out by Li and Prakash, 1999. The lower fluctuation at lower gas velocity is due the absence of fast moving bubbles and smaller bubbles which have near uniform sizes and moving at an almost uniform velocity. On the other hand in the churn turbulent flow regime, both smaller bubbles with lower velocity and larger bubbles

that move with higher velocity co-exist thus creating turbulence of varied magnitudes and different rates of heat transfer surface renewal. It should be pointed out that whereas it is a common knowledge that smaller bubbles move at low velocities, some that are trapped in the wake of larger bubbles move at the same velocity as the larger ones.

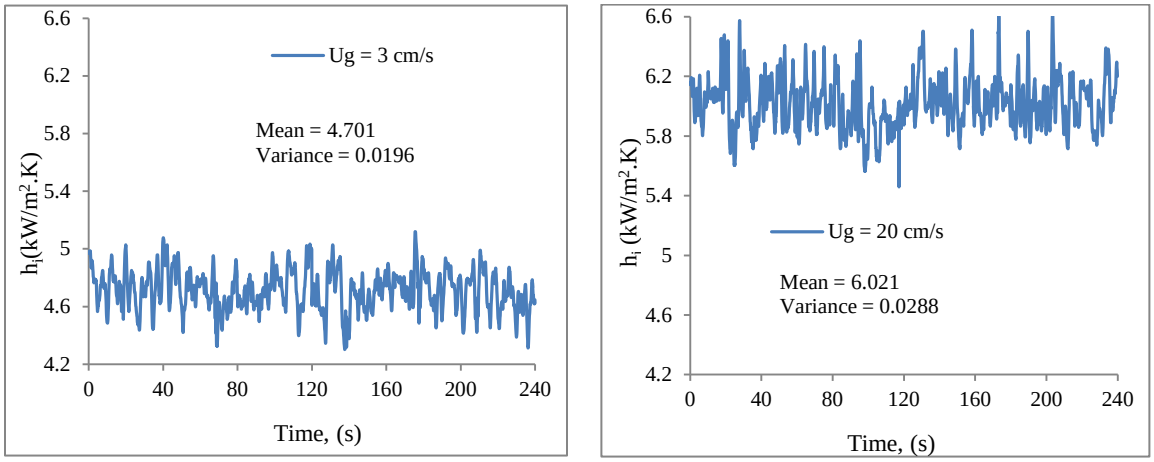

(a) (b)

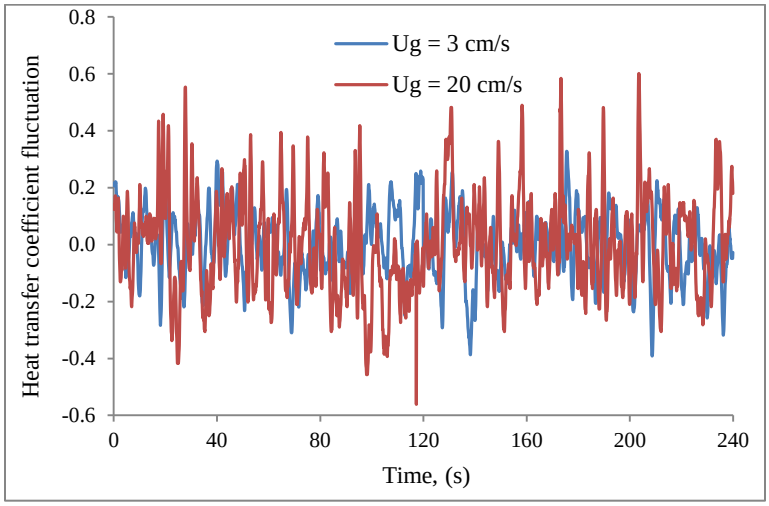

(c)

Figure 4.2 Instantaneous heat transfer coefficient signal (a) at 3 cm/s (b) at 20 cm/s (c) fluctuation comparison in terms of $h_i - h_{avg}$ at r/R=0.0 in 6-inch diameter column

4.3.2. Effect of Solids Loading and Superficial Gas Velocity on Heat Transfer Coefficient. In order to achieve economically high space-time yields, high slurry concentrations (typically 30-40 vol. %) need to be employed in the bubble column (Fox, 1990). The addition of solid particles which mimic the catalyst carrier in a commercial process such as F-T synthesis into a liquid changes the average thermo physical properties of the suspension and alters its apparent viscosity as well, Deckwer, 1980b. From the studies on bubble populations in bubble columns conducted by Li and Prakash, 2000 it was reported that adding solids up to 20 % by vol of the gas-free slurry, led to increased bubble rise velocity by about 20 %. These observations point to the fact that solids presence in gas-liquid system alters the behavior of the flow in the system. In this section the effect of solids loading up to 40 % vol on the heat transfer coefficient in 6-inch laboratory-scale bubble column and in 18-inch pilot plant-scale bubble column are investigated in connection with the discussed bubble properties in Section 3. Figures from Section 3 are re-plotted here for clarity and demonstrating the inter-relationships.

Figure 4.3 shows the effect of solids loading and superficial gas velocity on the heat transfer coefficient measured at the column center (r/R = 0.0) in 6-inch diameter empty column (Figure 4.3a) and in 18-inch diameter empty column (Figure 4.3b). It is observed that the heat transfer coefficient increases with increase in superficial gas velocity regardless of the solids loading, then reaches a plateau. It is noted that the heat transfer coefficient increases with superficial gas velocity and the rate of increase slows down significantly at superficial gas velocities above 25 cm/s. Similar observations have been made in the previous studies of Deckwer, 1980, Saxena et al., 1990, Li and Prakash,

1997, Yang et al., 2000, Abdulmohsin et al., 2010, Abdulmohsin and Al-Dahhan, 2012, Wu 2007, Wu et al, 2007, Wu and Al-Dahhan, 2011 and most recently Prakash, 2012.

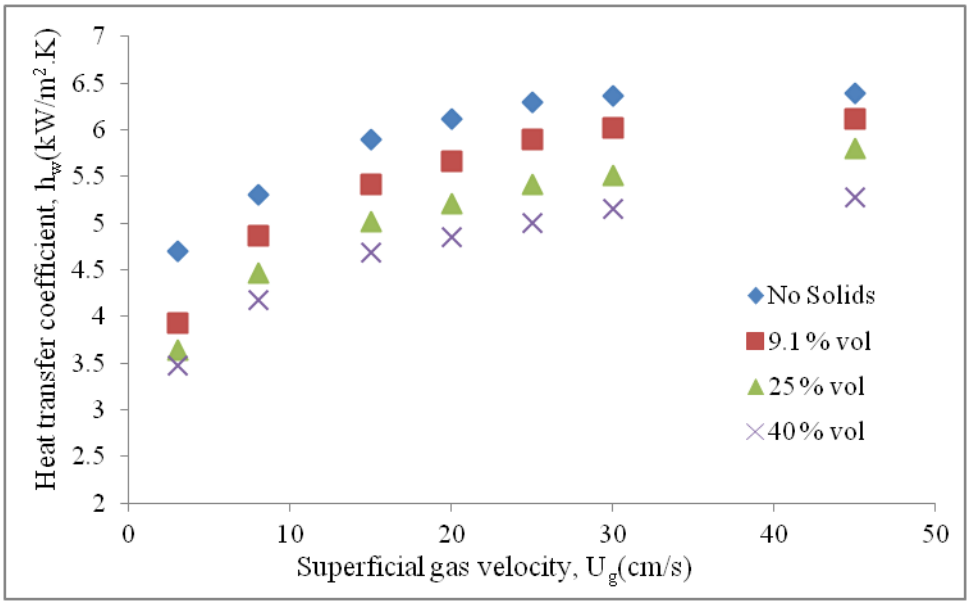

(a)

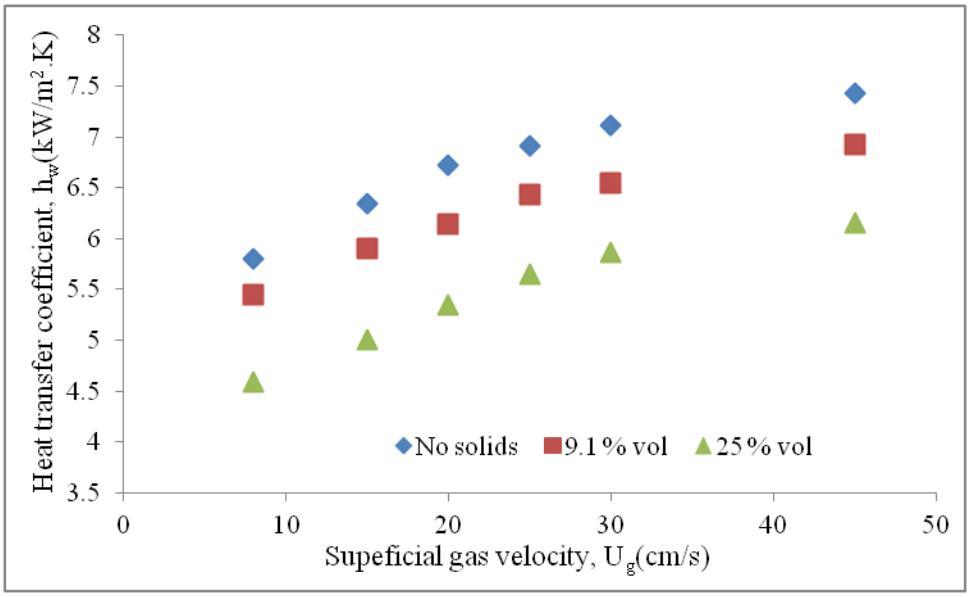

(b)

Figure 4.3 Effect of solids volume fraction and superficial gas velocity on heat transfer coefficient at r/R=0.0 in (a) 6-inch bubble column (b) 18-inch bubble column

They noted that the rate of increase in heat transfer coefficient is high for gas velocities less than 0.20 m/s and beyond this the increase becomes gradual.

Increasing superficial gas velocity leads to increased bubble frequency, bubble population and gas hold-up as well as the bubble chord length (which is characteristic of the bubble sizes) and axial bubble velocity as indicated in Section 3 and further illustrated in Figures 4.4-4.5. Figure 4.4 shows the effect of solids loading and superficial gas velocity on relevant bubble dynamics in 6-inch empty bubble column at the center of the column (r/R = 0.0). While Figure 4.5 shows the effect in 18-inch diameter column at the center of the column (r/R = 0.0). At Ug >25 cm/s the rate of increase in heat transfer coefficient falls, in a similar way the as the local gas hold up (Figure 4.4a), bubble chord length (Figure 4.4 c) as well as the axial bubble velocity (Figure 4.4d) but at a lower rate. This is an indication that there exists a close tie between the heat transfer rate and the bubble properties. It is important to point out that beyond Ug = 20 cm/s the bubble chord lengths starts to decrease while the axial bubble velocity continues to increase albeit negligibly. Bubbles break and coalesce, and the number of both large and small bubbles increases and the bubble size distribution spreads wider than the relatively uniform bubble size distribution in bubbly flow, (Figure 3.27). In the churn-turbulent flow regime the increase in the number of small bubbles is faster than that of large bubbles, so the mean bubble chord length decreases slightly with Ug as illustrated in Figure 4.5c and Figure 4.5c. However the axial bubble velocity continues to increase which indicates that the many smaller bubbles produced are trapped in the wake of larger bubbles which move at higher velocity thus a slight increase in the axial velocity despite a slight fall in bubble chord lengths with Ug.

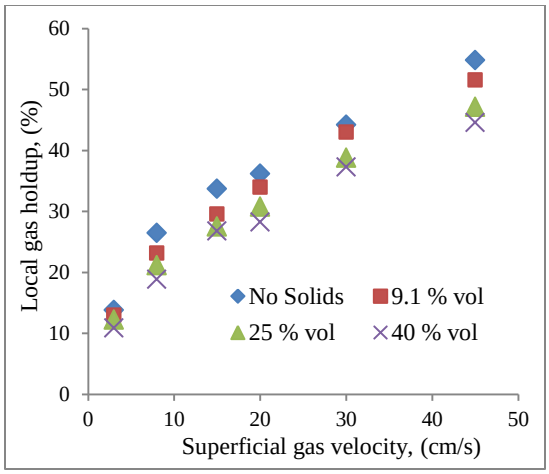

(a)

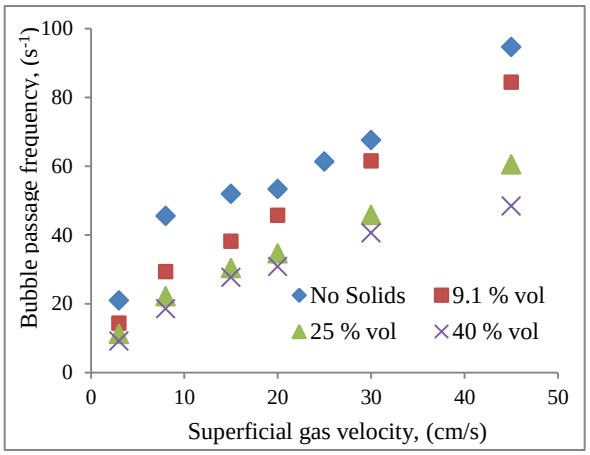

(b)

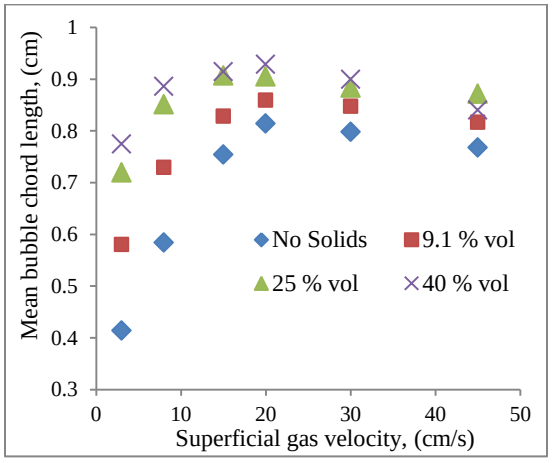

(c)

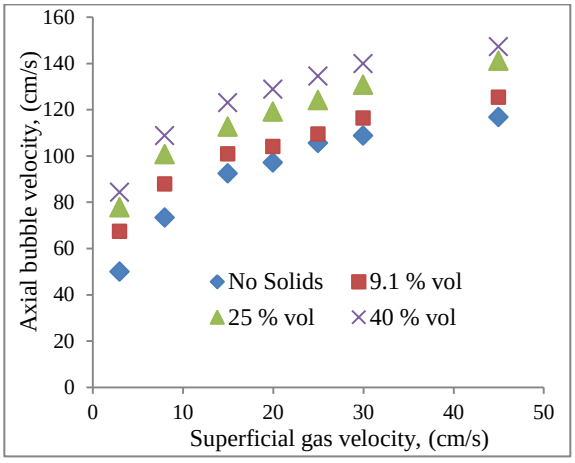

(d)

Figure 4.4 Effect of solids loading and superficial gas velocity in 6-inch diameter column on (a) Local gas holdup (b)Bubble passage frequency (c) Mean bubble chord length (d) Axial bubble velocity

Whereas some researchers have reported that adding solid particles to gas-liquid systems enhance the heat transfer coefficient, (Saxena et al., 1990; Deckwer et al., 1980; Yang et al., 2000; Wu 2007, 2011), a few others have reported the reverse trend, (Li and Prakash, 1997, Li, 1998; Jhawar 2011). Worth noting is that in these investigations,

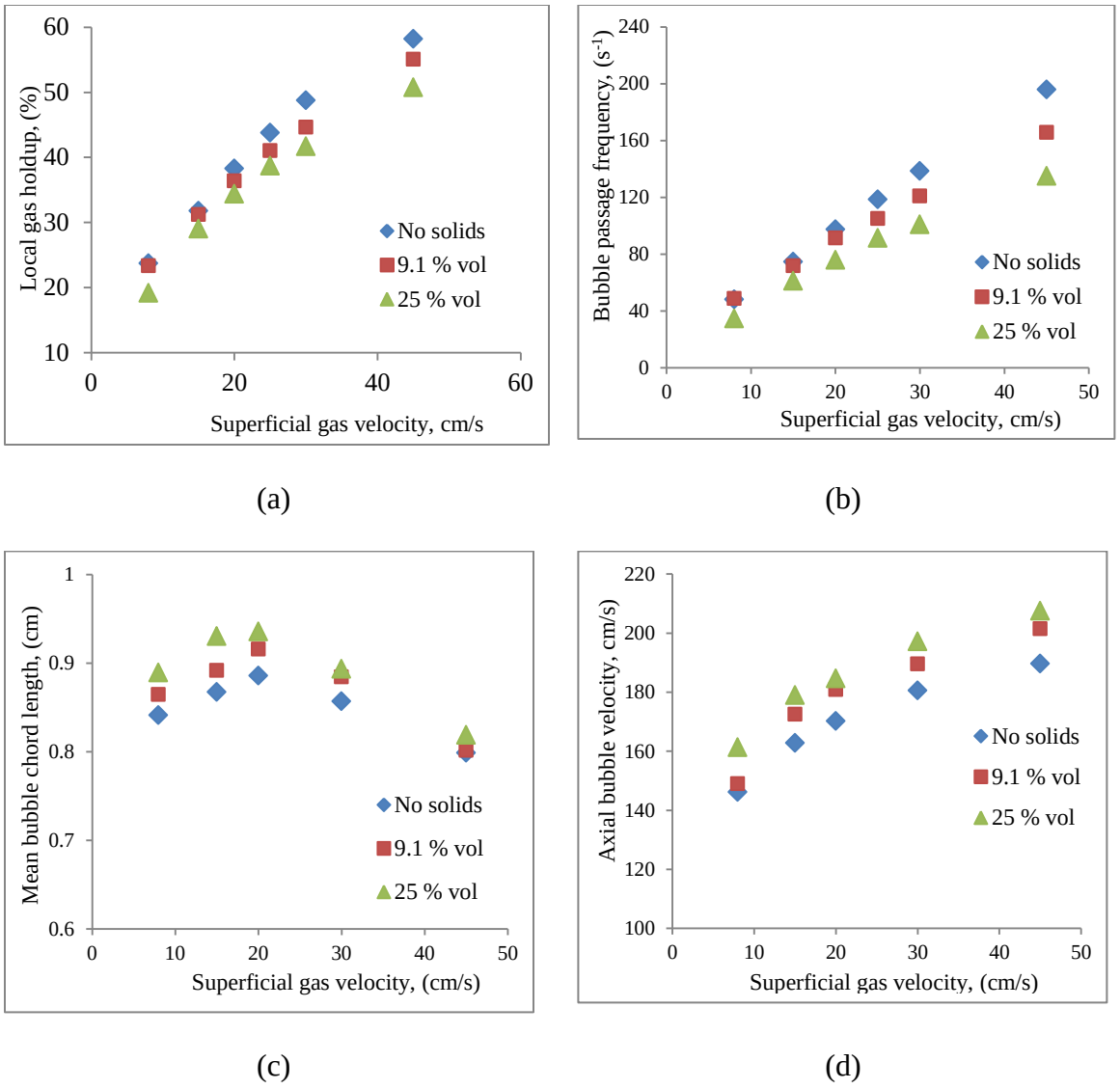

Figure 4.5 Effect of solids loading and superficial gas velocity in 18-inch diameter column on (a) Local gas holdup (b) Bubble passage frequency (c) Mean bubble chord length (d) Axial bubble velocity

different liquids, gases and solids were used. It is therefore debatable whether the effect of solids loading depends on the solids type and the gas-liquid system investigated. According to the results obtained in the current work, it can be observed that the addition of solids to the gas-liquid system leads to lower heat transfer coefficient, regardless of the

column diameter and superficial gas velocity, or radial location. Kumar et al., 1992 demonstrated that the local heat transfer coefficient has a direct connection to the bubble sizes. They showed that the heat transfer coefficient increases with an increase in bubbles size, since strong vortices are created behind the large bubbles hence intense mixing in the wake region, a short distance behind the bubble is expected. The phenomena encountered in the bubble columns correspond to the flow behavior at three flow regimes as reported by Chen et al., 1994 with the increase in the superficial gas velocity in a bubble column. Hence, at low superficial gas velocities, the heat transfer coefficients are relatively small because of the small bubble size in the homogenous flow regime. With increasing superficial gas velocity, the heat transfer coefficient increases due to the increase in bubble sizes hence their velocity, and their numbers and passage frequency over the heat transfer surface. This leads to an enhanced rate of the heat transfer surface renewal. Luo et al., 1999 also pointed out that in the churn turbulent flow regime, bubble coalescence and breakup rates come to equilibrium at a certain gas velocity thus the magnitude of the increase slows down.

The heat transfer variations with slurry concentration are comparable with bubble dynamics variations reported earlier on in Section 3 and Figures 4.4 and 4.5. Besides they are also consistent with those of Gandhi et al., 1999. The gas holdups reported earlier on and by several authors Saxena, 1989, Li and Prakash, 2001, decreased with increase in slurry concentration and the rate of decrease slowed at slurry concentrations above 20 %. These similarities in heat transfer and gas holdup variations suggest a role for underlying bubbles behavior in the heat transfer coefficients and rates. Li and Prakash 2001, attributed the decrease in heat transfer coefficient with solids to turbulence dampening

effects of higher apparent viscosity of the slurry suspension. The addition of solids which have higher thermal conductivity and higher heat capacity such as the glass beads used in this work would lead to enhanced heat transfer coefficient, while increased slurry viscosity would have a negative influence on the same, Jhawar, 2011. It has also been documented by several researchers that the heat-transfer coefficient decreases with increasing liquid viscosity in multiphase reactors, (Kang et al., 1985, Kim et al., 1986, Kumar and Fan, 1994, Cho et al., 2002) regardless of the particle size.

The decrease in the heat-transfer rate observed in this work has been attributed to an increase in the thermal boundary sublayer thickness around the heat transfer surface. Addition of solids leads to increase in the thermal boundary layer thickness that is responsible for the heat transfer resistance. The increased boundary layer results from increased pseudo-slurry viscosity due to a decrease in turbulence and an increase in viscous friction loss between the phases, thus increasing the resistance for conduction heat transfer. From the mechanistic point of view as will be illustrated in the next chapter, the conduction is required to occur before the convective heat transport occurs. Thus with increased thermal boundary layer, the resistance to the conduction is increased. Moreover, the particle movement is retarded with increasing viscosity, thereby reducing their attack on the thermal boundary layer around the heating source, Jhawar, 2011, consequently low rate of thermal layer renewal. It is also observed that axial bubble velocity increases with increased solids loading. But the population of the bubbles and the bubble passage frequency is greatly lowered with solids addition thus the frequency with which the heat transfer surface is renewed is also reduced.

Kumar and Fan, 1994 demonstrated that for a gas liquid and gas-liquid-solid systems it is that a thin liquid film of uniform thickness exists at the heat transfer probe surface and that the mass of fluid brought by the bubble wake is viewed to exchange heat by unsteady-state conduction at the outer edge of the thin film. They further claimed that the resistance to heat transfer is due to the thin film whose thickness depends on the liquid properties and the local hydrodynamics, followed by penetration and unsteady-state heating of a liquid mass element.

4.3.3. Effect of Solids Loading on Heat Transfer Coefficient and its Radial Variation. Few studies have reported the effect of high solids loading on the radial variation of the heat transfer coefficient, particularly in bubble columns operated at higher superficial gas velocity which are all desired in commercial applications like in the F-T synthesis process. Among the few reported studies include, Li and Prakash, 2001, Wu et al., 2007. Figure 4.6 and Figure 4.7 illustrate the effect of solids volume fraction and superficial gas velocity on radial profiles of the heat transfer coefficient in empty 6-inch bubble column and 18-inch bubble columns at superficial gas velocity of 45 cm/s.

In both the columns, significant radial differences are observed. Higher heat transfer values at the column center while close to the column wall, lower values of the heat transfer coefficient are noted. Additional data were collected at more radial locations to obtain the radial profiles of heat transfer coefficients in the bulk region for different gas velocities and slurry concentrations. The radial variation can be attributed to higher local turbulence generated by the large fast moving bubbles at the column center and slower smaller bubbles moving closer to the column wall at all the reported gas velocities and solids loading. Saxena et al., 1990 investigated in detail the effect of column

diameter on heat transfer. They reported that heat transfer coefficient measured in a 30.0 cm diameter slurry bubble column was greater than in a 10.8 cm diameter slurry bubble column. They attributed this increase to more intense mixing attained in larger column. Further details on the differences and scale effect will be examined later in Section 6.

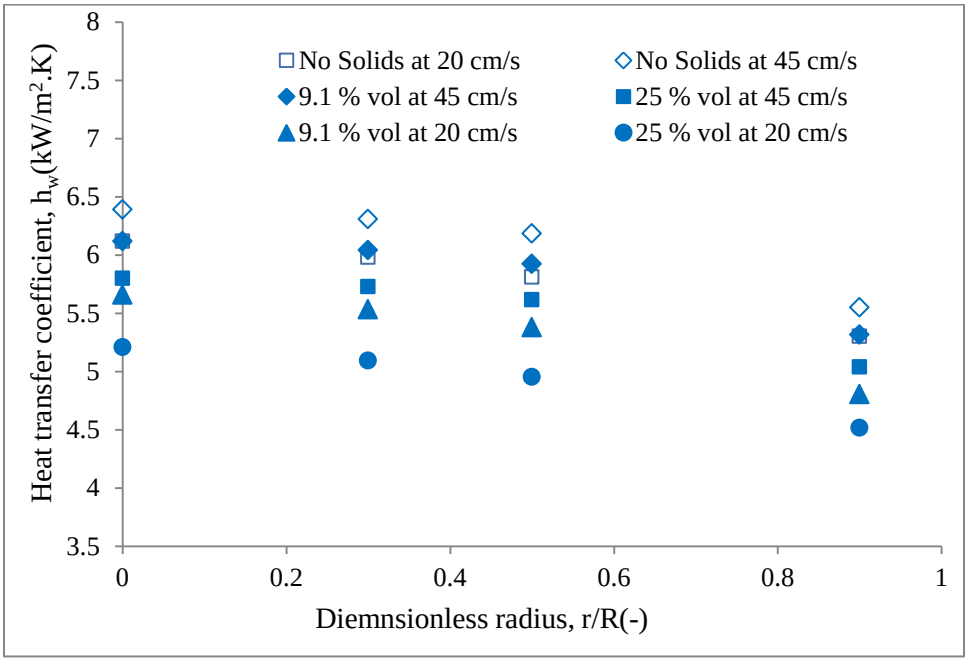

Figure 4.6 Effect of solids volume fraction on radial profiles of heat transfer coefficient in 6-inch bubble column

The radial heat transfer coefficient variation is justified from the local gas holdup radial profiles shown in Figure 4.8 and also as discussed in Section 3, Figures 3.22 and 3.26. Similar trends in profiles of other bubble properties were already discussed in Section 3, (Figure 3.27, 3.29, 3.32 and 3.35) and are therefore not re-plotted here in this section). Towards the center of the column, higher local gas holdup and higher bubble

passage frequency hence higher rate of heat transfer surface renewal at the central region of the column. With no solids, in the 6-inch column the radial profiles are nearly flatter in central region with a 2.5 % decrease in the heat transfer coefficient from r/R = 0.0 to r/R≤ 0.5 then a sharp (9 %) decline in the column wall region (r/R ≥ 0.6) on the average. Similar trends but steeper profiles, 5.3 % decrease at the column core (r/R ≤ 0.5) and 14 % decrease at (r/R ≥ 0.6) are observed in the 18-inch diameter column.

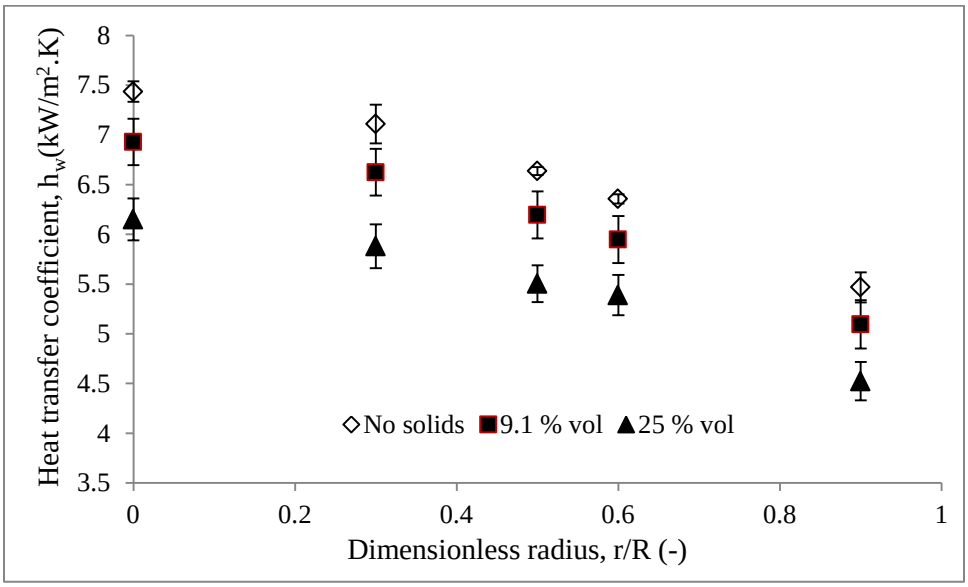

Figure.4.7 Effect of solids volume fraction on radial profiles of heat transfer coefficient in 18-inch bubble column at Ug = 45 cm/s

With increasing the slurry concentration, the bubble sizes (Table 4.1) become larger Figure 4.4c, Figure 4.5c and the probability of getting smaller bubbles decreases or shifts to larger values of the bubble chord lengths, Figure 4.9. Figure 4.9 shows the

distribution of the bubble sizes in terms of the bubble chord lengths in 6-inch diameter empty column (Figure 4.9a) and in 18-inch diameter empty column (Figure 4.9b) under

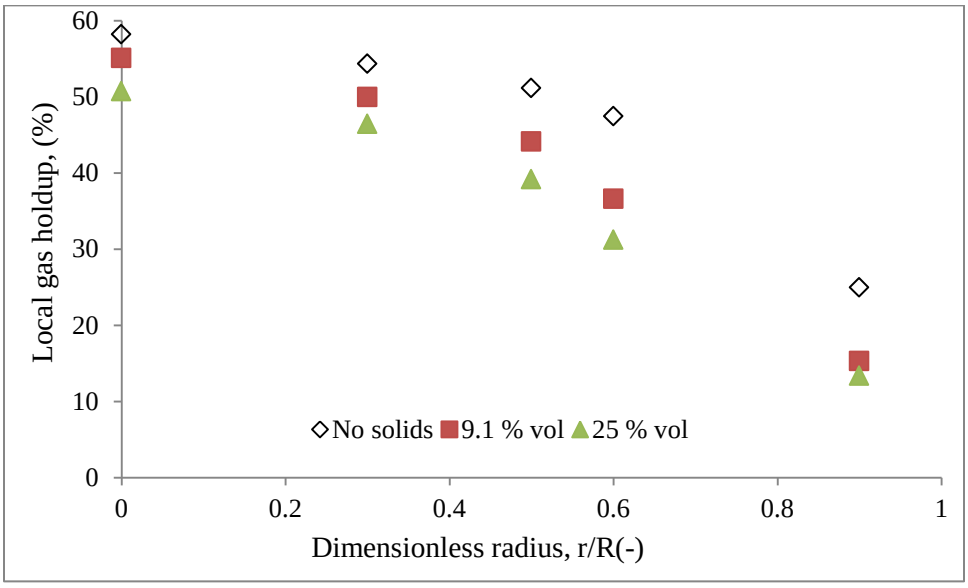

Figure 4.8 Effect of solids loading on the local gas holdup radial profiles in 18-inch diameter empty column at 45 cm/s

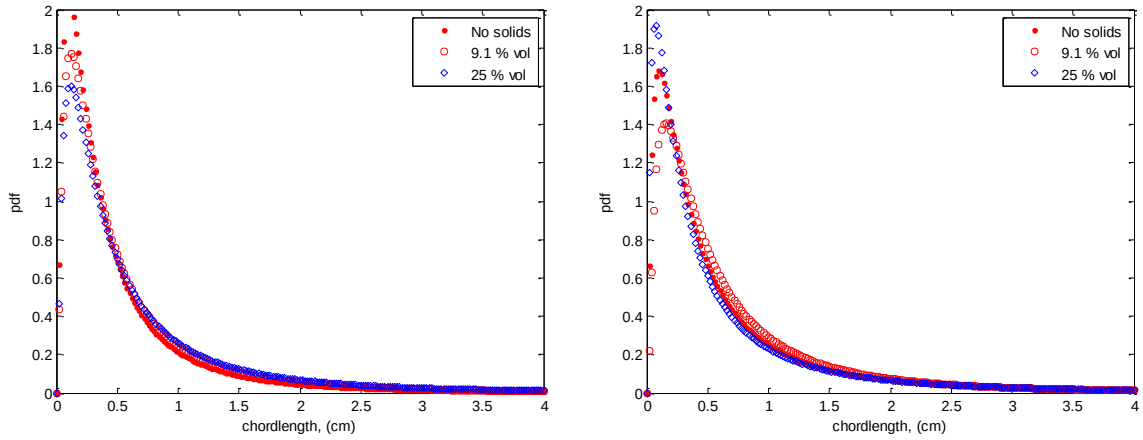

(a) (b)

Figure 4.9 Effect of solids loading on bubble chord length probability distributions in empty columns at r/R(-) = 0.0 in (a) 6-inch diameter (b) 18-inch diameter (Equation 3.8)

different solids loading. The figures 4.9a, b were plotted based on the criterion presented in Section 3.2.2.4. Further statistical analysis is done of the distributions as shown in Table 4.1 by providing the mean and variance.

Table 4.1 Statistical parameters for the bubble chord length distribution 6-inch and 18-inch columns with and without solids

Column	Solids loading	Mean	Variance
6-inch	No Solids	0.7199	1.1418
	9.1 % vol	0.8263	1.4261
	25 % vol	0.9828	2.4682
18-inch	No Solids	0.8026	1.9784
	9.1 % vol	0.8196	1.9974
	25 % vol	0.8245	2.7559

4.3.4. Comparison of the Heat Transfer Coefficient Measurements with Existing Data. There have been a large number of investigations on experimental measurement of heat transfer coefficient. A wide range of gas velocity, column diameter together with different gas–liquid and gas–liquid–solid systems have been studied in the published literature. A summary of these studies has been given by Hulet et al., 2009. Additional studies are also summarized in Appendix-A. It should be noted that the major effort has been on correlating the heat transfer data by means of empirical or semi-

empirical correlations but the use of these expression is limited to the experimental conditions on which they are based. In order to understand the comparative performance of these correlations, these have been plotted and illustrated in Figure 4.10. Figure 4.10 further shows a comparison between the measured time averaged heat transfer coefficients in this work taken at the column center r/R (-) = 0.0 for air-water 6-inch bubble column within the fully developed flow region (Z/D = 5.6) and the literature for both reported values and correlation predictions under atmospheric pressure and the reported values at similar operating conditions of Jhawar 2011, Wu et al., 2007; Li and Prakash, 1997; Schluter et al., 1995; Saxena et al., 1990; and Verma, 1989.

Verma, 1989 studied heat transfer rate in a 0.11 m diameter column with a height of 1.7 m equipped with a heat transfer surface that was 2 cm diameter and 33 cm long located within z/D = 5.2 -10.7 above the gas distributor. It was also observed that the heat transfer coefficient increased with increasing Ug and became all but nearly constant above a gas velocity of 0.12 m/s. Furthermore, the heat transfer coefficient was found to be independent of probe location within the sampling zone of z/D = 5.2-10.7. Based on the assumption that the heat transfer occurs by conduction to a thin boundary layer of liquid at the heat transfer surface, the authors experimental data was used for comparison in this work. Their results though generally lower than the measured in this work, lie within close range to each other as well as those measured by Wu, 2007 in a 16 cm diameter air-water bubble column and Jhawar, 2011 in a 28 cm diameter air-water bubble column using a similar probe as the one used in this work. In fact the values lie within 3 % an indication of higher level of accuracy and consistency. Schlüter et al., 1995 did not give the details of the experimental method used, thus it is hard to evaluate why their

results are larger than the measured values in this work or even to the others. The results in this work and those reported by Verma, 1989 Saxena et al., 1990, and Li and Prakash, 1997 were obtained using immersed cylindrical heaters. As reported by Saxena et al., 1990, column diameter can affect the heat transfer coefficient, and the heat transfer coefficient increases with the increase of the column diameter in a bubble column without internals.

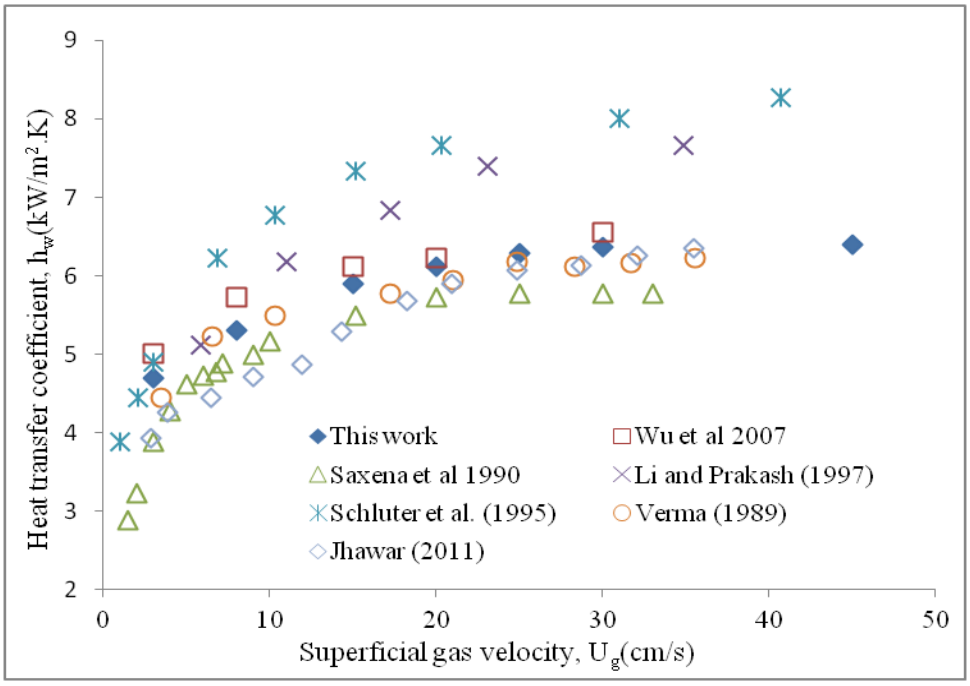

Figure 4.10 Comparison of the heat transfer coefficients measured in this work with the reported data in air-water bubble column at the column center, r/R (-) = 0.0

The heat transfer coefficient shows strong dependence on superficial gas velocity at low values up to 15 cm/s and weaker dependence at higher superficial gas velocities for all the correlations and measurements compared. The reported difference could be

attributed to difference in flow region over which such experiments were done, column diameters, or experimental and system conditions, limited data were used for the development of the correlation as well as the sparger effects. Abdulmohsin and Al-Dahhan, 2012 also claimed that such variation in measured heat transfer coefficient could be attributed to many uncertainties caused by different measurement techniques (probe) used and different operating and design conditions applied in these reported studies.

4.3.5. Effect of Dense Internals and Gas Velocity on Heat Transfer Coefficient without Solids. Most of the studies in bubble columns on transport parameters and hydrodynamics have been performed in empty bubble columns. Only a few researchers have reported the effect of internals on heat transfer coefficient in bubble columns including; (Saxena et al., 1990b; Saxena et al., 1992b; Schluter et al., 1995, Jhawar, 2011 and Abdulmohsin and Al-Dahhan, 2012). But the effect of dense internals that occupy higher CSA is still not evaluated and reported under the conditions that mimics an FT process. Thus the need to examine effect of dense internals on heat transfer coefficients in three-phase slurry bubble columns column such as those desired in the FT process. Figure 4.11 illustrates the effect of dense internals on the heat transfer coefficient and their radial profiles in 6-inch diameter bubble column.

The superficial gas velocity was calculated based only on the free cross-sectional area for the flow. It can be observed that under the same operating conditions and gas velocity, the heat transfer coefficient obtained in the presence of dense internals occupying 25 % of the column cross-section are higher than those obtained in the empty bubble column. Figure 4.12 shows similar profiles for the effect of dense internals on the heat transfer coefficient in 18-inch diameter bubble column. The systematic and detailed

studies illustrated in Section 3 has shown that with the hybrid probe in the same column and internals, small bubbles are formed with narrow range in size distribution, (Figure 3.31) while the coalescence to form larger bubbles are prevented from forming when the dense internals are used. Even though the smaller bubbles have lower rise velocity, their frequency is significantly increased and have higher residence time in the system thus enhanced holdup.

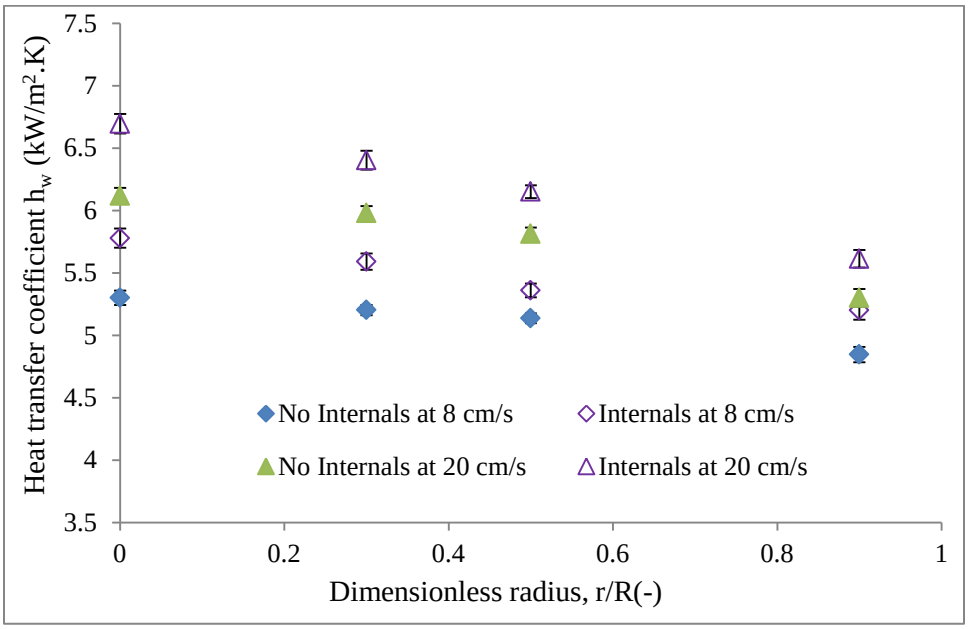

Figure 4.11 Effect of Internals on the radial profiles of the heat transfer coefficient in 6-inch bubble column Ug based on free CSA without solids

With higher gas holdup and bubble frequency, the rate of heat transfer surface renewal will be increased thus the observed increase in heat transfer coefficient with inclusion of dense internals. To illustrate the corresponding effect of the dense internals

on the radial profiles of bubble dynamics, only the gas holdup radial profiles are used since the radial profiles of the other bubble dynamic properties are more or less similar to those of gas holdup. Figure 4.13 shows the effect of dense internals on the local gas holdup radial profiles in 6-inch diameter column (Figure 4.13a) and in 18-inch diameter column (Figure 4.13b).

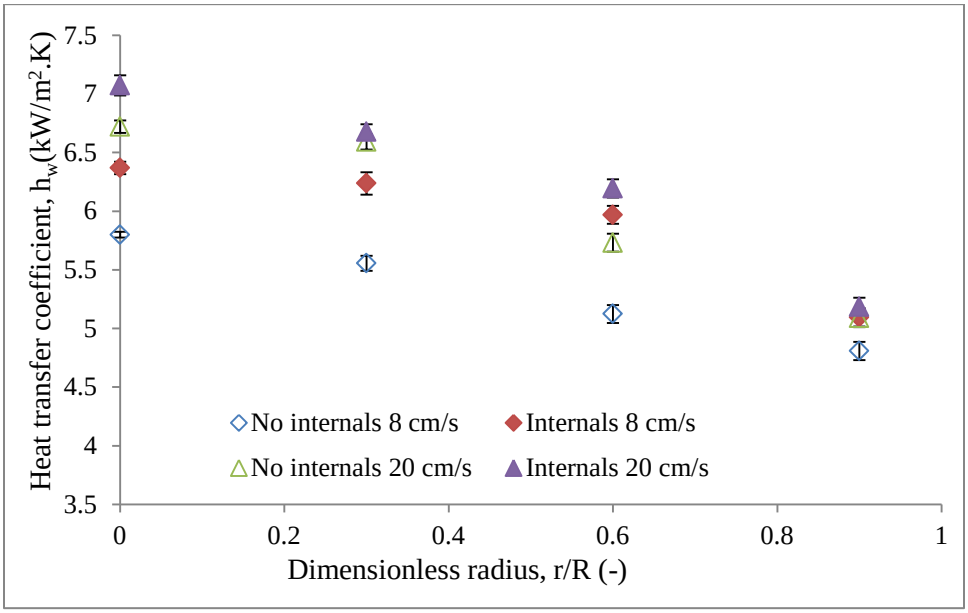

Figure 4.12 Effect of Internals on the radial profiles of the heat transfer coefficient in 18-inch bubble column Ug based on free CSA without solids

Studies in the current work reveal that the presence of dense internals increased the heat transfer coefficient in the column center by up to 8.5 % and 10 % in the 6-inch and 18-inch diameter columns, respectively, at lower superficial velocity (8 cm/s). At higher superficial gas velocity (20 cm/s) the dense internals enhanced the heat transfer

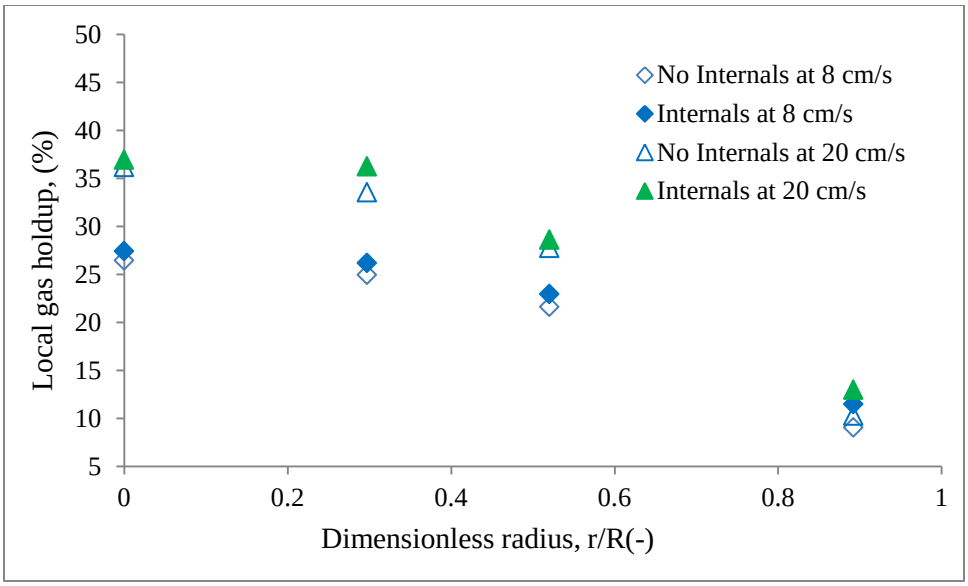

(a)

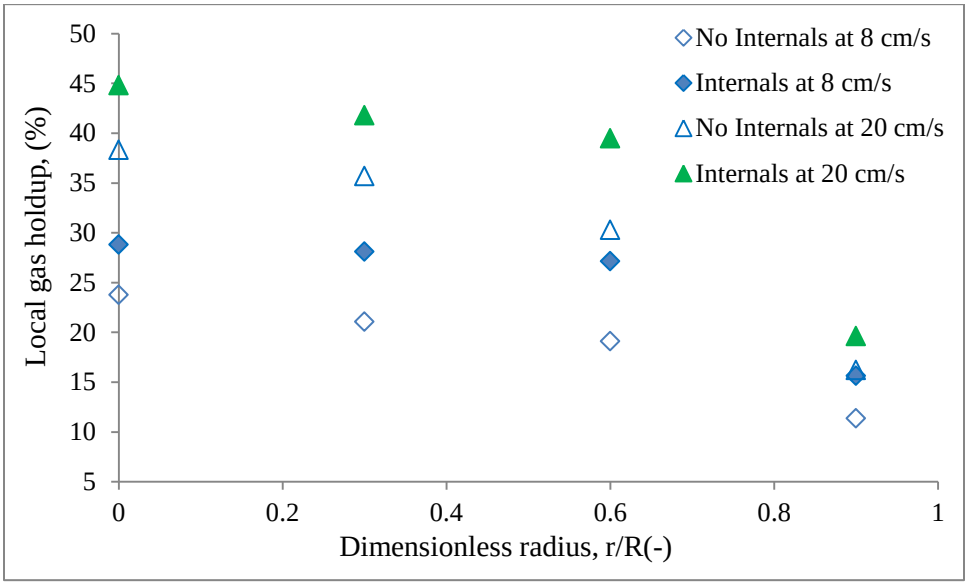

(b)

Figure 4.13 Effect of dense internals on the radial profiles of local gas holdup at different superficial gas velocities based on free CSA in (a) 6-inch diameter column and (b) 18-inch diameter column without solids

coefficient by up to 4.8 % and 2.8 % in the 6-inch and 18-inch diameter columns respectively. It is apparent from these observations that the influence of dense internals is

more significant at lower superficial gas velocities and become smaller in the higher range (churn turbulent flow regime) of gas velocity. The effect of dense internals on the bubble dynamics discussed in details in Chapter 3 reveal effect much like those on the heat transfer coefficient. As illustrated in Figure 4.13, the impact of dense internals on the local gas holdup radial profiles is more significant at lower superficial gas velocity (Ug = 8 cm/s). The local gas holdup is increased by 7 % at the column center and up to 22 % at the column wall region at 8 cm/s in 6-inch diameter column while an increase of 3 % at the column center and 18 % at the column wall region at 20 cm/s in 6-inch column. In 18-inch diameter column, the dense internals enhances the local gas holdup by 20 % at the column center and 37 % at the column wall region at 8 cm/s. At higher superficial gas velocity, 20 cm/s, dense internals enhanced the local gas holdup by 13 % at the column center and 21 % at the column wall region in 18-inch diameter.

Abdulmohsin and Al-Dahhan, 2012 also reported similar findings in heat transfer coefficient for an air-water system for studies conducted in 8-inch diameter column. They reported that compared with an empty bubble column (without internals), no significant effect was noted with internals covering low CSA of the column at 5 % of the total CSA at the same superficial gas velocity. However, when the internals coverage was increased to 22 % of the cross-sectional area, the heat transfer coefficient was enhanced by up to 19 % at low superficial gas velocity (0.03 m/s), while the effect of dense internals was smaller at high superficial gas velocity (0.2 m/s). Nevertheless, a key finding here is that the empty column results of heat transfer coefficient for a gas-liquid system can be extrapolated to those with dense internals if the Ug based on the free CSA is used.

Forret et al., 2003 also in their liquid dispersion studies in large bubble column with and without internals observed that the presence of internals gave rise to higher liquid backmixing due to large scale liquid recirculation intensity enhancement. Thus the dense internals would lead to better mixing that enhances the heat transfer rate. The resulting higher bubbles breakup rate and enhanced liquid recirculation velocity will also improve the wake enhanced heat transfer rates. Heat transfer measurements at different radial locations carried out by Li and Prakash, 1997 and Prakash et al., 2001 reported that the column center heat transfer coefficients were higher than the ones closer to the column wall heat transfer coefficients, due to the fact that large bubbles collect more dominantly at the center region. Besides that, obviously there existed more turbulence in the center as compared to near wall, due to possible wall effects.

4.3.6. Effect of Dense Internals and Solids Loading on the Heat Transfer Coefficient. From the two-phase studies in bubble columns, Kolbel et al., 1958, Zaidi et al., 1990 involving liquids of different viscosities, the effect of using different liquids with different viscosity as well as liquid phase thermal conductivity and heat capacity have demonstrated significant effect on the heat transfer rates. It is commonly accepted that the heat-transfer coefficient for gas-liquid and gas-liquid-solid increases with an increase in the gas velocity, the size of particles, and the thermal conductivity and heat capacity of the liquid, but decreases with an increase in the liquid viscosity (Kim and Laurent, 1991). Addition of solid particles would increase or decrease the average properties of suspension depending on solids, (Jhawar and Prakash, 2011). Previous studies on heat transfer in gas-liquid and gas-liquid-solid systems indicated that an increase in the liquid viscosity decreases the heat-transfer coefficient (Kato et al., 1981;

Kang et al., 1985; Deckwer, 1980; Kumar and Fan, 1994). The decrease in the heat-transfer coefficient with increasing liquid viscosity is possibly due to the fact that the thickness of the laminar sublayer in turbulent flow increases with liquid viscosity. Also the rate of surface renewal could be decreased. Figure 4.14 and Figure 4.15 show the variation of heat transfer coefficient in 6-inch and 18-inch diameter bubble columns respectively, without internals and with dense internals occupying 25 % of the column CSA at different superficial gas velocities based on the free cross-sectional area of the column.

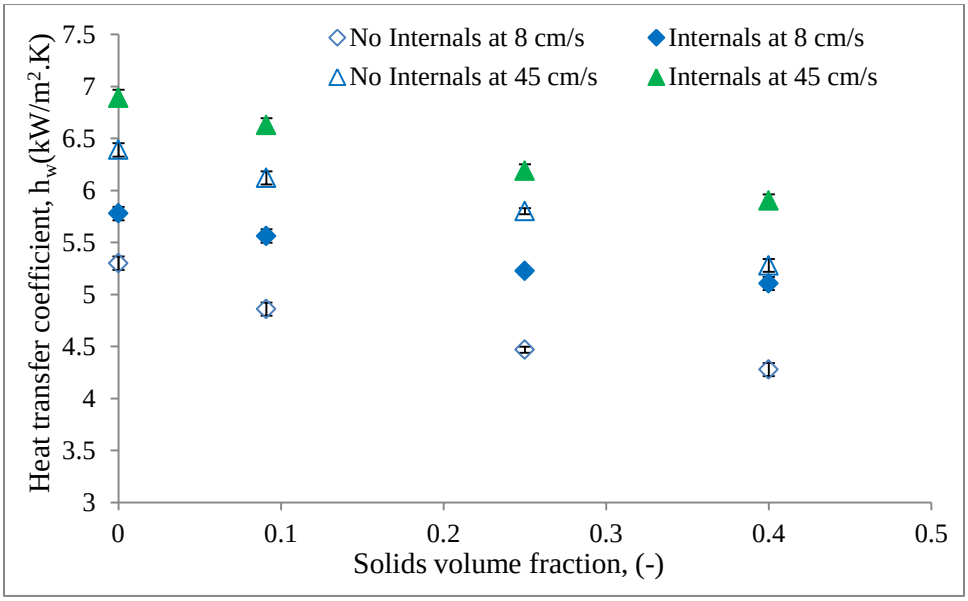

Figure 4.14 Impact of internals and solids loading in 6-inch bubble column on heat transfer coefficient at r/R(-)= 0.0 with Ug based on free cross-sectional area

It is evident from the figures that the heat transfer coefficient decreases with increase in slurry concentration in bubble columns with dense internals (25 %) and

without internals. However the rate of decrease in the heat transfer coefficient with increasing solids loading varies with the superficial gas velocity. Similar trends were observed for gas holdup and bubble passage frequency profiles, Figure 4.16. It is also noted that the impact of internals on the heat transfer coefficient is more significant at lower superficial gas velocity, at higher solids loading and more pronounced in the smaller column (6-inch). In fact with dense internals, an increase of up to 18 % is attained in the 6-inch column at 40 % vol solids loading in heat transfer coefficient as compared to 9 % increase in the heat transfer coefficient at no solids.

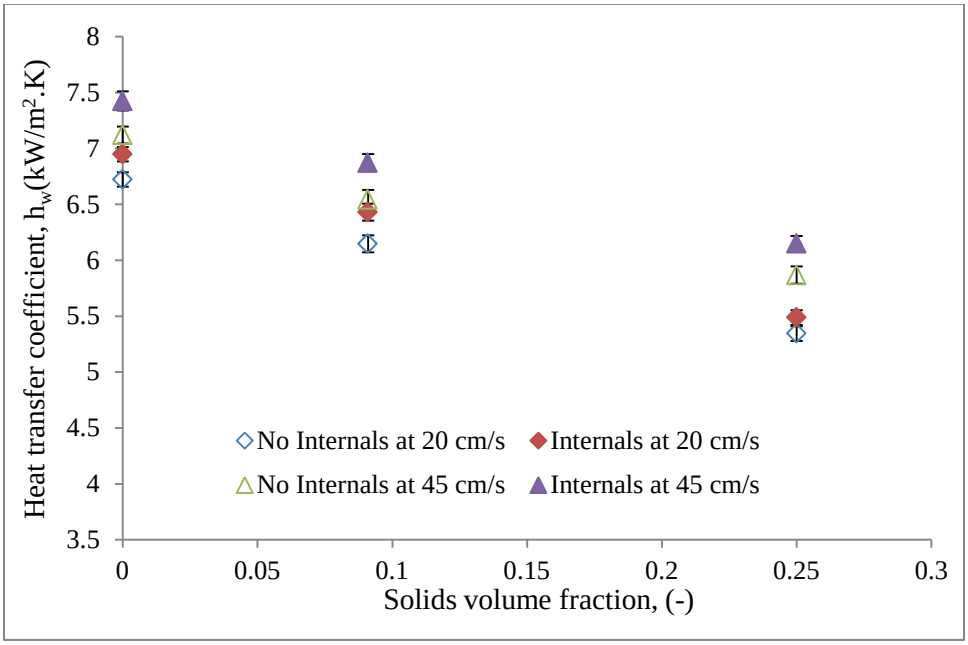

Figure 4.15 Impact of internals and solids loading in18-inch bubble column on heat transfer coefficient at r/R(-)= 0.0 with Ug based on free cross-sectional area

An increase of ~2 % in local gas holdup at 45 cm/s was attained in 6-inch column with or without solids while between ~14-17 % increase was attained at 8 cm/s. In 18-

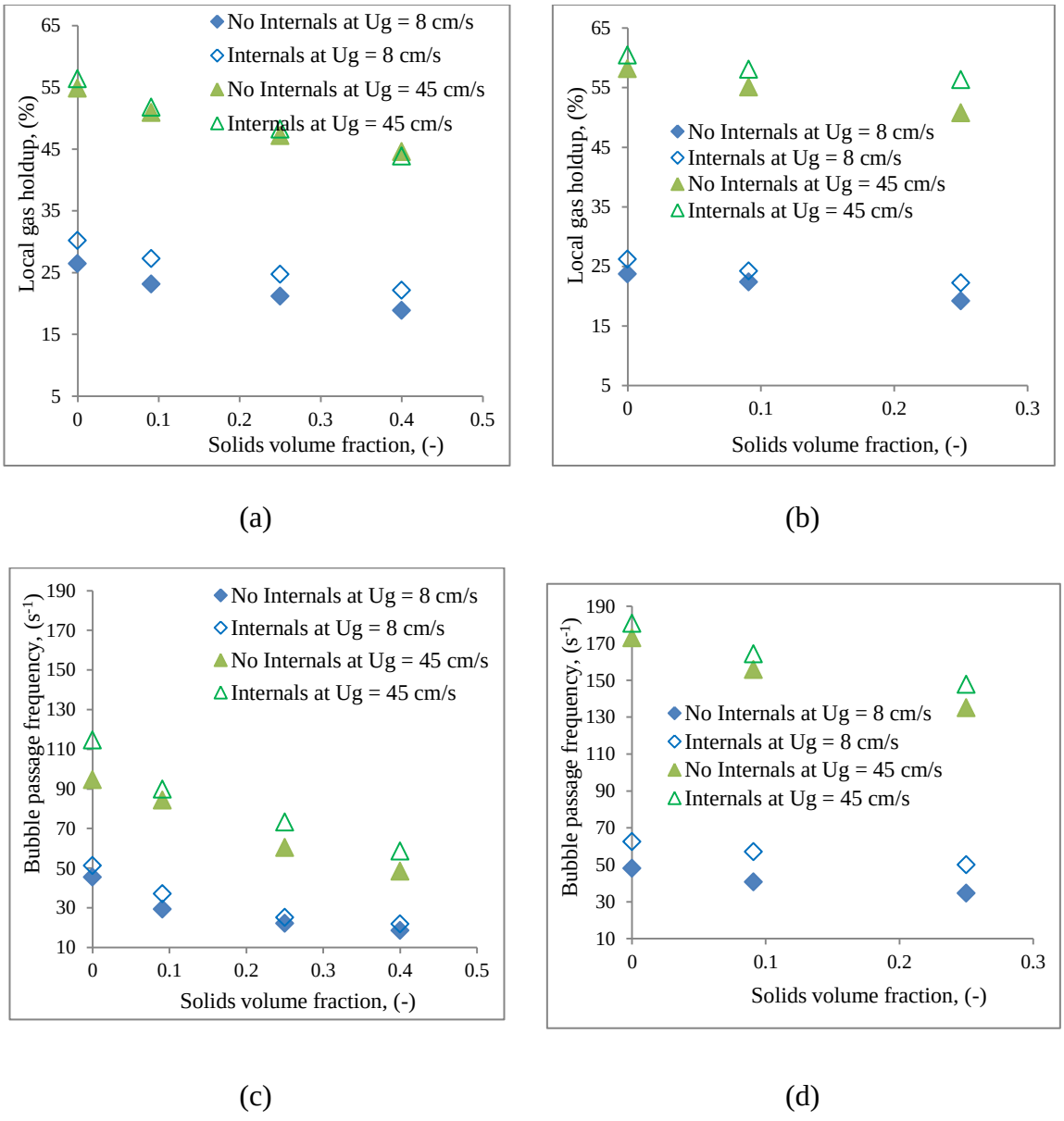

Figure 4.16 Impact of internals and solids loading on bubble dynamic parameters (a) local gas holdup in 6-inch column (b) local gas holdup in 18-inch column (c) bubble passage frequency in 6-inch column (d) bubble passage frequency in 18-inch column

inch diameter column, an increase in local gas holdup of between 3-9 % was attained at 45 cm/s while between 10 – 14 % increases at 20 cm/s. With the highest increase in both

columns attained at the highest solids loading used. Similar trends were observed for the bubble passage frequency.

As will be illustrated in Section 5, the heat transfer phenomenon is a sequential process where thermal diffusion occurs followed by convection into the bulk. The thermal boundary layer known as the film thickness is increased with solids addition. Increase in this layer leads to resistance in diffusive heat transfer. The increase in apparent suspension viscosity due to addition of particles also results in reduced turbulence, and decreased rate of surface renewal because of the solid particles dampening on the bubble wake turbulence (Li and Prakash, 1997).

It was demonstrated in Section 3 (see Figure 3.22) that the addition of glass-beads, solids only changes slightly the radial profiles of the gas hold up. Thus the resulting effect on the intensity of large-scale liquid recirculation velocity would be not significant. Thus, change in the rate of heat transfer due to addition of such solids could be mainly attributed to decreased turbulence in the gas-liquid-solids system since the glass bead solids lower the gas hold up and bubble passage frequency.

Finally, the hybrid probe used in this work gives an insight to further understand the underlying reason for the observed increase in heat transfer coefficient with the insertion of internals regardless of the solids loading.

4.4. MIMICKED HEAT EXCHANGING INTERNALS HEAT TRANSFER PROBE

4.4.1. Scope. As discussed before, the heat transfer coefficient measurements have been conducted by many researchers using flat plate type or rod assembly of the

heat transfer probes. In this section, of this work, heat transfer surface is simulated by using the modified rod type of heat transfer probe which is installed vertically in the mimicked heat exchanging tube (internals). A mimicked heat exchanging internals and heat transfer probe assembly is shown in Figure 4.17.

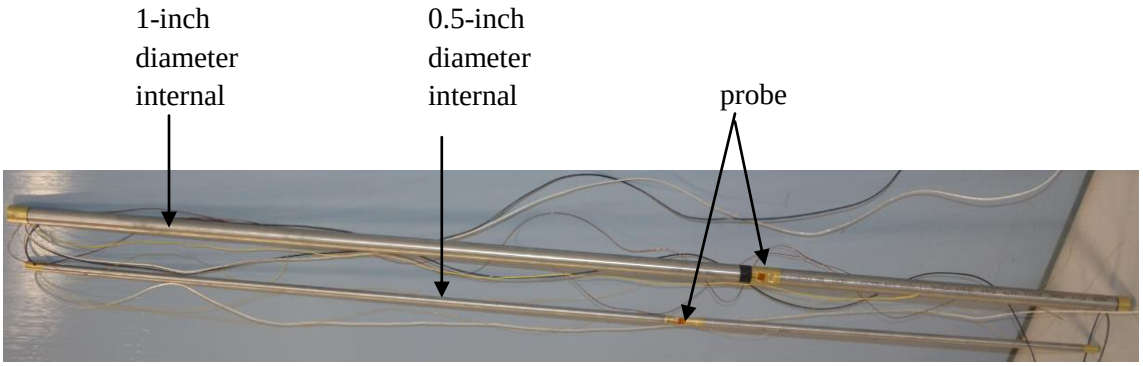

(a)

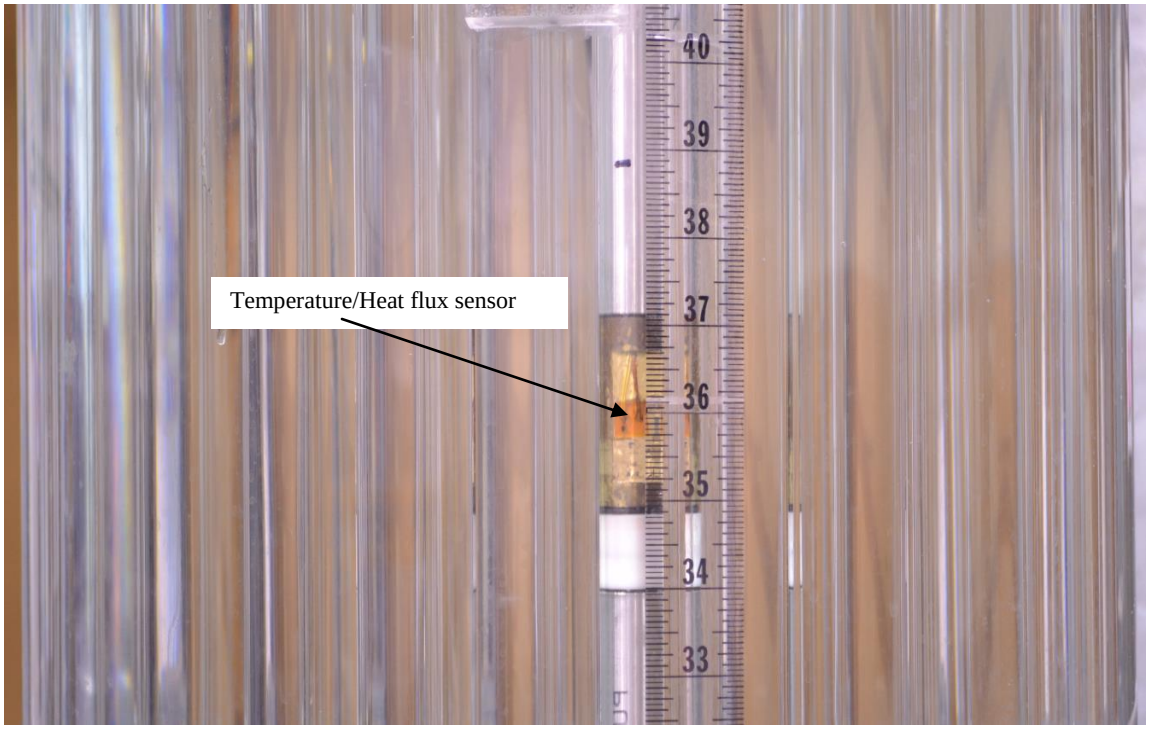

(b)

Figure 4.17 Advanced mimicked extended rod heat transfer surface probes (a) Image photos of half inch and one inch rods and (b) Image photo of the heat transfer rod among internals in the column

Two diameter tubes of heat transfer surface probes were simulated. The two consist of extended heat transfer probes, with stainless steel tubes 1/2" OD and 1" OD rods. Supporting honey-combed structures for holding the dense internals were used to keep these advanced mimicked heat transfer surface probes together. In order to investigate the role of different sizes of internals that occupy the same CSA (25 % of CSA) and hence configuration on heat transfer coefficient, the two diameters were used as discussed in Section 3. It should be noted that such measurements of the heat transfer coefficient were carried out at the same time as the bubble dynamic measurements.

The stainless steel tubes used in mimicked extended heat transfer surface probes were of the same length as the Plexiglas internals (1.83 m), and both ends of the stainless steel tubes were sealed by threaded caps (which can be any material, brass or Teflon caps) to avoid leaking. The heat transfer coefficient measurement elements are embedded at axial Z/D= 5.1 distance on the extended heat transfer probes above the gas distributor in 6 inch column and Z/D= 3.1 above the gas distributor in 18-inch column. The selected Z/D represent the fully developed flow region. To minimize heat loss by conduction, the elements were connected by Teflon fittings and rubber O-rings on the ends to avoid seepage into the cartridge heater that would compromise its functionality. These elements were designed adjustable to different axial locations, however owing to the technicality associated with the internals removal and position readjustments, in 18 inch column, only one axial position was chosen within the fully developed flow region Z/D= 3.1 above the gas distributor.

4.4.2. Assessment of Advanced Mimicked Heat Exchanging Internals Heat Transfer Probes. For comparison purposes with the results obtained from the L-shaped

heat transfer probe, the experiments were conducted in the air-water systems under ambient pressure in both 6-inch diameter column and the 18-inch diameter column and in the presence of dense internals. Though the experimental investigations were also performed on the effect of different axial locations in the 6-inch column, three axial positions all within the fully developed flow region, the observed differences even with the dense internals are within the margin of experimental error, thus not reported here. The results obtained by the elements for the air-water system are shown in Figure 4.18 in 6-inch column in which half inch dense internals were used while Figure 4.19 for the 18-inch column air-water system in which 1-inch dense internals were utilized. The standard deviations were noted to be less than 0.114 ($kW/m^2.K$) in 6-inch diameter heat transfer surface probes.

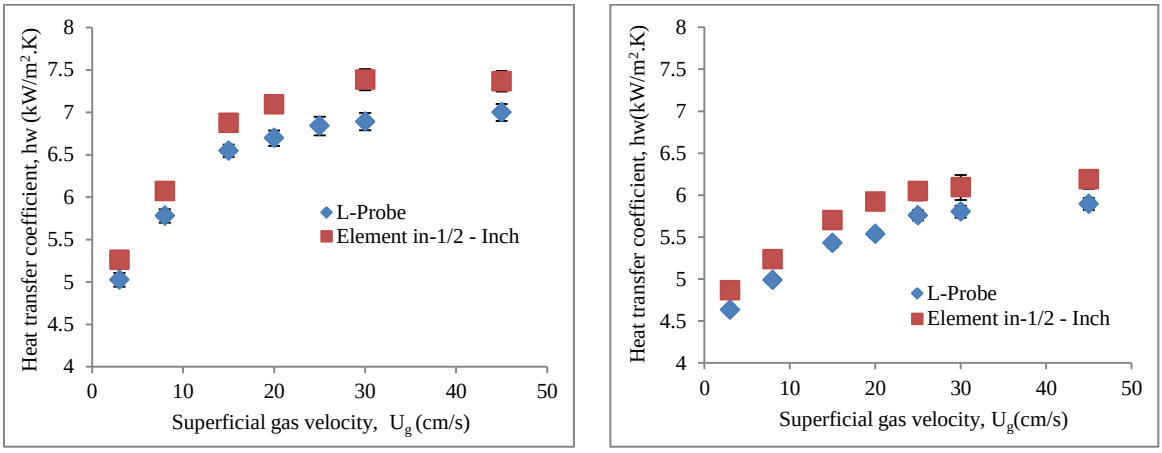

(a) (b)

Figure. 4.18 Comparison between the data obtained by embedded probe on the half-inch internal rod and those measured by single L-shaped probe at z/D = 5.1 in 6-inch column for an air-water system at (a) column center (b) column wall region

For both the columns it is observed that the heat transfer coefficient obtained by the elements (mimicked internal probe) is higher than those measured by the L-shaped rod probe at the same position with dense internals. However, the average deviation over the whole range of superficial gas velocity (based on free cross-sectional area) is less than 8 % in 6-inch column (i.e between 4 - 9 %) and less than 5 % in the 18-inch column (i.e between 3 – 6 %), with deviations being highest at lower gas velocity in the two columns. The deviations were even smaller closer to the wall region in both the columns.

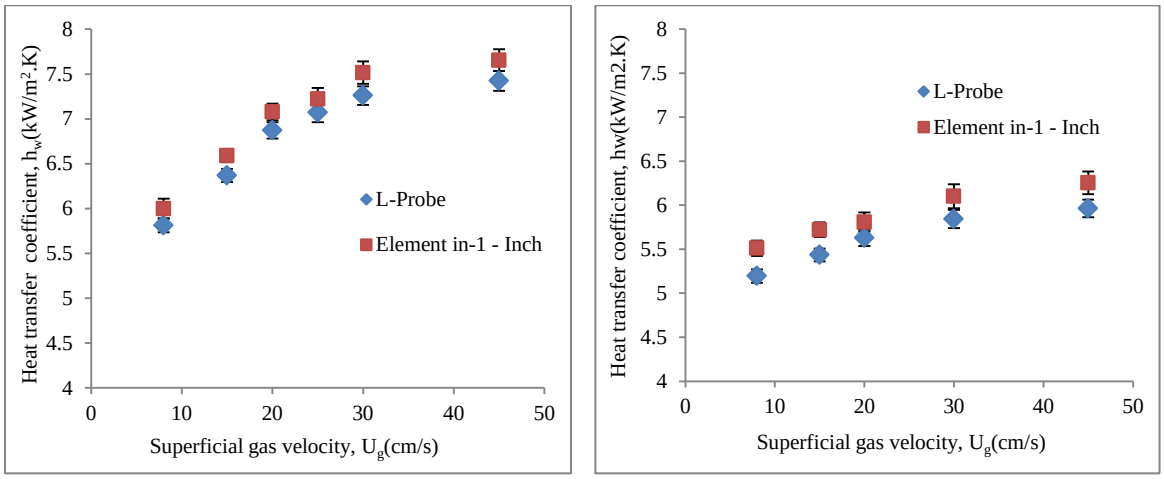

(a) (b)

Figure. 4.19 Comparison between the data obtained by embedded probe on the one-inch internal rod and those measured by single L-shaped probe at z/D = 3.1 in 18-inch column for an air-water system at (a) column center (b) column wall region

It is clear that when the heat transfer probe is embedded on the internals, consistently higher values of the heat transfer coefficient were relative to the L-shaped rod heat transfer probe in both the columns irrespective of the radial location of the probe were obtained. Thus it is necessary that the use of embedded heat transfer probes on the

internals be adopted for the heat transfer measurements in columns inserted with dense mimicked heat exchanging internals.

To assess the effect of different diameter of dense internals occupying the same cross-sectional area on the heat transfer coefficient, a comparison is made for the measurements obtained using the advanced mimicked extended heat transfer rods of half-inch diameter and one-inch diameter rods. Figure 4.20 shows a comparison of measurements obtained by the elements in 6-inch column using half inch diameter internals and 1-inch diameter internals both covering 25 % cross-sectional area of the column for air-water-glass beads with the solids loading at 25 % volume. It is noted from

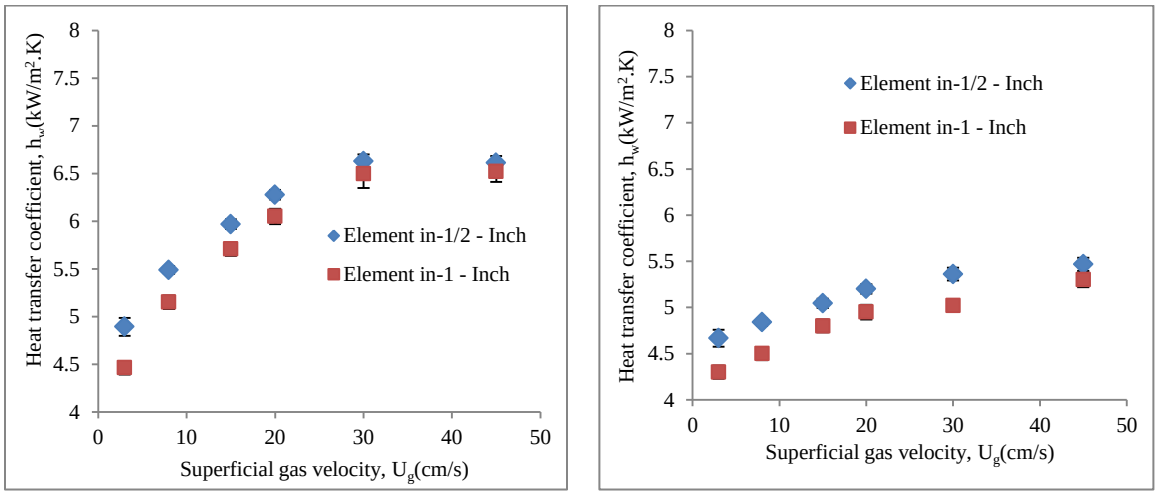

Figure 4.20 Comparison between the data obtained by embedded probe on the one-inch internal rod and those measured by the half-inch internal at z/D = 5.1 in 6-inch column for an air-water-glass beads system (25 % vol.) at (a) column center (b) column wall region

Figure 4.20 that half-inch internals gave consistently higher heat transfer coefficient values at the column center and close to the column wall region. This is expected as

depicted from the bubble properties discussed in Section 3 and illustrated by Figures 3.7, 3.8, 3.10 and Figures 3.13-3.18.

4.5. SUMMARY

Hybrid measurements technique for heat transfer coefficient and bubble dynamics was developed and successfully implemented in a 0.14 m ID bubble and 0.44 m ID bubble and slurry bubble columns. The effects of superficial gas velocity, dense internals, solids loading, and radial probe location on heat transfer coefficients were investigated. For the first time, the heat transfer coefficient has been studied in connection with bubble dynamics under conditions that mimic F-T reaction process with dense internals occupying 25 % CSA and high solids loading up to 40 % by volume. The findings and conclusions are summarized as follows:

The heat transfer coefficient increases with superficial gas velocity, although at higher superficial gas velocities, particularly beyond 20 cm/s the rate of increase is considerably small. When the operating conditions are maintained constant, the heat transfer coefficient in the center of the column is larger than those near the wall region, and the differences at higher superficial gas velocities are smaller than those at low superficial gas velocities.

The heat transfer coefficient obtained in empty column for gas-liquid system can be extrapolated to columns equipped with dense internals occupying 25 % of the CSA.

For gas-liquid-solids (glass-beads) systems, the heat transfer coefficient obtained in empty 6-inch diameter column cannot be extrapolated for 6-inch diameter column equipped with dense internals occupying 25 % of the CSA due to significant differences

obtained even when the gas velocity was based on free CSA. The extrapolation can be done for 18-inch column from the results in empty column to the column equipped with dense internals, using Ug based on free CSA. For the 6-inch column, some of the bubble properties such as local gas holdup and axial bubble velocity can be extrapolated only at higher gas velocities, ($\geq$ 20 cm/s) while the other bubble parameters such as bubble passage frequency and bubble sizes cannot be extrapolated.

With dense internals occupying 25 % of the CSA, the heat transfer coefficient increases, although the increase is more pronounced at low superficial gas velocities, a similar scenario as those of the bubble properties.

At low solids loading, the heat transfer coefficient in the slurry bubble column behaves nearly like that in a two-phase system. However, with further increase in solids loading, a decrease in the heat transfer coefficient was observed but the fall slows down beyond 25 % solids by volume.

The radial profile of heat transfer coefficients becomes flat towards the column core and changes only slightly with increasing solids loading, much like the gas holdup and bubble velocity, bubble sizes and bubble passage frequency radial profiles.

To assess the effect of internals on the heat transfer coefficient, new mimic heat exchanging internals with attached heat transfer coefficient measurement elements were constructed and assessed. Smaller diameter internals provided higher heat transfer rate as compared to the larger diameter elements. The impact of smaller diameter internals was equally and consistently higher on the bubble properties assessed in details in Section 3. It is also worth to note that the embedded heat transfer probe on the internals gave consistently higher values relative to the L-shaped rod heat transfer probe in both the

columns irrespective of the radial location of the probe. Thus the use of advanced embedded heat transfer probes on the internals would be necessary for the heat transfer measurements in slurry bubble columns inserted with dense mimicked heat exchanging internals.

5. MECHANISTIC ASSESSMENT OF HEAT TRANSFER COEFFICIENT BASED ON BUBBLE DYNAMICS

5.1. SCOPE

In order to predict the heat transfer rates and coefficients in bubble and slurry bubble columns, several correlations have proposed. These correlations have been developed based on either experimental studies on heat transfer in bubble columns or based on bubble dynamics studies. Thus the heat transfer studies have been performed separately from bubble dynamics studies under different operating conditions. However, as discussed in Section 2, and the previous chapters, bubble dynamics and heat transfer are closely related. Detailed critical review of the studies on heat transfer coefficient and bubble dynamics and hydrodynamics point at closely knit relation between the bubble dynamics and the heat transfer rate in two-phase and three-phase systems in general and bubble and slurry bubble columns in particular. Thus, there is a need to mechanistically asses how the heat transfer phenomenon in bubble columns is affected by different bubble properties that govern the flow behavior, including local gas holdup, bubble passage frequency, bubble velocity, bubble sizes, as well as their directions. In this chapter a systematic mechanism for predicting the heat transfer coefficient is presented and analyzed.

Turbulence and mixing that are induced by gas bubbles play important role in heat and mass transfer in gas-liquid and gas-liquid-solid systems. The high heat-transfer rate in multiphase flow systems particularly bubble and slurry bubble columns is mainly due to bubble induced turbulence (Yang et al., 2000, Kumar et al., 1992). Both experimental and theoretical results reported in the literature suggest that there is a series

of film and surface renewal that govern the heat exchange between a heat transfer surface and flowing fluid adjacent to the surface (Karst, 1962; Wasan and Ahluwalia, 1969; Yang et al., 2000; Kumar and Fan, 1994).

The film theory was first proposed by Nernst, 1904. It has been applied to both heat and mass transfer with some success. According to this model, steady-state mass transfer and hence heat transfer occurs by molecular diffusion across a stagnant, or laminar film at the interface between phases where the fluid is turbulent. The mass transferred across a unit area of the interface per unit time is assumed to be proportional to the concentration gradient between the bulk fluid and the interface such that

$$\dot{m} = -\frac{D}{\delta_e}(c_b - c_i) = -k(c_b - c_i) \tag{5.1}$$

Where D is the molecular diffusivity, δ_e is the effective film thickness, c_b is the average concentration in the bulk fluid and c_i the average concentration in the interface, $\dot{m}$ is the rate of mass transferred across a unit area of the interface and $k = \frac{D}{\delta_e}$ is the mass transfer coefficient. The analogous form of heat transfer can be derived in a similar manner that would give the heat flux, q and the heat transfer coefficient h as

$$\dot{q} = -\frac{\alpha}{\delta_e}(t_b - t_i) = -h(t_b - t_i) \tag{5.2}$$

Where α is the thermal diffusivity, δ_e is the effective film thickness, t_b and t_i are the average temperature of the bulk fluid and of the interface respectively, $\dot{q}$ the heat flux per unit area and $h = \frac{\alpha}{\delta_e}$ is the heat transfer coefficient. This model indicates a linear relationship between mass flux and the molecular diffusivity, D and hence the heat flux and the thermal diffusivity, α. It (the model) also oversimplifies the actual conditions near a phase boundary. Furthermore, the concept of the theory supposes that there exists a

stagnant film of a definite but unknown thickness. Therefore according to Azbel, 1981 this theory's main weakness is the introduction of a uniform film of thickness, δ_e.

Based on Fick's second law of unsteady diffusion (Higbie, 1935), proposed the penetration theory where mass or heat transfer is observed as time-dependent non-steady state process. The non-steady state phenomenon was not accounted for by the film theory. Mass transfer and heat transfer are assumed to occur during the repeated contacts of matter (gas/solid) with the liquid interface. Fresh liquid elements continually replace those interacting with the interface. During each contact period between the liquid element and the interface, mass or heat is transferred to the element. According to this theory, the contact time of the small eddies with the interface, is so short that the steady state characteristics do not develop therefore the transfer of heat or mass is by unsteady-state molecular diffusion. Besides, all the eddies are assumed to stay in contact with the interface for same length of time (θ) during which diffusion of matter (heat and mass) occurs into the eddy which can be described for a 1-D system by Equation 5.3;

Hence, the average heat transfer coefficient during the contact time θ between the fluid eddy and the heat transfer surface can be calculated as follows;

$$T = \begin{cases} T_b & at\ t = 0, \quad y \geq 0 \\ T_b & at\ y \to \infty, \quad t \geq 0 \\ T_i & at\ y = 0 \quad t > 0 \end{cases}$$

Then the average heat transfer coefficient, h_{avg} according to Higbie, 1935 becomes

$$h_{avg} = \sqrt{\left(\frac{\alpha}{\pi\theta}\right)\rho c_p} \tag{5.3}$$

Danckwerts, 1951 modified the penetration theory, (Higbie, 1935) and came up with the surface renewal model in-order to account for the different times of contact by different

eddies which have different sizes. Thus the fluid elements can have a surface residence time ranging from zero to infinity. Hence the average heat transfer coefficient becomes;

$$h_{avg} = \sqrt{(\alpha s)\rho c_p} \tag{5.4}$$

Where s is the fractional rate of surface renewal by the elements, a parameter not easy to determine.

Research conducted to investigate the characteristics of liquid film both experimentally and theoretically suggest that a thin film lies between a solid surface and the flowing fluid over the solid surface; Cooper, 1969, Moriyama and Inoue, 1996, Shedd & Newell, 2004. Thus to predict the heat transfer coefficient, using the film theory alone would not be appropriate due to its shortcoming stated earlier-on. While using the penetration theory alone would not be sufficient since different eddies have a distribution in the contact time. Surface renewal model would be more appropriate but on it's on, the presence of the stagnant liquid film would not be accounted for. Thus combining both the surface renewal and film theory is the most appropriate mechanism of estimating the heat transfer rate.

Accordingly, Wasan and Ahluwalia, 1969 developed a mechanistic model to predict heat transfer coefficient based on a mechanism where heat-transfer enhancement due to bubble passage expressed in terms of film theory and unsteady-state consecutive surface renewal model (also known as the modified penetration theory). Such mechanism suggests that there is a thin film of uniform thickness, δ, lying parallel to and covering the heat transfer surface. Due to the bubble motion around the film, a liquid element is moved to the outer surface of film from the bulk. In this case, heat is transferred to the element by unsteady state conduction during the contact period and then washed away. A

short time later another fluid element is moved to the same surface and the process repeats. Figure 5.1 illustrates the consecutive film and unsteady state surface renewal heat transfer mechanism from the heating source into the bulk fluid.

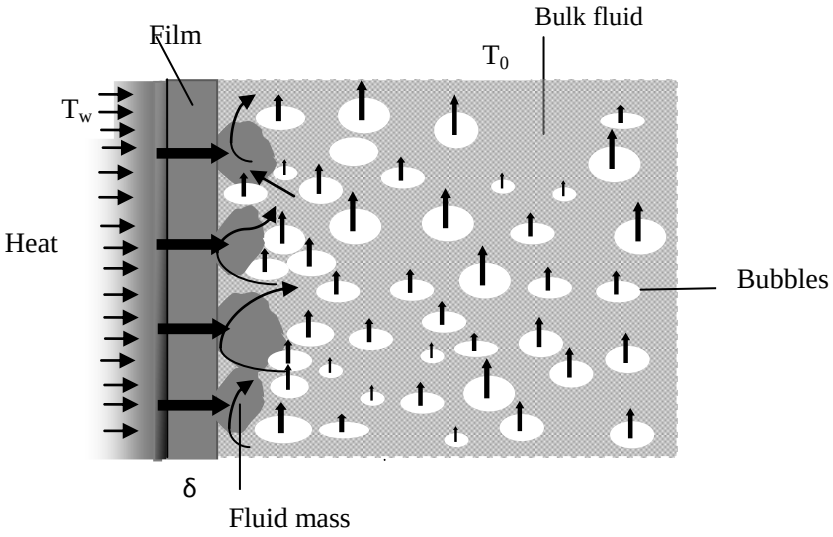

Figure 5.1 Consecutive film and unsteady state surface renewal mechanism, (modified from, Wasan and Ahluwalia, 1969)

This proposed approach differs from the concepts of the combination of film-penetration theory where the later recommended film theory for long contact times and penetration theory for short contact times. In Wasan and Ahluwalia's, 1969 approach, a uniform film (thinner than would be predicted by film theory alone) is regarded to lie adjacent to the heat transfer surface and a mass of fluid exchanges heat by unsteady state conduction at the outer edge of such film. Hence, there is a dynamic change of the temperature of the interface between the film and the fluid element. According to this approach, Wasan and Ahluwalia, 1969 developed a mechanistic model to predict heat

transfer coefficient from heat exchanging surface to flowing gas-liquid and gas-liquid-solid mediums as outlined below.

In such approach, the temperature of the fresh fluid element coming from the bulk to outer surface of the film is assumed to be uniform and equal to the bulk fluid temperature at time (t) = 0. By assuming no energy storage in the film, the instantaneous heat transfer rate to the fluid mass was given as

$$q = -k\left(\frac{\partial T}{\partial Y}\right)_{y=0} = h\left(T_w - T_{y=0}\right) \tag{5.5}$$

Where, y is the distance within the fluid mass measured from the edge of the film, and the film with a uniform film thickness δ, and the heat transfer coefficient, $h = k/\delta$.

The two dimensional unsteady state equation for heat conduction to the fluid mass is;

$$\frac{\partial T}{\partial t} = \alpha\left(\frac{\partial^2 T}{\partial y^2} + \frac{\partial^2 T}{\partial z^2}\right) \tag{5.6}$$

Where α is the thermal diffusivity given by, $\frac{k}{\rho C_p}$. By assuming an infinitely long heat source, which is normal to the heat flux direction, equation (5.6) can be simplified as follows:

$$\frac{\partial T}{\partial t} = \alpha\frac{\partial^2 T}{\partial y^2} \tag{5.7}$$

By using the Laplace transform the solution of equation (5.7) becomes

$$\overline{T} = \frac{T_0}{s} + c_1 e^{\sqrt{s/\alpha}y} + c_2 e^{-\sqrt{s/\alpha}y} \tag{5.8}$$

As $y \to \infty$, $e^{\sqrt{s/\alpha}y} \to \infty$, thus $c_1 = 0$.

So equation (5.7) becomes

$$\bar{T} = \frac{T_0}{s} + c_2 e^{-\sqrt{s/\alpha}y} \tag{5.9}$$

When equation (5.5) is transformed with respect to time, t, it yields;

$$\bar{q} = -k\left(\frac{\partial \bar{T}}{\partial Y}\right) = h\left(\bar{T}_w - \bar{T}_{y0}\right) \tag{5.10}$$

Differentiating equation (5.9) with respect to y then substitution into equation (5.10) and solving for c_2 gives;

$$c_2 = \frac{h}{(h+k)\sqrt{\left(\frac{s}{\alpha}\right)}}\left[\bar{T}_w - \frac{T_0}{s}\right] \tag{5.11}$$

Substituting c_2 from equation (5.11) into equation (5.9) gives

$$\bar{T} = \frac{T_0}{s} + \frac{h\, e^{-\sqrt{s/\alpha}y}}{(h+k)\sqrt{\left(\frac{s}{\alpha}\right)}}\left[\bar{T}_w - \frac{T_0}{s}\right] \tag{5.12}$$

Solving equation (5.8), combing its final equation with equation (5.5) and setting $y = 0$ yield:

$$\bar{q} = h\left[\left(\bar{T}_w - \frac{T_0}{s}\right) - h\left(\bar{T}_w - \frac{T_0}{s}\right)\frac{1}{h+k\sqrt{\frac{s}{\alpha}}}\right] \tag{5.13}$$

By taking inverse Laplace transform, substituting $h = k/\delta$, combining and utilizing equations 5.14, 5.15 and 5.16, equation 5.17 below will be obtained.

The total heat transfer over the contact time period is q_{t_c}.

$$q_{t_c} = \int_0^{t_c} q\, dt \tag{5.14}$$

The overall heat transfer rate q_{av} is the average over the contact time of the instantaneous heat transfer rate:

$$q_{av} = \frac{1}{t_c}\int_0^{t_c} q\, dt \tag{5.15}$$

Also with

$$q_{av} = h(T_w - T_0) \tag{5.16}$$

Accordingly, Wasan and Ahluwalia, 1969 proposed equation (5.17) for modeling the average heat transfer coefficient, h_w which depends on the film thickness δ, contact time, t_c, and the physical properties, k and α.

$$h_w = \frac{2k}{\sqrt{\pi \alpha t_c}} - \frac{k\delta}{\alpha t_c}\left[1 - e^{\frac{\alpha t_c}{\delta^2}} erfc \frac{\sqrt{\alpha t_c}}{\delta}\right] \quad (5.17)$$

where, k and α are thermal conductivity and thermal diffusivity of the liquid or slurry, respectively.

This model (equation 5.17) has been successfully used to predict the heat transfer coefficient in two-phase and three-phase flow systems (Kumar et al., 1992; Kumar and Fan, 1994; Li and Prakash, 1997; Yang et al., 2000). This model (Equation 5.17) can give local heat transfer coefficient $h_w(r)$ by locally having different estimated t_c and δ. The needed film thickness, δ, and the contact time t_c, have been estimated by different investigators using the few available empirical correlations. In this work, the needed contact time t_c will be developed, and the parameters related to it are examined.

5.2. EXPERIMENTAL SETUP

In order to illustrate the heat transfer in a mechanistic manner and based on the discussed model above, a simultaneous measurements of both the heat transfer coefficient and bubble dynamics were conducted in two scales of Plexiglas columns. The smaller scale was a 0.14 m inside diameter and 1.8 m height with dynamic bed height in all the experiments, maintained constant at a level of 1.56 m (z/D = 11.16) above the gas distributor by adjusting the amount of liquid loaded in the column. The larger scale consisted of a 0.44 m inside diameter and 3.66 m height with dynamic bed height in all

the experiments maintained constant at a level of 2.67 m (z/D = 6.0) above the gas distributor by adjusting the amount of liquid loaded in the column. In this study, compressed filtered oil-free dry air introduced continuously from the bottom of the columns was used as the gas phase. Soft filtered tap water was used as liquid phase. Glass beads with an average size of 150 μm and density of 2500 kg/m^3 was used as the solids/fines phase. The solids loading was based on the wet volume and the concentrations varied between 0 % vol – 25 % vol.

In both units perforated plates with triangular pitch hole pattern (6-inch column) and square pitch hole pattern (18-inch column) with a total free area of 1.09 % was used as the gas distributors. The superficial gas velocities were from 0.03 to 0.45 m/s based on free cross-sectional area of the column covering both the bubbly and churn turbulent flow regimes. The internals used in this study were vertical Plexiglas rods of 0.5-inch and 1-inch diameter (in the small scale column and the large scale column, respectively) occupying 25 % of the column cross-sectional area that simulates the Fischer-Tropsch synthesis process. The schematics of both the columns used, the internals used and and the general features of the experimental systems is the same as discussed in Sections 3-4. Combined probes consisting of both advanced four-point optical probe and a fast response heat transfer were used to simultaneously measure the local heat flux and surface temperature and the local bubble properties, including local gas hold up, bubble passage frequency, axial bubble velocity, specific interfacial area, as well as the bubble chord lengths which is characteristic of bubble sizes.

5.3. CONTACT TIME MODELING DEVELOPMENT

One of the two needed parameters in the mechanistic Equation (5.17) is the contact time, (t_c) between the fluid element and the thin film. Due to the limitation in the measurements and the unavailability of techniques, only a few models for the estimation of the contact time between the liquid elements and the thin film have been proposed. Kumar and Fan, 1994 assumed that the absolute bubble rise velocity can be taken as an estimate of the characteristic velocity of a fluid element near the heat transfer surface. They obtained the absolute bubble rise velocity by following each bubble frame by frame in the video recording over a certain distance. Therefore, during the heat-transfer enhancement by the bubble wake, the time available for heating by conduction before each fluid element passes the heat-transfer surface may be approximated. They assumed that all the fluid elements renew the probe surface at the same rate hence there is no distribution of residence time, which is in line with the penetration theory (Higbie, 1935). Thus, they proposed equation (5.18) to estimate the contact time in gas-liquid (bubble columns) and gas-liquid-solid (slurry bubble columns) systems.

$$t_c = \frac{L}{U_b} \tag{5.18}$$

where L is the vertical length of the heat flux sensor and U_b is the bubble rise velocity. So during this time, unsteady heat conduction occurs and starts at a distance from the heat transfer surface equivalent to the thickness of the thin film. One of the main drawbacks of this approach is that the video can only be used for transparent medium at very low gas velocity, hence minimized applicability in systems requiring higher gas velocities

Yang et al., 2000 alongside Kumar and Fan, 1994 assumed that the contact time is equal to the contact time between the bubbles and the film and used the same equation

proposed by the latter (Equation 5.18). While using a cylindrical rod-type of the heat transfer probe, Li and Prakash, 2001 assumed that the contact time, θ_c can be modeled as;

$$\theta_c = \frac{d_p}{U_{b,L}} \tag{5.19}$$

Where d_p is the diameter of the cylindrical probe while $U_{b,L}$ is the rise velocity of large bubbles. These approaches only provided single values for the contact time to obtain single averaged value of heat transfer coefficient using the mechanistic model of Equation (5.17). However, in the multiphase flow systems particularly bubble and slurry bubble columns, at a particular superficial gas velocity, populations of bubbles and their properties (velocity, size, passage frequency, specific interfacial area, local gas holdup) exist (Xue et al., 2004, Youssef and Al-Dahhan, 2009). Unfortunately accounting for this distribution has not been reported in the open literature. Theoretically with a reasonable measurement approach, the distribution in the contact time can be obtained from the above models.

In this work the distribution in the contact time estimation, boundary layer estimation and heat transfer coefficient calculations using Equation (5.17) is assessed using new approach in estimating contact time. In the measurements of local gas hold-up, a number of studies have been done by fiber optical probes. Schweitzer et al, 2001 using 2 points optical fibers to measure local gas holdup in fluidized beds and slurry bubble columns, demonstrated that the optical probe spends different amount of time in the gas phase as it does in the liquid and pseudo-slurry phase. Detailed experimental studies by Xue et al., 2004; Wu, 2007 and, Youssef and Al-Dahhan, 2009 have shown that the optical probe stays for different times in the liquid as it does in the gas bubbles. Moreover, the quantities of heat transfer coefficient and bubble dynamics vary along the

diameter or radial and the height of the column (containment of the gas-liquid and gas-liquid-solid systems).

Accordingly, local gas holdup is defined as the fraction of volume occupied by gas within a certain volume of interest within the fluid mixture (Xue, 2004, Schweitzer et al., 2001),

$$\varepsilon_{g,local} = \frac{V_{g,local}}{V_{g,local} + V_{l,local}} \tag{5.20}$$

This same definition can be extended to local gas holdup for pseudo-slurry mixture as well. By invoking the ergodic hypothesis, which states that "the ensemble average is equivalent to the time average," the spatially (volume) averaged local holdup can be replaced by its equivalent time-averaged local holdup which is the ratio of the time the probe tip spends in the gas bubbles to the sampling period thus.

$$\varepsilon_g = \frac{t_g}{t_g + t_l} \tag{5.21}$$

Where ε_g , t_g and t_l are the local gas holdup, time the fiber probe tip spends in the bubble and time the probe spends in the liquid, respectively, during a sampling time τ. Over such sampling time τ, N bubbles hit the fiber probe tip. The average time spent by the probe tip inside a bubble, $\bar{t}_g$ is given by:

$$\bar{t}_g = \frac{\varepsilon_g}{N}\tau \tag{5.22}$$

Similarly the average time the probe spends in the liquid element, $\bar{t}_l$ becomes

$$\bar{t}_l = \frac{\varepsilon_l}{\varepsilon_g}\bar{t}_g \tag{5.23}$$

Where, ε_l is the local liquid holdup

$$\varepsilon_l = 1 - \varepsilon_g \tag{5.24}$$

Substituting Equations (5.22) and (5.24) into Equation (5.23) gives the contact time between the thin film and the liquid element as:

$$\bar{t}_l = t_c = \left(1 - \varepsilon_g\right)\frac{\tau}{N} = \frac{\left(1-\varepsilon_g\right)}{N/\tau} = \frac{\varepsilon_l}{N/\tau} \tag{5.25}$$

It is worth noting that $\frac{\tau}{N}$ is the inverse bubble passage frequency ν^{-1} over the optical fibers tip and hence, over the heat transfer probe surface when the optical probe tips are mounted just off the heat flux sensor. This approach indeed shows that the contact time is a function of the local liquid holdup or gas holdup as $\varepsilon_l = 1 - \varepsilon_g$ and bubble passage frequency. Consequently, the variation of heat transfer coefficient with the contact time is via the bubble passage frequency and the local phase holdups that are determined by the bubble velocity, bubble sizes and the gas-liquid specific interfacial area. Since by the hybrid measurements, local gas holdup and local bubble passage frequency can be obtained, it is therefore possible to obtain the mean local contact time.

5.4. FILM THICKNESS ESTIMATION

The other parameter required in the mechanistic equation is the film thickness; δ. The film thickness accounts for the heat transfer resistance. Border diffusion layer model developed by Azbel, 1981, which is a modified film theory has been used by Kumar and Fan, 1994 and Yang et al., 2000 to predict the film thickness, δ. In this work, this model is used. According to this model, the distribution of the diffusing matter (mass or heat) in a turbulent stream has a four-layer structure. Namely, the diffusion sublayer δ, which is also known as the thermal boundary layer and is in contact with the solid interface, followed by the laminar viscous sublayer δ_0, then turbulent boundary layer and finally the

main turbulent stream. According to Azbel, 1981 the relation between the diffusion sublayer and the viscous sublayer is;

$$\delta = \left(\frac{\propto}{\upsilon}\right)^{1/n} \delta_0 \ , \tag{5.26}$$

where ν is the kinematic viscosity and α the thermal diffusivity. According to the experimental data for liquid-solid interface flows, it has been found that $n \cong 3$ (Azbel, 1981). The thickness of laminar viscous sublayer, δ_0 can be estimated by solving the Prandtl's boundary-layer equations; (Schlichting, 1968)

$$\frac{\partial u}{\partial t} + u\frac{\partial u}{\partial x} + v\frac{\partial u}{\partial y} = -\frac{1}{\rho}\frac{\partial p}{\partial x} + v\frac{\partial^2 u}{\partial y^2} \tag{5.27}$$

$$\frac{\partial u}{\partial x} + \frac{\partial v}{\partial y} = 0 \tag{5.28}$$

With the boundary conditions

$y = 0:$ $\quad u = v = 0;$

$y = \infty:$ $\quad u = U(x, t)$

Where U(x,t) is considered a known unsteady state potential flow to determine the pressure distribution, according to Schlichting, 1968. Thus using the square dimensions of the heat flux sensor utilized in this work as L=0.011 m leads to the thickness of laminar sublayer as follows

$$\delta_0 = \frac{8.68L}{\mathrm{Re}^{3/4}} \tag{5.29}$$

Hence the film thickness also known as the thermal boundary layer, δ can be calculated by combining Equations (5.26) and (5.29):

$$\delta = \frac{8.68L}{\mathrm{Re}^{3/4}\,\mathrm{Pr}^{1/3}} \tag{5.30}$$

Where the Reynold's number, Re and Prandtl's number, Pr are defined as $\mathrm{Re} = \frac{U_{axial} l_c \rho_l}{\mu_l}$, $\mathrm{Pr} = \frac{C_{p_l} \mu_l}{K_l}$ with the axial bubble velocity U_{axial}, bubble chord length l_c, the liquid density, ρ_l, liquid thermal conductivity, K_l, liquid viscosity, μ_l and the specific heat capacity of the liquid, C_{p_l}.

Using equations (5.25), for contact time and (5.30), for film thickness into the mechanistic equation (5.17) the predicted heat transfer coefficient can be obtained. It is also possible that rather than single values calculated for the mean, a distribution of the heat transfer coefficient can also be obtained.

5.5. RESULTS AND DISCUSSION

5.5.1. Contact Time Results and Discussion. Figures 5.2a, b show the contact time radial profiles obtained from the measured bubble properties in the 6-inch and 18-inch empty bubble columns respectively, at different superficial gas velocities. As indicated in the above section, the contact time is estimated in this work from the bubble passage frequency and local gas holdup, all of which are interrelated to the bubble sizes and bubble velocity. From Figure 5.2 it can be seen that the contact time slope increases continuously towards the column wall for both the 6-inch and 18-inch bubble columns yielding much like parabolic profiles similar to the measured heat transfer coefficient and the reported bubble velocity, frequency, local holdup and specific interfacial area. This is an indication that the contact time determines the heat transfer rate as it depends on these bubble properties. Close to the wall, higher contact times are estimated due to lower bubble passage frequency and low gas holdup. The low gas holdup and low bubble passage frequency leads to a lower rate of the heat transfer surface renewal.

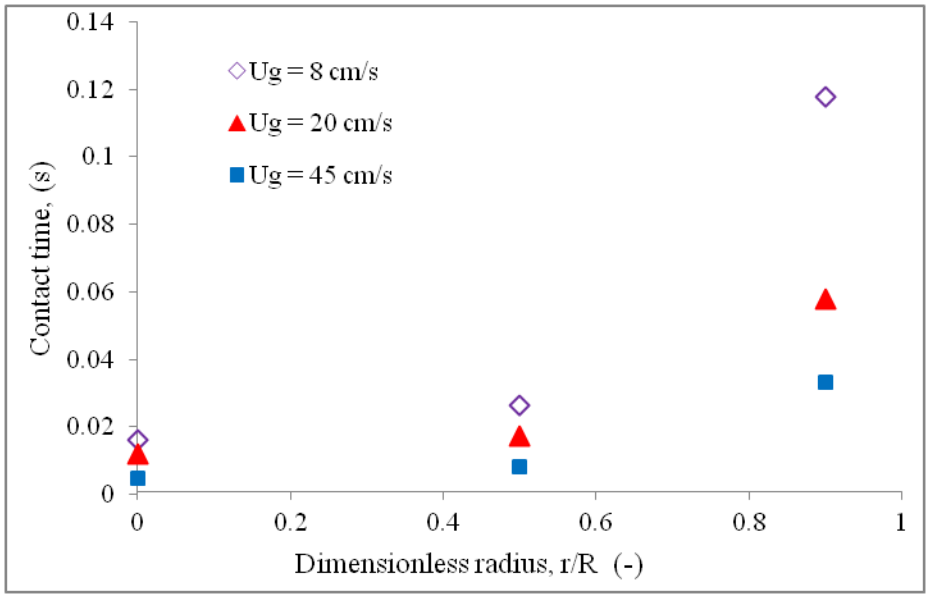

(a)

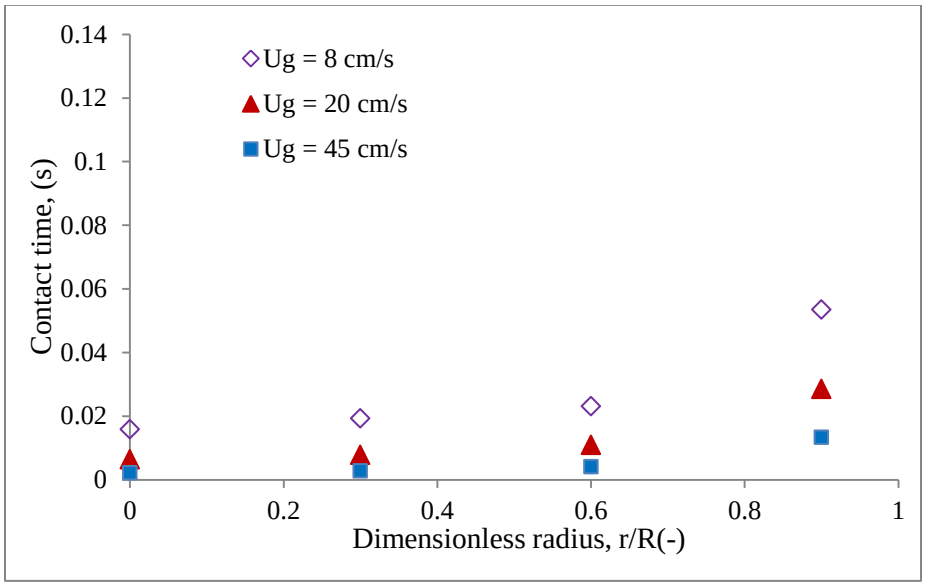

(b)

Figure 5.2 Effect of superficial gas velocity on radial profiles of contact time in empty bubble columns (a) 6-inch diameter column and (b) 18-inch diameter column

Figure 5.3 shows a comparison of the contact time with some of the reported methods in the literature. To obtain the contact time values predicted by the models of Kumar and

Fan, 1994 and Li and Prakash, 2001, the length L, of the heat flux sensor and the diameter of the heat transfer probe used in the current work has been utilized while the bubble rise velocity measured by the four-points optical probe used in this work has been used. As noted earlier on, at superficial gas velocities beyond 15 cm/s, the bubble velocity does not change significantly. Thus the two models give relatively close values to each other and remain nearly constant at 20 cm/s or more, since the length of the heat flux and probe diameter are fixed, the only determinant of the contact time becomes the bubble velocity. This represents clear shortcoming of such approach in estimating the contact time because the contact time is expected to vary (decrease) with increased superficial gas velocity where the mixing and circulation get enhanced. On the other hand, the proposed model predicts lower contact times at higher range of superficial gas

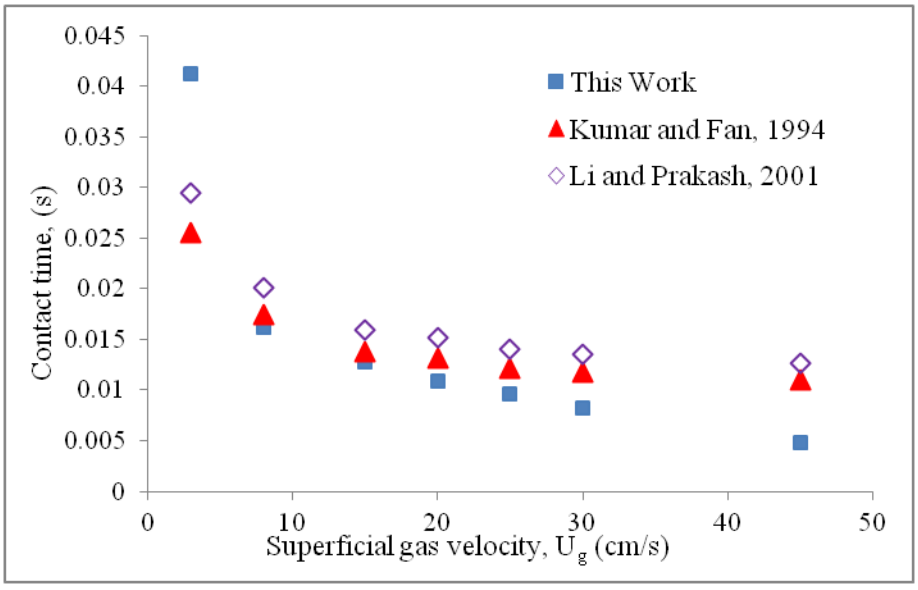

Figure 5.3 Contact time comparison with the reported models for air water system in the literature at the column center, r/R (-) = 0.0 in 18-inch diameter column

velocity than those of the other two models of Kumar and Fan, 1994 and Li and Prakash, 2000. This difference can be attributed to the proposed model being able to capture the change in contact time due to enhanced mixing and recirculation along with bubble coalescence and breakage. Further increase in local gas holdup and bubble passage frequency with superficial gas velocity is also reflected.

The distribution of estimated contact time is illustrated in Figure 5.4 for an 18-inch empty bubble column at r/R (-) = 0 at two superficial gas velocities. The significantly small variances point to the fact that there is little spread in the local holdup and bubble passage frequency at the point of measurements thus narrow contact time distribution. However, relatively wide spread in the contact time is observed at higher gas velocity. This is due to the fact that at higher gas velocity, both the population of larger and smaller bubbles up relative to lower gas velocity. Thus it is expected that the heat transfer coefficient variation due to variation in contact time has a wider spread at higher gas velocity.

The proposed contact time model, (equation 5.25) is simple but requires both the measurements of bubble passage frequency as well as local gas holdup. An equation to estimate the contact time is further proposed in Appendix D based on the model data.

5.5.2. Film Thickness Results and Discussion. For gas-liquid and gas-liquid-solid systems it is believed that a thin liquid film of thickness, δ exists at the probe surface and the mass of fluid brought by the bubble wake is viewed to exchange heat by unsteady-state conduction at the outer edge of the film. The resistance to heat transfer is due to the film (whose thickness depends on the liquid properties and the local hydrodynamics) followed by penetration and unsteady-state heating of an element of the

fluid. Thus, before the heat released from the probe can propagate very far in the lateral direction, it is swept into the wake. The fluid elements brought by the bubble wake of each bubble renew the probe surface, and the temperature of the fluid element sweeping the outer surface of the film is assumed.

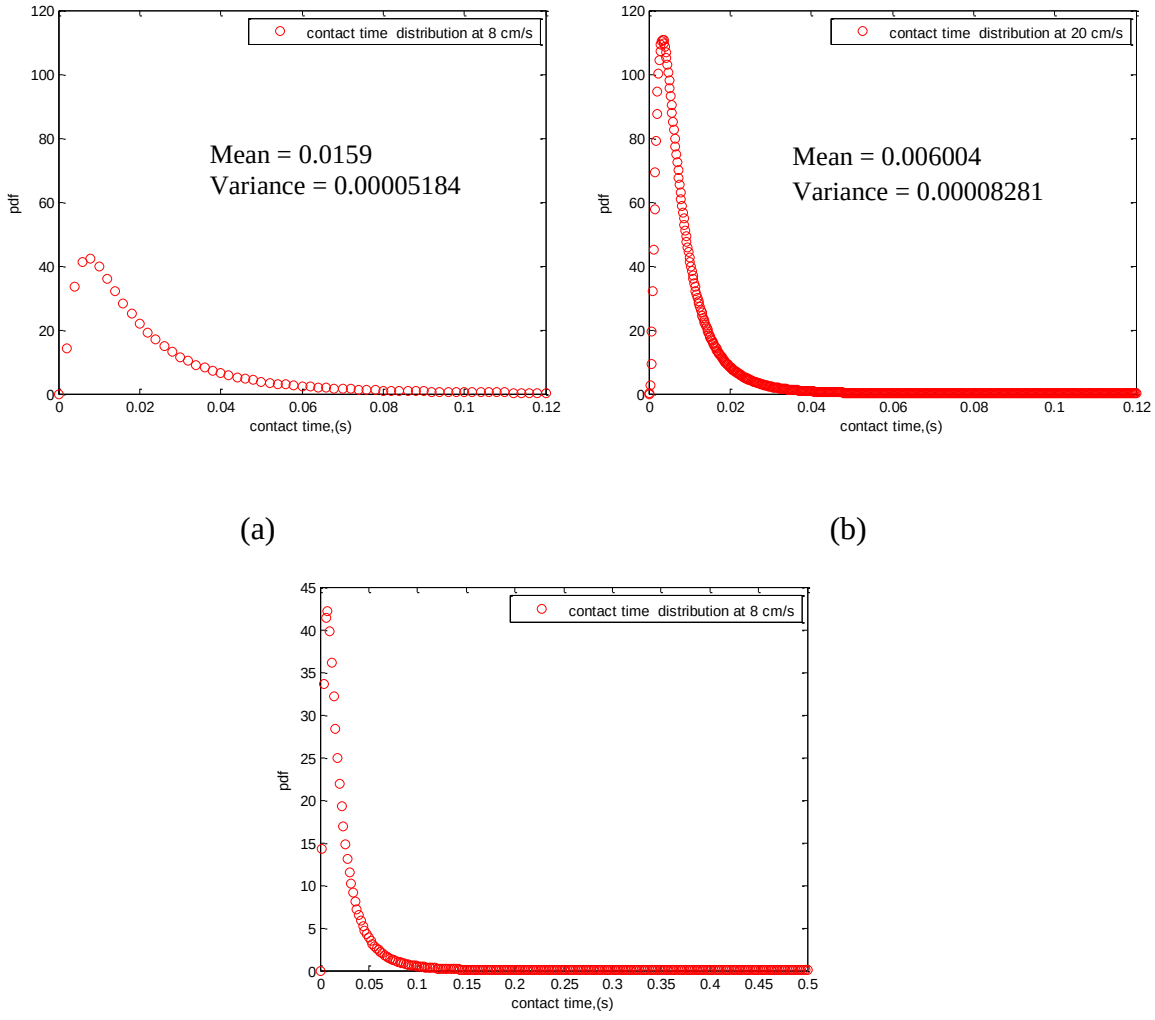

Figure 5.4 Distribution of the predicted contact time in 18-inch bubble column at r/R (-) = 0.0 (a) at Ug = 8 cm/s (b) at Ug = 20 cm/s (c) Entire view of (a)

Figure 5.5 illustrates the radial profiles of the estimated film thickness in 18-inch bubble column using Equation 5.30 and based on the bubble properties measured by the combined measurements technique. Even though maximum film thickness is obtained close to the column wall just like the contact time, with minimum at the column center, radial profiles are not necessarily similar. Increasing Ug from 8 cm/s to 45 cm/s leads to a decrease of film thickness by ~ 21 % and 9 % at the column center and wall region respectively with an average decrease of 15 %. At the lower gas velocity (8 cm/s), the wall region is also noted to have up to twice the film thickness at the column center and up to 2.4 times at higher gas velocity (45 cm/s). These variations can be attributed to higher local axial bubble velocity and liquid velocity and hence more intensity of mixing which gives rise to smaller δ at the column center and at higher superficial gas velocity.

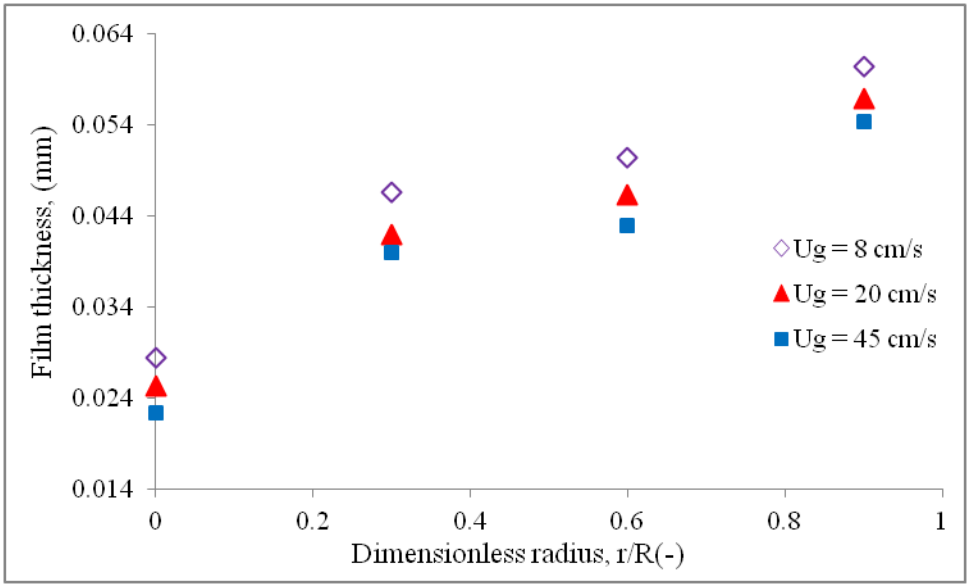

Figure 5.5 Effect of superficial gas velocity on radial profiles of estimated film thickness in 18-inch empty bubble column.

A parity plot obtained for the estimated film thickness for all the conditions of operation employed in this work (Equation 5.30) with the film thickness estimated using other correlations in the literature is shown in Figure 5.6. The other correlations used were as follows;

Kumar and Fan, 1994 and Yang et al., 2000 both used the equation;

$$\delta = \frac{6.14L}{\mathrm{Re}^{3/4}\,\mathrm{Pr}^{1/3}} \tag{5.31}$$

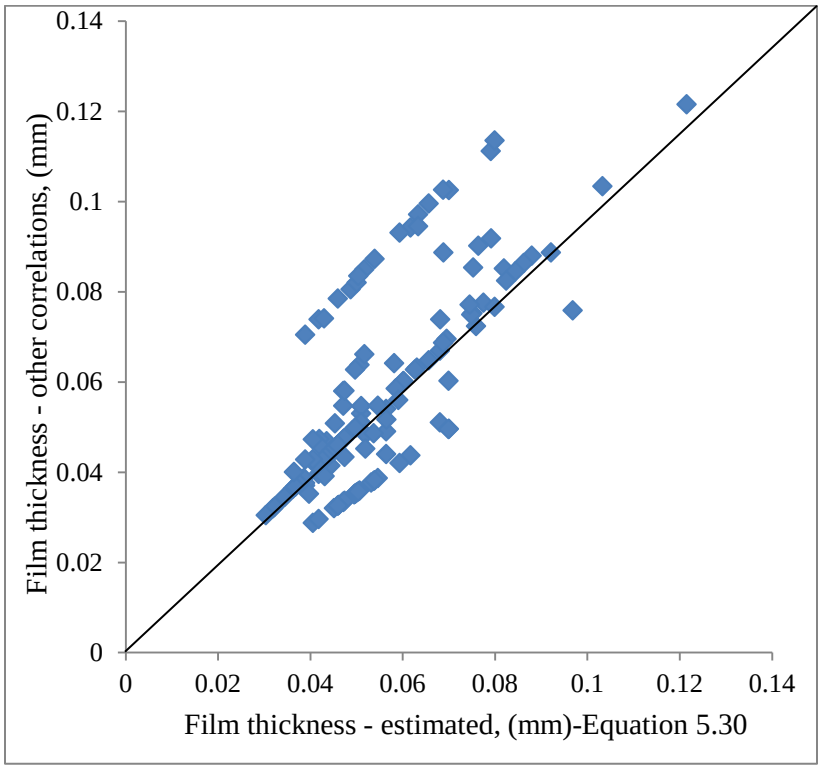

Figure 5.6 A parity plot of the estimated film thickness (Equation, 5.30) vs film thickness estimated from correlations of Kumar and Fan, 1994, Yang et al., 2000 and Li and Prakash, 2001 in bubble column

They both defined Reynolds number and Prandtl's number, respectively, as

$\mathrm{Re} = \frac{U_b L \rho_l}{\mu_l}$, $\mathrm{Pr} = \frac{C_{p_l} \mu_l}{K_l}$, with L being the vertical length of the heat transfer probe and U_b the bubble rise velocity. In this case the length of the heat flux sensor used in the current work has been utilized and the average upward bubble velocity measured by the four-point optical probe in the hybrid measurement has been used as the bubble rise velocity.

Li and Prakash, 2001 used a similar equation as above,

$$\delta = \frac{1.25 d_p}{{Re_p}^{1/2} Pr^{1/3}} \tag{5.31}$$

where d_p is the probe diameter and Re_p is the Reynolds number based on the diameter of the probe and defined as $\mathrm{Re} = \frac{U_{b,L} d_p \rho_l}{\mu_l}$, $\mathrm{Pr} = \frac{C_{p_l} \mu_l}{K_l}$ with $U_{b,L}$ being the bubble rise velocity of large bubbles. To obtain the bubble rise velocity of large bubbles, only the upward bubble velocity of the bubbles whose chord lengths were larger than the mean chord lengths were used. It is apparent that the differences between the predictions are due largely to the Reynolds numbers. The statistical difference between estimated film thickness the correlations of Kumar and Fan, 1994, Yang et al., 2000 and Li and Prakash, 2001 predictions are represented in terms of the average absolute relative difference (AARD) and absolute relative difference (ARD) and are defined as follows;

$$AARD = \frac{1}{N} \sum_{i=1}^{N} \left| \frac{\delta_{estimated} - \delta_{other\ corr}}{\delta_{estimated}} \right| \tag{5.32}$$

$$ARD = \left| \frac{\delta_{estimated} - \delta_{other\ corr}}{\delta_{estimated}} \right| \tag{5.33}$$

It was determined that the film thickness predicted by other correlations (Kumar and Fan, 1994, Yang et al., 2000 and Li and Prakash 2001) those estimated in the current work (Equation, 5.26) lie close to each other with an AARD of 15 %.

At any given superficial gas velocity, bubbles are formed of different sizes which move at different velocities hence a distribution in the bubble velocities and bubbles sizes (which are characterized by the bubble chord lengths). The distribution plots of the axial bubble velocity are provided in Appendix C. In Equation 5.29, the Reynolds number is a function of both axial bubble velocity and bubble chord lengths which have distributions. Thus a distribution of estimated film thickness is obtained as shown in Figure 5.7. A near statistical similarity is observed in the distributions with little difference in variance. As expected smaller film thickness is obtained at Ug = 20 cm/s than at Ug = 8 cm/s

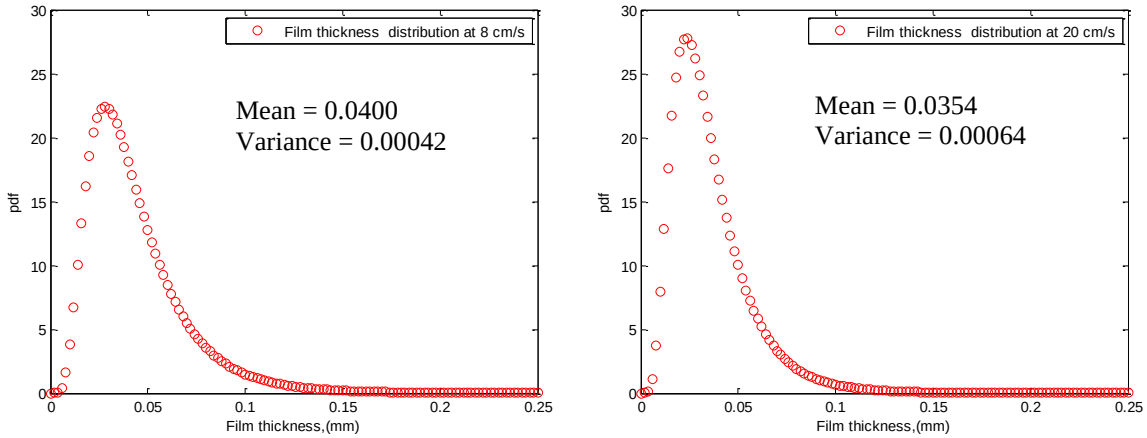

(a) (b)

Figure 5.7 Distribution of the estimated boundary layer thickness in 18-inch bubble column at r/R (-) = 0.0 (a) at Ug = 8 cm/s (b) at Ug = 20 cm/s

5.5.3. Heat Transfer Coefficient Results and Discussion. The effect of superficial gas velocity on radial profiles of the predicted heat transfer coefficient is presented here. Figure 5.8 compares the time averaged instantaneous heat transfer data estimated by Equation 5.16 at different radial locations from the center to the column wall for an air-water system for the gas velocity of 8 cm/s, 20 cm/s and 45 cm/s. It is observed that steepness of the radial profiles with superficial gas velocity increases from low gas velocity to higher gas velocity. For instance, at Ug = 8 cm/s the radial profile has an average steepness of 1.2 towards the column wall and this increases to 2.0 at Ug = 20 cm/s and 2.4 at Ug = 45 cm/s. This is consistent with the results of discussed bubble properties, such as Figure 4.10b. Higher values are thus predicted at the centre which could be attributed to higher local turbulence generated by higher wake intensity due to, higher gas holdup and bubble frequency, lower film thickness, faster moving bubbles in

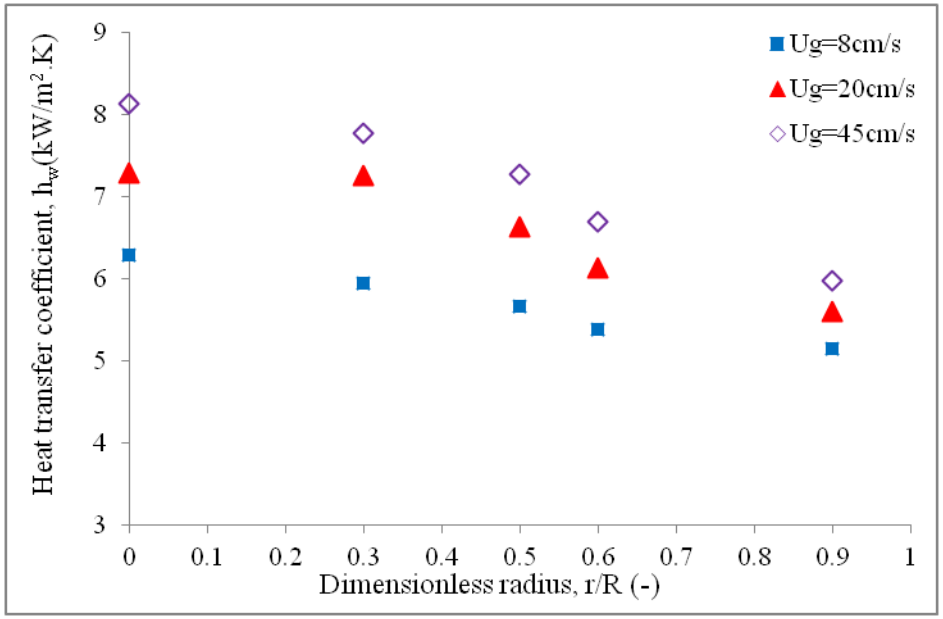

Figure 5.8 Effect of superficial gas velocity on radial profiles of predicted heat transfer coefficient in 18-inch empty bubble column

the central region of the column. Further to that it has been demonstrated that large bubbles move towards the column center with higher velocity while smaller bubbles move closer to the wall region downwards at lower velocity. It has also been demonstrated that the bubble passage frequency and gas holdup are much higher at column center and increase towards the column center. This higher bubble frequency and hold up leads to shorter contact times and thinner films on the heat transfer surface thus enhancing the rate of renewal of the heat transfer surface.

It is worth to note at this point that there are several studies reported in the literature about the parabolic profiles of the gas hold up as well as liquid velocity, (Hills, 1974; Ueyama et al., 1980; Nottenkamper et al., 1983, Wu and Al-Dahhan, 2001; Luo and Svendsen, 1991, Shaikh, 2007). The parabolic shape of radial heat transfer profiles are generally similar to radial profiles of gas holdup and liquid velocity reported in literature studies, but it should be noted, however, that heat transfer is affected by both liquid velocity and turbulence generated by bubbles among other bubble properties. Hence, a direct comparison with gas holdup, liquid velocity or any other bubble property profiles is not appropriate and may be misleading. The general however indicates that the wall region is relatively free of large bubbles or faster moving chain of bubbles. Indeed the measured bubble diameter is smaller near the wall region and larger in the center. The smaller diameter bubbles near the wall would have smaller wakes associated with them, resulting in a lower local heat transfer coefficient.

Figure 5.9 shows a comparison of the mean predicted heat transfer (Equation 5.16) coefficient values with the measured. The predicted heat transfer coefficients were obtained based on the bubble properties measured at the same time as the measurements

of the heat transfer coefficient using the heat transfer probe. At 8 cm/s the predicted heat transfer coefficient shown in Figure 5.10 are 7.3 % and 6.1 % higher than measured at the column center region ($r/R \leq 0.3$) and at the column wall region ($r/R \geq 0.6$), respectively. These differences increase further with gas velocity. At 45 cm/s an increase of 11.3 % and 9 % is noted. At the column center and higher gas velocity, much shorter contact times are estimated by the new model. At such short contact times, shorter than the response time of the heat flux probe, the heat transfer wake-enhanced phenomenon cannot be captured by the heat transfer probe. At the column wall region, relatively longer contact times are estimated. Nevertheless, the estimated heat transfer coefficient still fall within 12 % of the measured ones.

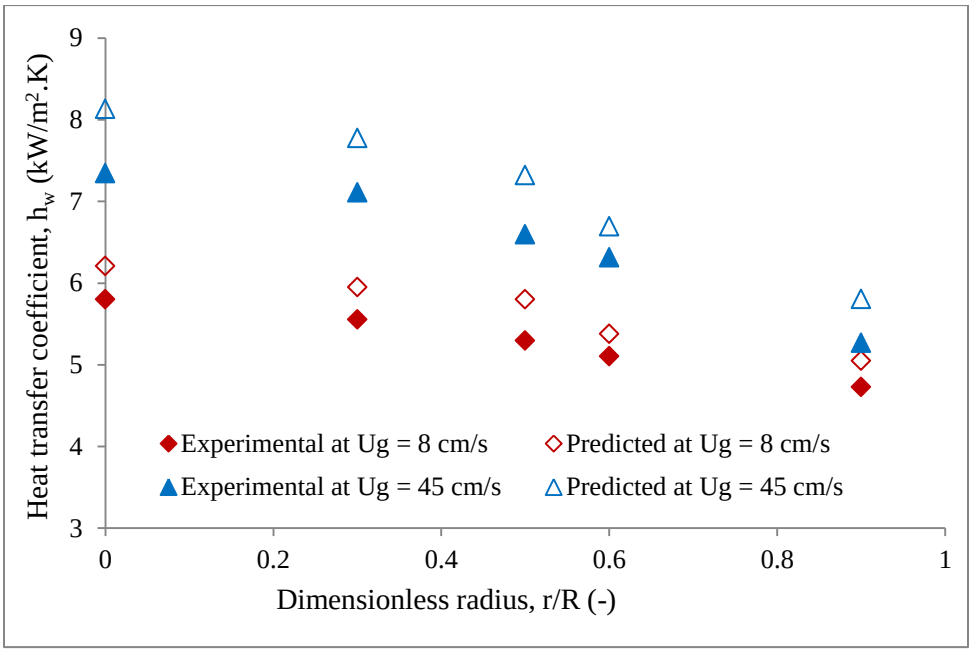

Figure 5.9 Comparison of the predicted heat transfer coefficient (Equation 5.16) with the measured heat transfer coefficient values in 18-inch bubble column without internals

To understand the comparative performance of the proposed model, a parity plot is used as illustrated in Figure 5.10. Figure 5.10 shows the predictions of the proposed model compared against the experimental data of the measured heat transfer coefficient using the fast response heat transfer probe developed and utilized in this work for a wide range of operating conditions, with the needed model parameters obtained from the hybrid technique measurements. To further assess the performance of the correlation model predictions statistically, the average absolute relative error (AARE) has been used and is calculated as follows:

$$AARE = \frac{1}{N}\sum_{i=1}^{N}\left|\frac{h_{w,predicted} - h_{w,experimental}}{h_{w,experimental}}\right| \tag{5.34}$$

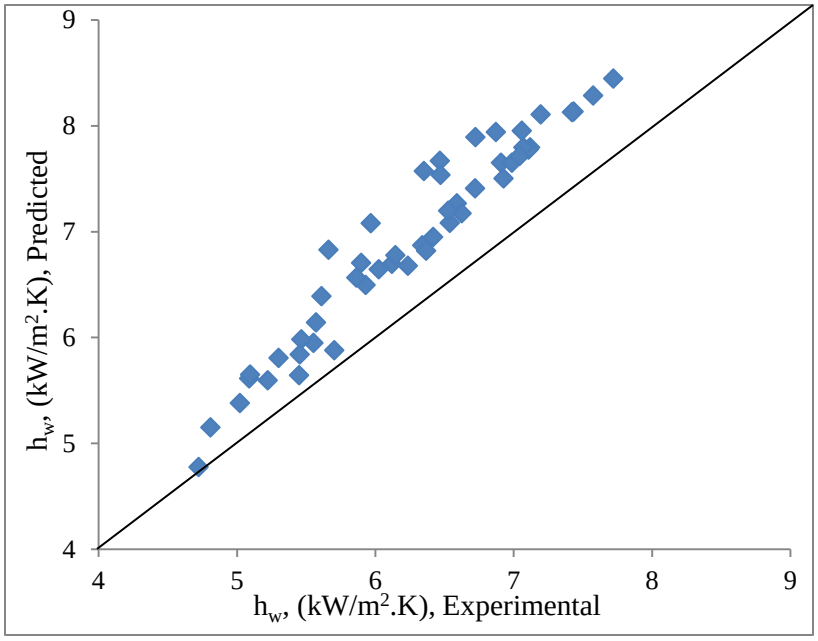

Figure 5.10 A parity plot of the predicted heat transfer coefficient-(Equation 5.16) vs the measured heat transfer coefficient values in the bubble columns at the same operating conditions

A very good agreement within 13 % was found between the predicted and the experimental values of heat transfer coefficient, in spite of the fact that the model over predicts the heat transfer coefficient at all the evaluated conditions. One of the main reasons why proposed model over predicts the heat transfer coefficient is that the new approach of estimating the contact time (Equation 5.24) predicts up to very low values of contact time. In fact, at 20 cm/s in 18-inch column, the estimated contact is 0.006, which is almost an order of magnitude less than the response time of the heat flux and temperature sensor.

5.5.4. Heat Transfer Coefficient and Bubble Dynamics Distribution. The reported heat transfer coefficient in the open literature shows the average values only. However in an industrial system at the same superficial gas flow rate, the values over time vary significantly. With distributions in the measured bubble properties as well as in both the contact time and film thickness, it is therefore possible that a distribution of the predicted heat transfer coefficient can be obtained. The simulated distribution was extracted from experimental data collected for a period of 90 seconds. In Figure 5.11 it is demonstrated that there is distribution of heat transfer coefficient both at 8 cm/s and at 20 cm/s. In fact a wider distribution in the heat transfer coefficient is reported at higher superficial gas velocity than lower gas velocity. Figure 5.12 and Figure 5.13 show the histogram for probability distribution of bubble chord lengths and axial bubble velocity respectively, at 8 cm/s and 20 cm/s in 18-inch diameter column without internals for an air-water system. At higher gas velocity there is growth in population of both large and small bubbles hence a wider spread of the bubble sizes (chord lengths). The different sizes of bubbles move at different velocities that creates different intensities of the heat

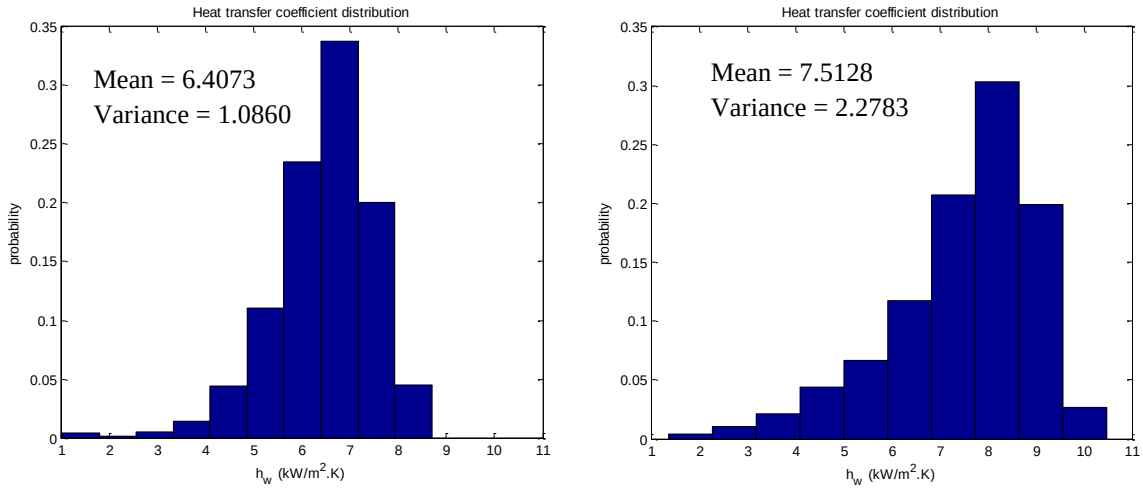

(a) (b)

Figure 5.11 Histogram of the probability distribution of predicted heat transfer coefficient in 18-inch empty bubble column at r/R = 0.0 (a) U_g = 8 cm/s (b) U_g = 20 cm/s.

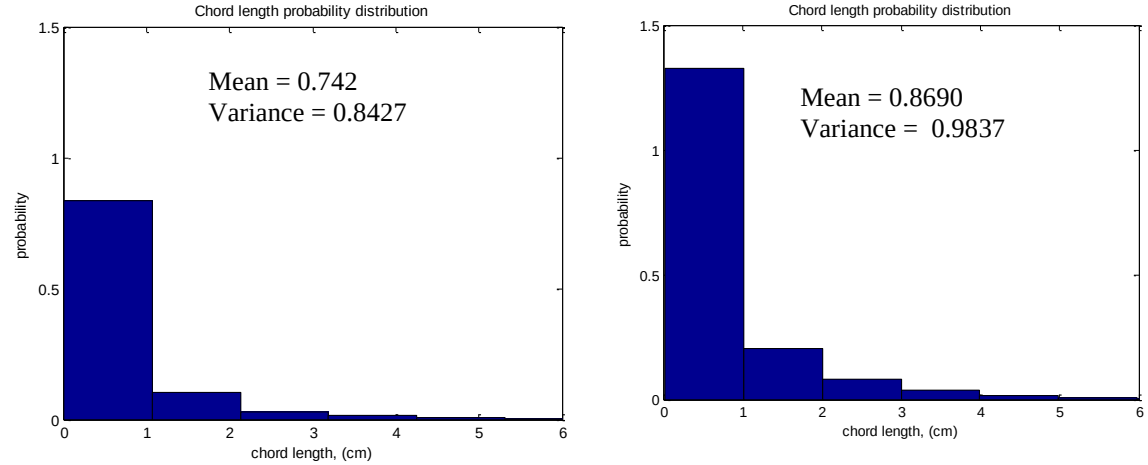

(a) (b)

Figure 5.12 Histogram of the probability distribution of bubble chord lengths in 18-inch empty bubble column at r/R = 0.0 (a) U_g = 8 cm/s (b) U_g = 20 cm/s.

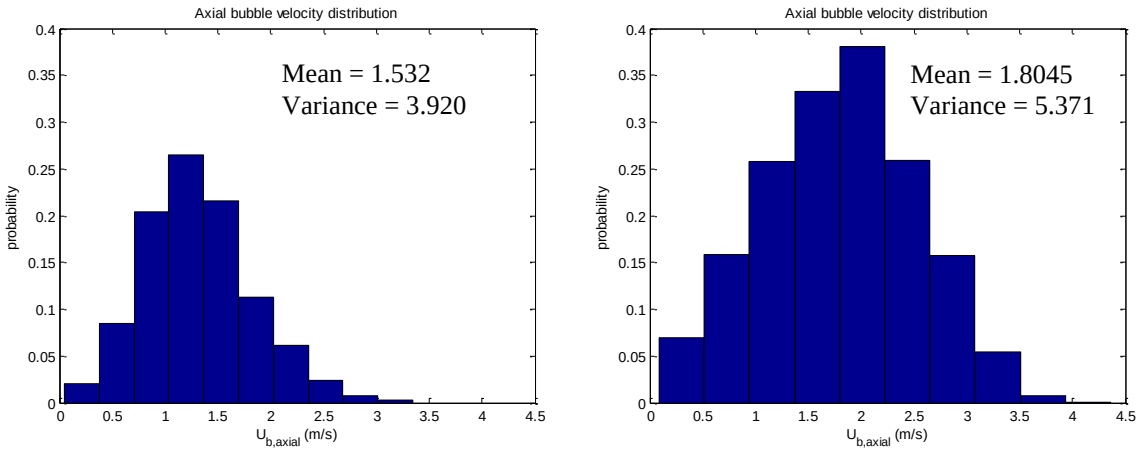

(a) (b)

Figure 5.13 Histogram of the probability distribution of the axial bubble velocity in 18-inch empty bubble column at r/R = 0.0 (a) U_g = 8 cm/s (b) U_g = 20 cm/s.

transfer surface renewal rate. It should also be pointed out that some of the smaller bubbles are entrained and dragged in the wake of larger ones and move at nearly same velocity as of the large bubbles. The mean of the distribution of heat transfer coefficient was found to be 1.8 % and 3.1 % higher than the predicted average at Ug = 8 cm/s and 20 cm/s, respectively

5.6. REMARKS

For the first time a correlation based on the local bubble properties has been proposed and used to estimate the contact time needed in the mechanistic approach equation and successfully implemented in the heat transfer estimation.

The mechanistic analysis shows that the contact time between the thin film and the liquid elements is a function of the local phase holdup and bubble passage frequency

all which are dependent on other bubble properties such as the specific interfacial area, bubble sizes and bubble velocity.

The heat transfer coefficient depends upon the combined effects of bubble parameters including; bubble frequency, local gas hold-up, bubble velocity and their distributions over the heating surface.

The variation of the local time averaged heat transfer coefficient with the contact time is via the bubble passage frequency and the local phase hold-ups.

6. EFFECT OF SCALE ON THE HEAT TRANSFER COEFFICIENT AND BUBBLE DYNAMICS IN BUBBLE AND SLURRY BUBBLE COLUMNS

This Section addresses the effect of column diameter on the heat transfer coefficient, local and overall gas holdup, bubble velocity, bubble frequency, and specific interfacial area in pilot-scale bubble and slurry bubble columns. The experimentally measured heat transfer coefficient and bubble dynamic parameters were obtained using the combined measurement techniques of both the heat transfer probe and 4-point optical probe in the presence and absence of dense internals and different solids loading.

6.1. SCOPE

Most of the reported studies in the literature on bubble columns have been performed on laboratory scale reactors mostly in diameters of about 0.25 cm (Krishna et al., 2001). However, the required large gas throughputs, necessitates the use of large-diameter reactors (typically in the range 5-10 m), and often in parallel, while tall reactors are desired to achieve high levels of conversion, (Krishna et al., 1997). The bubble column diameter is an important design parameter for bubble columns, especially in processes involving higher volumetric productivity such as methanol synthesis and the F-T process. Accordingly, the effect of column diameter has been a subject of extensive studies in the last few decades, resulting in a large volume of experimental data under a wide range of operating conditions. Despite all the efforts, none of these studies has attempted to address the effect of the column diameter on both the heat transfer rate and bubble dynamics simultaneously in the presence of dense vertical cooling internals and or solids of high loading.

Previous work has revealed that the presence of internals alters the flow field and has effects on the liquid velocity profiles (Bernemann, 1989; Chen et al., 1999, and Forret et al., 2003), bubble dynamics (Youssef, 2010, Chapter 3 of this work), bubble velocity profiles (Hamed, 2012), and turbulent intensities (Chen et al., 1999 and Forret et al, 2003), heat transfer coefficient, (Abdulmohsin and Al-Dahhan, 2012; Chapter 4 of this work). Several studies in the literature also indicate that increasing column diameter affects the hydrodynamics and hence the transport parameters such as heat transfer and mass transfer rates (Kolbel et al., 1958; Koide et al., 1979; Degaleesan, 1997; Li and Prakash, 2000; Krishna, 2000; Krishna et al., 2001; and Krishna and van Baten, 2002;).

Although bubble columns are relatively simple in mechanical construction, the task of extrapolating small diameter columns behavior to larger ones is always challenging, delicate and difficult. The extrapolation of data obtained in laboratory scale units to the commercial scale reactors requires a systematic approach based on the understanding of the scaling principles of bubble dynamics and of the behavior of two-phase dispersions and three-phase dispersions in large scale columns. Shaikh and Al-Dahhan, 2010; observed that the key to such extrapolation is the proper understanding of the complex hydrodynamic behavior because the dispersion and interfacial heat and mass transfer which often limit the chemical reaction rates are closely related to fluid dynamics of the system through gas–liquid contact area and the turbulence properties of the flow.

Thus, the influence of the diameter on the hydrodynamics is important so that the design correlations and models developed at laboratory scale can be extrapolated and confidently used to the satisfaction of the industrial scale needs. Whereas several researchers have investigated the influence of scale on gas hold-up, Shah et al., 1982;

Greary and Rice, 1992; Vandu and Krishna to mention a few, little attention has been paid to the influence of scale on other hydrodynamic parameters such as the bubble sizes, bubble velocity, local gas holdup as well as heat transfer. As outlined in chapter 3 and by a few other researchers, Xue et al., 2008; Wu, 2007 and Youssef and Al-Dahhan, 2009, these bubble properties are closely related. Hence, an understanding of the column diameter effect on their variation together with the accompanying influence on the heat transfer rates and coefficient in bubble and slurry bubble columns still requires close scrutiny.

For the commercial design or scale-up of the slurry bubble column reactor, an understanding of the flow behavior of bubbles with increasing column diameter is essential, because the similarity of bubble properties should be adjusted with increasing column diameter. It has been generally understood that in dynamic flow systems such as slurry bubble column reactors, the hydrodynamic stability and similarity have to be controlled and adjusted to provide the heterogeneous reactants with plausible conditions for effective contacting and reaction (Behkish et al., 2007; Zhang Zhao, 2006; Mirzaei et al., 2006; Duvenhage and Shingles, 2002; Gandhi et al., 1999).

Though bubble columns are easy to construct, the complexity of flow patterns and mixing in bubble columns, optimal design and sound scale-up procedures are still not fully understood (Deckwer and Schumpe, 1993; Li and Prakash, 2002). Furthermore, the flow behavior changes dramatically with the inclusion of heat exchanging internals, (Youssef, 2010; Bernemann, 1989; Shah et al., 1978; and Kafarov, 1975). Whereas bubble dynamics and heat transfer rate in bubble columns have been subjects of studies for decades, only a handful have investigated the effects of bubble properties on the heat

transfer coefficient on columns of different sizes, including (Saxena et al., 1989, Jhawar 2012). However, not a single work has been reported in the open literature (at least within our knowledge) on the effect of column diameter as well as solids loading effects on the bubble dynamics and subsequently their effect on the heat transfer coefficient in bubble columns equipped with dense heat exchanging internals. Therefore the core of this work is to experimentally assess the effect of column diameter and solids volume fraction on the heat transfer coefficient and bubble dynamics including the local and overall gas holdup, axial bubble velocity, specific interfacial area and bubble passage frequency. In order to achieve this, a combined measurements technique is used as described in the experimental section. Both the heat flux and the bubble dynamics are measured simultaneously to avoid effects of changing experimental operating conditions.

In this chapter, the effect of bubble column diameter on bubble dynamics and heat transfer characteristics in slurry bubble columns is presented and analyzed based on mainly data obtained from the experimental work done in 6-inch and 18-inch bubble columns. The two different column diameters were used at atmospheric pressure and room temperature to study overall and local gas hold-up, bubble velocity, bubble frequency, and bubble chord-lengths, and the heat transfer coefficient.

6.2. EXPERIMENTAL SETUP

The experiments were conducted in two scales of Plexiglas columns. The smaller scale was a 6-inch (0.14 m) inside diameter and 1.8 m height with dynamic bed height in all the experiments, maintained constant at a level of 1.56 m (z/D = 11.16) above the gas distributor by adjusting the amount of liquid, and liquid-solids loaded in the column. The

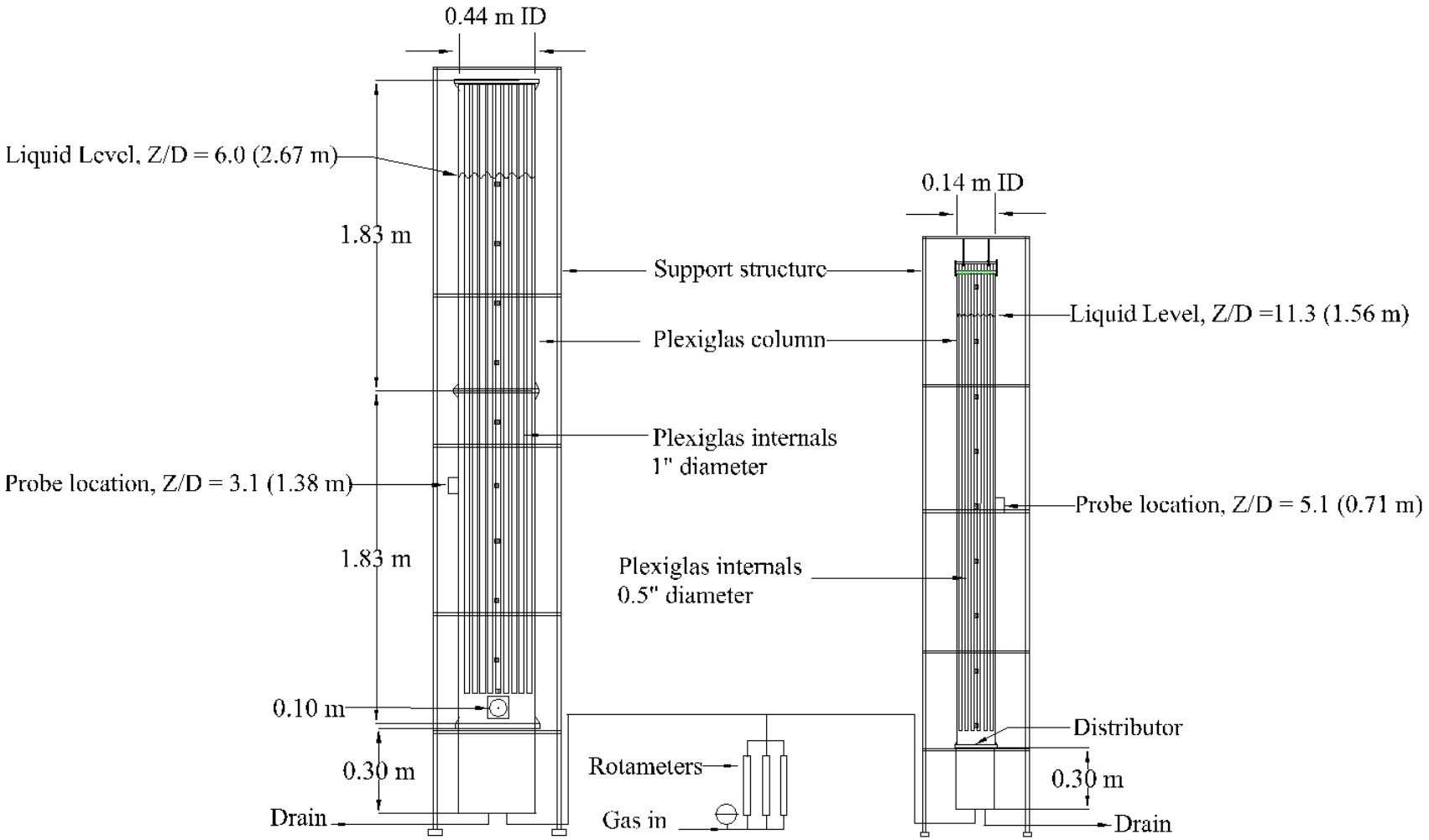

Figure 6.1 Schematic of the experimental structure and mimicked dense heat exchanging internals in both the 6-inch diameter column and 18-inch diameter column

larger scale consisted of an 18-inch (0.44 m) inside diameter and 3.66 m height with dynamic bed height in all the experiments, maintained constant at a level of 2.67 m (z/D = 6.0) above the gas distributor by adjusting the amount of liquid, and liquid-solids loaded in the column. A typical schematic diagram of the experimental setup for all the experimental work in this study with dense internals is shown in Figure.6.1. In this study, compressed filtered oil-free dry air introduced continuously from the bottom of the columns was used as the gas phase. Soft filtered tap water was used as liquid phase. Glass beads with an average size of 150 μm and density of 2500 kg/m^2 was used as the solids/fines phase. The solids loading is based on the wet volume-which is the volume of the glass beads together with the liquid in the pores. Since the glass beads used is nonporous, the wet volume was simply same as the volume of non-soaked beads and the concentrations varied between 0 % vol – 25 % vol. The solids volume fraction was defined as;

$$v_s = \frac{V_s}{V_s + V_L} = \frac{\varepsilon_s}{\varepsilon_s + \varepsilon_L} \tag{6.1}$$

In both units perforated plates with triangular pitch hole pattern (6-inch column) and square pitch hole pattern (18-inch column) with a total free area of 1.09 % was used as the gas distributors. The superficial gas velocities were from 0.03 to 0.45 m/s based on free cross-sectional area of the column covering both the bubbly and churn turbulent flow regimes. The superficial gas velocities were from 0.03 to 0.45 m/s based on the free cross-sectional area (CSA) of the column available for the flow.

The internals used in this study were vertical Plexiglas rods of 0.5 inch and 1 inch diameter (in the small scale column and the large scale column respectively) occupying 25 % of the column cross-sectional area that simulates the Fischer-Tropsch synthesis

process. Combined probes was used to simultaneously measure the local heat flux and surface temperature and the local bubble properties, including local gas hold up, bubble passage frequency, axial bubble velocity, specific interfacial area, as well as the bubble chord lengths which is characteristic of bubble sizes. The description of the combined probes has been given in Section 3 and Section 4.

The experimental conditions for the bubble dynamics and heat transfer measurements employed covered a wide range of superficial gas velocities in the homogenous and churn turbulent flow regimes, in the presence and absence of dense internals as summarized in Table 6.1 using an air-water system and air-water glass-beads system.

Table 6.1 Experimental conditions for the effect of column diameter

Dc (m)	Internals (% CSA)	Solids (% vol)	Radial Positions
0.14	0.0 %	0.0 %	r/R(-) = 0.0, 0.3, 0.5, 0.6, 0.9
0.14	0.0 %	9.1 %	r/R(-) = 0.0, 0.3, 0.5, 0.6, 0.9
0.14	0.0 %	25 %	r/R(-) = 0.0, 0.3, 0.5, 0.6, 0.9
0.14	25 %	0.0 %	r/R(-) = 0.0, 0.3, 0.5, 0.6, 0.9
0.14	25 %	9.1 %	r/R(-) = 0.0, 0.3, 0.5, 0.6, 0.9
0.14	25 %	25 %	r/R(-) = 0.0, 0.3, 0.5, 0.6, 0.9
0.44	0.0 %	0.0 %	r/R(-) = 0.0, 0.3, 0.5, 0.6, 0.9
0.44	0.0 %	9.1 %	r/R(-) = 0.0, 0.3, 0.5, 0.6, 0.9
0.44	0.0 %	25 %	r/R(-) = 0.0, 0.3, 0.5, 0.6, 0.9
0.44	25 %	0.0 %	r/R(-) = 0.0, 0.3, 0.5, 0.6, 0.9

Table 6.1 Experimental conditions for the effect of column diameter (cont.)

0.44	25 %	9.1 %	r/R(-) = 0.0, 0.3, 0.5, 0.6, 0.9
0.44	25 %	25 %	r/R(-) = 0.0, 0.3, 0.5, 0.6, 0.9

6.3. RESULTS AND DISCUSSION

In order to elucidate the effects of column diameter on heat transfer coefficient and bubble dynamics, the heat transfer data as well as bubble dynamics data of this study obtained in two pilot scale bubble columns of 6-inch (0.14 m) and 18-inch, (0.44 m) diameters are compared against each other. The effect of column diameter on the heat transfer coefficient is presented in light of the observed variation of the different bubble properties with the column diameter.

6.3.1. Effect of Column Diameter on the Heat Transfer Coefficient and Bubble Dynamics in Columns without Internals and without Solids. First, the effect of column diameter is discussed for empty bubble columns without solids. This should form a basis of comparison when solids are used.

6.3.1.1. Effect of column diameter on the heat transfer coefficient. The effect of column diameter on heat transfer coefficient has been studied by a few researchers including Jhawar and Prakash, 2011 and Saxena et al., 1989, 1990. To analyze the effect of column diameter on the heat transfer coefficient, the experimental data obtained from this study in two diameter columns are compared against each other. Figure 6.2 shows a comparison of the measured local time-averaged heat transfer coefficients in 6-inch and those obtained in 18-inch empty bubble columns for air-water systems in this work.

While Figure 6.3 shows the effect of column diameter and superficial gas velocity on the related bubble properties. It is noted that in both the columns, the heat transfer coefficient increases sharply up to U_g = 25 cm/s beyond which the rate of increase slows down. Increasing superficial gas velocity leads to increased bubble frequency, and bubble population and gas hold-up as well as the bubble chord length (which is characteristic of the bubble sizes) and axial bubble velocity. Below Ug = 25 cm/s, an increase in Ug leads to an average increase of 9 % and 7.5 % in the heat transfer coefficient in 6-inch and 18-inch columns, respectively. While from 25 cm/s onwards an average increase of 1.3 % and 1.8 % in the heat transfer coefficient in 6-inch and 18-inch columns respectively are attained. Similar trends have been observed in the related bubble dynamics shown in Figure 6.3.

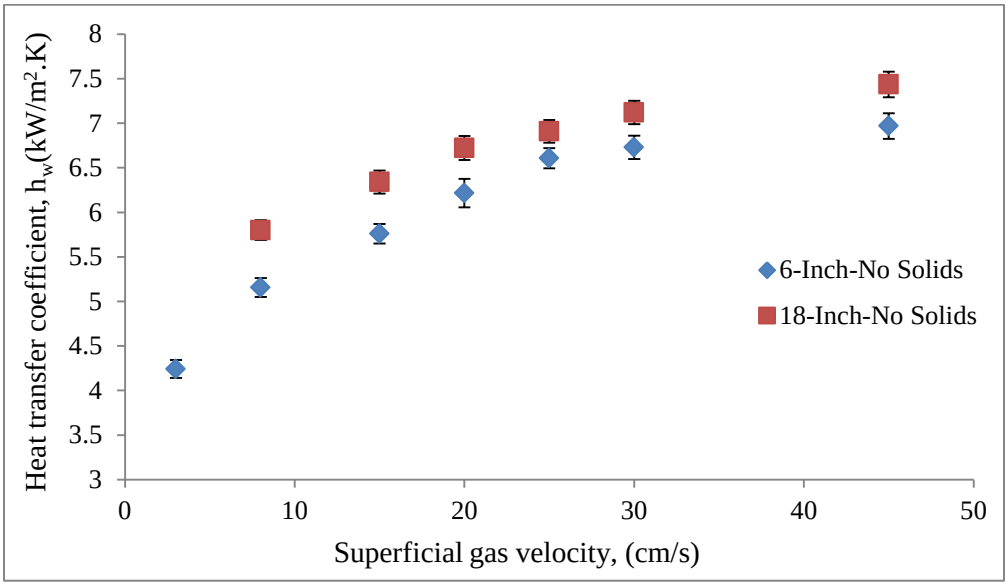

Figure 6.2 Effect of column diameter and superficial gas velocity on measured heat transfer coefficient for an air-water system without internals

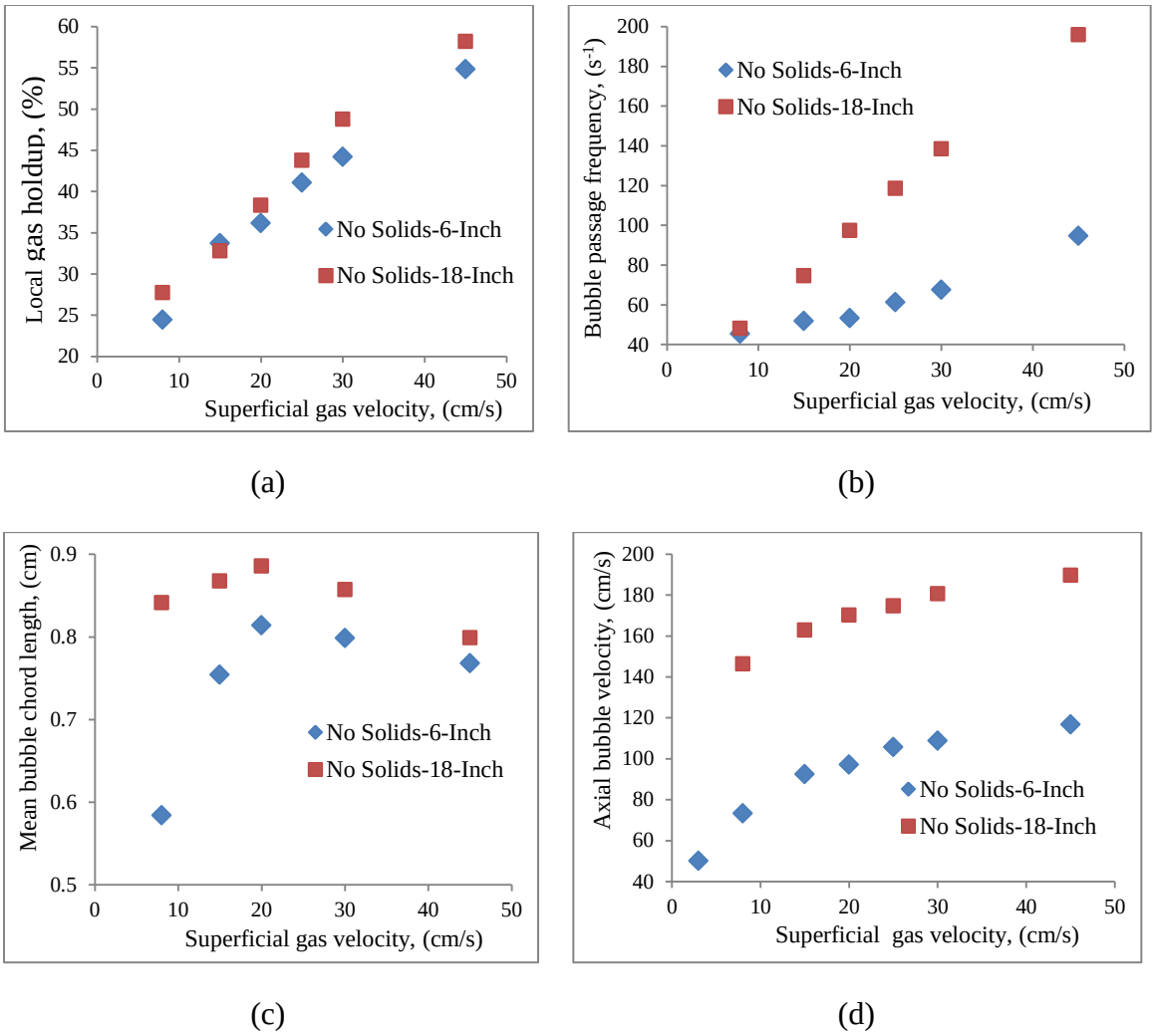

Figure 6.3 Effect of column diameter on bubble properties (a) Local gas holdup (b) Bubble passage frequency (c) Mean bubble chord length and (d) Axial bubble velocity at the column center, (r/R = 0.0) for an air-water system without internals at different superficial gas velocities

Whereas the local gas holdup and bubble passage frequency in both 6-inch and 18-inch columns increase almost linearly with the gas velocity, the mean bubble chord length increases with Ug until it is in deep churn-turbulent flow and then remains almost identical with increasing Ug. A sharp increase in the chord length with Ug is realized in the 6-inch column compared to the 18-inch at lower gas velocities. Similarly the increase

in gas velocity below 25 cm/s leads to an average increase in axial bubble velocity of 15 % and 8 % in 6-inch and 18-inch columns respectively. Beyond Ug = 25 cm/s an average increase in axial bubble velocity of 2.4 % and 1.6 % in 6-inch and 18-inch columns are attained.

The effect of the column diameter on the radial profiles of heat transfer coefficient at higher superficial gas velocities for an air-water system is shown in Figure 6.4. The heat transfer coefficient radial profiles obtained in the 18-inch column are generally larger than those in the 6-inch at the same operating condition with the difference getting smaller towards the column wall region. At 20 cm/s, the larger column has up to 10 % higher heat transfer coefficient at the column core region ($r/R \leq 0.3$) and 2.5 % at the column wall region ($r/R \geq 0.6$). At 45 cm/s the difference is even more, with 14 % higher at the column core region, $r/R \leq 0.3$ and 9 % higher at the column wall region, $r/R \geq 0.6$. This can be attributed to higher mixing intensity achieved in the larger column with increased gas velocity relative to the smaller column. Similar findings have been reported by other researchers including; Jhawar and Prakash, 2011; Saxena, 1990. Saxena et al., 1989 used a 1.9 cm diameter probe of conventional design placed at column center and compared the results obtained in the central region of bubble columns of 0.108 m and 0.305 m diameter. These authors observed a similar increase in heat transfer with column diameter and attributed it to better mixing achieved with large diameter.

The enhancement of the heat transfer coefficient with increased column diameter can be attributed to combined effects of; (i) increased gas holdup, Figure 6.5-6.6 ii) increased bubble passage frequency, Figure 6.7a, iii), increased specific interfacial area

per unit volume, Figure 6.7b iv) increased bubble velocity Figure 6.8 as well as, v) increased axial liquid circulation velocity (Figure 6.8), a subject of other study in our laboratories, Al-Mesfer, 2013. The effects of the column diameter on the overall gas holdup and on the radial profiles of the relevant bubble dynamics are discussed in the next section (Section 6.3.1.2-6.3.1.3).

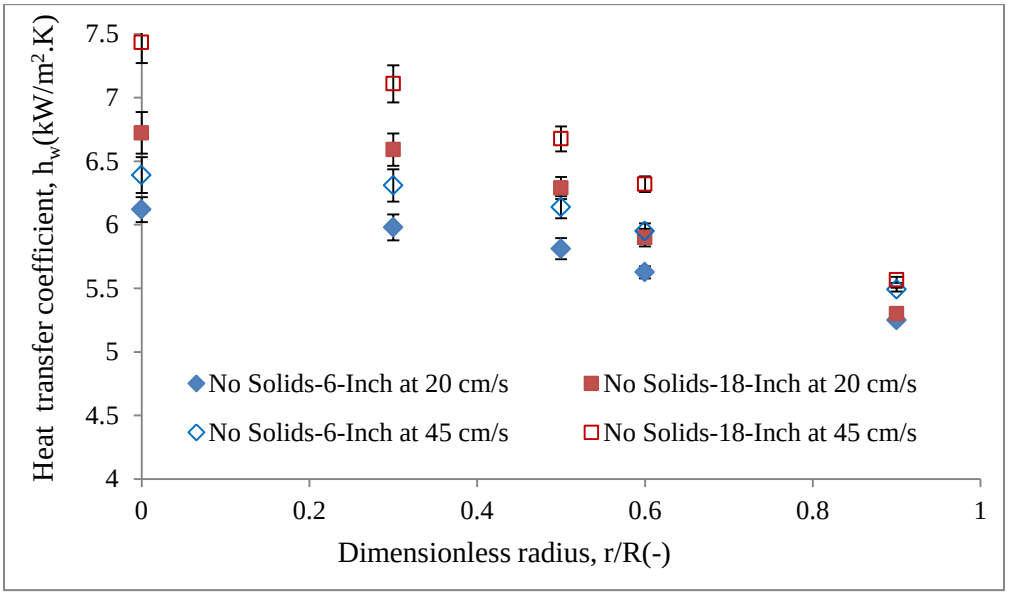

Figure 6.4 Effect of column diameter on radial profiles of heat transfer coefficient at different superficial gas velocities for an air-water system without internals

6.3.1.2. Effect of column diameter on the local and overall gas holdup. The overall gas holdup was determined by bed expansion method as described in Section 3. A comparison of the overall gas holdup measured in the two columns shows that the overall gas hold up is higher in the larger column for all the superficial gas velocities Figure 6.6. The difference diminishes at low gas velocity, but remains significant in the churn

turbulent flow regime. The estimated overall gas holdup in the larger column is higher than that in smaller column. A few findings reported in the literature point to a decrease in overall gas holdup with column diameter, Krishna et al., 1997. Wu, 2007 indicated that the column diameter effect ceases for columns of diameter greater than 15 cm.

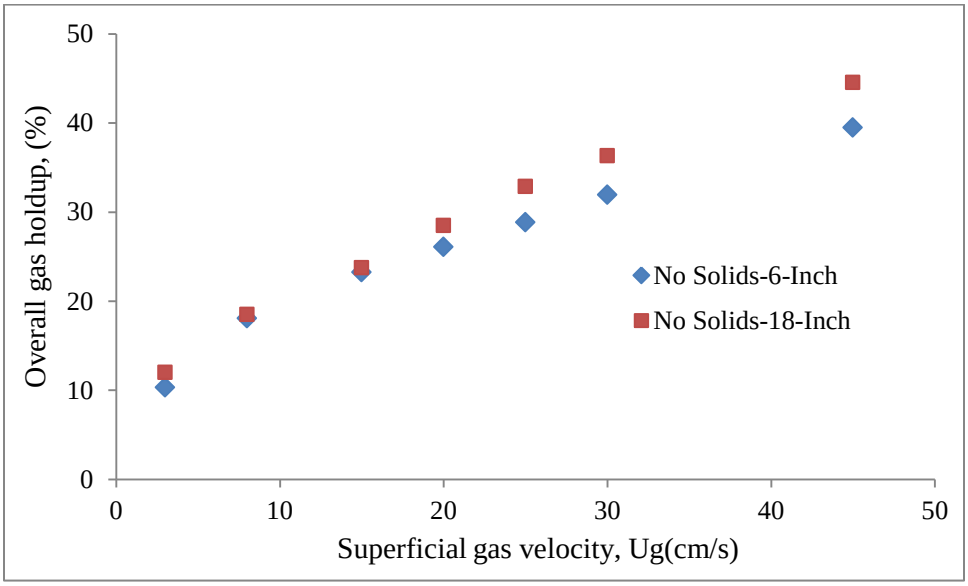

Figure 6.5 Effect of column diameter and superficial gas velocity on overall gas holdup.

The radial profiles of the local gas holdup are shown in Figure 6.6 to give insight into how the column diameter affects the local variations in gas holdup. At 20 cm/s up to 12 % higher gas holdup is attained in 18-inch column than in the 6-inch at the column core region while a 19 % higher at the column wall region, with an average radial gas holdup increase of 16 %. When the gas velocity is increased to 45 cm/s, higher gas holdup which is 10 % more than in the smaller column is attained at the column core while up to 30 % higher gas holdup is attained in the larger column than the smaller

column in the column wall region, with 22 % higher gas holdup on the average attained than in the 6-inch column. This indicates that with the overall increase in bubbles population with gas velocity, the growth in number of smaller bubbles which tend to move closer to the column wall is much higher in the larger column than in the smaller column.

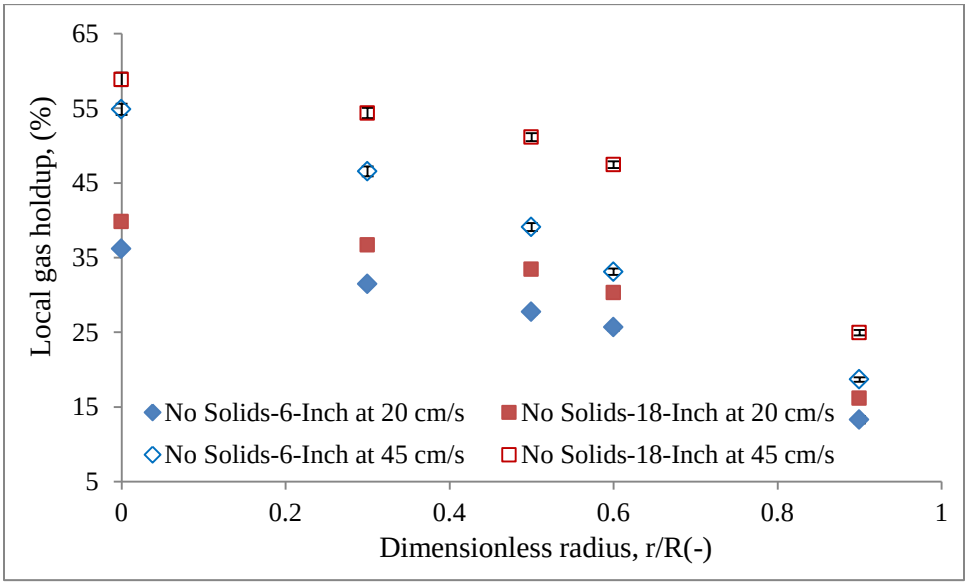

Figure 6.6 Effect of column diameter on the radial profiles of local gas holdup at different gas velocities in empty columns for air-water systems

6.3.1.3. Effect of column diameter on the bubble passage frequency and specific interfacial area. Few studies have examined the bubble passage frequency in bubble columns, (Xue, 2004, Wu, 2007, Shin et al., 2009, and Youssef and Al-Dahhan, 2010). However, only Shin et al., 2008, reported the effect of column diameter on the bubble passage frequency. Figure 6.7 presents the effect of column diameter on the radial

profiles of bubble passage frequency (Figure 6.7a) and Specific interfacial area (Figure 6.7b) at different gas velocities in bubble columns for air-water systems. It is observed that the bubble passage frequency is significantly higher in the column of larger diameter particularly at the column core. This is due to large population of bubbles injected in the larger column. The radial profiles of bubble passage frequency, like gas holdup is governed by bubble slip velocity generated by the net radial force and turbulent dispersion, thus most of the bubbles move towards column center.

Measurements spanning the diameter of the column show that higher interfacial area exists in the center of the column with gradual decrease towards the column wall region. Since the bubble frequency, gas holdup, and specific interfacial area are interwoven parameters, one can confidently expect that an increase in both gas holdup and interfacial area will result with an increase in bubble passage frequency. It is clear from Figure 6.7b that the interfacial area increases with superficial gas velocity. The specific interfacial area largely depends on the shape of the bubbles. Ellipsoidal, spherical cap, and skirted bubbles (Bhaga and Weber, 1981), as well as very irregular bubble shapes, are found deep in the churn turbulent flow regime as a result of coalescence and break-up phenomena, hence the higher interfacial area at 45 cm/s relative to 20 cm/s.

It was found that larger interfacial area existed at the column's center than in the region near the wall, which is similar to the findings of Xue, 2004, Xue et al., 2008, Youssef and Al-Dahhan, 2009 and Youssef, 2010. This difference is due to enhanced rates of breakup and coalescence among bubbles in the central region of the column in the churn turbulent flow regime, which was confirmed by the bubble frequency measured by the optical probe, shown in Figure 6.7a. An increase in bubble passage frequency

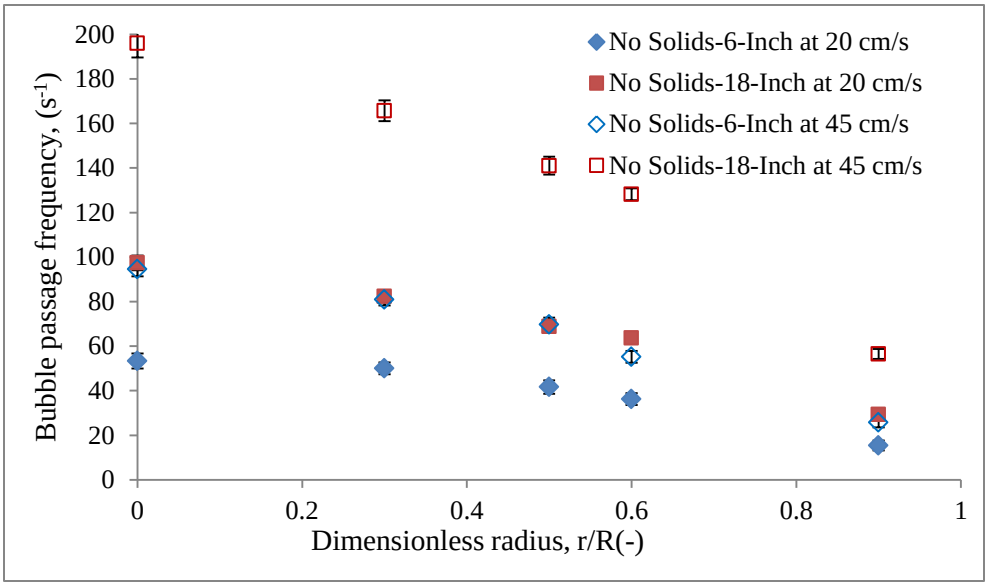

(a)

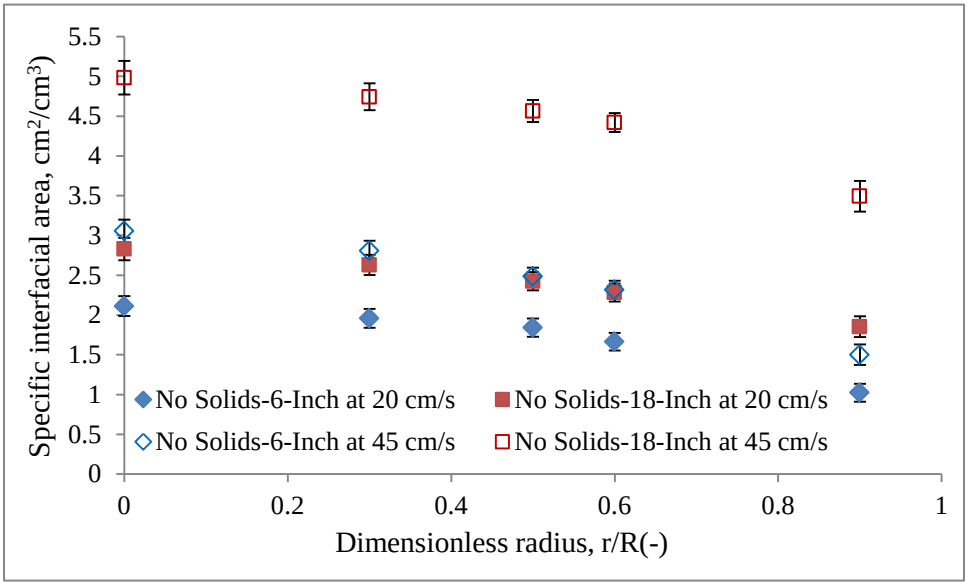

(b)

Figure 6.7 Effect of Column diameter on the radial profiles of (a) Bubble passage frequency and (b) Specific interfacial area at different gas velocities in empty columns for air-water systems

leads to increase in specific interfacial area. The same trend was observed and explained by Wu, 2007 in empty bubble columns. The rate of bubble coalescence and breakup is

more intense in the larger diameter column due to higher turbulence and mixing attained. This is further confirmed by the more steep radial profiles of gas holdup in the 18-inch column. Hence higher interfacial area is attained in the 18-inch column than in the 6-inch at the studied gas velocities. In fact at 20 cm/s the 18-inch diameter gave a radial average of 37 % higher interfacial area. While up to 81 % higher radial specific interfacial area was attained in the 18-inch than the 6-inch column at 45 cm/s. Thus the effect of column diameter on the interfacial area increases with the superficial gas velocity in empty columns.

6.3.1.4. Effect of column diameter on the radial profiles of axial liquid velocity. It has been demonstrated by Gupta, 2002 and Hamed, 2012 that at any given location (r,Z), the axial bubble velocity $U_b(r)$, depends mainly on two factors: the local liquid velocity, $U_l(r)$ and the local slip velocity, $U_s(r)$ at that location, (Equation 6.2).

$$U_b(r) = U_l(r) + U_s(r) \tag{6.2}$$

While a number of studies have reported the variation of the liquid axial velocity with increased column diameter, (Degaleesan, 1997; Forret et al., 2003; and Krishna and Sie, 2000). Forret et al., 2006 demonstrated that the axial liquid circulation velocity increased with column diameter. The increase in column diameter increases turbulence which causes an increase in the liquid velocities (Kumar, 1994 and Degaleesan, 1997). In order to demonstrate the column diameter effect on the large scale axial liquid velocity profiles, the following equation proposed by Wu and Al-Dahhan, 2001 for bubble columns without solids is employed;

$$V_L(r) = V_{LO}\left[1 - 2.65 * m^{0.44} * c\left(\frac{r}{R}\right)^{2.65*m^{0.44}*c}\right] \tag{6.3}$$

With the value of the liquid velocity radial profile steepness parameter, m and wall holdup parameter, c obtained from the following dimensionless groups which were determined by fitting the experimental data of computer automated radioactive particle tracking (CARPT) data. The correlation was developed based on the data obtained in

$$m = 2.188 * 10^{3} {Re_G}^{-0.598} {Fr_G}^{0.146} {Mo_L}^{-0.004} \quad (6.4a)$$

$$c = 4.32 * 10^{-2} {Re_G}^{0.2492} \quad (6.4b)$$

$$Re_G = \frac{D_c U_g (\rho_L - \rho_g)}{\mu_L}, \qquad Fr_G = \frac{{U_g}^2}{g D_c}, \qquad Mo_L = \frac{g {\mu_L}^4}{(\rho_L - \rho_g) {\sigma_L}^3}$$

columns without internals. Where V_{LO} is the centerline axial liquid velocity in the bubble column which can be obtained from either experiments or correlations. In the current work, the centerline liquid velocity has been determined using the correlation of Riquarts, 1981 (Equation 6.5). Since it is not only easy to use but also gives centerline liquid velocity which is in close agreement with a good number of correlations in the literature, more so the artificial neural network (ANN) of Shaikh, 2007 that uses data obtained at a wide range of operating and design conditions in bubble columns.

$$V_{L0} = 0.21 (g D_c)^{0.5} \left(\frac{{U_g}^3}{g \nu_L} \right)^{1/3} \quad (6.5)$$

Since liquid measurement was not carried out in the current work, only the simulations obtained from the correlation have been presented.

Figure 6.8 illustrates the simulated radial profiles of the axial liquid velocities for 6-inch and 18-inch columns without solids or internals. The axial liquid velocity in the 18-inch column is significantly higher than that of 6-inch column. Particularly at the column center ~ 1.7 times that of the 6-inch column. With such increase in the axial liquid velocity with column diameter, an enhanced mixing is attained in the larger

column. Therefore higher rate of the heat transfer surface renewal is attained in the larger column than the 6-inch hence, higher heat transfer coefficient as shown in figure 6.4.

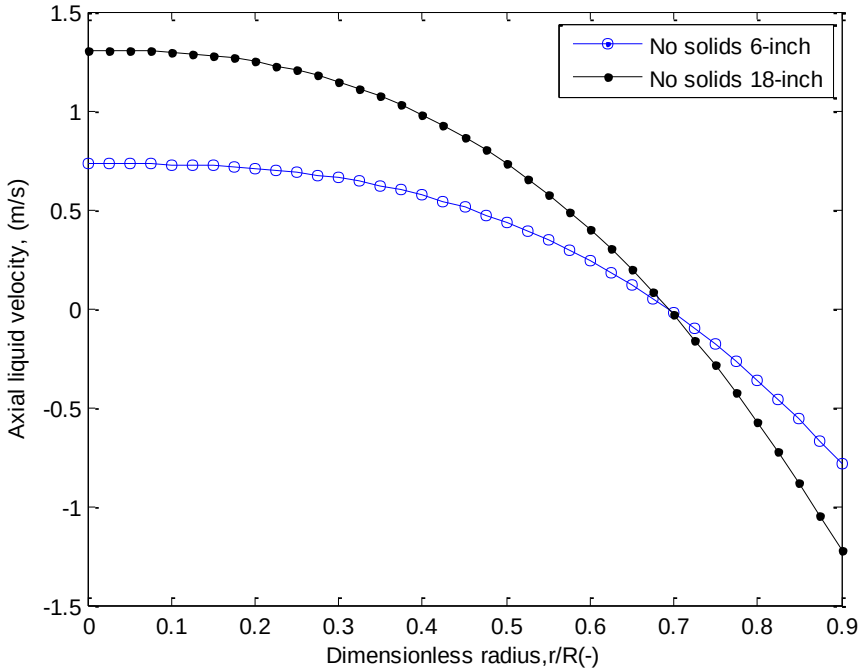

Figure 6.8 Effect of column diameter on the radial profiles of axial liquid velocity in empty columns and no solids at Ug = 45 cm/s.

6.3.2. Effect of Column Diameter on the Heat Transfer Coefficient and Bubble Dynamics in Columns without Internals with Solids. Having discussed the effect of column diameter in empty column with no solids, this section focuses on the effect of column diameter for empty bubble columns with solids.

6.3.2.1. Effect of column diameter on the heat transfer coefficient. Whereas, some researchers have reported increase in heat transfer coefficient with addition of solids, Kölbel et al., 1960; Deckwer et al., 1980; Saxena et al., 1989c, Saxena and Chen,

1994; Yang et al., 2000, others have reported a decrease in heat transfer coefficient. Jhawar and Prakash, 2011 using glass beads similar to those used in this work as the solid/fines with air as the gas phase and water as liquid phase, demonstrated that the heat transfer coefficient decreases with increase in solids loading. This corroborates the earlier findings of Michael and Reichert, 1981 and of Li and Prakash, 1997, 2001.

Figure 6.9 illustrates the effect of column diameter at different solids loading on the heat transfer coefficient at Ug = 45 cm/s. In this work a decrease in heat transfer coefficient was observed with increasing solids fraction in both the large and small column as illustrated in Figure 6.9. Although for air-water-glass beads system solids loading (addition of glass beads) leads to increase in bubble sizes with higher velocities, the increased solids loading leads to an increase in the boundary layer thickness which increases resistance to the heat transfer rate Li and Prakash, 2001. Furthermore the

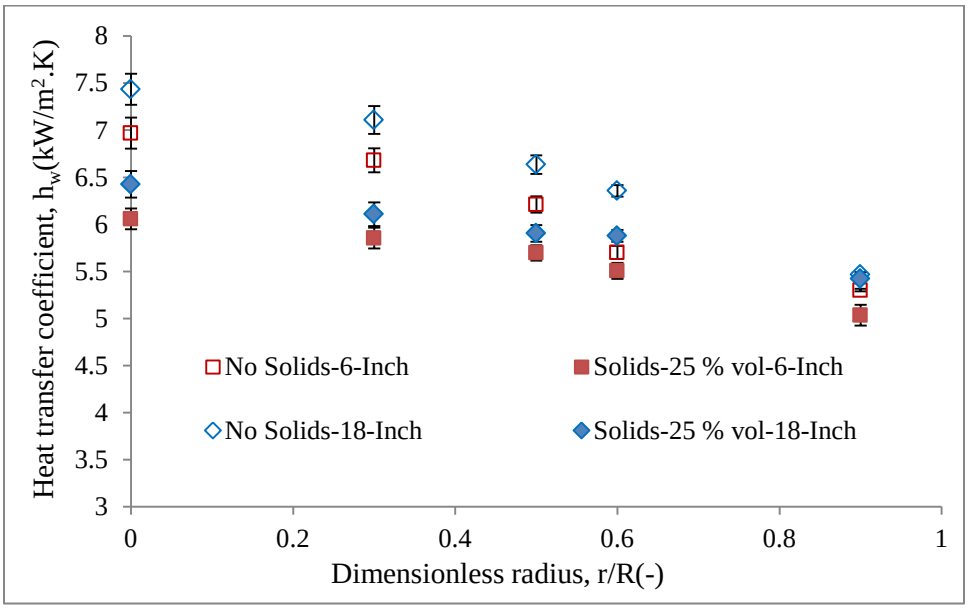

Figure 6.9 Effect of column diameter on the radial profiles of heat transfer coefficient in empty columns for air-water-glass beads system at Ug = 45 cm/s

increase in apparent slurry viscosity due to addition of the solids results in lower turbulence, because of the small solid particles dampening on the bubble wake induced turbulence. Besides, the hydrodynamic boundary layer thickness increase would have a negative impact on heat transfer coefficient (Jhawar, 2012). These observed phenomena of reduced turbulence can be as a result of decreased local gas holdup, (Figure 6.10), decreased bubbles population and bubble passage frequency (Figure 6.10b), and a decrease in specific interfacial area (Figure 6.11) with addition of solids. Thus the combined influence of bubbles passage frequency, specific interfacial area, and gas holdup dominates leading to decreased heat transfer coefficient. With 25 % solids loading, the heat transfer obtained in the 18-inch column is 5.7 % higher on the average than those obtained in the 6-inch diameter column while without solids, 4.3 % higher heat transfer coefficient than in the 6-inch was obtained in the 18-inch column averagely.

6.3.2.2. Effect of column diameter on the local gas holdup. Figure 6.10 shows the effect of column diameter on the radial profiles of local gas holdup. At 25 % solids, the radial local gas holdup obtained in 18-inch column is 23 % higher than in the 6-inch column on the average with least effect at the column center and highest at the column annulus region. Without solids the influence of the column diameter is even greater with a radial average of 26 % higher in the larger column. Though the use of solids leads to a general decrease in gas holdup, the slope of the gas holdup radial profiles is slightly increased. A 5.6 % increase in the slope of the gas holdup in 6-inch column while an increase of 7 % was realized in the 18-inch when 25 % vol solids was used. This variation is likely to enhance the intensity of the large-scale liquid/slurry recirculation to

some extent. Thus the influence of the column diameter becomes more pronounced on the heat transfer coefficient when the solids are used.

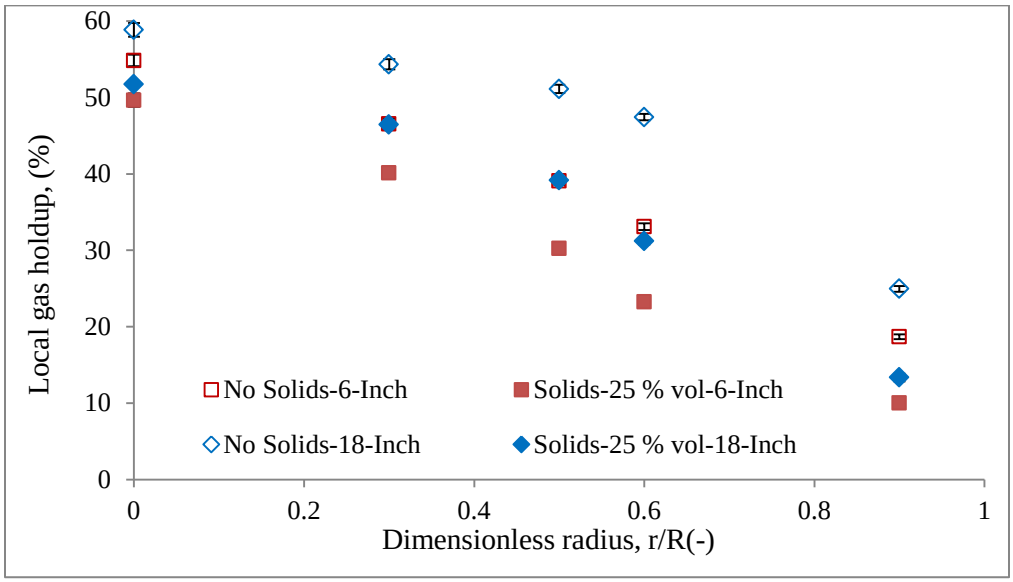

Figure 6.10 Effect of column diameter on the radial profiles of local gas holdup in empty columns for air-water-glass beads systems at Ug = 45 cm/s

6.3.2.3. Effect of column diameter on bubble passage frequency and specific interfacial area. The bubble passage frequency radial profiles have similar trends as those of local gas holdup with and without solids. Figure 6.11 illustrates the effect of column diameter on the bubble passage frequency (Figure 6.11a) and specific interfacial area (Figure 6.11b) for empty columns with and without solids. In the 18-inch column the bubble passage frequency is twice that in the 6-inch column almost at each of the radial locations, without solids or with 25 % vol solids. The specific interfacial area is noted to decrease with the solids loading. This is due to an increase in bubble coalescence forming

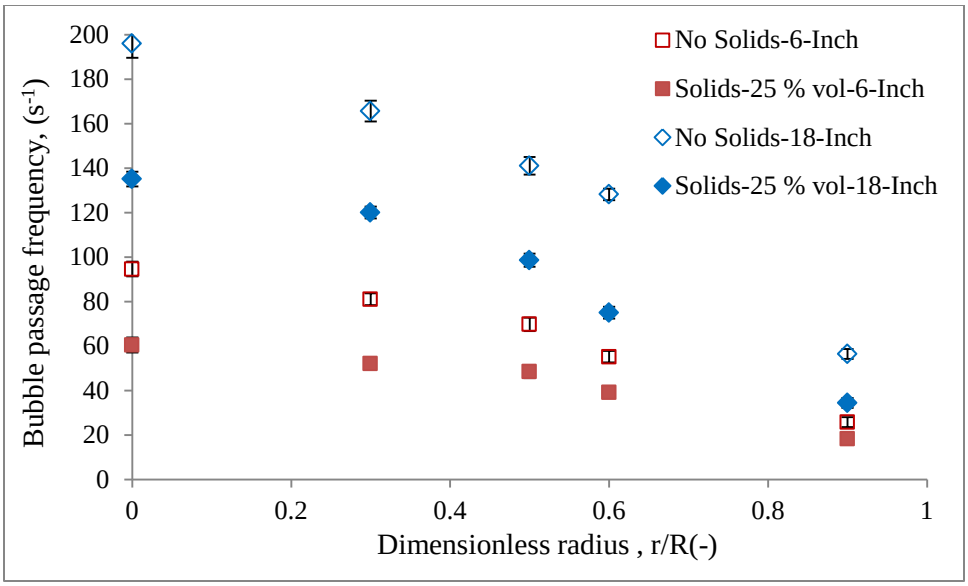

(a)

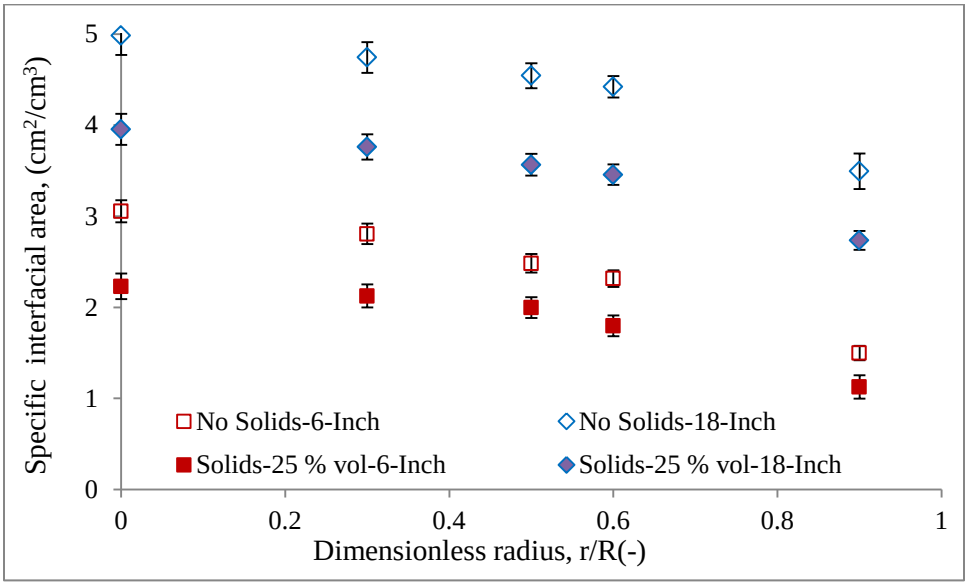

(b)

Figure 6.11 Effect of column diameter on the radial profiles of (a) Bubble passage frequency and (b) Specific interfacial area in columns for air-water-glass beads systems at Ug = 45 cm/s

larger bubbles hence a decrease in total interfacial area (Zahradnick et al., 1992). With increasing column diameter, increased interfacial area is observed much like of the gas

holdup and the bubble passage frequency. Without solids, the specific interfacial area obtained in the 18-inch column is 51 % higher than those of 6-inch at the column core region. However when 25 % solids are used, the 18-inch column gives 65 % higher interfacial area than the 6-inch column at the core region. In both cases the interfacial area obtained at the column wall region in the 18-inch almost twice those in the 6-inch column. This confirms the trends obtained with the local gas hold up in the preceding section. The higher specific interfacial area obtained in the larger column could be attributed to higher breakup rate due to greater turbulence that gives large bubbles population with higher frequency.

6.3.2.4. Effect of column diameter on the axial bubble velocity. The axial bubble velocities defined as magnitude of the velocity of bubbles moving parallel to the column orientation were obtained as outlined in Section 3.3.3.5. Figure 6.12 presents the effect of column diameter and solids loading on the radial profiles of the axial bubble velocity in the two pilot scale bubble columns for air-water and air-water glass beads systems as obtained by the 4-point optical probe. It is observed that without solids, the axial bubble velocity in the larger column is up to 50 % higher than that of the smaller scale column at the column center, r/R = 0.0 and up to 63 % higher at the column wall region. When 25 % vol. solids are used, the larger column gave 45 % higher axial bubble velocity at the column center than in the 6-inch and up 71 % higher close to the wall region. The enhancement of liquid circulation caused by the increase in column diameter (Kumar, 1994, Degaleesan, 1997, and Hamed, 2012) enhances gas circulation, hence the higher axial bubble velocity. Moreover, with the solids, the increase in the column

diameter allows the formation of larger bubbles (Figure 6.3c) that churn at higher axial bubble velocities than in smaller diameter column.

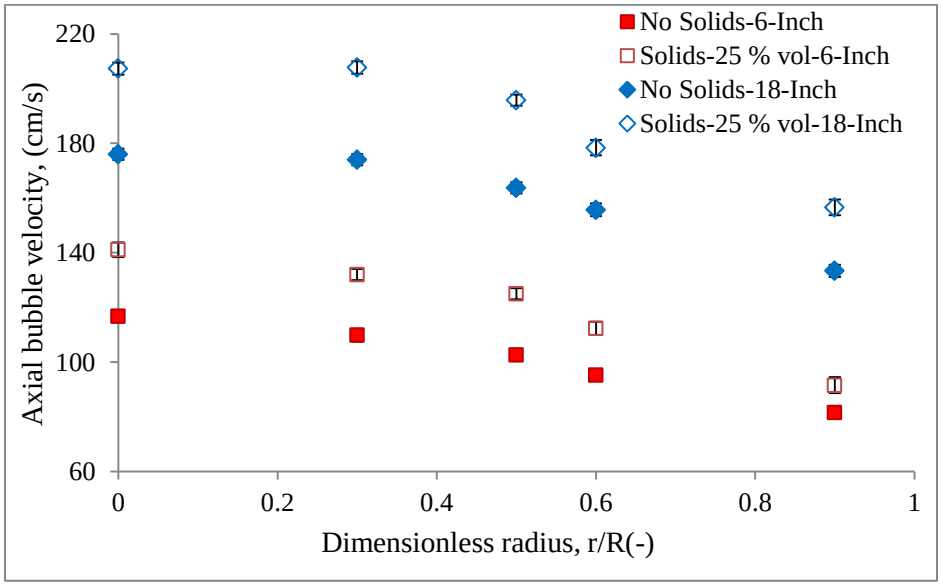

Figure 6.12 Effect of column diameter and solids loading on the radial profiles of axial bubble velocity at Ug = 45 cm/s

6.3.3. Effect of Column Diameter on the Heat Transfer Coefficient and Bubble Dynamics in Columns Equipped with Dense Internals. In the highly exothermic reactions such as the FT synthesis process, the removal of the heat generated by the chemical reaction is necessary. Thus there is need to examine the effect of column diameter with internals as presented in this section.

6.3.3.1. Effect of column diameter on the heat transfer coefficient. To demonstrate the effect of column diameter in the presence of dense internals, the empty column results were used for reference. Figure 6.13 shows the radial profiles of the heat

transfer coefficient in two columns, 6-inch and 18-inch diameter at Ug = 45 cm/s based on free CSA without solids. In the presence of dense internals, at the column centre region, the 18-inch column gave ~7 % higher values of the heat transfer coefficient than

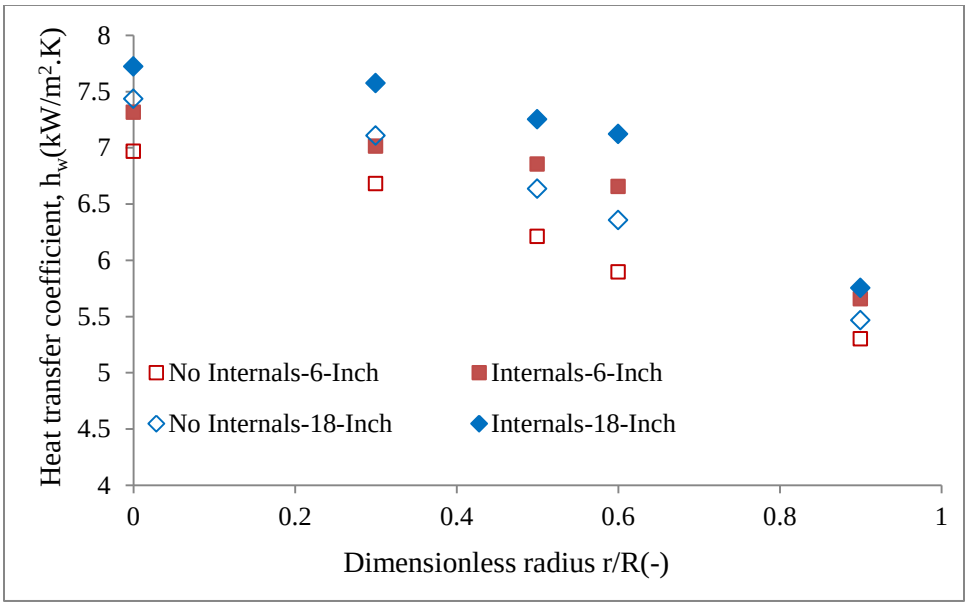

Figure 6.13 Effect of column diameter on radial profiles of the heat transfer coefficient at Ug = 45 cm/s based on free CSA.

6-inch column. While at the column wall region, r/R = 0.9, about 3 % higher values were obtained with an average of 6.2 % higher heat transfer coefficient in the 18-inch than the 6-inch column. Without internals, the 18-inch column gave ~5.6 % higher values on the average than the 6-inch diameter column. These findings are consistent with the reported bubble dynamics in sections 6.3.3.2-6.3.3.4.

6.3.3.2. Effect of column diameter on the local gas holdup. The effect of column diameter on local gas holdup radial profiles in columns with dense internals and

without solids at Ug = 45 cm/s based on the free CSA is shown in Figure 6.14. The local gas holdup obtained with the 18-inch column is 23 % higher on the average than those of 6-inch without internals. In the presence of dense internals, the gas holdup is ~ 25 % higher in the 18-inch column averagely than the 6-inch column

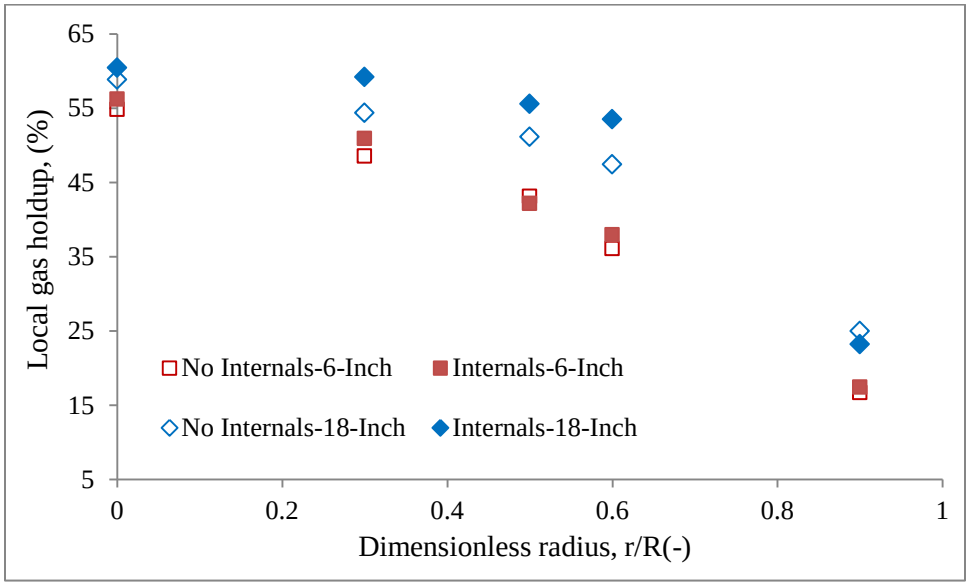

Figure 6.14 Effect of column diameter on the radial profiles of local gas holdup at Ug = 45 cm/s based on free CSA.

6.3.3.3. Effect of column diameter on bubble passage frequency. When the columns are inserted with dense internals, the radial profiles of both the bubble passage frequency and the specific interfacial area are not significantly changed. However like the local gas holdup with and without solids, the larger column gave higher values. Figure 6.14 illustrates the effect of column diameter on the bubble passage frequency for columns equipped with dense internals at Ug = 45 cm/s based on free CSA. In the 18-

inch column the bubble passage frequency is twice that in the 6-inch column without internals and 1.86 times that of 6-inch on the average when dense internals are used.

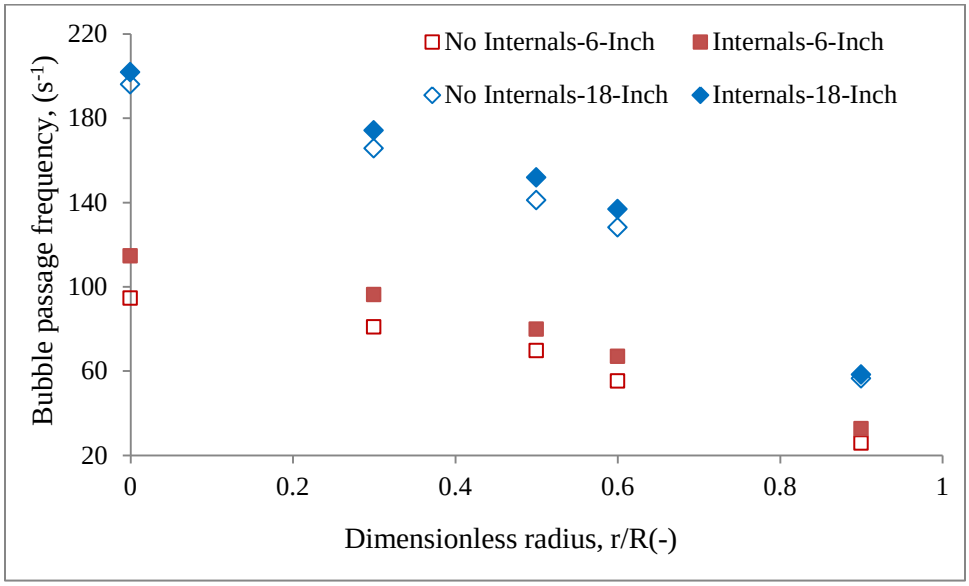

Figure 6.15 Effect of column diameter on the radial profiles of bubble passage frequency at Ug = 45 cm/s based on free CSA.

6.3.4. Development of Heat Transfer Coefficient Empirical Correlation for Columns without Internals. While there exists several empirical and semi-empirical correlations in the literature for heat transfer coefficient prediction in bubble columns, most of these correlations provide only the wall-region heat transfer coefficient. Numerous correlations have been proposed in the past for the prediction of heat transfer coefficients. These correlations are summarized elsewhere in Wu, 2007 and Hulet et al., 2009. However, these correlations can predict well only at their own studied experimental conditions, which were mainly in smaller columns ~ 8 cm diameter operated in the

homogenous flow regime and hence not much benefit to systems that desire operation in the heterogeneous flow regime such as FT process and Liquid phase methanol synthesis.

To aid the design and scale-up of bubble column and slurry bubble column reactors, there is need for empirical or semi-empirical correlation that can predict heat transfer coefficients over a wide range of operating conditions, involving solids and thus slurry system with wide range in physical properties of liquid, alongside the column size (diameter). In this work, power-law empirical correlation has been developed. In order to develop the empirical correlations of heat transfer coefficient in bubble and slurry bubble columns, only data obtained in the current work of heat transfer coefficients measured in two columns of 6-inch (0.14 m) diameter and 18-inch (0.44 m) diameter. The experimental measurements were conducted in two and three phase systems covering wide range of both liquid/slurry properties and gas flow rates, and accounts for the different liquid properties. Deckwer, 1980 was the first to propose the heat transfer coefficient relation as follows;

$$\frac{h}{\rho C_p U_g} \propto \left(\frac{{U_g}^3}{gv}\right)^{-0.25} \left(\frac{\mu C_p}{K}\right)^{-0.5} \tag{6.6}$$

Or in terms of dimensionless numbers, generally is given as;

$$St = \beta \, (Re \, Fr \, Pr^{a})^{\,b} \tag{6.7}$$

Different researchers have subsequently defined the dimensionless groups and modified the coefficient β and the exponents a, b in equation 6.7 to fit their experimental data, (Yang et al., 2000, Wu, 2007). Similarly, the form that fits the measured heat transfer coefficient experimental data of the current work has been proposed, (Equation 6.8) for the center-line heat transfer coefficient. The correlation proposed in this work estimates the centerline heat transfer coefficient h_c in bubble and slurry bubble columns and the

power law final form was selected based on the least square regression method as follows;

$$h_c = 3.413 \times 10^{-5}\, {U_g}^{-0.52}\, \rho_{sl} {C_p}_{sl} {D_c}^{0.14} \left[\left(\frac{D_c U_g \rho_{sl}}{\mu_{sl}} \right) \left(\frac{{U_g}^2}{D_c g} \right) \left(\frac{C_{p,sl} \mu_{sl}}{K_{sl}} \right)^{2.54} \right]^{0.254} \quad (6.8)$$

The center-line was chosen as the point of reference in developing the above equation, (Equation 6.8) since the heat transfer coefficient at the column center has been found to be the highest along a radial direction. Based on the radial profiles of heat transfer coefficients measured, and discussed in the current work, the h_c is ~ 16 % higher the wall region heat transfer coefficient. Besides it (h_c) is ~7 % higher than radial average heat transfer coefficient. Hence it can provide useful indication and close approximation from an engineering point of view.

All the units are consistently in cgs. The effective slurry viscosity, μ_{sl} thermal conductivity, K_{sl} density, ρ_{sl} and heat capacity, ${C_p}_{sl}$ can be evaluated from the physical properties of both the solid and liquid as follows;

$$\rho_{sl} = \emptyset_s \rho_s + \rho_l (1 - \emptyset_s) \quad (6.9)$$

$$C_{p,sl} = w_s C_{p,s} + C_{p,l} (1 - w_s) \quad (6.10)$$

To estimate the thermal conductivity of the slurry, the equation proposed by Tareef (1940) can be adopted;

$$K_{sl} = K_l \frac{2K_l + K_s - 2\emptyset_s (K_l - K_s)}{2K_l + K_s - \emptyset_s (K_l - K_s)} \quad (6.11)$$

While for high solids loading (>5 vol %), a widely tested semi-theoretical correlation of Vand, 1948 that has also been recommended by Suh and Deckwer, 1989 based on their analysis of heat transfer coefficients in three-phase fluidized beds can be employed in calculating the apparent slurry viscosity.

$$\mu_{sl} = \mu_l \exp\left[\frac{2.5\emptyset_s}{1 - 0.609\emptyset_s}\right] \quad (6.12)$$

The properties of the collected parameters such as column diameter, and liquid-solid suspension are shown in Appendix D, Table D-1. A parity plot for the measured and the estimated heat transfer coefficient is also given in Appendix D. The relative error produced by the correlation, (Equation 6.8) (6 %) is less than that of the proposed mechanistic model highlighted in Section 5, (13 %). This difference is attributed to the fact that Equation 6.8 was developed by fitting to the measured heat transfer coefficient data while the mechanistic model has no fitting.

6.4. REMARKS

The variation of heat transfer coefficient and bubble dynamics with column diameter in bubble and slurry bubble columns equipped with dense internals occupying 25 % of the CSA was examined based on the data of this study obtained by using combined measurements technique.

The higher heat transfer coefficient is reported in the larger column regardless of solids or internals use. With the effect of column diameter being more pronounced in the column core region. Similar trends on the effect of the bubble dynamics have also been realized. The local and overall gas holdup, specific interfacial area, bubble passage frequency, bubble sizes and the axial bubble velocity is increased with increase in column diameter.

The observed increase in heat transfer coefficient in the central region of column is related to increase in the large scale liquid circulation velocity with column diameter

which can in turn be related to increase in the axial bubble velocities of large bubbles. Besides, higher gas holdup and bubble passage frequency attained in the larger column lead to enhanced heat transfer rate due to increased heat transfer surface renewal.

A general heat transfer coefficient correlation which accounts for column diameter effects and the liquid and gas physical properties on the heat transfer has been proposed to predict the center line heat transfer coefficient in bubble and slurry bubble columns.

7. CONCLUDING REMARKS AND RECOMMENDATIONS

In this section concluding remarks and summary of the key findings of this work alongside with recommendations for future work in bubble columns with and without dense internals are presented.

7.1. CONCLUDING REMARKS

This work has investigated the heat transfer coefficients and bubble dynamics in bubble columns without internals and with dense internals both under two-phase and three-phase systems that mimic cold flow conditions of the FT process. Among the outstanding features of this work is that for the first time, a combined measurements technique that consists of four-point fiber optical probe and fast response heat transfer probe was developed and used simultaneously to capture both the heat transfer coefficient and the bubble dynamics at the same time. The effect of dense internals and high solids loading on bubble dynamics and heat transfer coefficient was assessed in pilot scale bubble columns. Columns of different scales were utilized to assess the effect of column diameter in both in the presence and absence of dense internals. Besides, a contact time needed in the mechanistic equation for the heat transfer coefficient prediction was developed based on the local bubble properties.

7.1.1. Bubble Dynamics. The impact of dense internals, internals size and configuration and high solids loading was assessed on the bubble dynamic parameters including local and overall gas holdup, bubble chord length, bubble passage frequency, specific interfacial area, and axial bubble velocity and radial bubble velocity. The overall and local gas holdup, bubble sizes, bubble passage frequency, specific interfacial area,

and axial bubble velocity increased with superficial gas velocity, regardless of solids loading or internals use. However the overall and local gas holdup, specific interfacial area, and bubble passage frequency decreased with the increase in solids loading. Slight increase in axial bubble velocity and bubble sizes was attained with the increase in solids loading. Analysis of the distribution of the bubble chord lengths in the column center showed that a wider spread with increasing solids loading was attained than with no solids with effect of solids loading being significantly higher at lower range than higher range of superficial gas velocity. It was also noted that the probe measurements with upward and downward orientation are necessary for the bubble dynamic study, particularly towards the column wall region and high superficial gas velocities where more bubbles move downward than those moving upwards.

The internals size and configuration were also noted to have notable effect on the bubble properties. With dense small sized internals smaller bubble sizes with higher specific interfacial area in a unit volume and higher bubble passage frequencies were attained, the overall gas holdup and local gas hold up were only but slightly enhanced which is within the margin of error while the axial bubble velocity was slightly reduced. More difference in the centerline and the wall region was noted with the local gas holdup thus higher intensity of large scale liquid recirculation expected with smaller sized internals.

This work also found that it is possible to extrapolate the local and overall gas holdup studies from the empty bubble columns to those equipped with the dense internals by matching the gas velocity based on the free cross-sectional area available for the flow. Particularly in the 6-inch diameter column where the gas holdups are within 3 % of each

other. In the 18-inch column, the internals were found to enhance the local and overall gas holdup therefore extrapolation may not be possible. It was also established that the addition of solids does not have significant impact on the radial profiles of the local gas holdup.

The larger diameter column exhibited higher values than the 6-inch column for all the measured bubble properties at the same operating conditions.

7.1.2. Heat Transfer Coefficient. Heat transfer coefficient measurement methodology was simultaneously employed alongside bubble dynamics measurements. The measurements were first verified in air-water system and then extended to air-water-glass beads systems with and without internals to mimic the cold flow conditions of the Fischer-Tropsch synthesis process. The heat transfer coefficient was noted to increase with increase in superficial gas velocity, with the rate of increase being higher at lower superficial gas velocity and then the increase becomes significantly small from 20 cm/s. Consistently higher heat transfer coefficient was obtained at the column center relative to the column wall regions as well as other radial locations for all the operating conditions, with or without solids and regardless of internals presence. These findings were found to be consistent with those already reported by other researchers.

The presence of dense internals was found to enhance the heat transfer coefficient with the effect being higher at lower superficial gas velocity. The heat transfer coefficient obtained in empty column for gas-liquid system can be extrapolated to columns equipped with dense internals occupying 25 % of the CSA since the enhancement of the heat transfer coefficient with the internals was relatively small up to 5 %.

7.1.3. Effect of Column Diameter. The column diameter was found to have effect on the heat transfer coefficient as well all the bubble dynamic parameters including overall and local gas holdup, bubble passage frequency, specific interfacial area, bubble chord length and the axial bubble velocity. Larger column diameter was found to increase the heat transfer coefficient, enhance the local and overall gas holdup, bubble passage frequency, bubble chord lengths and axial bubble velocity, with and without internals or solids.

7.2. RECOMMENDATION FOR FUTURE WORK

- The current work was limited to ambient temperature and pressure while the liquid phase methanol synthesis (LPMeOH) synthesis and FT synthesis involve a 3-phase system running at high pressure and temperature. Therefore, it is important to adopt a study where mimic FT conditions are applied on both heat transfer and bubble dynamics to assure the validity of the findings and results of the current work.
- The studies of heat transfer coefficient and bubble dynamics still need to be done with different gas-liquid-solids systems since some studies have reported increase in heat transfer coefficient while others a decrease and it is thought the different phenomena observed can be attributed to different gas-liquid-solid systems employed.
- This work presents a deep insight on the influence of dense internals and high solids loading on the heat transfer coefficient and bubble dynamics in bubble columns. However as a first step this study was limited to the air-water-glass beads system. It is therefore recommended to use hydrocarbon system which is of industrial interest.

- In future studies, a computational fluid dynamics (CFD) should be implemented to examine and validate the experimental data obtained from the four-point optical probe and integrate the heat transfer to it to simulate. Information obtained from the hybrid measurements technique in the current work provides detailed understanding of the relation between heat transfer and bubble dynamics and also positions CFD as an alternative method for obtaining essential information regarding the performance of bubble and slurry bubble columns.
- The effect of different configurations and sizes of dense internals on both heat transfer and bubble dynamics still need to be examined in columns of larger diameters such as 18-inch diameter column.
- The effect of height of internals above the surface of gas distributor needs to be investigated along with different configurations and sizes of sparger (gas distributor) on the heat transfer coefficient and bubble dynamics.
- Integrate the measurements and findings of the current work with those obtained from Computed Tomography (CT), which gives gas holdup distribution and flow regime identification and the Radioactive Particle Tracking (RPT) technique that gives turbulent parameters, liquid velocity, phase residence time and eddy diffusivity.
- A single probe that combines both the heat transfer coefficient and the bubble dynamics measurements needs to be developed and implemented

APPENDIX A

HEAT TRANSFER STUDIES SUMMARY

Table A.1 Summary of heat transfer and hydrodynamics studies in bubble and slurry bubble columns with vertical internals.

Author(s)	System used	Column and sparger features	Internals specifications	Investigated subject and/or parameters
Kölbel and Langheim, 1958 (US 2,852,350)	CO+H2-watery solution of Fe(NO3)3 and Cu(NO3)2	1.4 m diameter – 12 m height	360 pipes that reduces to 270 at 3 m above the gas inlet, to 180 after 3 further meters and finally to 90 by moving 3 more meters higher.	Improvement of cooling system design
Kölbel and Ackermann, 1958 (US 2,853,369)	Gas-slurry (no details given)	Applicable to any column with diameter 30 cm up to 3m and above, and more than 1.5 m in height	Vertical shafts (circular or hexagonal) with cooling tubes within or in between the circular shafts or various arrangements within the hexagonal ones	Overcoming the liquid recirculation "rolling movement" and backmixing
Carleton et al., 1967	Nitrogen-water and oxygen-cobalt catalyzed sodium sulphite	wide range of column diameters as well as packing materials and sizes		Gas holdup, pressure drop, gas and liquid RTD, and interfacial area
Voyer and Miller, 1968	Nitrogen-water and Nitrogen-NaOH solution	5.5" diameter-0.67 to 7.8ft/ sieve plate (5% free area, 0.15" diameter holes at ½" triangular pitch)	½" 6 mesh cylindrical screen packing and ½" 6 mesh corrugated screen packing (corrugated and each layer perpendicular to the next one).	Interfacial area
Shah et al., 1978	Nitrogen-water	Glass: 6.35 cm diameter/sparger details not specified	6, 16 and 23 glass rods (0.004m diameter); 2 and 4 glass rods (0.011 m diameter); 1 glass rod (0.032 m diameter); 1, 2, and 4 screen baskets (0.019 m diameter) and 1 screen basket (0.038 m diameter). The smaller baskets were a) empty, b) filled with 0.0032 m polyethylene packing and c)	Gas holdup and backmixing

			filled with 0.0159 m diameter glass rods. The larger baskets were a) and b) same as above and c) filled with 0.032 m diameter rod. (Rods were all 1.143 m tall)	
Kölbel and Ralek, 1980	Syngas-catalyst slurry	Not Specified	Vertical honeycombed shafts with cooling pipes arranged centrally around or in corners	Liquid backmixing and catalyst efficiency
O'Dowd et al., 1987	Nitrogen-water-glass spheres	10.8 cm diameter column – 1.94 m height/perforated plate with 72 holes of 0.001 m diameter	Internal baffles: 5 vertical rods (1 central and 4 around at 90 deg. each)of 0.019m diameter and 1.88 m height	Solids dispersion coefficient, local gas holdup and bubble size and interfacial area
Yamashita, 1987	Air-water system	31 cm diameter/single nozzle of 60 mm diameter downwards on central axis (10 cm above bottom)	Single rod of 6 mm diameter (hanging 36.5 cm above bottom)	Overall gas holdup
		Multi rods and pipes: Small separation *(6mm): 18, 44, 70 and 85 internals of 14mm diameter. Large separation (≥8mm): 37, 28, 21 and 10 internals of 22mm diameter. 9 internals of 60 mm diameter. 9 internals of 48 mm diameter.		
		16 cm diameter/single nozzle of 27.6 mm diameter horizontally on side wall (10 cm above bottom)	Single pipe and rod (sitting on bottom)	
		Multi rods and pipes: Large separation *(≥8mm): 2 internals of 14, 22, 38 and 20 mm diameter 5, 6, and 11 internals of 22 mm		

		diameter		
		8 cm diameter/single nozzle of 10 mm diameter horizontally on side wall (4.2 cm above bottom)	Single pipe and rod	
Saxena et al., 1991	Nitrogen-Therminol 66-red iron oxide powder	10.8 cm diameter/perforated plate	Single cylindrical probe (19, 31.8, and 50.8 mm diameter) and bundle of 7 tubes of 19 mm diameter each in a triangular pitch of 36.5 mm	Heat transfer, gas holdup
Saxena et al., 1992	Air-water Air-water-glass beads	30.5 cm diameter – 3.3 m height/perforated plate of 0.8mm diameter orifices in square arrangement of 9.5 mm pitch	5, 7, and 37 Stainless Steel tubes (the latter in 3 bundles of 3 concentric hexagonal rows) of 19 mm diameter each and the pitch is 36.5 mm	Overall gas holdup
Saxena and Rao, 1993	Nitrogen-Therminol-Magnetite	Same as Saxena et al. (1992)	37 Stainless Steel tubes in a bundle of 19 mm diameter each in equilateral pitch of 36.5 mm	Overall gas holdup
Saxena and Chen, 1994	Air-water	Same as Saxena et al. (1991) Same as Saxena et al.(1992)	1 and 7 tubes bundle	Hydrodynamics and heat transfer
	Air-water-solids (glass beads (50 μm), magnetite (37.5, 49, 58, 69, 90.5 μm), red iron oxide powder (1.02, 2.38μm)) Nitrogen-Therminol Nitrogen-Therminol-Solids (red iron oxide (1.7 μm), magnetite (28, 36.6, 37μm)	Same as Saxena et al. (1991)		
	Nitrogen-Therminol Nitrogen-Therminol-Solid	Same as Saxena et al. (1992)	37 tubes bundle, pitch as Saxena et. al. (1992)	

Pradhan et al., 1993	Air-aqueous CMC solution	0.102m diameter column – 2.5 m height/64 holes of 1.5mm diameter each in a 1.2 cm triangular pitch	Helical coils (made of 6mm Co tube) of 3.5 cm and/or 6.8 cm diameter in 2.5 cm pitch and bundles of vertical straight tubes (Stainless Steel with 1.2, 1.5, and 2.0 cm outer diameters)	Overall gas holdup and pressure drop
Chen et al., 1999	Air-water Air-Drakeoil	18" (44cm) diameter/301 holes of 0.77mm diameter each on 14 concentric circular rings at 1.5 cm apart	16 Aluminum tubes of 1" diameter each in two bundles at r/R=0.39 and 0.61	Gas holdup and its radial profile, liquid recirculation velocity, turbulent stresses and eddy diffusivities
De et al., 1999	Air-sodium sulphate Air-butanol Air-glycerine	0.05 m diameter column – 2.5 m height/plate sparger	Helical coils of 3.5 cm diameter and straight tubes of 1.2 cm and 1.5 cm diameter	Overall gas holdup
Maretto and Krishna, 2001	Syngas-paraffin $C_{16}H_{34}$-Co based catalayst	7 m diameter – 30 m dispersion height	Vertical cooling tubes and spacer sieve trays	Reactor productivity and reaction kinetics modeling
Forret et al., 2003	Air-water	1 m diameter/perforated plate: 312 holes of 2mm diameter and 50 mm pitch	56 tubes of 63 mm diameter each and a 10.8 cm square pitch	Liquid mixing-axial dispersion coefficient
Larachi et al., 2006	Air-water	Simulated lab scale 19 cm diameter and pilot scale 100 cm diameter	Tubes of 1" diameter and triangular pitch in 4 arrangements: dense (253 tubes), sparse (31 tubes), star/wall clearance (121 tubes), star/core clearance (132 tubes)	CFD simulations (gas holdup, liquid axial velocity and turbulent kinetic energy)
Balamurugan and Subbarao, 2006	Gas (Air) – liquid (NA)	15 cm diameter/perforated plate with 126 holes of 0.2 cm diameter each in 1 cm square pitch	21 and 41 Stainless Steel helical springs of 1.9 cm coil diameter made of 0.5 mm wire	Bubble size and holdup
Youssef and Al-Dahhan, 2009	Air-water	0.19 m diameter – 2 m height/perforated plate: 225 holes of 1.32 mm diameter, arranged in a triangular pitch, with a total free area of 1.09%.	12 and 48 Plexiglas rods of ½" diameter each located in two concentric circles and in triangular pitch, respectively	Gas holdup and its radial profile, and bubble dynamics.
Abdulmohsin	Air-water	0.19 m diameter – 2 m	12 and 48 Plexiglas rods of ½" diameter each	Heat transfer coefficient

and Al-Dahhan, 2012		height/perforated plate: 225 holes of 1.32 mm diameter, arranged in a triangular pitch, with a total free area of 1.09%.	located in two concentric circles and in triangular pitch, respectively	and its radial profile.
Jhawar and Prakash, 2011	Air-water-glass beads	0.15 m diameter and 2.5 m high/ sintered steel plate distributor	15 tube bundle (0.95 cm OD) located within 10 cm radius	Column diameter, heat transfer, center-line liquid velocity, overall gas holdup, bubble rise velocity
Youssef et al., 2013	Air-water	0.45 m diameter – 3.8 m height/perforated plate: 241 holes of 3 mm diameter, arranged in a triangular pitch, with a total free area of 1.09%.	16 Plexiglas rods of 1" diameter each in two concentric circles and 17 and 27 cm triangular pitch, respectively (5 % CSA occupied) 75 Plexiglas rods of 1" diameter triangular pitch, respectively	Hydrodynamics in pilot scale column: Effect of internals on Gas holdup and its radial profile, interfacial area, bubble chord lengths

APPENDIX B

THE HEAT TRANSFER COEFFICIENT MEASUREMENT TECHNIQUE

PROCEDURE

Scope

In this work, a combined measurement of both the heat transfer coefficient and bubble dynamics was utilized. To investigate the heat transfer coefficients in bubble and slurry bubble columns, with and without dense internals, the following section outlines the sequence of operation as well as the technical information for heat transfer studies and measurements.

B.1 Components of the heat transfer coefficient measurement technique

1. Heat transfer probe

The detailed structure of the heat transfer probe is outlined in Chapter 4. The sensitivity of the probe is 0.02s, thermal resistance of 0.003 ^{o}F ft^{2}-hr/BTU, and heat capacity values of 0.01 BTU ^{o}F/ft^{2}-hr of the micro-foil heat flux sensor No. 20453-1(G161) are as provided on the information sheet available from the manufacturer (RdF Corporation, 23 Elm Ave. Hudson, NH 03051 USA 800-445-8367, 603-882-5195 FAX 603-882-6925). The sensor is designed for heat flow levels up to 50 BTU/ft^{2}-sec., and operating temperature ranges from -300 ^{0}F to + 400 ^{0}F, with an accuracy of ± 3 %.

2. Thermocouple probe

The thermocouple probe contains a set of three T-type thermocouples purchased from Omega Engineering Inc. each of whose specifications are (TMTSS-125U-12). Each thermocouple is a subminiature transition joint probe (type T, 0.125" O.D. stainless steel sheath, 12" length, ungrounded junction), with the work temperature of up to 500 ^{o}F.

3. Amplifier

Since the signal of the heat flux sensor is in the range of microvolts amplication of the measured signals was done by using an amplifier JH4300-AC obtained from JH

Technology, Inc.. The guaranteed operating temperature of the amplifier was in the range -10 ~ +60 ^{o}C, and the temperature stability of ~ ± (0.02 % span +1.3 microvolts) per ^{o}C, or better. The data acquisition period is suggested to be no longer than 60 minutes due to the effect of the operating temperature on the amplifier.

4. DC power supply

The DC power supply used in the experiments is a HY 5003 model manufactured by RSR Electronics, Inc.. The regulated output voltage is 0-50V, and the regulated output current is 0-3A. The voltage indication accuracy is ±1% +2 digits, and the current indication accuracy is ±2%+2 digits.

5. Data acquisition instruments

The data acquisition instruments were produced by National Instruments Corporation, including a SCXI-1000 chassis block, SCXI-1102 module kit, SCXI-1303 terminal block, SCXI-1349 with a 2m cable, and NI PCI-6281 multifunction I/O board. All the components were assembled and connected after the purchase, and the data acquisition program was also developed on LabVIEW launch pad and implemented using LabVIEW software.

B.2 Operating and DAQ procedures of heat transfer probe technique

During the experiments using the heat transfer probe technique, the following procedures were followed:

- Mount the heat transfer probe and thermocouple probe to the ports of the slurry bubble column at the desired axial location and the radial positions.
- Tighten the fittings to prevent the liquid leaks through the connection points.

- Properly connect the power input lines of the heater in the heat transfer probe to the DC power supply.
- Connect the thermocouple wires (blue-Pos. (+), red-Neg.(-)) of the microfilm sensor to one of the channels numbered from 0 to 7 in the SCXI-1303 terminal block.
- Connect the heat flux sensor wires (white-Pos.(+), red-Neg.(-)) to the input of the amplifier, and then connect the output of the amplifier to one of the channels numbered from 8 to 32 in the SCXI-1303 terminal block.
- Connect the thermocouple wires of the thermocouple probe to one of the channels numbered from 0 to 7 in the SCXI-1303 terminal block.
- Load the required amount of liquid and solid into the slurry bubble column.
- Operate the slurry bubble column at the designed condition for about 20 minutes, and then switch on the power of the chassis (SCXI-1000) and start the temperature measurement program on the PC.
- When the system reaches steady state, collect the temperature data several (3-5) times to obtain the average the temperature difference between the probe surface and the bulk.
- Switch on the DC power supply of the heater and the power of the amplifier, and then start the heat flux measurement program on the PC.
- After 20-30 minutes, when the signal of heat flux becomes stable, collect both the heat flux data and temperature data simultaneously using the heat flux measurement program. At this point the measurement is complete

- Once the data acquisition is completed, each of the files can be opened and viewed in Ms Excel or MATLAB.

APPENDIX C

ADDITIONAL RESULTS OF THE BUBBLE DYNAMICS IN BUBBLE AND SLURRY BUBBLE COLUMNS

Scope

Bubble dynamics in bubble and slurry bubble columns was assessed in Section 3 in columns with dense internals and without internals. The aim of this section is to provide additional bubble dynamics data and contact time data for the proposed mechanistic model.

C.1 Bubble Passage Frequency and Specific interfacial area

The observed effects of size and configuration of internals on the bubble passage frequency and specific interfacial area are consistent with those of local gas holdup at the same gas velocity as discussed under Section 3. Higher bubble passage frequency is obtained when internals are used. The half-inch internals provide consistently highest bubble passage frequency at all radial locations regardless of the area used for calculating the gas velocity.

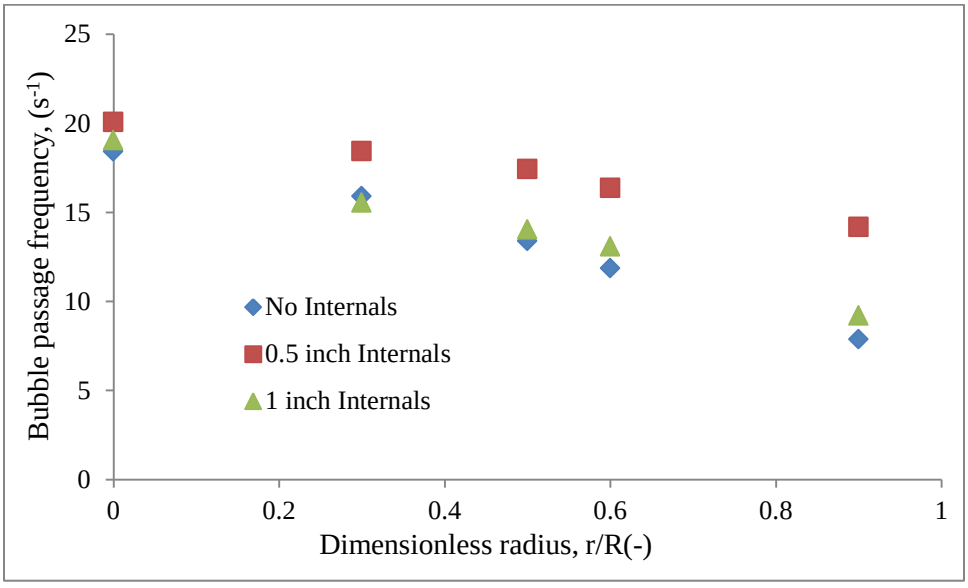

(a)

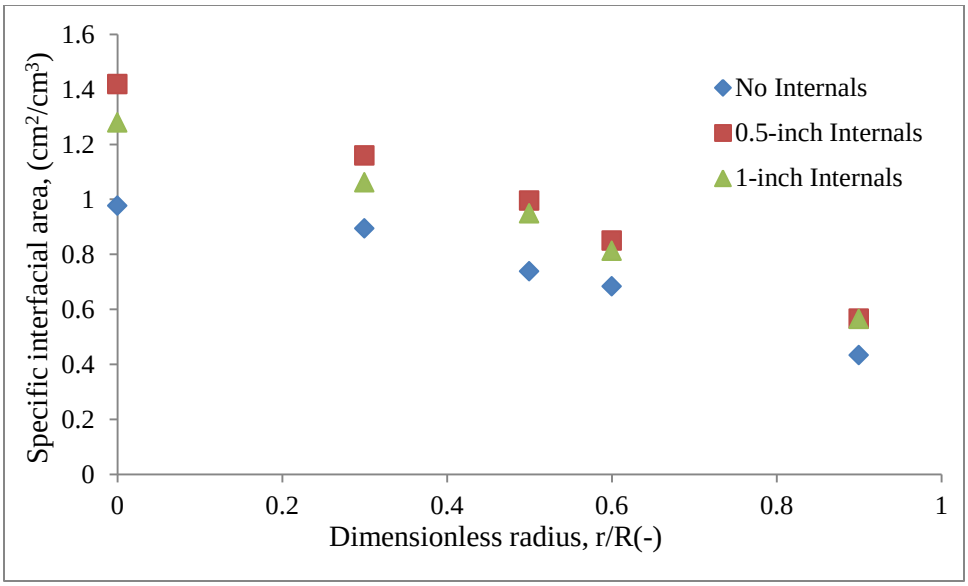

(b)

Figure C.1. Effect of size of internals on radial profiles of (a) Bubble passage frequency (b) Specific interfacial area at U_g = 3 cm/s

C.2. Impact of Internals on the contact time in bubble and slurry bubble columns

The impact of internals on the contact time predicted by the model, (Equation 5.21) vs the superficial gas velocity for 6-inch column at r/R = 0.0 is shown in Figure C.2. with superficial gas velocity based on both the total CSA and free CSA of the column. A significant difference is noticed on the effect of internals at lower gas velocity which becomes less with increasing gas velocity. This is consistent with the bubble dynamics that were discussed in Section 3 of this dissertation. It was pointed out that the effect of internals was significant at lower superficial gas velocity (based on free CSA or total CSA) on both the bubble passage frequency and local gas holdup and negligible at higher gas velocity.

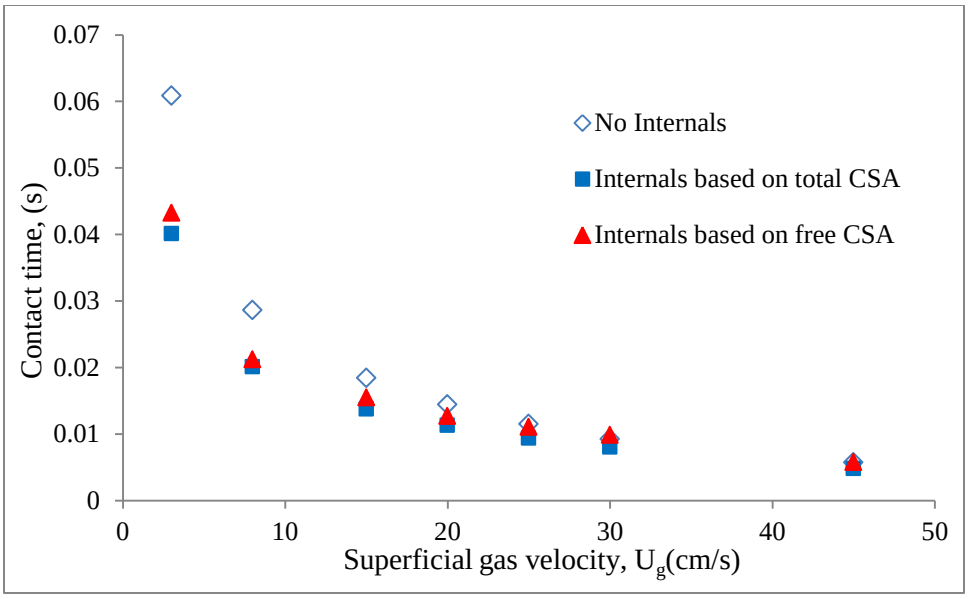

Figure C.2. Effect of internals on the predicted contact time in 6-inch column at r/R(-) = 0.0

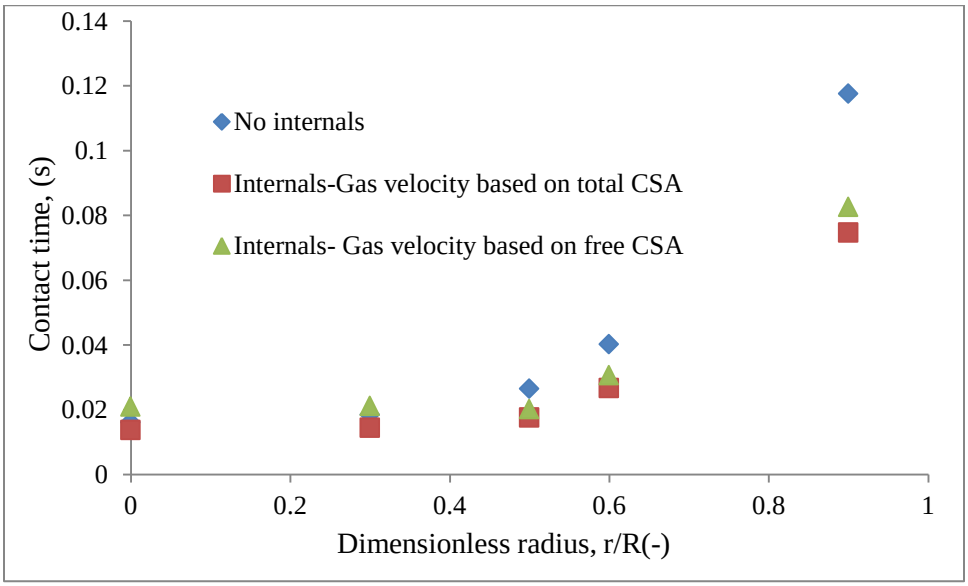

Figure C.3. Effect of internals on radial profiles of predicted contact time at gas velocity, 8 cm/s

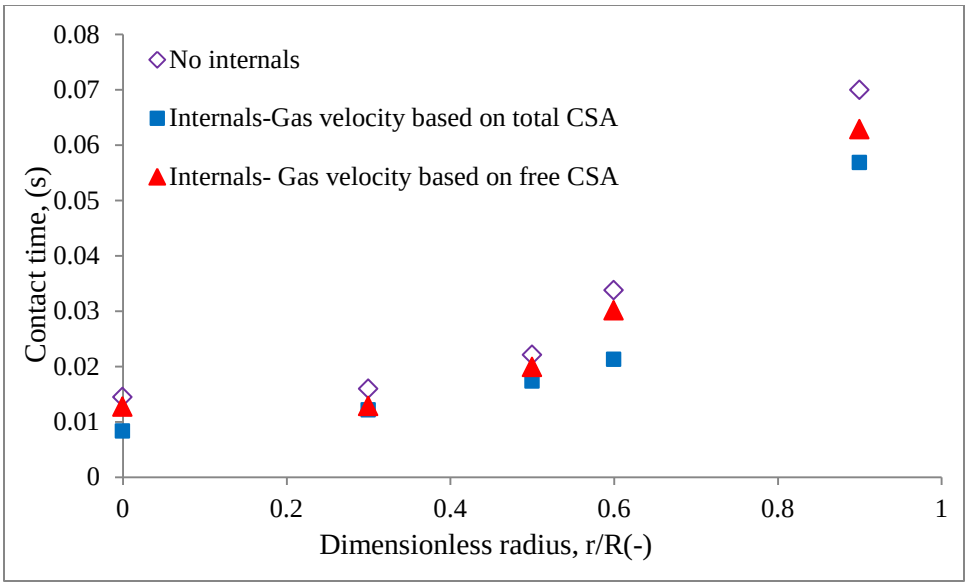

Figure C.4 Effect of internals on radial profiles of predicted contact time at gas velocity, 20 cm/s

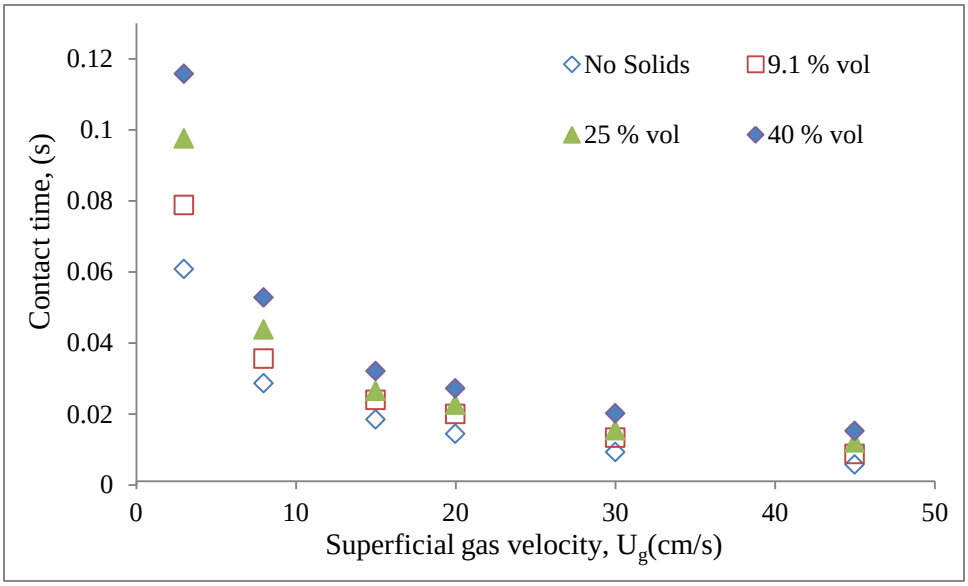

Figure C.5. Effect of solids volume fraction on the contact time at r/R = 0.0 in 6 Inch bubble column

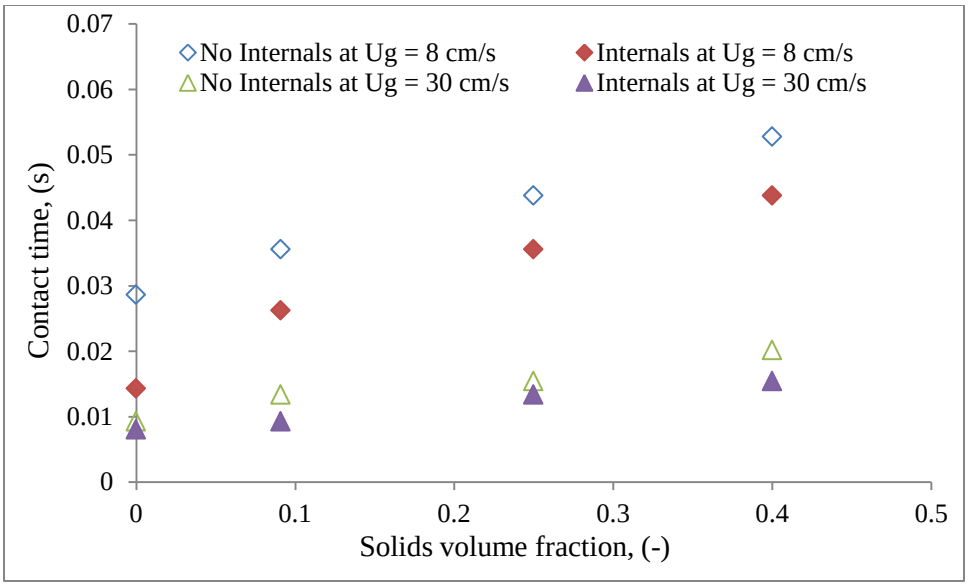

Figure C.6. Combined effect of internals and solids volume fraction on contact time in 6-inch bubble column at r/R (-) = 0.0

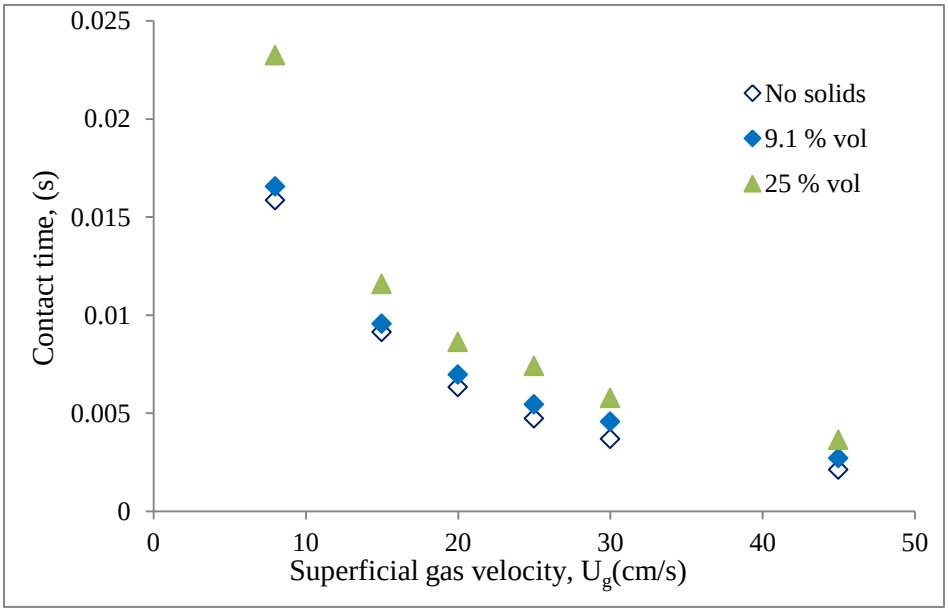

Figure C.7. Impact of solids volume fraction on contact time in 18-inch column at r/R(-) = 0.0

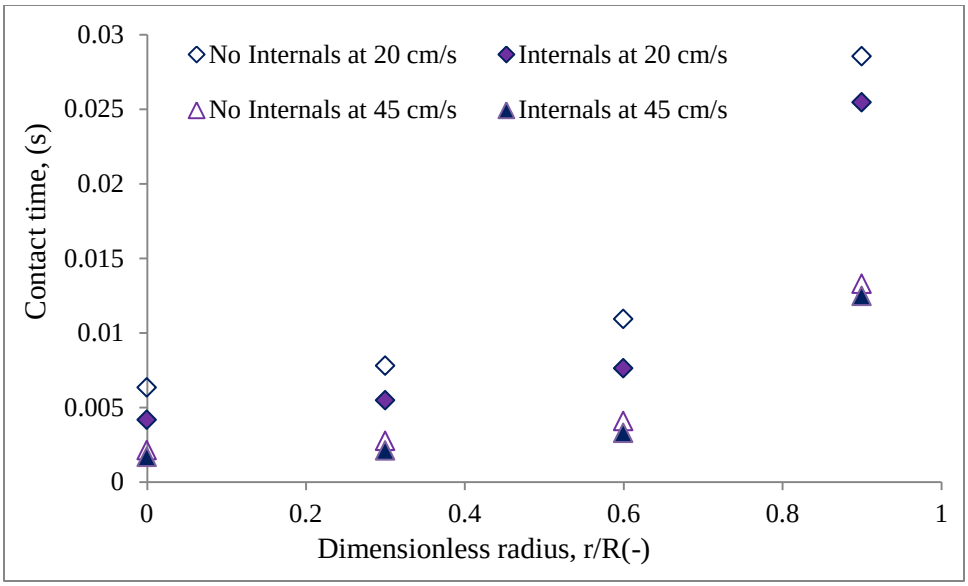

Figure C.8. Effect of internals on radial profiles of the estimated contact time in 18-inch column

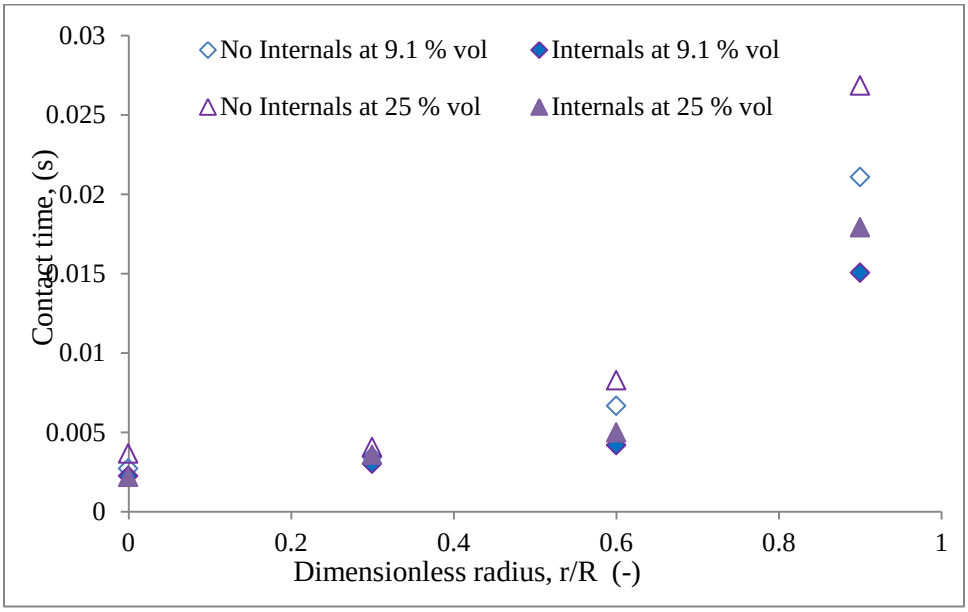

Figure C.9. Combined effect of internals and solids volume fraction on the radial profiles of the contact time in 18-inch column at Ug = 45 cm/s based on free CSA

APPENDIX D

DEVELOPMENT OF EMPIRICAL CORRELATIONS

D.1. Empirical Correlation for Heat Transfer Prediction in Slurry Bubble Columns

Based on the generated database from the experimental measurements using the heat transfer probe, (part of the combined measurements technique) a power law correlation has therefore been developed. The power law correlation was selected based on the least square regression method, with the final form as follows,

$$h_c = 3.413 \times 10^{-5} {U_g}^{-0.52} \rho_{sl} {C_p}_{sl} {D_c}^{0.14} \left[\left(\frac{D_c U_g \rho_{sl}}{\mu_{sl}} \right) \left(\frac{{U_g}^2}{D_c g} \right) \left(\frac{C_{p,sl} \mu_{sl}}{K_{sl}} \right)^{2.54} \right]^{0.254} \qquad (D.1)$$

Table D.1. Parameters collected in the database

Parameters	Range
Column diameter	0.1397 -0.4445 m
Superficial gas velocity	0.03 - 0.45 m/s
Density of liquid-solid suspension	998-134 kg/m^3
Viscosity of liquid-solid suspension	0.0005-0.0587 Pa.S
Heat capacity of liquid-solid suspension	2224-4183 J/kg.K
Thermal conductivity of liquid-solid suspension	0.6-0.634 w/(m.K)
Internals (% CSA)	0.0 % CSA, 25 % CSA

Figure D.1 shows a parity plot of the predicted heat transfer coefficient vs the experimental (measured) heat transfer coefficient. The Absolute Average Relative Error (AARE) was found to be 6 %, which implies a close match between the predictions and measurements. Where the AARE was defined as follows;

$$AARE = \frac{1}{N}\sum_{i=1}^{N}\left|\frac{h_{c,predicted} - h_{c,experimental}}{h_{c,experimental}}\right| \qquad (D.2)$$

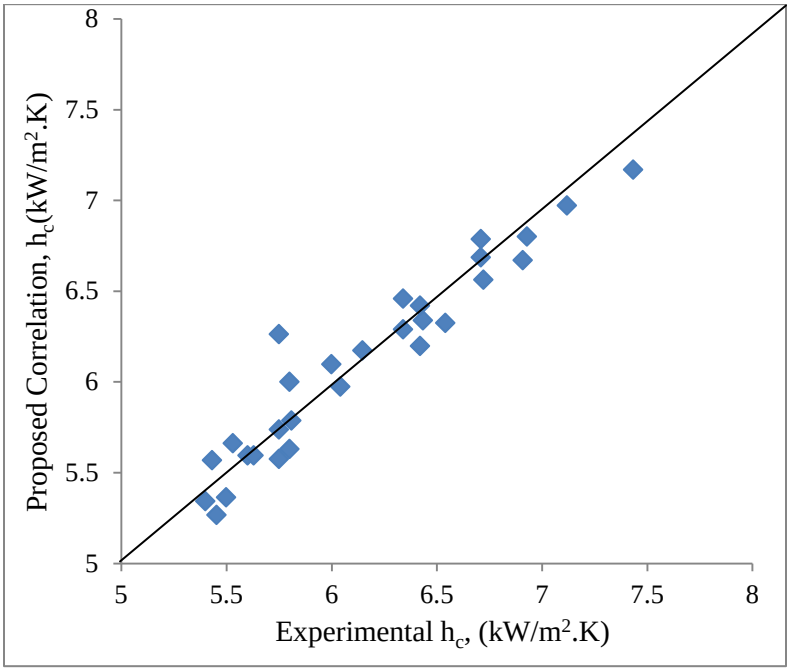

Figure D.1. A parity plot of the proposed correlation vs experimental heat transfer coefficient

D.2 Empirical Correlation for Contact Time needed in the Mechanistic Equation of Heat Transfer

According to the mechanistic model for the contact time estimation proposed in Section 5, the contact time is a function of both local gas holdup and bubble passage frequency. The local gas holdup can be estimated from the empirical correlations or the artificial neural network correlations available in the literature, (Degaleesan, 1998, Shaikh 2007). However the bubble passage frequency cannot easily be obtained due to lack of correlations. Thus, attempt has been made to see if the contact time, t_c can be

represented by an empirical correlation with parameters that can easily be obtained such as local gas holdup. Based on the data obtained from the combined measurements technique, the measured local bubble properties have been used to propose the following straight forward equation for predicting the contact time between fluid elements and the thin film at any local point in the column.

$$t_c = 0.0007\varepsilon_g(r)^{-2.184} \qquad (D.3)$$

Where, $\varepsilon_g(r)$ is the local gas holdup. Assessment of the performance of the proposed contact time correlation, (Equation D.3) relative to that of the mechanistic contact time model is done by using a parity plot. Figure D.2 shows the parity plot of the predicted contact time using the mechanistic model of the current work vs. proposed contact time based on data of the mechanistic model.

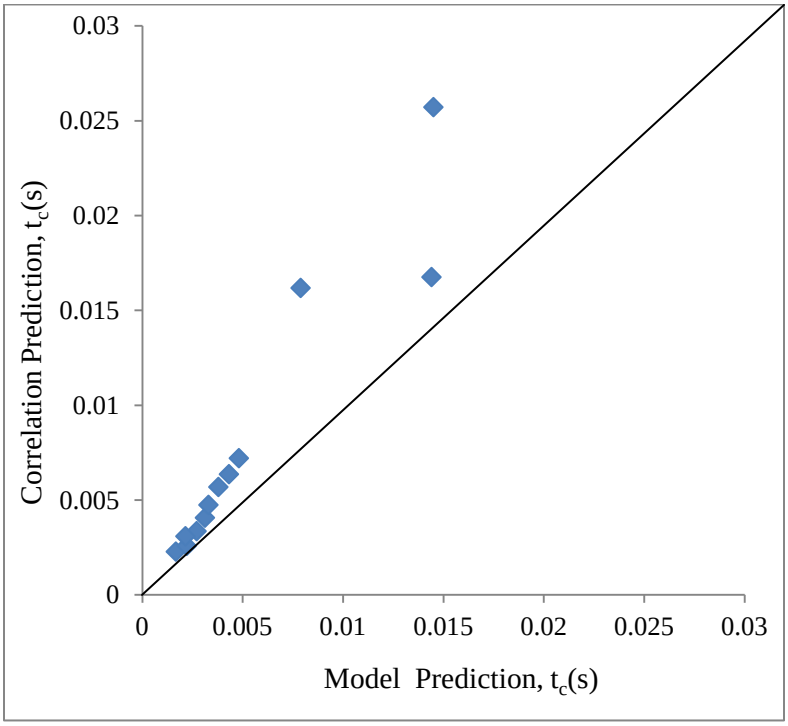

Figure D.2. A parity plot of the predicted contact time vs the mechanistic model

The Absolute Average Relative Error (AARE) was found to be 33 %. Where the AARE has been defined as;

$$AARE = \frac{1}{N}\sum_{i=1}^{N}\left|\frac{t_{c,predicted} - t_{c,model}}{t_{c,model}}\right| \qquad (D.4)$$

The resulting error is significant particularly at higher values of the contact times. It is obvious that correlating the contact time with local gas holdup alone is not adequate. Therefore, further evaluation of the relationship between the contact time and other key parameters that can describe the effects of bubbles properties such as passage frequency need to be examined. Accordingly, development of a modified correlation for the contact time is recommended.

BIBLIOGRAPHY

1. A. Mirzaei, M. Faizi and R. Habibpour, Applied Catalysis, 306, 98 (2006).

2. Abdulmohsin, R., and Al-Dahhan, M., 2012 Impact of internals on the heat transfer coefficient in a bubble column, Industrial & Engineering Chemistry Research. 51, 2874−2881

3. Akita, K. and Yoshida, F., 1974. Bubble size, interfacial area, and liquid-phase mass transfer coefficient in bubble columns. Ind. Eng. Chem. Process Des. Develop., 13(1), 84-91.

4. Al Mesfer K.M. "Effect of Dense Heat Exchanging Internals on the Hydrodynamics of Bubble Column Reactors using Non-invasive Measurement Techniques", Ph.D. Thesis, Missouri University of Science and Technology, Rolla, MO, 2013.

5. Anabtawi MZA, Abu-Eishah SI, Hilal N, Nabhan NBW. Hydrodynamic studies in both bi-dimensional and three-dimensional bubble columns with a single sparger. Chem Eng Process 2002; 1:1–6.

6. Azbel, D., 1981. Two-phase flows in chemical engineering. Cambridge University Press, Cambridge.

7. Baker, C.G.J., E.A. Armstrong and M.A. Bergougnou, Heat Transfer in Three Phase Fluidized Beds, Powder Technol. 21, 195-204 (1978).

8. Balamurugan, V. and Subbaro, D. bubble size and holdup in bubble columns with vibrating internals, AIChE Spring National Meeting (2006).

9. Barghi, S., Prakash, A., Margaritis, A. and Bergougnou, M.A., 2004. Flow regime identification in a slurry bubble column from gas holdup and pressure fluctuation analysis. The Canadian Journal of Chemical Engineering. 82, 865-870.

10. Bauer, M., and Eigenberger, G., Multiscale Modeling of Hydrodynamics, Mass Transfer and reaction in Bubble Column Reactors, Chemical Engineering Science, Vol. 56, (2001), pp. 1067-1074.

11. Behkish A, Men Z, Inga RJ, Morsi BI. Mass transfer characteristics in a large-scale slurry bubble column reactor with organic liquid mixtures. Chem Eng Sci 2002; 57:3307–24.

12. Behkish, A., Hydrodynamic and Mass Transfer Parameters in large-scale Slurry Bubble Column Reactors, Ph.D. Thesis, University of Pittsburgh, Pittsburg, PA, 2004.

13. Behkish, R. Lemoine, L. Sehabiague, R. Oukaci and B. I. Morsi, Chem. Eng. J., 128, 69, 2007.

14. Bernemann, K., 1989. On the hydrodynamics and mixing of the liquid phase in bubble columns with longitudinal tube bundles, Ph.D. Thesis, University of Dortmund, Germany.

15. Bhaga D., and Weber M. E., 1981. Bubbles in viscous liquids: shapes, wakes and velocities, J Fluid Mech, 105: 61-85.

16. Bouaifi M, Hebrard G, Bastoul D, Roustan M. A comparative study of gas holdup, bubble size, interfacial area and mass transfer coefficients in stirred gas–liquid reactors and bubble columns. Chem Eng Process 2001; 40:97–111.

17. Carleton, A. J.; Flain, R. J.; Rennie, J.; Valentin, H. H., Some properties of a packed bubble column, Chemical Engineering Science, 22, 1839-1845, 1967.

18. Carra, Sergio; Morbidelli, Massimo, 1987. Gas-liquid reactors. Chemical Industries (Dekker), 26 (Chem. React. React. Eng.), 545-666.

19. Chen, J., P., Gupta, S., Degaleesan, M. H., AI-Dahhan, M. P., Dudukovic and B. A., Toseland, 1998, Gas holdup distributions in large-diameter bubble columns measured by computed tomography', Flow Measurement and Instrumentation, 9(2), 91-101.

20. Chen, J.; Li, F.; Degaleesan, S.; Gupta, P.; Al-Dahhan, M. H.; Dudukovic, M. P.; Toseland, B. A. Fluid Dynamic Parameters in Bubble Columns with Internals. Chem. Eng. Sci. 1999, 54 (13-14), 2187–2197.

21. Chen, R.C., Reese, J., Fan, L.-S., 1994. Flow structure in a three-dimensional bubble column and three-phase fluidized bed. AIChE. Journal 40, 1093–1104.

22. Chiu, T.M. and E.N. Ziegler, "Heat Transfer in Three Phase Fluidized Beds", AlChE J. 29, 677-685, 1983.

23. Cho, Y. J.; Woo, K. J.; Kang, Y.; Kim, S. D. Dynamic characteristics of heat transfer coefficient in pressurized bubble columns, Chemical Engineering and Processing. 41 (2002) 699- 706.

24. Choi K.H. and Lee K.W. Behavior of Gas Bubbles in a Concentric Cylindrical Airlift Column, Korean J. of Chem. Eng., 1992 9(2), 66-73

25. Cooper, M. G. (1969). The microlayer and bubble growth in nucleate pool boiling, International Journal of Heat and Mass Transfer, 12, 915-933.

26. Crabtree, J.R., and Bridgewater, J.; Chem. Eng. Sci. 1971, 20 (839).

27. D.W. Holladay, C.W. Hancher, D.D. Chilcote, and C.D. Scott, Biodegradation of phenolic waste liquors in stirred-tank, columnar and fluidized-bed bioreactors, Proc. IChE Symp. Ser., 74, 241–252, 1978.

28. Danckwerts, P. V., 1951. Significance of liquid-film coefficients in gas absorption. Journal of Industrial and Engineering Chemistry (Washington, D. C.), 43 1460-1467.

29. Deckwer, W. D.; Louisi, Y.; Zaldi, A.; Ralek, M. Hydrodynamic properties of the Fischer_Tropsch slurry process. Ind. Eng. Chem. Process Des. Dev. 1980b, 19, 699–708.

30. Deckwer, W.-D. and Schumpe, A., 1993. Improved tools for bubble column reactor design and scale-up. Chemical Engineering Science 48, 889–911.

31. Deckwer, W.D., On the Mechanism of Heat Transfer in Bubble Column Reactor, Chem. Eng. Sci. 35, 1341-1 346 (1980a).

32. Deckwer, W.-D., 1992. Bubble column reactors, Chichester.

33. Deckwer, W.-D.; Alper, E. Katalytische suspensions reacktoren. Chem. Eng. Technol. 1980, 52, 219–228.

34. Degaleesan S, Dudukovic M, Pan Y. Experimental study of gas induced liquid-flow structures in bubble columns. AIChE J 2001;47: 1913–31.

35. Degaleesan, S., "Fluid Dynamic Measurements and Modeling of Liquid Mixing in Bubble Columns," D.Sc. Thesis, Washington University, St. Louis, MO (1997).

36. Diesterwerg, G., Fuhr, H., and Reher, P., (1978), Die Bayer-Turmbiologie, Industrieabwasser, 7.

37. Drew, D. A., 1983, Mathematical Modeling of two-phase flows, Ann. Rev. Fluid Mech., 15,261-291.

38. Dudukovic, M. P.; Larachi, F.; Mills, P. L. Multiphase reactors revised. Chem. Eng. Sci. 1999, 54, 1975–1995.

39. Dudukovic, M.P., Opaque multiphase flows: experiments and modeling. Expt. Ther. Flu. Sci., 26 (6-7), 747-761, 2002.

40. Ellenberger, J. and Krishna, R., A unified approach to the scale-up of gas-solid fluidized bed and gas-liquid bubble column reactors. Chem. Eng. Sci., 49 (24B), 5391 5411, 1994.

41. F. Fischer, H. Tropsch, Brennstoff-Chem. 4 (1923) 276.

42. Fan L. S, Matsuura A, Chern SS. Hydrodynamic characteristics of a gas–liquid–solid fluidized bed containing a binary mixture of particles. AIChE J 1985; 31:1801–10.

43. Fan, L.-S. Gas-liquid-solid fluidization engineering; Butterworths Series in Chemical Engineering: Boston, MA, 1989.

44. Fan, L.-S., G. Q. Yang, D. J. Lee, K. Tsuchiya and X. Luo, Some Aspects of High-Pressure Phenomena of Bubbles in Liquids and Liquid-Solid Suspensions, Chem. Eng. Sci. 54, 4681, 1999.

45. Forret A, Schweitzer J-M., Gauthier T, Krishna R, Scweich D. Influence of scale on the hydrodynamics of bubble column reactors: an experimental study in columns of 0.1, 0.4 and 1 m diameters. Chem Eng Sci 2003; 58:719–24.

46. Forret, A., Schweitzer, J. M., Gauthier, T., Krishna, R., and Schweich, D., 2006. Scale up of slurry bubble reactors, Oil & Gas Science and Technology, 61(3), 443-458.

47. Forret, A.; Schweitzer, J. M.; Gauthier, T.; Krishna, R.; Schweich, D. Liquid dispersion in large diameter bubble columns, with and without internals. Can. J. Chem. Eng. 2003, 81, 360–366.

48. Fox, J. M., Fischer-Tropsch Reactor Selection, Catal. Lett., 7, 281, 1990.

49. Franz, K., Borner, T., Kantorek, H.J., & Buchholz, R. (1984). Flow structures in bubble columns. German Chemical Engineering, 7, 365}374.

50. Frijlink, J.J., 1987. Physical aspects of gassed suspension reactors. Ph. D. Thesis, Delft University of Technology, Delft, The Netherlands

51. Gandhi, A. Prakash and M. A. Bergougnou, Powder Technol., 80 (1999).

52. Gandhi, B., A. Prakash and M.A. Bergougnou, Effects of Sparger Height and Orifice Orientation on Solids Dispersion in a Slurry Bubble Column, Can. J. of Chem. Eng. 77, 383-391 (1999).

53. Geary, N.W. and Rice, R.G., Circulation and Scale-up in bubble columns. AIChE J., 38 (1), 76-82, 1992.

54. Geerlings, J.J.C., Wilson, J.H., Kramer, G.J., Kuipers, H.P.C.E., Hoek, A., Huisman, H.M., Fischer-Tropsch Technology – From Active Site to Commercial Process," Applied Catalysis A: General, Vol. 186, (1999), pp. 27-40.

55. Groen, J.S., Oldeman, R.G.C., Mudde, R.F., & Van Den Akker, H.E.A. (1996). Coherent structure and axial dispersion in bubble column reactors. Chemical Engineering Science, 51(10), 2511}2520.

56. Gupta, P., 2002. Churn-turbulent bubble columns - experiments and modeling. D.Sc. Thesis, Washington University in St. Louis, Saint Louis, MO, USA.

57. Gupta, P., Ong, B. C., Al-Dahhan, M. H., Dudukovic, M. P., and Toseland, B. A., 2001. Hydrodynamics of churn turbulent bubble columns: gas-liquid recirculation and mechanistic modeling, Catalysis today, 64, 253-269.

58. Hanning Li. Heat Transfer and Hydrodynamics in a Three-Phase Slurry Bubble Column. Ph.D. Thesis, The University of Western Ontario London, Ontario Canada, 1998.

59. Hebrard, G., Bastoul, D., & Roustan, M. (1996). Influence of the gas sparger on the hydrodynamic behaviour of bubble columns. Transactions of the Institution of Chemical Engineers, 74 (Part A), 406}414.

60. Highbie, R., Trans. AIChE, 31, 365 (1935)

61. Hills, J.H., Radial Non-Uniformity of Velocity and Voidage in a Bubble Column", Trans. Instn. Chem. Engrs. 52, 1-9 (1974).

62. Hulet, C., Clement, P., Tochon, P., Schweich, D., Dromard, N., and Anfray, J., 2009. Literature Review on Heat Transfer in Two and Three-Phase Bubble Columns, Int. J. Chem. Reactor Eng., 7.

63. IEO, 2007. International Energy Outlook, Department of Energy. Washington, DC, USA.

64. IEO, 2012. International Energy Outlook, Department of Energy. Washington, DC, USA.

65. Inga, J. R. and B. I. Morsi, Effect of Catalyst Loading on Gas/Liquid Mass Transfer in a Slurry Reactor: A Statistical Experimental Approach, Can. J. Chem. Eng. 75(5), 872–881 (1997).

66. J. Chen, P. Gupta, S. Degaleesan, M.H. Al-Dahhan, M.P. Dudukovic, B.A. Toseland, Flow Meas. Instr. 9 (1998) 91.

67. J. Duvenhage and T. Shingles, Catalysis Today, 71, 301 (2002).

68. Jhawar, A.K, Effects of Internals Configurations on Heat Transfer and Hydrodynamics in Bubble Columns – With and Without Solid Particles. Ph.D. Thesis, The University of Western Ontario London, Ontario, Canada, 2011.

69. Jhawar, A.K., Prakash, A., 2007. Analysis of local heat transfer coefficient in bubble column using fast response probes. Chemical Engineering Science. 62, 7274-7281.

70. Jhawar, A.K., Prakash, A., 2012. Heat Transfer in a Slurry Bubble Column Reactor: A Critical Overview. Ind. Eng. Chem. Res. 51, 1464-1473.

71. Joshi, J.B., Computational flow modelling and design of bubble column reactors. Chem. Eng. Sci., 56, 5893-5933, 2001.

72. Joshi, J.B.; Veera U P.; Prasad, V. C.; Phanikumar, D.V.; Deshphande, N. S.; Thakre, S.S. and Thorat, B.N. Gas Hold-up structure in bubble column reactors. PINSA 64, A, No.4, July,1998, 441-567

73. K. Zhang and Y. Zhao, Chem. Eng. Sci., 61, 1459 (2006).

74. Kafarov, V.V., Kruglik, A.E., and Trofimov, V.I., 1975. Comparative evaluation of the effect of installation of some standard heat exchangers in bubble-type columns on the average gas content and structure of liquid-phase streams.

75. Kang, Y., I.S. Suh and S.D. Kim, Heat Transfer Characteristics of Three Phase Fluidized Beds, Chem. Eng. Comm. 34, 1-13 (1985).

76. Kantarci, N., Borak, F., and Ulgen, K.O. Bubble column reactors. Process Biochemistry 40 (2005a): 2263 - 2283.

77. Kantarci, N., Ulgen, K.O., and Borak, F. "A study on hydrodynamics and heat transfer in a bubble column with yeast and bacterial cell suspensions." The Canadian Journal of Chemical Engineering 83.August (2005b): 764 - 773.

78. Karamanev, D., Nagamune, T., and Endo, I., Hydrodynamic and mass transfer study of a gas-liquid-solid draft tube spouted bed bioreactor. Chem. Eng. Sci., 47 (13-14), 3581-3588, 1992.

79. Kato, Y., K. Uchida, T. Kago and S. Morooka, "Liquid Holdup and Heat Transfer Coefficient between Bed and Wall in Liquid-Solid and Gas-Liquid-Solid Fluidized Beds", Powder Technol. 28, 173-1 79 (1981).

80. Kemoum, A., Rados, N., Al-Dahhan, M., Dudukovic, M., Mills, P., Leib, T., and Lerou, J., “Gas Holdup in a Trayed Cold-Flow Bubble Column”, Chem. Eng. Sci, 56, 1197-1205 (2001).

81. Kim, S. D.; Kang, Y.; Kwon, H. K. Heat transfer characteristics in two- and three phase slurry-fluidized beds. AIChE J. 1986, 32, 1397–1400.

82. Kim, S. D.; Laurent, A. The State of Knowledge on Heat Transfer in Three-Phase Fluidized Beds. Int. Chem. Eng. 1991, 31, 284.

83. Kim, S.D., Kang, Y., 1997. Heat and mass transfer in three-phase fluidized-bed reactors – an overview. Chemical Engineering Science. 52, 3639-3660.

84. Kluytmans, J.H.J., van Wachem, B.G.M., Kuster, B.F.M., Schouten, J.C., 2001. Gas holdup in a slurry bubble column: influence of electrolyte and carbon particles. Industrial Engineering Chemical Research 40, 5326–5333.

85. Kölbel, H., Borchers, E., and Martins, J. "Wärmeübergang in blasensäulen. III. Messungen an gasdurchströmten suspensionen." Chemie Ingenieur Technik 32.2 (1960): 84 - 88.

86. Kolbel, H.; Ralek, M. Catal. Rev. Eng. Sci. 1980, 21, 225.

87. Korte, H., 1987. Heat transfer in bubble columns with and without internals, Ph.D. Thesis, University of Dortmund, Germany.

88. Krishna R, Van Baten J. M. “Mass transfer in bubble columns.” Catal Today 2003; 79–80:67–75.

89. Krishna R., (2000), “A Scale-up Strategy for a Commercial Scale Bubble Column Slurry Reactor for Fischer-Tropsch Synthesis.” Oil and Gas Science and Tech. 55 (4) 359-393.

90. Krishna, R. and Sie, S.T., Design and Scale-Up of the Fischer-Tropsch Bubble Column Slurry Reactor. Fuel Process Technol., 64 (1-3), 73-105, 2000.

91. Krishna, R. and van Baten J.M., “A strategy for scaling up the Fischer–Tropsch bubble column slurry reactor,” Topics in Catalysis Vol. 26, Nos. 1–4, December 2003.

92. Krishna, R., Deswart, J.W.A., Ellenberger, J., Martina, G.B., and Maretto, C., Gas Holdup in Slurry Bubble-Columns - Effect of Column Diameter and Slurry Concentrations. AIChE J., Vol 43 (Iss 2), 311-316, 1997.

93. Krishna, R., J. M. van Baten, M. I. Urseanu and J. Ellenberger, “Design and Scale-Up of the Bubble Column Slurry Reactor for Fischer-Tropsch Synthesis,” Chem. Eng. Sci. 56, 537–545 (2001).

94. Krishna, R., Van Baten, J.M., and Urseanu, M.I., Scale effects on the hydrodynamics of bubble columns operating in the homogeneous flow regime. Chem. Eng. Tech., 24 (5), 451-458, 2001.

95. Kumar S., Kusakabe K., Raghunathan., K, Fan, L.S. Mechanism of Heat Transfer in Bubbly Liquid and Liquid-Solid Systems: Single Bubble Injection. AIChE J., 1992, 38(5), 733-741.

96. Kumar, B.S., Moslemian, D., & DudukovicH, M.P. (1995). A gamma ray tomographic scanner for imaging void fraction distribution in bubble columns. Flow Measurement and Instrument, 6(1), 61}73.

97. Kumar, R., and N. R. Kuloor, "The formation of bubbles and drops," Advances in Chemical Engineering, 8, 255 (1970).

98. Kumar, S. B., 1994, Computed tomographic measurements of void fraction and modeling of the flow in bubble columns, Ph.D. Thesis, Florida Atlantic University.

99. Kumar, S., Fan, L. S., 1994., "Heat Transfer Characteristics in Viscous Gas-Liquid and Gas-Liquid-Solid System," AICHE J., 40, 745-755

100. Kumar, S.B., Moslemian, D., & DudukovicH, M.P. (1997). Gas holdup measurements in bubble columns using computed tomography. The American Institute of Chemical Engineers Journal, 43(6), 1414}1425.

101. Larachi, F.; Desvigne, D.; Donnat, L.; Schweich, D. Simulating the effects of liquid circulation in bubble columns with internals. Chem. Eng. Sci. 2006, 61 (13), 4195–4206.

102. Lehman, J. and Hammer, J., (1978), Continuous fermentation in tower fermentor, I European congress on biotechnology, Interlaken, Part 1, 1.

103. Li H., Prakash, A., Margaritis, A., and Bergougnou, M.A., 2003. Effects of micron-size particles on hydrodyanamics and local heat transfer in a slurry bubble column. Powder Technonlgy, 133, 171-184.

104. Li, H., and Prakash, A. "Heat transfer and hydrodynamics in a three-phase slurry bubble column." Industrial Engineering Chemistry and Research 36 (1997): 4688-4694.

105. Li, H., and Prakash, A., 2001. Survey of heat transfer mechanisms in a slurry bubble column. The Canadian Journal of Chemical Engineering, 79, 717-725.

106. Lin, T.J., and Fan, L.S. "Heat transfer and bubble characteristics from a nozzle in high-pressure bubble columns." Chemical Engineering Science 54 (1999): 4853 - 4859.

107. Luewisutthchat, W.; Tsutsumi, A.; Yoshida, K. Bubble characteristics in multiphase flow systems: bubble sizes and size distributions. J. Chem. Eng. Jpn. 1997, 30 (3), 461 466.

108. Luo X, Lee DJ, Lau R, Yang G, Fan L. Maximum stable bubble size and gas holdup in high-pressure slurry bubble columns. AIChE J 1999; 45:665–680.

109. Luo, Hean; Svendsen, Hallvard F., (1991). Turbulent circulation in bubble columns from eddy viscosity distributions of single-phase pipe flow, Can. J. of Chem.

110. Macchi, A., H. Bi, J. R. Grace, C. A. McKnight and L. Hackman, "Dimensional Hydrodynamic Similitude in Three-Phase Fluidized Beds," Chem. Eng. Sci. 56, 6039–6045 (2001).

111. Magiliotou, M., Y. Chen and L.S. Fan, "Bed-Immersed Object Heat Transfer in a Three Phase Fluidized Bed", AlChE J. 34, 1043-1 047 (1988).

112. Maretto, C., and Krishna, R. "Modelling of a bubble column slurry reactor for Fischer-Tropsch synthesis." Catalysis Today 52 (1999): 279 - 289.

113. Menzel, T., in der Weide, T., Staudacher, O., Wein, O., & Onken, U. (1990). Reynolds shear stress for modeling of bubble column reactors. Industrial & Engineering Chemistry Research, 29(6), 988}994.

114. Michael, R., and Reichert, K.H. "Heat transfer of polyethylene-hydrocarbon dispersions in bubble column reactors." The Canadian Journal of Chemical Engineering 59.October (1981): 602 - 605.

115. Mohamed Hamed "Hydrodynmaics, Mixing, and Mass Transfer in Bubble Columns with internals" Ph.D. Thesis, Washington University: Saint Louis, Missouri, 2012.

116. Moriyama, K. & Inoue, A. (1996). Thickness of the liquid film formed by a growing bubble in a narrow gap between two horizontal plates, Transactions of the ASME, 118, 132-139.

117. Nernst, W.Z. Phys.Chem., 47, 52 (1904)

118. Nigam, K.D.P.; Schumpe, A. Three-Phase Sparged Reactors; Overseas Publishers Association B.V.: Amsterdam, 1996.

119. Nottenkamper, R., A. Steiff and P.M. Weinpach, "Experimental Investigation of Hydrodynamics of Bubble Columns", Ger. Chem. Eng. 6, 147-155 (1983).

120. Ong, B. C., Gupta, P., Youssef, A., Al-Dahhan, M. and Dudukovic, M. P., 2009. Computed Tomographic Investigation of the Influence of Gas Sparger Design on Gas Holdup Distribution in a Bubble Column, Ind. Eng. Chem. Res., 48, 58–68.

121. P.J. van Berge, R.C. Everson, Stud. Surf. Sci. Catal. 107 (1997) 207.

122. Pohorecki, R.; Moniuk, W.; Zdrojkowski, A.; Bielski, P. Hydrodynamics of a pilot plant column under elevated temperature and pressure. Chem. Eng. Sci. 2001, 56, 1167–1174.

123. Pradhan, A. K.; Parichia, R.; K.; De, P. Gas hold-up in non Newtonian solutions in a bubble column with internals. Can. J. Chem. Eng. 1993, 71, 468–471.

124. Prakash A, Margaritis A, Li H. Hydrodynamics and local heat transfer measurements in a bubble column with suspension of yeast. Biochem Eng J 2001;9:155 63.

125. Raje, A., Inga, J.R., Davis, B., "Fischer-Tropsch Synthesis: Process Considerations Based on Performance of Iron-based Catalysts," Fuel, Vol. 76, (1997), pp. 273-280.

126. Riquarts, H. P. (1981). A physical model for axial mixing of the liquid phase for heterogeneous flow regime in bubble columns. German Chemical Engineering, 4, 18}23.

127. S. Barghi, A. Prakash, A. Margaritis, M. A. Mergougnou, Can. J. Chem. Eng. 2004, 82, 865.

128. S.B. Kumar, N. Devanathan, D. Moslemian, M.P. Dudukovic, Chem. Eng. Sci. 49 (1994) 5637.

129. Safoniuk, M., J. R. Grace, L. Hackman and C. A. McKnight, "Use of Dimensional Similitude for Scale-Up of Hydrodynamics in Three-Phase Fluidized Bed," Chem. Eng. Sci. 54, 4961–4966 (1999).

130. Saxena SC, Rao NS, Saxena AC. "Heat Transfer and Gas Holdup Studies in a Bubble Column: Air-Water-Glass Bead System", Chem. Eng. Commun. 96, 31-55 (1990a).

131. Saxena SC, Rao NS, Saxena AC. "Heat Transfer and Gas Holdup Studies in a Bubble Column: Air-Water-Sand System", Can. J. Chem. Eng. 70, 33-41 (1992).

132. Saxena SC, Rao NS, Saxena AC. "Heat Transfer from a Cylindrical Probe Immersed in a Three Phase Slurry Bubble Column", Chem. Eng. J. 44, 141-156 (1990b).

133. Saxena, S.C., and Chen, Z.D. "Hydrodynamics and heat transfer of baffled and unbaffled slurry bubble columns." Reviews in Chemical Engineering 10.3,4 (1994): 195 - 400.

134. Saxena, S.C., Verma, A.K., Vadivel, R., and Saxena, A.C. "Heat transfer from a cylindrical probe in a slurry bubble column." International Communications in Heat and Mass Transfer 16.2 (1989c): 267 - 281.

135. Schlichting, H., "Boundary Layer Theory", McCraw-Hill, New York, NY (1968).

136. Schlüter, S., Steiff, A., Weinspach, P.-M., 1995. Heat transfer in two- and three-phase bubble column reactors with internals. Chemical Engineering and Processing, 34, 157-72.

137. Schweitzer J.M., Bayle, J., Gauthier, T (2001) " Local gas hold-up measurements in fluidized bed and slurry bubble column", Chemical Engineering Science 56, 1103-1110.

138. Sehabiague L., Modeling, Scaleup and Optimization of Slurry Bubble Column Reactors for Fischer-Tropsch Synthesis, Ph.D. Thesis, University of Pittsburgh, Pittsburg, PA, 2012.

139. Shah, Y. T., Ratway, C. A., and Mcilvried, H. G., 1978. Back-mixing characteristics of a bubble column with vertically suspended tubes, Transactions of the Institution of Chemical Engineers, 56(2), 107-112.

140. Shah, Y.T., Kelkar, B.G., Godbole, S.P., Deckwer, W.D. "Design Parameters Estimations for Bubble Column Reactors," AIChE, Journal, Vol. 28, (1982), pp. 353-379.

141. Shaikh, A., 2007. Bubble and slurry bubble column reactors for syngas to liquid fuel conversion: mixing, flow regime transition, and scale-up, D.Sc. Thesis, Washington University in St. Louis, Saint Louis, MO, USA.

142. Shedd, T. A. & Newell, T. A. (2004). Characteristics of the liquid film and pressure drop in horizontal, annular, two-phase flow through round, square and triangular tubes, Journal of Fluid Engineering, 126, 807-817.

143. Shimizu K, Takada S, Minekawa K, Kawase Y. Phenomenological model for bubble columnreactors: prediction of gas holdups and volumetric mass transfer coefficients. Chem Eng J 2000; 78:21–8.

144. Shin I. S., Son S.M., Kim U. Y., Kang Y., Kim S. D., and Jung H. 2009., "Multiple effects of operating variables on the bubble properties in three-phase slurry bubble columns." Korean J. Chem. Eng., 26(2), 587-591.

145. Suh, I.S. and W.D. Deckwer, "Unified Correlation of Heat Transfer Coefficient in Three-Phase Fluidized Beds", Chem. Eng. Sci. 44, 1455-1 458 (1989).

146. Tang C, Heindel TJ. Time-dependent gas holdup variation in an air–water bubble column. Chem Eng Sci 2004; 59:623–32.

147. Tang, W.T. and Fan, L.S., Gas-liquid mass transfer in a three-phase fluidized bed containing low density particles. Ind. Eng. Chem. Res., 29 (1), 128-133, 1990.

148. Tareef, B.M., "Thermal Conductivity of Colloidal Systems", Colloidal J. of USSR 6, 545 (1940).

149. Tsuge, H., and S. Hibino, "Bubble formation from an orifice submerged in liquids," Chem. Eng. Comm., 22, 63 (1983).

150. Ueyama, K., S. Morooka, K. Koid, H. Kaji and T. Miyauchi, "Behavior of Gas Bubbles in Bubble Columns", Ind. Eng. Chem. Proc. Des. Dev. 19,592-599 (1980)

151. Van Baten J. M., and Krishna R. Scale effects on the Hydrodynamics of Bubble Columns Operating in the Heterogeneous Flow Regime. Chemical Eng. Research and Design, 2004, 82(A8): 1043–1053

152. Vand, V., "Viscosity of Solutions and Suspensions", J. Phys. Chem. 52, 277 (1948).

153. Vandu, C.O. and Krishna, R., Influence of scale on the volumetric mass transfer coefficient in bubble columns. Chem. Eng. and Proc., 43, 575-579, 2004a.

154. Vandu, C.O. and Krishna, R., Volumetric mass transfer coefficients in slurry bubble columns operating in the churn-turbulent flow regime. Chem. Eng. and Proc., 43, 987- 995, 2004b.

155. Veera UP, Kataria KL, Joshi JB. Effect of superficial gas velocity on gas hold-up profiles in foaming liquids in bubble column reactors. Chem Eng J 2004; 99:53–8.

156. Verma, A.K., 1989, Heat transfer mechanism in bubble columns. Chem Eng J, 42: 205–208.

157. Vinit P. C. Hydrodynamics and Mass Transfer in Slurry Bubble Columns: Scale and Pressure Effects. Ph.D. Thesis, Eindhoven University of Technology, The Netherlands, 2007.

158. Wang S, Arimatsu Y, Koumatsu K, Furumato K, Yoshimato M, Fukunaga K, et al. Gas holdup, liquid circulating velocity and mass transfer properties in a mini-scale external loop airlift bubble column. Chem Eng Sci 2003; 58:3353–60.

159. Wasan, D. T.; Ahluwalia, M. S. Consecutive Film and Surface Renewal Mechanism for Heat and Mass Transfer from a Wall. Chem. Eng. Sci. 1969, 24, 1535.

160. Wender, I., 1996. Reactions of Synthesis Gas, Fuel Processing Technology, 48, 189-297.

161. Wilkinson, P. M., A. P. Spek and L. L. van Dierendonck, "Design Parameters Estimation for Scale-Up of High Pressure Bubble Columns," AIChE J. 38(544), (1992).

162. Wu, C. Heat Transfer and Bubble Dynamics in Slurry Bubble Columns for Fischer Tropsch Clean Alternative Energy, Ph.D. Thesis, Washington University: Saint Louis, MO, 2007.

163. Wu, C., Al-Dahhan, M.H., and Prakash, A. "Heat transfer coefficients in a high pressure bubble column." Chemical Engineering Science 62.1-2 (2007): 140 -147.

164. Xue, J. Bubble velocity, size and interfacial area measurements in bubble columns, Ph.D. Thesis, Washington University, Saint Louis, MO, 2004.

165. Xue, J., Al-Dahhan, M., Dudukovic, M., P., and Mudde, R., F., 2008. Bubble velocity, size, and interfacial area measurements in a bubble column by four-point optical probe, AIChE J., 54(2), 350-363.

166. Yagi, H. and Yoshida, F. Oxygen Absorption in Fermenters-Effects of Surfactants, Antifoaming Agents, and Sterilized Cells. J. Ferment. Tech., 52, 905-916, 1974.

167. Yang, G. Q.; Luo, X.; Lau, R.; Fan, L. S. Heat-Transfer Characteristics in Slurry Bubble Columns at Elevated Pressures and Temperatures. Ind. Eng. Chem. Res. 2000, 39, 2568-2577

168. Yang, G.Q. and Fan, L.S., Axial liquid mixing in high-pressure bubble columns. AIChE J., 49 (8), 1995-2008, 2003.

169. Yasunishi, A.; Fukuma, M.; Muroyama, K. Measurement of behavior of gas bubbles and gas holdup in a slurry bubble column by a dual electroresistivity probe method. J. Chem. Eng. Jpn. 1986, 19 (5), 444–449.

170. Youssef Ahmed A. Fluid Dynamics and Scale-up of Bubble Columns with internals, Ph.D. Thesis, Washington University: Saint Louis, MO, 2010.

171. Youssef Ahmed A.; Al-Dahhan M.H.; Impact of Internals on the Gas Holdup and Bubble Properties of a Bubble Column. Ind. Eng. Chem. Res. 2009, 48, 8007–8013.

172. Yuanxin Wu, and M. H. Al-Dahhan "Prediction of axial liquid velocity profile in bubble columns" Chemical Engineering Science 56 (2001) 1127}1130.

173. Zahradnik, J.; Drapal, L.; Kastanek, F.;Reznickova, J. Hydrodynamics and mass transfer characteristics of sectionalized aerated slurry reactors. Chem. Eng. Process., 31, 263-272, 1992.

174. Zaidi, A., Deckwer, W.D., Mrani, A., and Benchekchou, B. "Hydrodynamics and heat transfer in three-phase fluidized beds with highly viscous pseudoplastic solutions." Chemical Engineering Science 45.8 (1990): 2235 - 2238.

175. Zhang, K. and Y. Zhao, "A Scale-Up Strategy for Low-Temperature Methanol Synthesis in a Circulating Slurry Bubble Reactor," Chem. Eng. Sci. 61, 1459–1469 (2006).

VITA

Moses Odongo O. Kagumba was born in Migori, Kenya on November 21, 1978. In May 2004, he received a BSc. with Honors in Chemistry and Mathematics from the University of Nairobi, Nairobi, Kenya. After teaching Chemistry and Mathematics for 3.5 years, at Mbita High School, he joined Missouri University of Science and Technology, (Missouri S&T), formally UMR for masters degree program in Chemistry. After 2 semesters before completing the masters program, he switched to Chemical Engineering in June of 2009 at Missouri S&T. In April 2013, he received his Ph.D. in Chemical Engineering from Missouri University of Science and Technology, Rolla, Missouri, USA.

He has had conference publication and a number of presentations; including at the American Institute of Chemical Engineers 2012 annual conference. He has been a member of American Institute of Chemical Engineers, (AIChE) since May 2010.

Listed below are the publication and presentations he has given among others.

Publications

- M.O. Kagumba, Y. Abdulaziz, and M.H. Al-Dahhan, "Effect of Internals and Solids Loading on Bubble Dynamics in Slurry Bubble Columns". 2012 AIChE Annual Meeting, October 28-November 2, David L. Lawrence Convention Center, Pittsburgh PA, U.S.A

Presentations

- M.O. Kagumba, and M.H. Al-Dahhan, "Combined Heat Transfer Coefficient and Bubble Dynamics Measurements in Bubble Columns: Assessment of a Mechanistic Approach", 2012 AIChE Annual Meeting, October 28-November 2, David L. Lawrence Convention Center, Pittsburgh PA, U.S.A

- M.O. Kagumba, Y. Abdulaziz, and M.H. Al-Dahhan, "Effect of Internals and Solids Loading on Bubble Dynamics in Slurry Bubble Columns". 2012 AIChE Annual Meeting, October 28-November 2, David L. Lawrence Convention Center, Pittsburgh PA, U.S.A

- Stoyan Nedeltchev*, Moses Kagumba and Muthanna Al-Dahhan "Flow Regime Identification in a Bubble Column with a Conically-Shaped Inlet Based On Optical Probe Data and Different Entropies" 1st International Symposium on Multiscale Multiphase Process Engineering October 4-7, 2011, Ishikawa Prefecture Japan